Editorial

Foreword to the special volume on geology of the Mongolian Altay

Mongolia is a land of endless skyline and steppe, rugged mountains and deserts, which hide away a great mineral potential. This country attracts geologists and mining companies from all over the world. Although the collaboration between former Czechoslovakia and Mongolia has had a long tradition, in fact going back as far as into 1950's, it was broken after political changes in early nineties. While Czech geologists drew back, Mongolia began to open up to numerous foreign prospecting and exploration companies. The cooperation in geology between Czech Republic and Mongolia resumed in 1997 within the frame of the Czech International Development Cooperation. The first projects were focussed on geological mapping and geochemical reconnaissance/prospecting works, the current deal mainly with the environmental problems and hydrogeology.

Modern geological works starting after opening of Mongolia to foreign geologists have brought new insight into older, mainly Russian, geological maps. New approaches yielded numerous data on tectonics, sedimentology, geochemistry and radiometric dating. The first stage of this renewed geological research effort culminated by publishing of a new terrane subdivision for Mongolia compiled by Badarch et al. (2002). It at last put the Mongolian regional geology within the broader geotectonic context of the Central Asian Orogenic Belt (CAOB). This belt known also as Altaids was a site of major crustal growth in the Phanerozoic times, representing one of the largest accretionary terrains on the Earth (for review see e.g. Mossakovsky et al. 1993; Şengör 1993; Dergunov 2001; Jahn 2004; Yakubchuk 2005; Windley et al. 2007 or Kröner et al. 2007).

Traditionally, the geological structure of Mongolia is subdivided into the northern and southern domains. The northern domain is considered to be a Caledonian orogen with relics of Precambrian rocks, whereas the southern domain

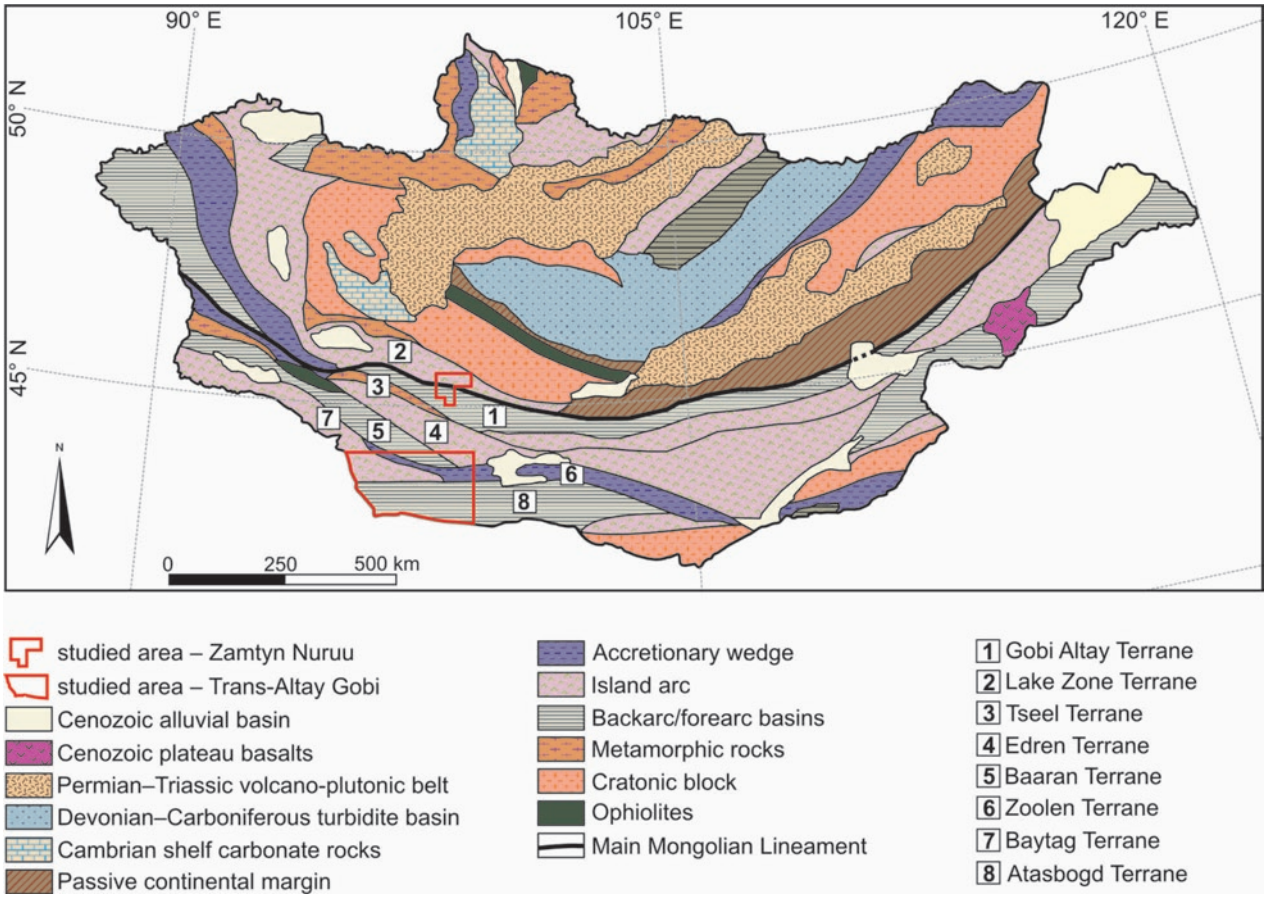

Fig. 1 Geological subdivision of Mongolia showing Zamtyn Nuruu and Trans-Altay Gobi areas as well as names of terranes discussed in the following papers. Simplified from Badarch et al. (2002).

is interpreted as a Variscan orogen. The two are divided by the so-called Main Mongolian Lineament – a regional topographic and structural boundary separating mostly Precambrian and Lower Palaeozoic rocks in the north from dominantly Middle–Upper Palaeozoic units in the south. The geological evolution of CAOB is characterised by accretion of various terranes between the Siberian, Tarim, and Sino-Korean cratons within time span of *c.* 1000–250 Ma (Windley et al. 2007). Collision culminated by extensive terrestrial volcanic activity in the SW Mongolia during the Permian and ended by the Early Mesozoic closure of the Mongolsk–Ochotsk marine basin (in the NE part of today's Mongolia). The Late Cretaceous–Palaeogene was in Mongolia a period of development similar to a platform evolution accompanied by within-plate magmatic activity (see Sinica 1993; Hendrix et al. 1996; Dergunov 2001; Barry et al. 2003 and references therein). The tectonic reactivation of the region was triggered by the collision of the Eurasian plate with the Indian subcontinent in the Late Cenozoic times. The E–W trending, recently active intra-continental faults accommodating deformation stress in the Himalayan region are responsible for the "horst" and "graben" topography of the SW Mongolia (e.g. Tapponier and Molnar 1979; Cunningham et al. 1996; Bayasgalan 1999; Vassallo et al. 2007; Cunningham 2008).

Although numerous geological publications have appeared since the Badarch's synthesis, it still represents the most systematic and comprehensive work summarizing geology of Mongolia. This geological subdivision presented in Fig. 1 hence provides basis also for all papers published in this Volume. The translation of local geographical terms used in the texts and figures is given in Tab. 1.

The original papers forming this volume of the *Journal of Geosciences* span from the extensive geological mapping, geochemical prospection and hydrogeological works performed in the SW Mongolia in the frame of the Czech International Development Cooperation in years 1999–2006 under the supervision by the Ministry of Environment of the Czech Republic.

The paper concerned with granites of the Trans-Altay Gobi results from the maps and data collected within the project "Geological and Geochemical Mapping of the Trans-Altay Gobi on a Scale of 1 : 200,000" carried out by the GEOMIN Co., Jihlava, in 1999–2003. Also the geological map of the Trans-Altay Gobi on the scale 1 : 500,000 that is enclosed in the current Volume summarizes results of the field campaign in the remote desert area on the south-western edge of Mongolia, along the border with China.

All remaining papers represent data acquired during the field work on the project "Geological mapping of the Mongolian Altay on the scale of 1 : 50,000" undertaken by the Czech Geological Survey. The Mongolian counterpart involved the Mineral Resources and Petroleum Authority of Mongolia (MRPAM), Geological Investigation Centre (GIC) and the geological departments of the Mongolian University of Science and Technology (MUST).

Pavel HANŽL, Guest Editor

Acknowledgements I appreciate the authors who spend much time preparing and finalizing papers in this Volume, beyond the scope of Czech International Development Cooperation projects, from which published data are gathered. This volume owes very much to editor-in-chief, handling editors, reviewers and other people who took the time to proofread it.

I would like to gratefully acknowledge the financial and logistic support during the field campaign by the Ministry of Environment of the Czech Republic, the Czech Embassy in Ulaanbaatar, the Czech Geological Survey, the Mineral Resources and Petroleum Authority of Mongolia, the Geological Investigation Centre of Mongolia, the Central Geological Laboratories, the Department of Geology and Mineral Resources of Ministry of Industry and Trade of Mongolia and the Geological Department of the Mongolian University of Science and Technology.

This work would not be possible without the support and co-operation of local authorities and people living in Chandman somon and Ekhin Gol. We owe also many thanks to the people we had pleasure to work with in Mongolia: students, helpers, drivers and mechanics.

Tab. 1 Translation of common Mongolian geographic terms used in this Volume

Aymag	province	Nuur	lake
Bulag	spring	Ovoo	shamanistic tumulus
Gol	river	Somon	district
Gov, Gobi	desert	Tolgoi	hill
Khudag	well	Uul	summit, mountain
Nuruu	mountain range		

References

Badarch G, Cunningham WD, Windley BF (2002) A new terrane subdivision for Mongolia: implications for the Phanerozoic crustal growth of central Asia. J Asian Earth Sci 20: 87–100

Barry TL, Saunders AD, Kempton PD, Windley BF, Pringle MS, Dorjnamjaa D, Saandar S (2003) Petrogenesis of Cenozoic basalts from Mongolia: evidence for the role of asthenospheric versus metasomatized lithospheric mantle sources. J Petrol 44: 55–91

Bayasgalan A, Jackson J, Ritz JF, Carretier S (1999) Forebergs, flower structures, and the development of large intracontinental strike-slip faults: the Gurvan Bogd fault system in Mongolia. J Struct Geol 21: 1285–1302

Cunningham WD (2008) Structural and topographic characteristic of restraining bend mountain ranges of the Altai, Gobi Altai and easternmost Tien Shan. In: Cunningham WD, Mann P (eds) Tectonics of Strike-Slip Restraining and Releasing Bends. Geol Soc of London Spec Pub 290: 219–238

Cunningham WD, Windley BF, Dorjnamjaa D, Badamgarov J, Saandar M (1996) A structural transect across the Mongolian Altai: active transpressional mountain building in central Asia. Tectonics 15:142–156

Dergunov AB ed. (2001) Tectonics, Magmatism, and Metallogeny of Mongolia. Routledge, London, pp 1–288

Hendrix MS, Graham SA, Amory JY, Badarch G (1996) Noyon Uul syncline, southern Mongolia: Lower Mesozoic sedimentary record of the tectonic amalgamation of central Asia. Geol Soc Am Bull 108: 1256–1274

Jahn BE (2004) The Central Asian Orogenic Belt and growth of the continental crust in the Phanerozoic. In: Malpas J, Fletcher CJN, Ali JR, Aitchinson JC (eds) Aspects of the Tectonic Evolution of China. Geol Soc London Spec Pub 226: 73–100

Kröner A, Windley BF, Badarch G, Tomurtogoo O, Hegner E, Jahn BM, Gruschka S, Khain EV, Demoux A., Wingate MTD (2007) Accretionary growth and crust formation in the Central Asian Orogenic Belt and comparison with the Arabian-Nubian shield. In:, Hatcher RD, Jr., Carlson MP, McBride JH, Martínez Catalán, JR (eds) 4-D Framework of Continental Crust: Geological Society of America Memoir 200: 181–209

Mossakovsky AA, Ruzhentsev SV, Samygin SG, Kheraskova TN (1993) Central Asian fold belt: geodynamic evolution and history of formation. Geotectonics 6: 3–33

Şengör AMC, Natalin BA, Burtman VS (1993) Evolution of the Altaid tectonic collage and Paleozoic crustal growth in Eurasia. Nature 364: 299–307

Sinica SM (1993) Jurassic and Lower Cretaceous of central Mongolia. In: The works of combined Russian-Mongolian palaeontology expedition, vol 42. pp 1–236 (in Russian)

Tapponier P, Molnar P (1979) Active faulting and Cenozoic tectonics of the Tienshan, Mongolia and Baykal region. J Geophys Res 84(B7): 3425–3459

Vassallo R, Ritz JF, Braucher R, Jolivet M, Carretier S, Larroque C, Chauvet A, Sue C, Todbileg M, Bourlès D, Arzhannikova A, Arzhannikov S (2007) Transpressional tectonics and stream terraces of the Gobi-Altay, Mongolia, Tectonics 26: TC5013, doi:10.1029/2006TC002081

Windley BF, Alexeiev D, Xiao W, Kröner A, Badarch G (2007) Tectonic models for the accretion of the Central Asian orogenic belt. J Geol Soc, London 164: 31–47

Yakubchuk A (2005) Geodynamic evolution of accreted terranes of Mongolia against the background of the Altaid and Transbaikal-Mongolian collages. In: Seltmann R, Gerel O Kirwin DJ (eds) Geodynamics and Metallogeny of Mongolia with a Special Emphasis on Copper and Gold Deposits. IAGOD Guidebook Series 11, London, pp 13–24

Foreword

In memory of Jaroslav Aichler

When we were working with Jarda on the last version of his manuscript on gold from the Zamtyn Nuruu area in the end of March 2008, no one expected that it would be his last publication and he would not live to see it published. In consequence, we would like to dedicate this issue of the *Journal of Geosciences* to commemorate his personality.

Jaroslav Aichler was born in 1955 in Litoměřice in a medical family where he got intellectual and emotional upbringing. He also gained fundamentals in arts during grammar school education. A wide interest in science brought him to the study of geology at Mining University in Ostrava where he graduated in 1979. Here he also met his future wife Zorka. Their marriage was a happy one with two, now adult children Jaroslav and Madla.

Jaroslav entered a job at a branch of the Czech Geological Survey in the town of Jeseník in 1980. He was involved in the great exploration and metallogenic projects concerned with base metals and gold ores in the Jeseníky Mts. In the years 1983–1990 he was head of the state prospecting project in the Jeseníky Mts. area. In these years of the geological boom in the Jeseníky Mts., Jarda's personality had matured in cooperation with a mineral resources group lead by Petr Orel and a geological mapping team headed by Jan Cháb. From this period comes his remarkable work on gold-bearing mineralization in black shales of the Andělská hora ore district. His outstanding professional as well as human qualities, honesty, enthusiasm and endurance lead the management of the Czech Geological Survey to appoint Jaroslav at the age of 28 the director of the Regional office in Jeseník which he remained until his death.

The coming of new computer technologies revealed a new horizon and he devoted himself to their implementation into processing of geological data. The spread of the Internet supported his visions about the flow and presentation of geological information. The time has shown that Jarda was a step ahead again. As the informatics manager he set up the Information Portal of Czech Geological Survey, hosting numerous science and popularisation sites today.

Experience in economic geology and ore prospecting took Jaroslav in many countries, e.g. Tanzania, Australia or China. For many years he was the executive secretary of the IAGOD, a worldwide institution incorporating more than ten thousands ore geologists, and he participated in numerous international conferences and workshops. The work on the geochemical prospecting and ore reconnaissance of the Zamtyn Nuruu area in the Mongolian Altay within a Czech International Development Cooperation project conducted by the Czech Geological Survey was the culmination of his activities abroad. His endurance, chosen methodologies and sound scepticism accompanied by great erudition lead to the discovery of several geochemical anomalies and interesting ore indications in the area so far considered as sterile.

Those who had the opportunity to meet Jaroslav either at work or privately always felt that they had encountered a person of a honest heart and outstanding abilities. His gift to mitigate conflicts and his short and smart comments on various situations, either at work meetings, in remote wilderness or at an informal evening, filled everybody by motivation, joy and hope for the future. Unfortunately, he himself ran out of inspiration on April 18, 2008.

The loss is hardly retrievable not only for his friends or the staff of the Czech Geological Survey but for the whole Czech geology and foreign partners. Jarda's scientific publications, web pages, popular lectures and mostly his personality will surely continue stimulating next generations of geologists to reveal secrets hidden in the Earth's interior.

Pavel HANŽL, with contribution of Petr MIXA and Petr OREL

Journal of Geosciences, 53 (2008), 123–138 DOI: 10.3190/jgeosci.025

Original paper

Prospection for gold and new occurrences of gold-bearing mineralization in the eastern Mongolian Altay

Jaroslav AICHLER[1†], Jan MALEC[1*], Josef VEČEŘA[1], Pavel HANŽL[1], David BURIÁNEK[1], Tamara SIDORINOVÁ[1], Zdeněk TÁBORSKÝ[1], Khasbar BOLORMAA[2], Dolgor BYAMBASUREN[2]

[1] *Czech Geological Survey, Klárov 3, 118 21 Prague 1, Czech Republic; jan.malec@geology.cz*
[2] *Geological Investigation Centre, Songino Khayrkhan District, PO Box 37/307; Ulaanbaatar, Mongolia*
[†] *deceased*
[*] *Corresponding author*

Geological mapping and regional geochemical prospection on a scale of 1:50,000, covered an area of about 4,000 km^2 in the Zamtyn Nuruu region of the eastern Mongolian Altay. Northern part of the region is formed by the Lake Zone Terrane, the southern by the Gobi Altay Terrane; these two units are separated by the Bogd fault. The panned-concentrate heavy mineral survey was combined with the dry stream-sediment geochemistry, both being complemented by lithogeochemical sampling.

The dry stream-sediment geochemistry proved to be a suitable method for regional prospection in semiarid to arid areas of Mongolia. The morphology and composition of placer gold grains were studied in order to estimate the distance from the primary source, and to constrain the nature of prospective primary mineral deposits. Based on the results of the regional geochemical survey and geological mapping, follow-up works were focused on prospective areas including the reconnaissance field works, detailed geochemical sampling, and geophysical measurements.

New occurrences and signs of Au, Cu, Zn and (Ba)-As-Sb-Hg mineralizations were discovered. The ascertained gold-bearing mineralizations are represented namely by Au and Au-(Ag) quartz veins in basic metavolcanic rocks of the Neoproterozoic Khan Taishir and volcanic rocks of the Permian Delger Khangay formations. Gold locally accompanies vein–disseminated base metal mineralization in some Proterozoic and Lower Palaeozoic formations. A prospective occurrence of clastic gold in Mesozoic conglomerates and sandstones was found at the northern edge of the Zamtyn Nuruu around the Samoandamba Uul. The geochemical survey has revealed a contrast in occurrence of ore indices between the two terranes formig the studied area. While the Lake Terrane and, especially, the Neoproterozoic Khan Taishir Formation are rich in gold and base metal showings, the Gobi Altay Terrane is barren.

Keywords: geochemical prospecting, gold, Mongolian Altay, Lake Terrane, Khan Taishir Formation
Received: 4 April 2008; accepted 10 June 2008; handling editor: M. Štemprok

1. Introduction

The geological survey in the eastern part of the Mongolian Altay was carried out within the framework of project of the International Development Cooperation of the Czech Republic in 2004–2006. The aim of the project was to conduct a comprehensive geological and geochemical mapping on a scale of 1:50,000 covering eleven map sheets, followed by hydrogeological mapping on a scale 1:100,000. An assessment of the mineral potential and a survey of newly found occurrences of ore mineralization, industrial rocks and minerals were additional objectives of the project. All field and laboratory data were compiled and managed using a geographic information system (GIS) (Krejčí and Hanžl 2006). A single occurrence of Cu mineralization and four non-metal occurrences were registered in the surveyed area by MRPAM (Mineral Resources and Petroleum Authority of Mongolia). In adjacent areas, granite-related ore mineralizations (Pb-Zn, Cu, Au) and Au-mineralization in metamorphosed rocks were recorded as sporadic (Dejidmaa et al. 2001). The results of geochemical survey indicated a number of areas with expected primary ore mineralization. New ore occurrences and ore showings were later studied and documented. Some of them were evaluated as perspective and recommended for a follow-up exploration.

An overview of geological and prospecting works and data was presented in the final report (Hanžl and Aichler 2007) available in the Geological Information Centre of MRPAM and in the Czech Geological Survey-Geofond. The current paper brings general information about methodology and the results (with a special emphasis on gold mineralization). The background analytical data cannot be shown due to constraints stipulated by the contract with the MRPAM.

1.1. Geographic position

The studied area in SW Mongolia is located along the boundary between the Gov Altay and Bayankhongor Aymags (regions) in the somons (districts) of Chandman, Erdene, Baatsagaan, and Bayantsagaan. The mountain ranges occupy about 60 % of the mapped area and they are represented by the Khar Argalantyn Nuruu in the north, the Zamtyn Nuruu and the Bayan Tsagaan Nuruu in the central part and the Gichigeney Nuruu (with the highest peak Ulaan Ovot Uul reaching an altitude of 3,359 m) in the south. They trend in general NW–SE to W–E, and have steep and rugged slopes often cut by narrow and deep valleys. The mountain ranges are separated from each other by intermountain endorheic depressions filled often by lakes. The largest of them, Boon Tsagaan Nuur, is located in the NE part of studied area in the Valley of Lakes at *c.* 1,300 m a.s.l.

This region is arid, especially in intermountain depressions, which do not receive more than 200 mm of rain in a year. Only parts of the mountain regions can be considered as semiarid with annual precipitation up to 350 mm (arid: less than 250 mm, semiarid: 250–500 mm; Nicols 1999).

2. Geological setting and ore mineralization

Central Asia represents a mosaic of microcontinents, collapsed ocean basins, and associated accretionary volcanosedimentary complexes, subduction-related igneous arcs and anorogenic intrusive massifs (Hendrix et al. 1992). Geologically, Mongolia is built by a number of tectonic zones (Dergunov 2001), which form a part of the extensive Central Asian Orogenic Belt (Mossakovsky et al. 1993). This belt developed between the Siberian Block in the N, the Tarim Block in the SW and the Sino-Korean Block in the S within time span of *c.* 1000–250 Ma (for review see Windley et al. 2007).

Traditionally, the geological structure of Mongolia is subdivided into the northern and southern domains. The northern domain is considered as a Caledonian orogen with relics of Precambrian rocks, whereas the southern domain is interpreted as a Variscan orogen. The two are separated by the so-called Main Mongolian lineament – a regional topographic and structural boundary separating mostly Precambrian and Lower Palaeozoic rocks in the north from dominantly Middle–Upper Palaeozoic units in the south (Badarch et al. 2002). The surveyed area is situated along the boundary, which separates two different structural zones: the northerly Lake Zone and the southerly Mongolian Altay Zone (Rauzer et al. 1987). The boundary between these zones is formed by a major E–W oriented fault (Rauzer et al. 1987), which coincides with the western continuation of the recently re-activated Bogd fault (Tapponier and Molnar 1979) known also as the North Gobi Altay fault system (Cunningham et al. 1996).

The Lake Zone corresponds to the Lake Terrane exhibiting an island-arc character and the Mongolian Altay Zone to Gobi Altay Terrane interpreted as a former forearc/backarc (Badarch et al. 2002). Geological outline of the studied area is given in Fig. 1.

2.1. Geology of the Zamtyn Nuruu area

The *Lake Terrane* in the studied area is composed of slightly metamorphosed volcanosedimentary sequences of the Neoproterozoic to Lower Palaeozoic ages, which alternate in tectonic mosaic with highly metamorphosed rocks of the Zamtyn Nuruu and Alag Khadny crystalline complexes and with relics of oceanic crust. The Permian volcanic and volcanoclastic sequences cover the Lower Palaeozoic rocks mainly in the NE and SW parts of the outcrops. These are tectonically incorporated into the structure of the Lake Terrane along its southern boundary.

The *Gobi Altay Terrane* is represented by the Bayan Tsagaan subzone (Dergunov 2001) built by slightly metamorphosed Lower Palaeozoic volcanoclastic sequences and Devonian–Carboniferous volcanoclastic sediments of a forearc/backarc character (Badarch et al. 2002). Metamorphic rocks are exposed only in tectonic slices along the northern boundary of the Carboniferous Tsokhoriin Nuruu Fm. and along the Bogd fault (Hrdličková et al. this volume). The basement is formed by the Chandman Khayrkhan Crystalline Complex.

Plutonic rocks of the Palaeozoic age in the Lake Terrane include undifferentiated bodies of gabbros and granites in the Zamtyn Nuruu Crystalline Complex, the granitic Burdnii Gol Massif of Cambrian age, and the Permian Shar Oroy Massif built by granites with an alkaline affinity (Hanžl et al. 2007 this volume). The Carboniferous Chandman Massif is formed by intermediate to acid intrusive rocks of the Gobi Altay Terrane (Economos et al. in print).

Following a Late Palaeozoic phase of tectonic consolidation of Central Asia, the ocean-basin closure continued in the Early Mesozoic along the southern margin of the newly enlarged Asian continent (Sengör 1984) and the Palaeozoic–Early Mesozoic tectonic evolution was terminated by a continental collision during the closure of the Mongolsk–Ochotsk marine basin (Dergunov 2001).

In the Zamtyn Nuruu, Mesozoic sequences represented by Upper Jurassic–Lower Cretaceous continental sediments and volcanics developed in a rift regime – in

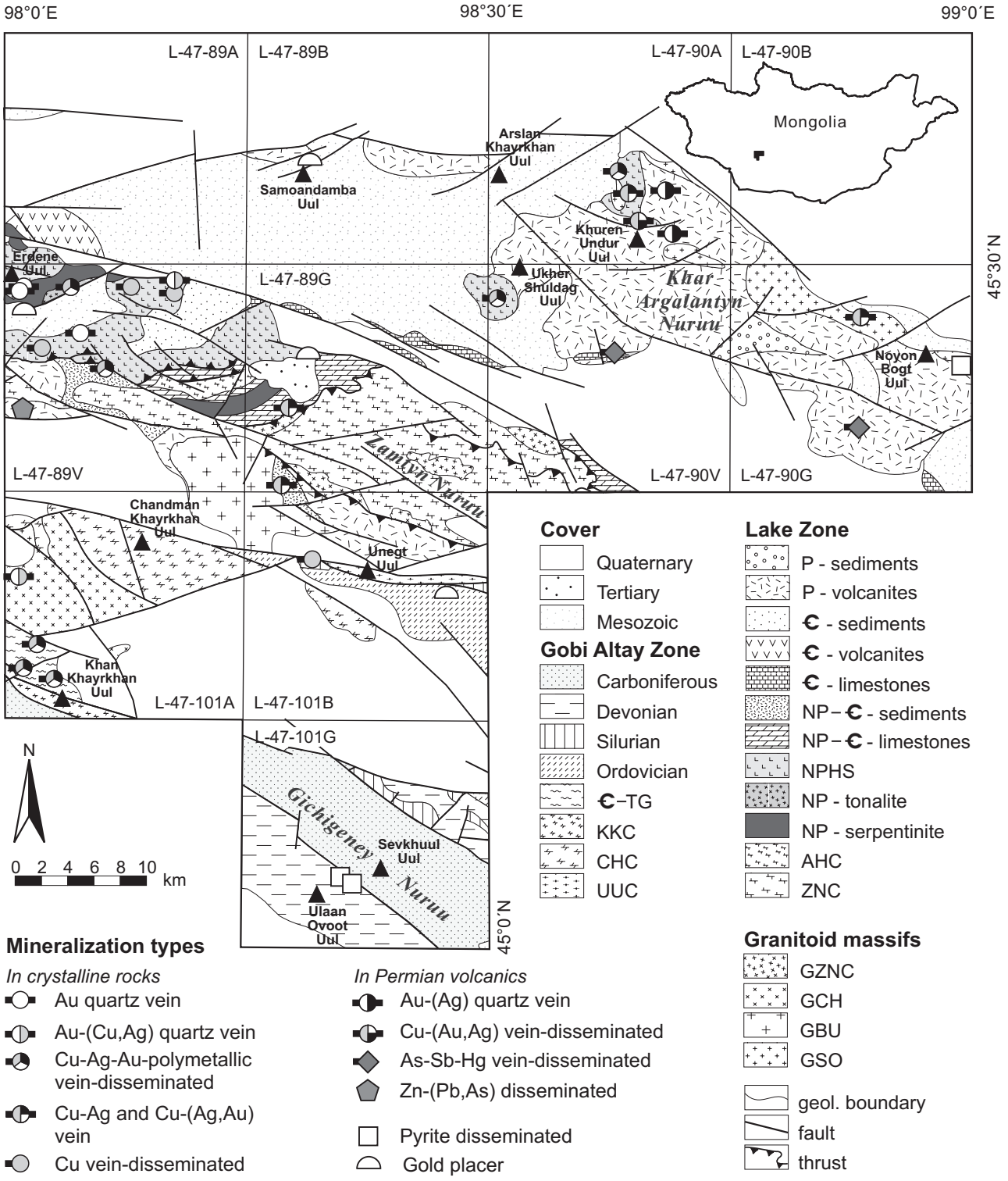

Fig. 1 Geological outline of the studied area in the eastern Mongolian Altay and the main occurrences of ore mineralizations (according to Hanžl and Aichler 2007).

Abbreviations used: TG – Tugrug Fm., NPHS – Khan Taishir Fm.; crystalline complexes: KKC – Khan Khayrkhan, CHC – Chandman Khayrkhan, UUC – Unegt Uul, AHC – Alag Khadny, ZNC – Zamtyn Nuruu; granitoid massifs: GZNC – intrusive rocks of the Zamtyn Nuruu, GCH – Chandman, GBU – Burdnii Gol, GSO – Shar Oroy; NP – Neoproterozoic, Є – Cambrian, P – Permian

the Mesozoic Gobi-Altay rift zone (Yanshin 1976; Yarmolyuk 1983, 1986; Kovalenko et al. 1995). Progressive cessation of tectonic processes initiated throughout the whole Mongolia in the end of the Early Cretaceous, and the Late Cretaceous–Palaeogene saw a period of development similar to a platform evolution (Yanshin 1976). Sediments of this period are not preserved.

The tectonic reactivation of the region was triggered by a collision of the Eurasian Plate with the Indian Subcontinent in the Late Cenozoic, whereby the E–W oriented faults accommodated deformations in the Himalayan region (Tapponier and Molnar 1979). Generally, the studied area has a typical fault-controlled topography, where mountain ranges are separated by intermountain basins. The Neogene–Quaternary detrital sediments filled endorheic intermountain depressions. The area has a very young type of relief as it is supposed for the adjacent Gobi Altay range (Vassallo et al. 2007).

2.2. Ore mineralization of Zamtyn Nuruu

In terms of geological units and related mineralization, the Lake Terrane corresponds to Nuuryn metallogenic belt and the Gobi Altay Terrane hosts the Bayangovi metallogenic belt (Dejidmaa and Badarch 2005).

The *Nuuryn metallogenic belt* hosts the following types of deposits: Cyprus-type Cu-Zn-Ag-(Au) sulphides, iron formation, Au-sulphide quartz veins and stockworks associated with disseminated Au, Au-Cu skarns, W greisens, porphyry Au-Cu, PGE-rich podiform Cr, talc-carbonate, gabbroic Ni-Cu and Ti-Fe. Mineral deposits of the Lake Terrane were described by Shaandar (2003) who recognized their economic importance.

The *Bayangovi metallogenic belt* is characterized especially by deposits and occurrences of Au-(carbonate)-quartz veins, Cu-Ag quartz veins and stockwork deposits related to regionally metamorphosed rocks and to calc-alkaline granites (Dejidmaa and Badarch 2005). The map of deposits and occurrences of Mongolia on a scale 1:1,000,000 together with their description was compiled by Dejidmaa et al. (2001). Dejidmaa et al. (2005) published also a review of mineral deposit models for Mongolia.

3. Methodology of the geochemical prospecting and exploration for mineral deposits

The regional geochemical prospection was carried out on eleven sheets of map on the scale 1:50,000. The main objective of regional geochemical study was to reveal potentially mineralized zones, ore-bearing structures and/or mineral deposits. The panned-concentrate survey on a scale of 1:50,000 was used as a basic method for regional geochemical prospection in pre-Quaternary formations and it was combined with the dry stream-sediment survey. These two methods were complemented by whole-rock geochemistry and, optionally, by sampling of lake sediments or soils.

All sampling sites were documented by field photography, magnetic susceptibility measurements and collecting of mineralized and weathered rock materials for laboratory examination.

Reconnaissance field work and detailed prospection were focused to prospective areas determined by regional geochemical survey and geological mapping. Identification of more than twenty potential fields of gold-bearing mineralizations was based on a distinction of heavy-mineral concentrate (HMC) anomalies, element-indicators in stream sediments, on finds of ore occurrences and on recognition of geological settings suitable for ore mineralization. To a various extent, we used a more detailed geochemical sampling, geophysical measurements, reconnaissance tours, and trenching in search for the primary ore mineralization.

3.1. Panned-concentrate drainage survey

Samples of *c.* 15 kg (10 litres) were taken from wet but mostly dry intermittent river beds in a grid of approx. 1 sample per 2 km^2 (or ~ 1 sample per 1 km^2 in pre-Quaternary outcrop areas). The sampling frequency was adjusted to the geological situation, geomorphology and drainage pattern. A denser sampling pattern was appropriate in a rugged terrain with well-developed drainage pattern and in geologically complex and/or perspective areas. Lower sampling density was employed in a flat relief with a thick sedimentary cover. Large intermountain depressions filled with Quaternary sediments were not sampled at all. The HMC samples were sieved when wet (mesh size 2 mm) and hand-panned to obtain a grey concentrate. Semiquantitative mineralogical analyses of 2.5 thousand HMC samples were carried out in the laboratory of the Geological Research Centre in Ulaanbaatar. The following heavy minerals were identified (according to their importance for ore-prospection): gold, pyrite, chalcopyrite, galena, malachite, azurite, metal copper, metal lead, secondary lead minerals, bismutite, scheelite, cassiterite, molybdenite, barite, fluorite, magnetite, ilmenite, chromite, Mn-minerals, a Ta-Nb mineral, xenotime, monazite, zircon, radioactive zircon, apatite, titanite, rutile, anatase, leucoxene, kyanite, sillimanite, andalusite, and spinel. The results of HMC analyses were stored in ESRI personal geodatabase. Two sets of distribution maps were compiled and plotted using the ArcGIS software on

a scale 1:50,000 including possible source areas of gold and selected heavy minerals (see examples of maps on *http://www.geology.cz/mongolia*).

3.2. Stream-sediment survey

Stream-sediment geochemistry was found to be an efficient method for outlining potentially mineralized areas. Finer (silt) fractions of alluvial sediments represent well the geochemistry of the drainage pattern and also reduce a "nugget effect" during sampling (Fletcher 1997). This method can be effectively used also in regional prospection for gold as shown by Xie and Wang (1991).

In streams with a low silt fraction, a modified method of sampling was employed. Composite samples collected along a stream were sieved in the field to obtain about 6 kg of the fraction under 2 mm. The density of sampling was approximately 1 sample per 2 km^2 for pre-Quaternary geological units. The samples were dried and sieved (–80 mesh) at the field camp, later treated (drying, sieving, pulverization) in the Central Geological Laboratory in Ulaanbaatar and subsequently analysed in the Acme Analytical Laboratories, Vancouver, Canada. The basic set of 36 elements including Au (detection limit 0.2 ppb) was determined by ICP-MS after acid decomposition. A set of 232 samples was additionally analysed for Pt, Pd and Rh with Au by ICP-MS (15 g-splits to get a more representative analyses of these elements subject to nugget effect).

The data set of 1,222 stream-sediment analyses was statistically evaluated using MS Excel and a freeware programme for geochemical data plotting – GCDkit (Janoušek et al. 2006). The principal elemental associations were defined on the basis of upper coefficients of correlation for anomalous values and considering bedrock geology. The single-element distribution maps with delineated anomalous source areas of principal elemental associations were compiled and plotted on a scale 1:50,000 (ArcGIS software).

3.3. Whole-rock geochemistry

Whole-rock samples of selected petrographic types were collected during geological mapping to determine the geochemistry of individual geological formations. Lithogeochemical grab sampling was used during a detailed prospection in some specified and perspective areas to assess the contents of ore elements-indicators.

Major-element oxides, C and S were analysed by ICP-ES and trace elements including REE by ICP-MS (Groups 4B and 1DX) in ACME Labs. Loss on ignition (LOI) was determined after heating to 1000 °C. The data were processed by the GCDkit software (Janoušek et al. 2006). The bulk composition of the rocks in a given geological unit was normalised to the average composition of the Continental Crust. Plotting using the box-and-whisker graphs to delineate formations that underwent hydrothermal processes/overprint (e.g. Reiman and Caritat 1998) was found particularly useful.

3.4. Mineralogical study of gold and accompanying heavy minerals

The morphology and composition of gold grains in placer deposits were studied to determine the nature of placer gold, which could serve as an indicator in search for the source area, and the setting of primary mineral deposit (Malec 2007). The gold grains were examined under a stereoscopic microscope and photographed using the electron microscope CamScan 3200 in the X-ray Microanalysis Facility (LAREM) of the Czech Geological Survey in Prague. Besides the morphology were tested the presence of secondary coatings of pure gold and their thickness and porosity. The composition of grain surface and of single gold particles in polished sections was analyzed by the energy dispersive microanalyzer (EDS) Link ISIS manufactured by Oxford Instruments. The minerals intergrown with gold were identified by the same procedure. Polished sections were prepared after embedding gold grains into epoxy resin. The polished specimens were examined under the ore microscope in order to recognize possible inhomogeneities (zoning, secondary coatings on pure Au, inclusions or intergrowths).

The distance of placer gold particles from a primary source was estimated from their morphology, mechanical disturbances on the grain surface, presence and thickness of secondary coatings of pure gold, and from mineral intergrowths (see Morávek et al. 1992 for experience from the Bohemian Massif). The data on gold grain shape show a clear relationship to the distance of transport from the primary source as approved by the literature. For instance the effect of "hammering" causes the change in shape of fluvially transported gold grains and the attendant abrasion affects their surface texture (Knight et al. 1999; Youngson and Craw 1999).

3.5. Ore mineral study

Selected samples of vein, ore and gossan material collected during the geological mapping and reconnaissance tours were processed in the Laboratory of the Geological Research Center in Ulaanbaatar by standard petrography and ore microscopic methods. Some of thin and polished sections were studied in the Mineralogical Laboratory of the Czech Geological Survey in Prague, where also analyses of ore minerals by the Link ISIS were carried out.

4. Results

4.1. Distribution and character of gold in intermittent streams

Gold is distributed very irregularly in the surveyed area as seen on the maps of heavy mineral concentrate (HMC) and stream-sediment geochemistry (Hanžl and Aichler 2007). Alluvial gold was found more commonly in the areas with exposed rocks of the Khan Taishir Fm. Isolated alluvial gold indications were identified also in other Neoproterozoic crystalline complexes. Gold scarcely appeared also in the drainage sediments within the low-grade to unmetamorphosed Palaeozoic and Mesozoic volcanosedimentary formations. Occurrences of placer gold associated with Mesozoic clastic sediments were newly discovered in the Samoandamba Uul.

Taken together, gold was determined in 175 of 2,500 collected HMC samples. The size of gold grains varies from dust to 0.2–1 mm across or to small nuggets. Its colour is always gold-yellow with metallic lustre. The shape of alluvial gold grains is variable and depends on the origin as well as the length of transport as is documented by results of morphological study (Fig. 2).

Short transport of gold particles corresponding to hundreds of metres is characteristic of gold from the Erdene Uul (map sheet L-47-89V) and the Ovoot am (L-47-101G). Gold from the Unegt Uul–W area (L-47-101G) is interpreted to have undergone a longer transport (~1.5 km). For gold from Samoandamba (L-47-89B) and Ulaan Uul–E (L-47-101B) areas, a transport in the order of several kilometres is assumed. In the case of placer gold from Neogene alluvial terraces in Bayan Tolgoi (L-47-89G), it might have been even longer.

Placer gold from the studied localities of the eastern Mongolian Altay has mostly a similar composition. In general, the gold is typically of a high fineness (>900) and, except for minor Ag, devoid of any other admixture. A small amount of gold grains of a lower fineness was found in Erdene Uul, in the samples from the Neogene alluvial terrace sediments (L-47-89G) and Ovoot am area (L-47-101G). A more detailed treatment of the placer gold morphology and composition is a part of descriptions of some selected localities in the Chapter 4.3.

4.2. Gold-bearing mineralizations

The presence of primary gold-bearing mineralizations was indicated by clastic gold in the heavy mineral concentrates and by Au contents in stream sediments. In the course of the reconnaissance studies some showings of gold-bearing mineralizations were found, which several are considered to be of a potential economic importance. The distribution of gold-bearing occurrences is shown in the Fig. 1.

The following types of Au-bearing mineralizations were discovered in the studied area:

- Au and Au-(Ag, Cu) quartz veins in crystalline complexes,
- Au-(Ag) quartz veins in Permian mafic volcanic rocks,
- gold-bearing base metal quartz-carbonate veins,
- other showings of gold-bearing mineralizations,
- gold placers.

4.2.1. Au and Au-(Ag, Cu) quartz vein mineralizations

Gold-bearing mineralization of this type is associated almost exclusively with the rocks of the Khan Taishir Fm. The formation was defined and assigned to the Neoproterozoic (Vendian according to Markova 1975) in the Khan Taishir Mts. ridge south of the Altay town. Presently the formation is considered to be of Vendian–Cambrian age (Dergunov 2001), as confirmed by radiometric dating (Badarch et al. 2002; Khain et al. 2003). Geological, petrographic and geochemical data from the Khan Taishir Fm. point to a dismembered ophiolite sequence (Hanžl and Aichler 2007) with prevailing basaltic volcanic rocks, sporadic deep-water sediments and boudins of serpentinites. This accords with Zonenshain and Kuzmin (1978), who described the ophiolite association in the Khan Taishir Massif.

Fig. 2 Morphology and internal structures of placer gold grains from the eastern Mongolian Altay. ⇨
Alluvial sediments, Erdene Uul area, L-47-89-V: **a** – irregular gold grain with a moderately worked surface, SEI; **b** – detail of the gold grain surface on the Fig. 2a, SEI; **c** – isometric grain with a moderately worked surface, SEI; **d** – plate of gold with slightly worked surface, SEI; **e** – oblong irregular gold grain with a very slightly modified morphology, SEI; **f** – irregular slightly worked forked gold, SEI; **g** – flat, irregular, moderately worked gold grain with rests of clay and limonite on the surface, SEI; **h** – intergrowths of gold (admixture of 6.9 wt. % Ag; bright) with albite and quartz (dark), polished section, BEI; **i** – inclusion of digenite with bornite (dark) in gold containing 5.6 wt. % Ag (light grey), polished section, BEI.
Alluvial sediments, Ovoot Am area, L-47-101-G: **j** – flat slightly worked gold grain with admixture of 14.2 wt. % Ag, SEI.
Neogene alluvial terrace sediments, Bayan Tolgoi area, L-47-101G: **k** – rounded flake of gold with a strongly modified shape, SEI; **l** – detail of the surface of the gold flake on the Fig. 2k, SEI.
Alluvial sediments, Unegt Uul-W area, L-47-101G: **m** – flat and intensively worked gold grain, SEI.
Quaternary sediments, Unegt Uul–SEE area, L-47-101B: **n** – isometric gold grain with a slightly modified morphology, SEI; **o** – flat gold nuggets, photomicrograph.
(SEI = secondary electron image; BEI = backscattered electron image).

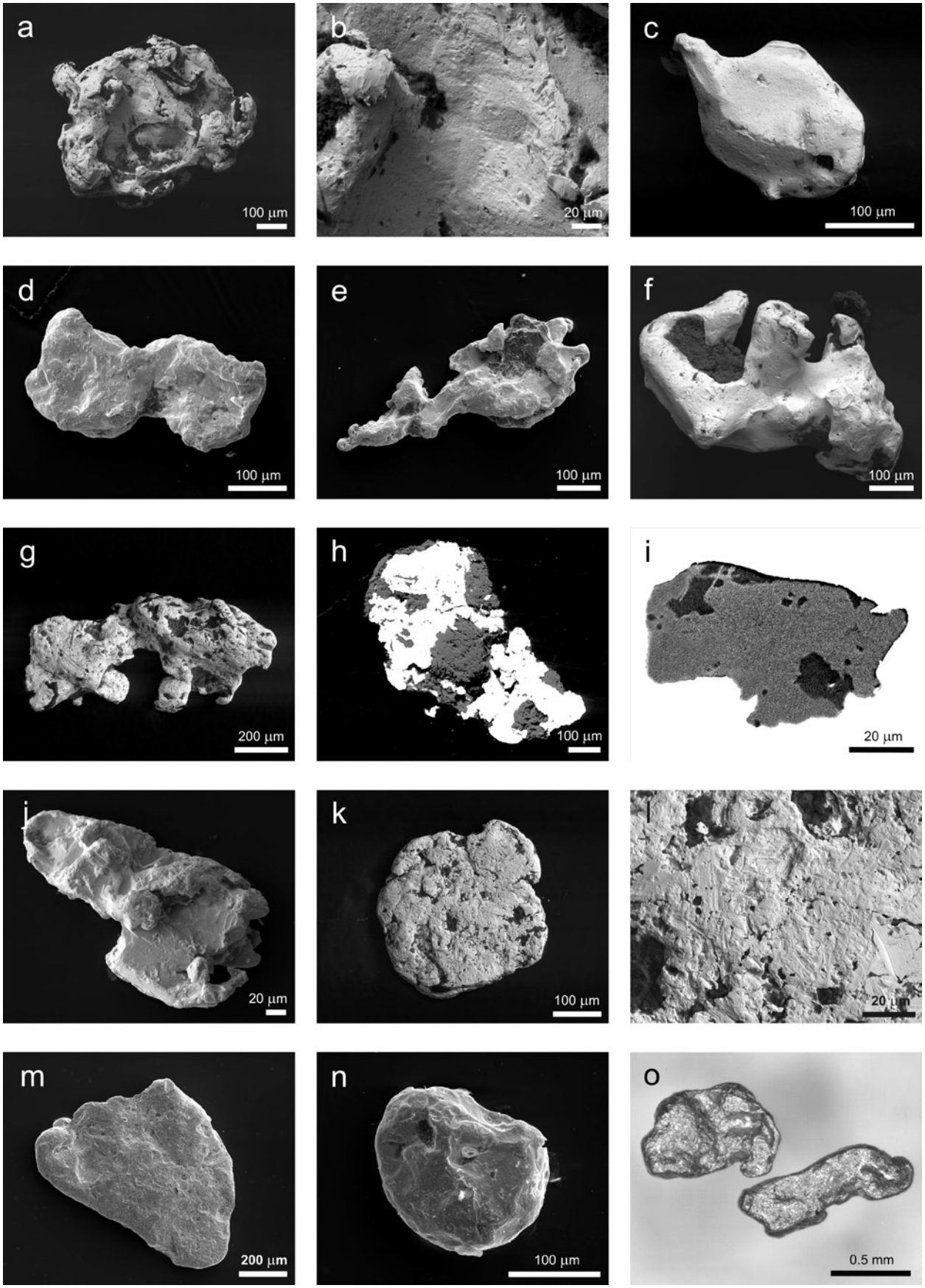
a
100 µm
b
20 µm
c
100 µm
d
100 µm
e
100 µm
f
100 µm
g
200 µm
h
100 µm
i
20 µm
j
20 µm
k
100 µm
l
20 µm
m
200 µm
n
100 µm
o
0.5 mm

The Khan Taishir Fm. occurs in two regions in the surveyed territory. The larger one is exposed E and SE of the Erdene Uul Mt. in the NW part. Small exposures crop out in erosion windows at the footwall of the Permian rocks in the Khar Argalantyn Nuruu Mts. in the E part of the region. The Khan Taishir Fm. has been thrusted from the north over the Alag Khadny and Zamtyn Nuruu crystalline complexes.

The Au-quartz vein type showing related to the Khan Taishir Fm. was discovered namely on the SE slopes of the Erdene Uul Mt. (L-47-89V, Fig. 3). The local rock association represents a nearly complete ophiolite sequence (Perfiliev and Kheraskov 1980) dominated by various types of metabasalts, gabbros, green schists and agglomerate tuffs enclosing lenses of limestones. The ophiolite sequence was intruded by tonalites and all the rocks were metamorphosed under the greenschist facies conditions (Fig. 4).

Fig. 3 The Erdene Uul Mt. range, viewed from the south.

The Au and Au-(Ag, Cu) quartz ± carbonate veins and veinlets have tabular to lenticular shapes and form *en-echelon* sets of lenses mostly parallel with the foliation dipping to the SW or WSW (Fig. 5). The veins outcropping on the tops of local rocky ridges are flat or mildly inclined filling extensional fractures. All the veins have the lengths of several to 10–20 metres and occur isolated or in *en-echelon* sets. Their thickness varies from 10 to 50 cm and does not exceed 1.5 m. Gold grade varies from traces to first g/t of Au.

The veins are dominated by white to grey-white medium-grained quartz, with a lesser amount of carbonates and albite. Ore mineral association is formed by pyrite, less commonly by chalcopyrite, pyrrhotite, malachite, goethite, hydrogoethite and gold. Sericitization, carbonatization and pyritization (Fig. 5) are the typical wall-rock alterations (forming aureoles 0.X to 2–3 m thick around the veins).

Native gold forms minute grains, mostly of an irregular shape but also more or less isometric or flat, as described from HMC samples taken from alluvial sediments in the mountain valleys and from alluvial fans beneath the outcrop areas. Quartz, albite, K-feldspar, hornblende(?), clinopyroxene(?), chlorite, biotite, Ti-oxide (rutile), limonite, sporadically also pyrite, digenite and bornite were found in form inclusions or intergrowths with gold (Fig. 2h–i). The fineness of gold ranges from 750 to 1,000, the majority of values fluctuating between 900 and 950 (median 920). This means that the gold of a low purity is rare.

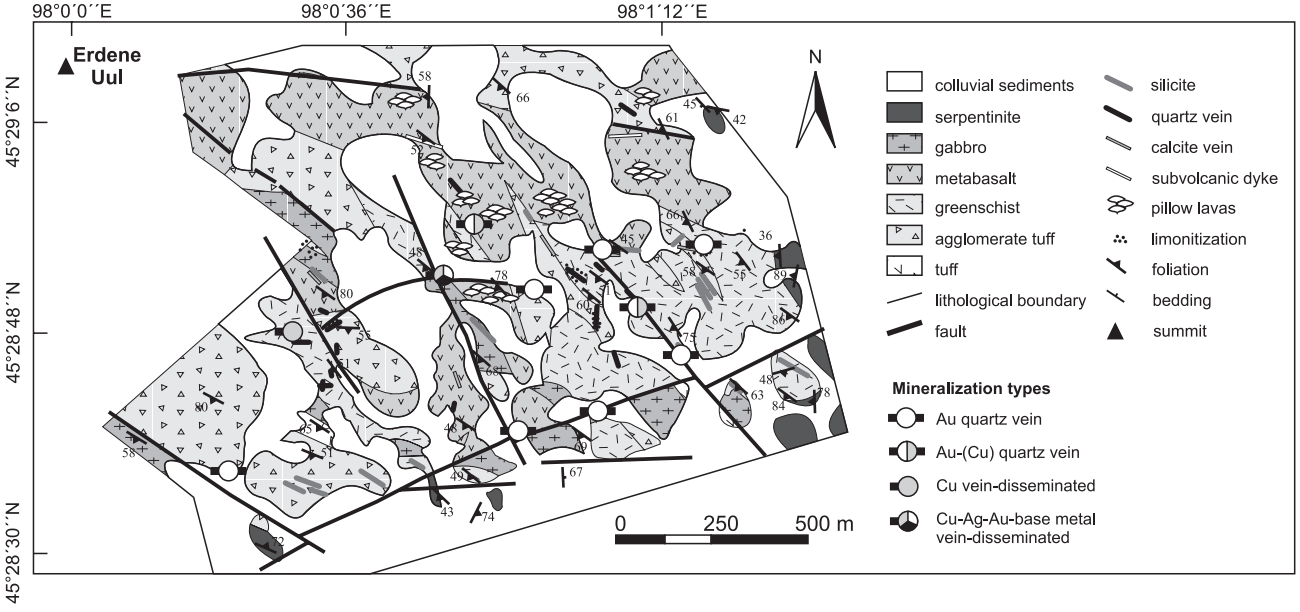

Fig. 4 Geological sketch of the Erdene Uul prospective area.

Fig. 5 Gold-bearing quartz vein arranged *en-echelon* to the foliation of the host basalt metatuffs and accompanied by wall-rock alteration, Erdene Uul Mt. area.

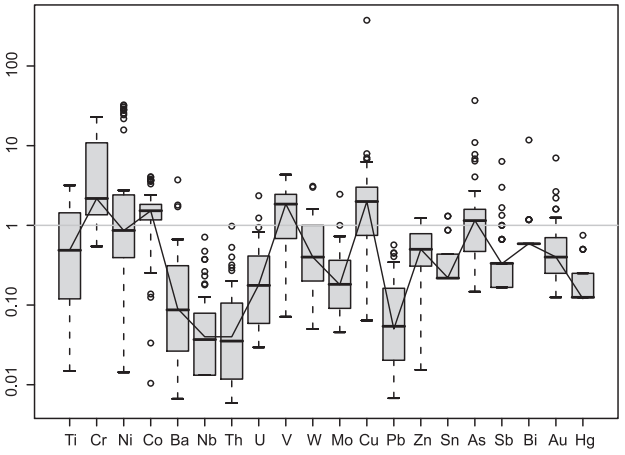

Fig. 6 Bulk chemistry of the Khan Taishir Fm. rocks. Normalization values (bulk continental crust) according to Reiman and Caritat (1998). For each element, the box represents 50 % of the population (limited by two quartiles); the horizontal line inside is the median and the "whiskers" show the total range without outliers denoted by small circles (Janoušek et al. 2006).

The composition and the character of gold-bearing veins and the high fineness of gold support the likely hydrothermal-metamorphic origin of the gold mineralization. The element distribution in the rocks of the Khan Taishir Fm. characterized by anomalous concentration of Au, Cu and other ore elements (Fig. 6) may suggest an important role for hydrothermal processes during its metamorphic development.

4.2.2. Au-(Ag) quartz mineralization

The occurrences of Au-(Ag) quartz vein mineralization were found in Permian volcanic rocks on the northern slopes of the Khar Argalantyn Nuruu Mts. (L-47-90A).

Three volcanic and volcanoclastic formations of a continental origin were recognised. The Khar Argalantyn Fm. was originally designated by Borzakovskii et al. (1985) as a Lower Permian complex. The Delger Khangay Fm. was firstly described by Mosiondze (in Zabotkin et al. 1983) as a Upper Permian complex and reclassified to Lower Permian as was the Khov Fm. occurring along the southern part of the Lake Terrane (Hanžl and Aichler 2007). Nevertheless, all Permian volcanic rocks are of a similar age and share analogous geochemical character in this part of the Lake Terrane. They appear to represent various products of lateral variations in subaerial volcanic activity including lava flows, agglomerates, ignimbrites, tuffs and continental volcanoclastic sediments. The major-element data from the Permian volcanic rocks show a compositional variation from rhyolite, trachydacite and trachyte to trachyandesite and trachybasalt. Except for rhyolites, these volcanic rocks have an alkaline affinity (Hanžl and Aichler 2007).

The Au-(Ag) quartz veins were observed east of the Khuren Ondor Uul Mt. (L-47-90A). They are associated with the Permian volcanic rocks of the Delger Khangay Fm. being composed of trachytic andesites, basaltic andesite and subordinate basalts, rhyolites and their tuffs. Irregularly distributed gold-bearing veins are north of the contact with the Lower Permian Shar Oroy Massif built by reddish medium- to coarse-grained granites–granodiorites. The field relations along the contact of the granites with volcanic rocks of the Delger Khangay Fm. suggest a cogenetic relationship. Veins of white-grey quartz and quartz-carbonate lenses and silicified zones do not exceed 0.X m in thickness and several metres in length. In addition to quartz and carbonates they contain mostly pyrite, chlorite, and traces of malachite. The grade of sampled veins varies from 0.X to first ppm Au. Magnetite with disseminated Cu-mineralization (chalcopyrite, chalcocite, covelline, malachite) and disseminated stibnite are common in mafic volcanic rocks in the vicinity of gold-bearing veins.

4.2.3. Au-Cu-Ag base metal mineralization

Occurrences of auriferous base metal veins and disseminated mineralization were found in exposures of the Khan Taishir and Maykhan Tsakhir formations in the Lake Terrane and of Tugrug Fm. in the Gobi Altay Terrane.

A mineralized NNE–SSW trending zone was ascertained in the central part of a block built by the Khan Taishir Fm. southwest of the Ukher Schuldag Uul. The zone, 3–10 m thick and 140 m long, occurs in cracked basalt metatuffs. The rocks are limonitized and bleached having ochre-yellow to brown-yellow colours. Limonitized quartz-carbonate veins and stringers carrying sulphides, common pyrite impregnations and large gossan are present here. In such massive gossans with increased contents of Au, Ag, Cu, and Pd, native gold, pyrite, goethite, hydrogoethite and scarce native copper were identified in polished sections (Fig. 7).

The existence of a mineralized zone was indicated by elevated Au contents in stream sediments. The absence of alluvial clastic gold in HMC samples indicates that probably only fine gold-bearing sulphidic mineralization can be expected in this area.

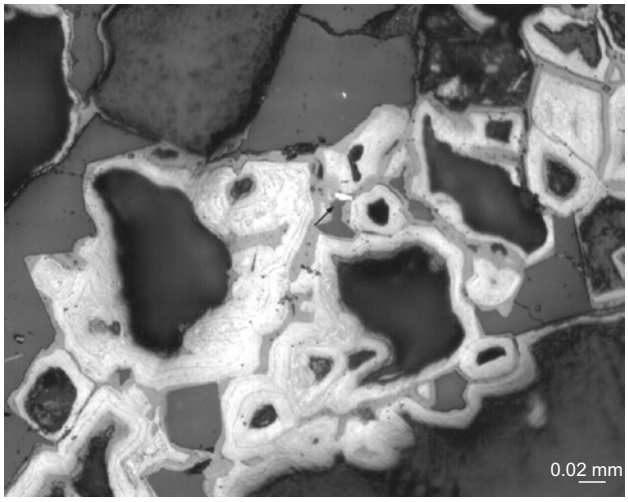

Fig. 7 Tiny gold grain (white indicated by black arrow) in the goethite–hydrogoethite (light) gossan layer, accompanied by quartz (dark grey). Photomicrograph of the polished section, reflected light. Ukher Schuldag Uul–SW.

Exceptionally, metal-rich samples of gossan above a gold-bearing base metal quartz-carbonate vein 20 cm thick and of an unknown length was discovered in a local slope cut (15.39 g/t Au, 61.1 g/t Ag, 25 ppb Pd). Similar limonitized zones with quartz-carbonate veins and veinlets with common disseminated pyrite in the altered wall rocks were described also in the northern parts of the Khan Taishir Fm. (L-47-89V). These are mostly E–W striking. However, the reconnaissance samples taken from these zones did not yield increased gold contents.

An occurrence of Au-Cu mineralization was also found in a swarm of limonitized 10–20 cm thick quartz-carbonate veins/lenses hosted by chloritized and limonitized andesite–basalt metatuffs in the surroundings of the Khanangiin Khokh Uul (L-47-89V). The width of a N–S trending zone is *c.* 15 m and the length exceeds 150 m. Its mineralization was indicated by increased gold contents in stream sediments.

Showings of gold in association with base metal (Cu, As, Zn, Pb, Ag) veins were ascertained in the Cambrian Tugrug Fm. composed of siliceous chlorite-sericite schists with intercalations of greenschists and quartzites N and NW of the Khar Khayrkhan Uul (L-47-101A). Low content of Au and elevated contents of silver were found in a quartz vein in silicified limestones of the Maykhan Tsakhir Fm. in the Tuymert Tsakhir Tolgoi area (L-47-89V). Tetrahedrite, covellite, malachite, azurite and antimony oxides were identified among ore minerals.

4.2.4. Other showings of gold-bearing mineralization

Gold in the HMC samples or increased contents of Au in stream sediments were detected also in other geological formations within the surveyed territory. However, their primary sources could not be identified.

Gobi Altay Terrane. Geochemical mapping only sporadically showed scattered Au anomalies indicating most likely local occurrences of gold-bearing quartz ± carbonate vein/veinlet mineralizations associated with the Ordovician (Bayan Tsagaan Fm.), Devonian (Gichigeney Fm.) and Carboniferous (Tsokhoriin Nuruu Fm.) rocks in the Gichigeney Nuruu Mts. (L-47-101G).

Quartz veins and/or silicified zones with pyrite in chlorite schists and greenschists of the Ordovician Bayan Tsagaan Fm. are proposed to be a possible primary source of alluvial gold in the Ovoot am area (L-47-101G). Two flat gold grains with a different fineness (~980 and 860) intergrown with chlorite and accompanied by pyrite and barite were studied. Their morphology reflects a short transport, with a distance not exceeding several hundreds of metres (Fig. 2j).

A gold grain (~0.2 mm) studied from the area W of the Unegt Uul Mt. (L-47-101B) is slightly to moderately mechanically worked (Fig. 2m), isometric and likely of high purity (~ 990 according to its surface analysis). Calcite was identified in the intergrowths. The length of transport can be estimated from several hundreds of metres to about 1.5 km. The gold probably originated from calcite-quartz veins associated with the granites of the Unegt Uul Crystalline Complex.

Lake Terrane. Besides the Erdene Uul region, other potential areas of gold-bearing mineralization were determined in the Lake Terrane. Gold found by geochemical mapping indicates also local occurrence of Au-mineralizations in other areas of the Khan Taishir Fm. (L-47-89V, G, 90A). Low sulphide quartz-carbonate veins are considered as the likely source of clastic gold. On the contrary, fine gold detected in stream sediments comes probably from gold-bearing base-metal vein(s) and/or disseminated mineralization.

The origin of unique clastic gold in the Zamtyn Nuruu Crystalline Complex (L-47-89V, G) can be related either to quartz veins with base metal sulphides hosted by gneisses, amphibolites and calc-silicate rocks, or if associated with scheelite, to quartz veins in mica schists.

Solitary occurrence of alluvial gold north of the Khuren Undur Uul Mt. accompanied by scheelite, pyrite and barite may have been derived from quartz veins, locally with common magnetite, confined to the granites of the Shar Oroy Massif (L-47-90A).

The presence of Au together with other elements-indicators (As, Sb, Hg) detected in stream sediments shows the occurrence of As-Sb-Hg (± Pb-Zn) vein or disseminated mineralization confined to the E–W trending zone in cracked acid volcanic rocks of the Permian Khar Argalantyn Fm. (L-47-90G).

4.3. Gold placers

Gold placers are scarce in the studied area and the observed contents of gold in Neogene terrace and Quaternary alluvial sediments are mostly low and irregular. A prospective occurrence of gold in Mesozoic conglomerates and sandstones was discovered in the northern part of the Zamtyn Nuruu area.

4.3.1. Erdene Uul–S

Gold placers in alluvial sediments are known from the southern slopes of the Erdene Uul Mt. (L-47-89V, Fig. 8). A slight change in morphology of gold grains with a size ranging from 0.2 to 2.5 mm and only an exceptional secondary coating testify for a short transport. Their shapes are mostly irregular, but also more or less isometric and sometimes flat; the crystal planes are abundant, as well. The fineness of gold fluctuates mostly between 900 and 950. Frequent intergrowths of gold with rock-forming minerals (quartz, albite, chlorite etc.) reflect the character of the primary mineralization, i.e. metamorphic sulphide-poor quartz veins and/or veinlets. These occur in the rocks of the Khan Taishir Fm. exposed in the Erdene Uul mountain range above the placer (see Chapter 4.1). The distribution of gold in alluvial sediments is very irregular. The Erdene Uul placer represents an intact alluvial placer of a small extent and low potential, which is occasionally exploited by the local illegal miners.

Fig. 8 View of alluvial fans on the southern slopes of the Erdene Uul Mt.

4.3.2. Ulaan Uul–SEE

The source of placer gold from intermittent streams was traced in the southern slopes of the Ulaan Uul range SEE of the Unegt Uul Mt. (L-47-101B). The gold grain features (such as morphology and fineness of surficial parts corresponding to ~1,000) indicate a transport over a distance in an order of few kilometres (Fig. 2d–e). An erosional remnant of Quaternary sediments of alluvial fans (sands and silty sands) on an ancient peneplain surface was identified as the source of the scarce gold.

4.3.3. Neogene terrace sediments, Bayan Tolgoi

Traces of placer gold accompanied by barite, pyrite and common titanite were identified in gravels and sands of large Neogene terraces of the Oshin Fm. and of Quaternary drainage sediments in Bayan Tolgoi (L-47-89G). The morphology of strongly reworked flat gold grains and the presence of surficial films of secondary enriched Au (Fig. 2k–l) indicate a long transport estimated at several to tens of kilometres. The varying fineness (1,000, 934 and 802) may imply two distinct primary sources of gold, i.e. hydrothermal and/or metamorphogenic veins confined to tectonic zones in crystalline complexes, or subvolcanic ore deposits.

4.3.4. Mesozoic sediments

A prospective occurrence of placer gold in the Mesozoic sediments was newly discovered in the northern part of

the Zamtyn Nuruu representing a conglomerate-hosted clastic Au type (Dejidmaa et al. 2005).

Mesozoic sequences in the studied area are represented by continental sediments and volcanic rocks of the Late Jurassic–Early Cretaceous ages that developed in a rift regime (Yarmolyuk 1983). Mesozoic sediments are divided into four formations: Toromkhon, Undurukhin, Anaday Khudag and Khulsan Gol (Rauzer et al. 1987).

The *Toromkhon Fm.* is the lowermost Mesozoic sequence. The contact with the underlying Neoproterozoic/Palaeozoic rocks is transgressive. Sediments of the Toromkhon Fm. consist of poorly to extremely poorly sorted conglomerates, breccias and sandy conglomerates with rare siltstone horizons. Poorly sorted and subangular clasts in massive conglomerates without grading indicate rapid deposition in arid/semiarid conditions. The degree of lithification is relatively low and thus they are interpreted as sediments of proximal facies of alluvial fans (Gilíková et al. 2007).

The sediments of the *Undurukhin Fm.* form up to 13 m thick cycles consisting of conglomerates fining upwards into sandstones, mudstones and marls. There are frequent wash-outs at the base of these cycles. Contact with the Toromkhon Fm. at the footwall is transitional with local wash-outs. The colour of sediments changes from red-brown to ochre-brown up to greenish brown-yellow shades. The grain size decreases upwards similarly to consolidation and degree of sorting in sediments. Bedding is monoclinal, gently dipping to the NW.

Irregularly dispersed gold was found in the profile of clastic sediments of both the Toromkhon and Undurukhin formations and in alluvial sediments of erosion furrows and valleys north of the Samoandamba Uul Mt. (Fig. 9) on map sheet L-47-89B. Mesozoic sediments are underlain by Permian volcanic sequence (rhyolites, trachydacite, trachybasalts and their tuffs).

Fig. 9 The central part of the gold placer in Mesozoic/Quaternary sediments north of the Samoandamba Uul Mt. (top of the horizon).

Gold released from Mesozoic sediments concentrates at the bottom of erosion furrows being lodged in crevices in the bedrock composed of sandstone benches or thresholds built by Permian volcanic rocks. The size of gold grains from these intermittent streams varies from 0.2 to 3.5 mm (Fig. 10), but nuggets exceeding 10 mm were also found (Fig. 10i). The morphology of grains was moderately to strongly affected by rounding and/or surface scratching. The flat shapes of gold grains prevail but isometric and irregular shapes are also relatively common. The distance of transport was estimated at a few kilometres but their re-deposition from older sediments cannot be excluded. The panned-concentrate sampling showed that the gold is accompanied by magnetite, ilmenite, chromite, and minor cassiterite with cinnabar.

The fineness of gold ranges between 950 and 1,000, occasionally reaching 900–950 (median 998). The coatings of secondarily enriched Au were found in case of gold particles with fineness of about 960 or less. Inhomogeneous internal structures – small domains with sharp outlines, irregular or lobate exsolutions of gold with distinctly enhanced Ag contents – were observed in some gold grains and nuggets (Fig. 10j–k). These textures may represent two or more generations of gold, or more likely products of recrystallization during diagenesis of sediments and/or weathering of primary occurrences. Inclusions of quartz, muscovite, K-feldspar and calcite were found in bigger gold grains (Fig. 10l) but it is not clear whether they represent intergrowths or were squeezed into the grains. On the other hand, small gold particles are free of inclusions or intergrown minerals.

Primary sources of gold are supposed to be most likely uniform, probably belonging to hydrothermal or metamorphic veins in crystalline complexes of the Khan Taishir Fm. Less likely source represent Permian volcanics, as is also documented by the petrography of clasts in Mesozoic sediments.

Gold is less abundant and irregularly distributed in Mesozoic sediments but their volume is enormous. The base of these sediments was determined at a depth of about 280 m by the geophysical methods (VES and reflection seismic profiling) at the northern contact with the Permian volcanic rocks (Valtr 2007). The E–W zone north of the Samoandamba Uul Mt. with outcropping sediments of the Toromkhon and Undurukhin formations was recommended for a detailed follow up exploration. Moreover, it is worth noting that these Mesozoic sedimentary sequences and their erosional remnants are known from other parts in the north of the surveyed area (Hanžl and Aichler 2007).

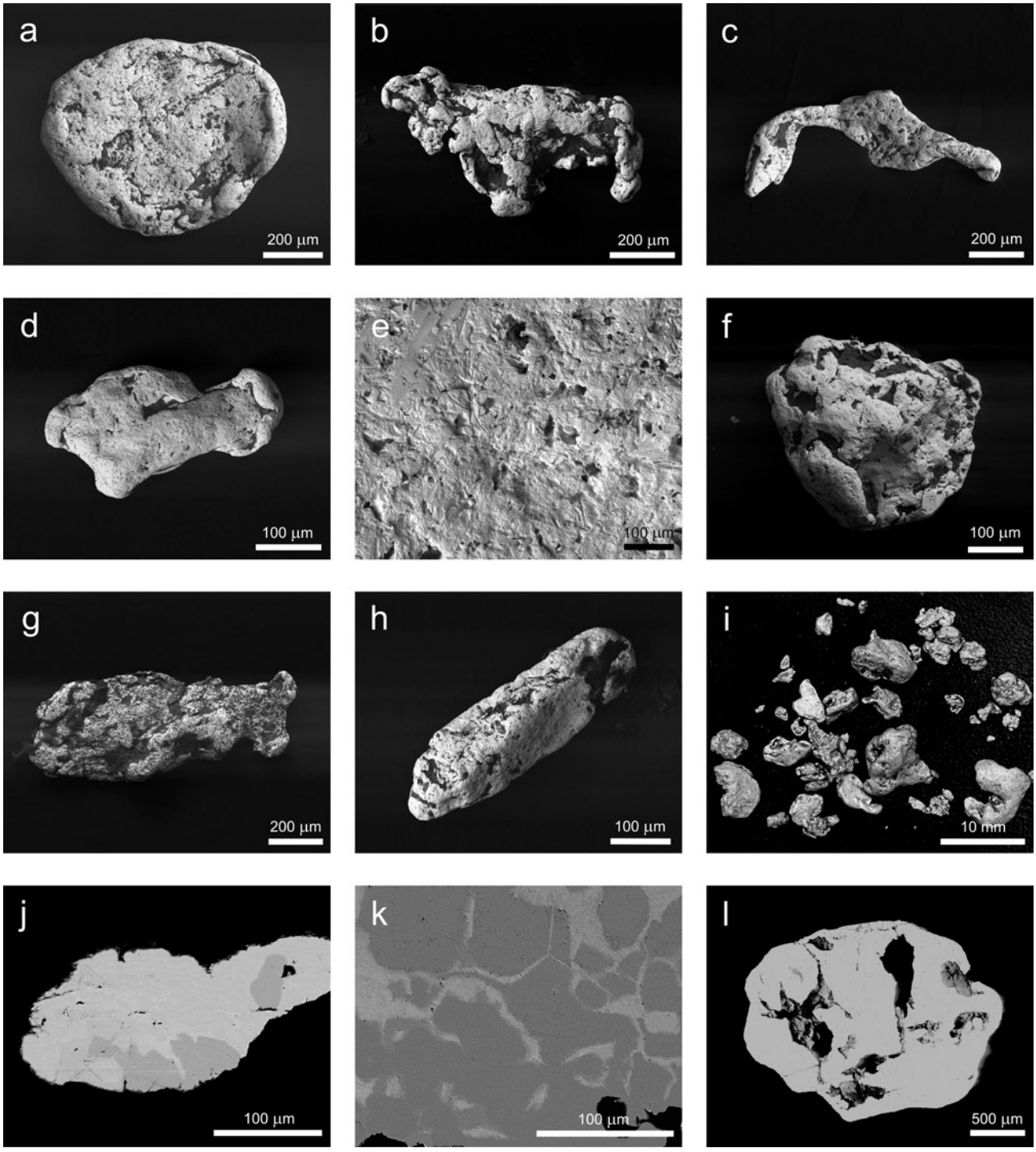

Fig. 10 Morphology and internal structures of placer gold grains from the Samoandamba–N area, L-47-89-B: **a** – intensively worked and rounded flake of pure gold indicative of a long transport, SEI; **b** – irregular flat and moderately worked gold grain, SEI; **c** – oblong moderately worked gold grain, SEI; **d** – flat, rounded, and moderately worked gold grain, SEI; **e** – detail of the surface of the gold particle on the Fig. 10e, SEI; **f** – isometric alluvial gold grain with slightly modified morphology, SEI; **g** – moderately worked flat gold grain, SEI; **h** – slightly worked oblong crystal of gold, SEI; **i** – gold nuggets from alluvial sediments, macro photo; **j** – polished section of an irregular gold grain; small domains of gold with admixture of 7.8 wt. % Ag (dark) in pure gold (bright), BEI; **k** – polished section of a flat nugget; small fields of gold containing 9.2 wt. % of Ag (dark) in pure gold (bright) represent probably recrystallization products, BEI; **l** – polished section of a nugget with inclusions of muscovite, K-feldspar, quartz, and calcite, BEI. (SEI = secondary electron image; BEI = backscattered electron image).

5. Conclusions

The area of about 4,000 km^2 in the eastern part of the Mongolian Altay Mts. region was mapped on a scale of 1:50,000 in the framework of the International Development Cooperation of the Czech Republic in 2004–2006. Regional geochemical mapping involved the panned heavy-mineral survey, geochemistry of dry stream-sediments from intermitent streams and whole-rock lithogeochemistry.

- The morphologies and compositions of placer gold grains were studied as a length of transport indicator, and in order to constrain the possible source of auriferous mineralizations. The gold with fineness over 900 and free of other impurities (except for Ag) is characteristic of the studied area.
- New occurrences and indices of Au, Ag, Cu, Zn, Pb and (Ba)-As-Sb-Hg mineralizations were discovered in some of the prospective areas.
- The surveyed part of the **Lake Terrane** has a potential for finding an economic gold-bearing mineralization.
- The Neoproterozoic Khan Taishir Fm. is supposed to host locally Au and Au-(Cu) veins and gold-bearing base metal vein–disseminated mineralization bound to metamorphosed (greenschist-facies) basic volcanic sequences.
- The Au-(Ag) quartz veins hosted by basic volcanic rocks of the Lower Permian Delger Khangay Fm. were ascertained in the area of the Khar Argalantyn Nuruu Mts.
- Low gold contents accompany also the As-Sb-Hg-(Ba) vein–disseminated mineralization confined to acid volcanic rocks of the Permian Khar Argalantyn Fm. The Ag-rich base metal quartz veins occur in silicified marbles of the Neoproterozoic–Palaeozoic Maykhan Tsakhir Fm.
- No prospective ore indications were found in the crystalline rocks of the Zamtyn Nuruu and Alag Khadny crystalline complexes or related to undifferentiated Palaeozoic plutonic rock bodies.
- In the **Gobi Altay Terrane**, the occurrences and showings of slightly auriferous base metal (Cu, As, Zn, Pb, Ag) veins were ascertained in siliceous chlorite-sericite schists with layers of greenschists and quartzites of the Cambrian Tugrug Fm.
- Sporadic discontinuous Au anomalies indicate more likely only indications of auriferous vein mineralizations bound to the Ordovician (Bayan Tsagaan Fm.), Devonian (Gichigeney Fm.) and Carboniferous (Tsokhoriin Nuruu Fm.) rock sequences.
- Gold placers associated with the **Upper Jurassic/ Lower Cretaceous, Neogene and Quaternary sediments** are not common. Only newly discovered placers confined to the Mesozoic conglomerates and sandstones in the Samoandamba area are supposed to have an economic potential.

Acknowledgments. The project was conducted by the Czech Geological Survey in a close cooperation with the Geological Information Centre of Mongolia and the Mineral Resources and Petroleum Authority of Mongolia (MRPAM). The authors warmly thank to all members of the Czech Zamtyn Nuruu-50 expedition for their assistance in field and sample processing, in particular to J. Holák and Z. Novotný. Special thanks are due to Kh. Gantumur, the former Chief Geologist of MRPAM for his support of project. K. Hrdličková is acknowledged for the technical assistance during preparation of the paper. O. Gerel and J. Zachariáš are thanked for helpful reviews; M. Štemprok is acknowledged for the careful editorial handling.

References

Badarch G, Cunningham WD, Windley BF (2002) A new Terrane subdivision for Mongolia: Implications for the Phanerozoic crustal growth of central Asia. J Asian Earth Sci 20: 87–100

Borzakovskii YA et al. (1985) Making of geological map and map of raw deposits of the western Mongolia (W of meridian 102°) on the scale 1:500,000 with explanatory text. Period I, maps M-46B, L-47A, B, V, G. Zarubezhgeologia, Moscow

Cunningham WD, Windley BF, Dorjnamjaa D, Badamgarov J, Saandar M (1996) A structural transect across the Mongolian Altai: active transpressional mountain building in central Asia, Tectonics 15: 142–156

Dejidmaa G, Badarch G (2005) Summary of pre-accretionary and accretionary metallogenic belts of Mongolia. In: Seltmann R, Gerel O, Kirwin DJ (eds) Geodynamics and metallogeny of Mongolia with a special emphasis on copper and gold deposits. CERCAMS/NHM London, SEG-IAGOD Field Trip, 14–16 August 2005, 8th Biennial SGA Meeting, pp 25–29

Dejidmaa G, Bujinlkham B, Eviihuu A, Enkhtuya B, Ganbaatar T, Moenkh-Erdene N, Oyuntuya N (2001) Distribution map of deposits and occurrences in Mongolia (on the scale 1:1,000,000). MRPAM – Geological Information Center, Ulaanbaatar

Dejidmaa G, Dorjgotov D, Gerel O, Gotovsuren A (2005) Preliminary description of mineral deposit models (types) for Mongolia. In: Seltmann R, Gerel O, Kirwin DJ (eds) Geodynamics and Metallogeny of Mongolia with a Special Emphasis on Copper and Gold Deposits. CERCAMS/NHM London, SEG–IAGOD Field Trip, 14–16 August 2005, 8th Biennial SGA Meeting, pp 31–52

Dergunov AB (2001) Tectonics, Magmatism, and Metallogeny of Mongolia. Routledge, London, pp 1–304

Economos R, Hanžl P, Hrdličková K, Buriánek D, Said LO, Gerdes A (in print) Geochemical and structural constraints on the magmatic history of the Chandman

Massif of the eastern Mongolian Altay Range, SW Mongolia. J Geosci

Fletcher WK (1997) Stream sediment geochemistry in today's exploration world. In: Gubins AG (ed) Proceedings of Exploration 97: Fourth Decennial International Conference on Mineral Exploration, pp 249–260

Gilíková H, Budil P, Čech S, Hanžl P, Otava J, Svobodová M, Ziegler V (2007): Cretaceous sediments of the Eastern part of the Mongolian Altay. In: Breiter K (ed) Proceedings of the 3rd Meeting of the Czech Geological Society, Volary, 19–22 September 2007, pp 15 (in Czech)

Hanžl P, Aichler J (eds) (2007) Geological Survey of the Mongolian Altay at a scale of 1 : 50,000 (Zamtyn Nuruu – 50). Final report of the International Development Cooperation project of the Czech Republic. Czech Geological Survey, Brno & MPRAM, Ulaanbaatar, pp 1–376

Hanžl P, Buriánek D, Hrdličková K, Aichler J, Gerdes A, Byambasuren D (2007) Granitoid massifs of the Zamtyn Nuruu area, SW Mongolia. In: Breiter K (ed) Proceedings of the 3rd Meeting of the Czech Geological Society, Volary, 19–22 September 2007, pp 27

Hendrix MS, Graham SS, Carroll AR, Sobel ER, Mc Knight CL, Schulein BJ, Wang Z (1992) Sedimentary record and climatic implications of recurrent deformation in the Tianshan: evidence from Mesozoic strata of the north Tarim, south Junggar and Turpan basins, northwest China. Geol Soc Am Bull 104: 53–79

Janoušek V, Farrow CM, Erban V (2006) Interpretation of whole-rock geochemical data in igneous geochemistry: introducing Geochemical Data Toolkit (GCDkit). J Petrol 47: 1255–1259.

Khain EV, Bibikova EV, Salnikova EB, Kröner A, Gibsher AS, Didenko AN, Degtyarev KE, Fedotova AA (2003) The Palaeo-Asian ocean in the Neoproterozoic and Early Palaeozoic: new geochronologic data and palaeotectonic reconstructions. Precambr Res 122: 329–358

Knight JB, Morison SR, Mortensen JK (1999) The relationship between placer gold particle shape, rimming, and distance of fluvial transport as exemplified by gold from the Klondike District, Yukon Territory, Canada. Econ Geol 94: 635–648

Kovalenko VI, Yarmolyuk VV, Bogatikov OA (1995) Magmatism, Geodynamics and Metallogeny of Central Asia. Miko Commercial Herald Publishers, Moscow, pp 1–272

Krejčí Z, Hanžl P (2006) Geoscience data management – Mongolian Altay Project. In: Vernadsky SGM RAS: 3rd International Conference GIS in Geology, Extended Abstracts, Russian–French Metallogenic Laboratory, Moscow, p 33–35

Malec J (2007) Study of gold particles from the Zamtyn Nuruu and Mongolian Altay obtained during heavy mineral survey undertaken in the years 2004–2006. In: Hanžl P, Aichler J (eds) Geological Survey of the Mongolian Altay at a scale of 1:50,000 (Zamtyn Nuruu – 50). Final report of the International Development Cooperation project of the Czech Republic. Czech Geological Survey, Brno & MPRAM, Ulaanbaatar

Marinov NA, Zonenshain LP, Blagonravov VA (eds) (1973) Geology of the People's Republic of Mongolia: Volume 1, Stratigraphy. Nedra Press, Moscow, pp 1–582

Markova NG (1975) Lower and Middle Palaeozoic Stratigraphy of the Western Mongolia. Nauka, Moscow (in Russian)

Morávek P et al (1992) Gold in the Bohemian Massif. Czech Geological Survey. Prague, pp 1–245 (in Czech)

Mossakovsky AA, Ruzhentsev SV, Samygin SG, Kheraskova TN (1993) Central Asian fold belt: geodynamic evolution and history of formation. Geotectonics 6: 3–33

Nicols G (1999) Sedimentology and Stratigraphy. Blackwell Science Ltd, London, pp 1–355

Perfiliev AS, Kheraskov NN (1980) Diabase complexes and the origin of layering of Earth's crust: tectonic layering of the lithosphere. Nauka, Moscow, pp 64–104 (in Russian)

Rauzer AA, Zhanchiv DI, Golyakov VI, Ykhina IF, Ivanov IG, Tsukernik AB, Afonin VV, Smirnov IG, Bykhover VI, Kravtsev AV, Baatarkhuyag A, Skoryukin MI, Khodikov IV, Mantsev NV, Okaemov SV, Mischin VA, Enkhsajkhan T (1987) Report on results of geological mapping on scale 1:200,000 in the south-western part of Mongolian Altay in 1983–1986, Mongolian National Republic. Tekhnoexport, Moscow, pp 1–352 (in Russian)

Reimann C, Caritat P de (1998) Chemical Elements in the Environment. Factsheets for the Geochemist and Environmental Scientist. Springer-Verlag, Berlin, pp 1–398

Sengör AMC (1984) The Cimmeride orogenic system and the tectonics of Eurasia. Geol Soc Am Spec Pap 195: pp 1–82

Shaandar P (2003): Geology and mineral resources of the Lake Zone. Mongolian Geoscientist 23: 18–19

Tapponier P, Molnar P (1979) Active faulting and Cenozoic tectonics of the Tien Shan, Mongolia and Baykal region. J Geophys Res 84(B7): 3425–3459

Valtr V (2007) Geophysical prospection in Zamtyn Nuruu 2005–2006. In: Hanžl P, Aichler J (eds) Geological Survey of the Mongolian Altay at a scale of 1:50,000 (Zamtyn Nuruu – 50). Final report of the International Development Cooperation project of the Czech Republic. Czech Geological Survey, Brno & MPRAM, Ulaanbaatar

Vassallo R, Jolivet M, Ritz JF, Braucher R, Larroque C, Sue C, Todbileg M, Javkhlanbold D (2007) Uplift age and rates of the Gurvan Bogd system (Gobi-Altay) by apatite fission track analysis. Earth Planet Sci Lett 259: 333–346

Windley BF, Alexeiev D, Xiao W, Kröner A, Badarch G (2007): Tectonic models for accretion of the Central Asian Orogenic Belt. J Geol Soc, London 164: 31–47

Xie X, Wang X (1991) Geochemical exploration for gold: a new approach to an old problem. J Geochem Explor 40: 25–48

Yanshin AL (ed) (1976) Map of Mesozoic and Cenozoic tectonics of the Mongolian People's Republic: 4 sheets, scale 1:15,000,000. USSR Academy of Sciences, Moscow

Yarmolyuk VV (1983) Late Palaeozoic Volcanism in the Continental Rift Structures of Central Asia. Nauka, Moscow, pp 1–198 (in Russian)

Yarmolyuk VV (1986) Characteristics of structural position of continental rift structures in Mongolia. Izv Akad Nauk SSSR, Ser geol 9: 3–15 (in Russian)

Youngson JH, Craw D (1999) Variation in placer style, gold morphology, and gold particle behavior down gravel bed-load rivers; an example from the Shotover/Arrow–Kawarau–Clutha River system, Otago, New Zealand. Econ Geol 94: 615–633

Zabotkin LB et al. (1983) Report on results of geological mapping on scale 1:200,000 in the Central-Gobi region of Mongolian National Republic in 1979–1982. Moscow (in Russian)

Zonenshain LP, Kuzmin MI (1978) The Khan-Taischir ophiolitic complex of Western Mongolia, its petrology, origin and comparison with other ophiolitic complexes. Contrib Mineral Petrol 67: pp 95–109

Journal of Geosciences, 53 (2008), 139–165 DOI: 10.3190/jgeosci.027

Original paper

Petrology and age of metamorphosed rocks in tectonic slices inside the Palaeozoic sediments of the eastern Mongolian Altay, SW Mongolia

Kristýna HRDLIČKOVÁ[1*], Khasbazaar BOLORMAA[2], David BURIÁNEK[1], Pavel HANŽL[1], Axel GERDES[3], Vojtěch JANOUŠEK[1]

[1] *Czech Geological Survey, Klárov 3, 118 21 Prague 1, Czech Republic; kristyna.hrdlickova@geology.cz*
[2] *Geological Investigation Centre, Songino Khayrkhan District, PO Box 37/307, Ulaanbaatar, Mongolia; khasbolorma@yahoo.com*
[3] *Institut für Geowissenschaften, J. W. Goethe Universität, Altenhöferallee 1; 60438 Frankfurt am Main; Germany; gerdes@em.uni-frankfurt.de*
[*] *Corresponding author*

Three crystalline complexes were newly described in the area of the junction between the Mongolian Altay and Gobi Altay in the surroundings of Chandman Sum, SW Mongolia. Khan Khayrkhan, Chandman Khayrkhan and Unegt Uul crystalline complexes were distinguished on the basis of their geological position, distinct petrography, metamorphic style and contrasting geochronological data. These units are situated along the northern margin of the Gobi-Altay Terrane and at first sight seem to have a very simple and uniform history. However, detailed studies reveal a more complex and varied evolution.

The Unegt Uul Crystalline Complex is a tectonic mélange of leucogranites, amphibolites and mica schists exposed between the branch of the Bogd fault in the north and Lower Palaeozoic sediments in the south. Metamorphic rocks suffered a prograde metamorphic event reaching temperatures of *c.* 650 °C and pressures of 6–7.5 kbar estimated from amphibolites. This Complex represents the oldest of the three units; the age of leucogranite formation corresponds to Cambrian (518 ± 5 Ma).

Chandman Khayrkhan Crystalline Complex is also restricted by Bogd fault from the north but southern boundary is limited by an intrusive contact with the Chandman Massif. It is composed of orthogneisses and migmatites with amphibolite and calc-silicate lenses. The Complex was affected by a HT, likely periplutonic, metamorphic event and subsequent retrogression. While the rocks of the Chandman Khayrkhan Crystalline Complex remain undated, the age of the granitic rocks in the Chandman Massif itself are Early Carboniferous (345 ± 2 Ma).

The Khan Khayrkhan Crystalline Complex has tectonic contacts with the surrounding Palaeozoic volcanosedimentary units. It is built by orthogneisses, amphibolites, paragneisses and mica schists. Metamorphic style corresponds to a prograde event with peak at *c.* 670 °C and 7–10 kbar. The crystallization age for the granitic protolith to the orthogneisses was the latest Devonian (363 ± 3 Ma).

Keywords: Variscan metamorphism, P–T calculations, ICP-MS, U-Pb zircon dating, Mongolian Altay, Gobi Altay Terrane
Received: 4 April 2008; accepted 2 July 2008; handling editor: W.S. Faryad

The online version of this article (doi: 10.3190/jgeosci.027) contains supplementary electronic material.

1. Introduction

Generally speaking, there is lack of data on conditions and timing of metamorphism in Mongolia and the SW part of the country is no exception. In contrast, numerous works have been concerned with Cenozoic faults (e.g. Molnar and Tapponnier 1975; Bayasgalan et al. 1999; Cunningham et al. 2003; Vassallo et al. 2007) as well as Palaeozoic (Dergunov 2001 or Windley et al. 2007 for review) or Mesozoic (e. g. Yarmolyuk and Kovalenko 2001) volcanosedimentary complexes. Geochronological data and tectonostratigraphic reconstructions have been assembled recently for the region of south-western Mongolia (Kepezhinskas et al. 1991; Badarch and Tomurtogoo 2001; Badarch et al. 2002; Buchan et al. 2002; Khain et al. 2002, 2003; Kovach et al. 2005; Kozakov et al. 2005; Helo et al. 2006).

Traditionally, the territory of Mongolia has been subdivided into northern and southern domains, which are separated by the so-called Main Mongolian lineament – a regional topographic and structural boundary dividing mostly Precambrian and Lower Palaeozoic rocks in the north from dominantly Middle–Upper Palaeozoic units in the south (Marinov et al. 1973; Badarch et al. 2002). The studied area is situated right along this boundary, which separates here the two different structural zones, the Lake

Zone in the north and the Gobi Altay Zone in the south (Rauzer et al. 1987). The Lake Terrane represents, according to Badarch et al. (2002) a former island arc and Gobi Altay Terrane is interpreted as a backarc/forearc basin.

Metamorphic domains are insufficiently known in the Mongolian and Gobi Altay mountain ranges. New metamorphic complexes were described during the geological survey of Zamtyn Nuruu area (Hanžl and Aichler 2007; see Introduction to this Volume), where the south-eastern Mongolian Altay and eastern Gobi-Altay ranges merge south of the Bogd fault in the Gichigeney Nuruu and Bayan Tsagaan Mts. These Unegt Uul (UUC), Chandman Khayrkhan (CHC) and Khan Khayrkhan (KKC) crystalline complexes recorded medium- to high-temperature and medium-pressure conditions. This paper brings first petrologic and P–T data from the metamorphic rocks in the western part of the Gobi-Altay Terrane, complemented by geochemical and isotopic analyses as well as U-Pb zircon and monazite dating.

2. Geological setting

The studied region is situated in the SW Mongolia, approximately 740 km SW of Ulaanbaatar at the junction of south-eastern Mongolian Altay (Gichigeney Nuruu range) with eastern Gobi Altay (eastern Bayan Tsagaan range represented by Unegt Uul and Chandman Uul).

Geologically, Mongolia is built by a number of tectonic zones that form the part of the extensive Central Asian Orogenic Belt – CAOB (Mossakovsky et al. 1994) known also as Altaids (Sengör et al. 1993). This belt has developed between the Siberian Block in the north, the Tarim Block in the south-west and the Sino-Korean Block in the south. It is characterized by an accretion of various terranes of different origin (Sengör et al. 1993; Windley et al. 2002; Jahn et al. 2004) and evolved during time span of 1000–250 Ma (Windley et al. 2007). Nevertheless, the tectonic evolution of the CAOB in north-eastern Mongolia culminated during the closure of

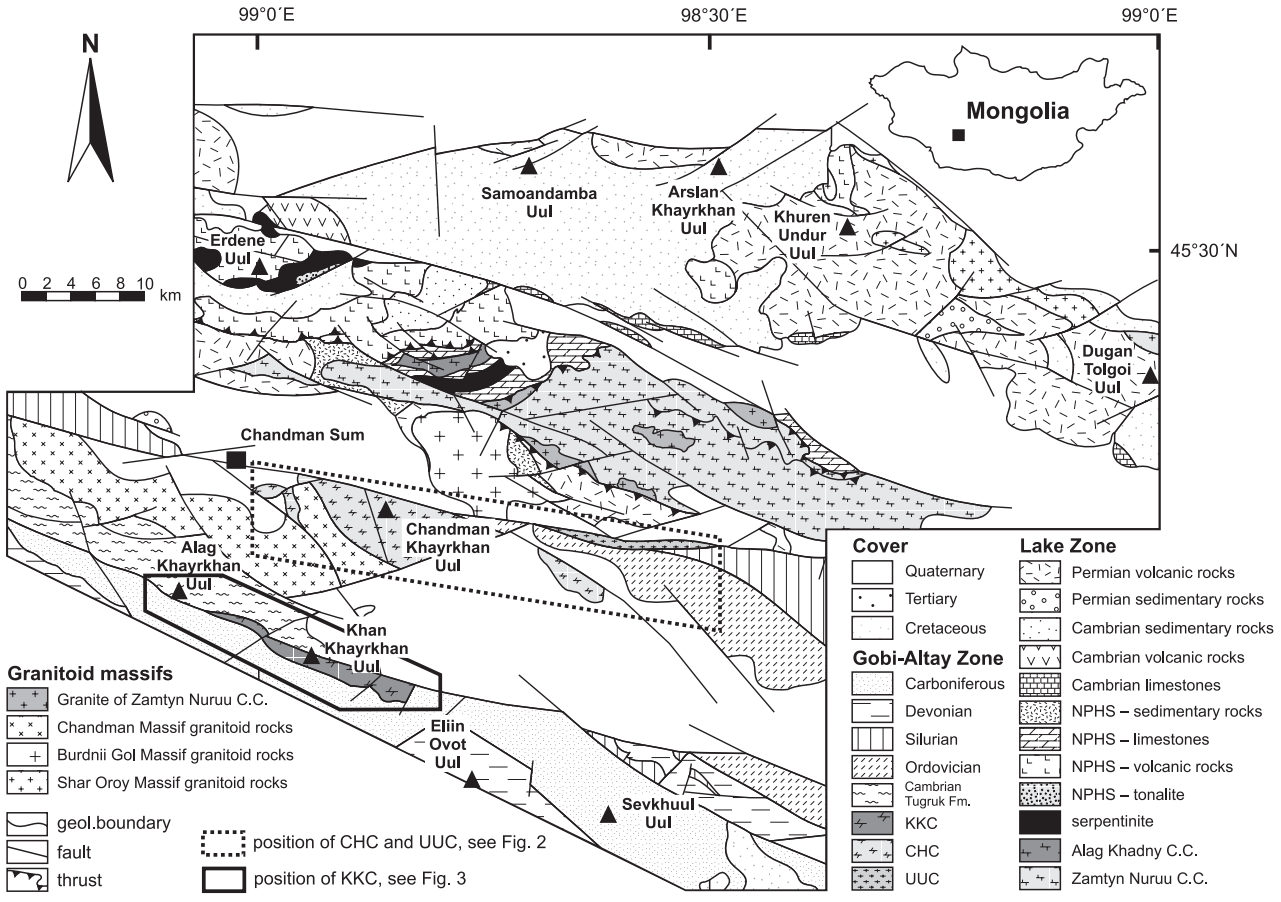

Fig. 1 Geological outline of the studied area in the easternmost Mongolian Altay (based on Hanžl and Aichler 2007 and results presented in this Volume). KKC – Khan Khayrkhan Crystalline Complex; CHC – Chandman Khayrkhan Crystalline Complex; UUC – Unegt Uul Crystalline Complex, NPHS – Khan Taishir Fm.

the Mongolian–Okhotsk marine basin in Early Jurassic times (Yarmolyuk and Kovalenko 2001).

The studied area is a part of the Gobi-Altay domain of the Altay orogen extending eastward from Russia and eastern Kazakhstan, through the northern China to south-western Mongolia. The Gobi-Altay Terrane most likely represents the south-western continental margin of the Siberian Plate (Xiao et al. 1992). According to Badarch et al. (2002), it forms a long narrow belt rimming the northern margin of the southern domain of Mongolia. It is composed of Cambrian (?) marine sediments and volcanoclastic rocks metamorphosed under greenschist-facies conditions accompanied by Palaeozoic sediments, with volcanic and volcanoclastic rocks of a forearc/backarc character. The sequence was intruded mainly by Carboniferous to Permian granite plutons.

Three metamorphic units were recognized in the eastern part of the Gobi-Altay Terrane in a form of tectonic slices inside the Palaeozoic sediments and volcanoclastic rocks. The Chandman Khayrkhan and Unegt Uul crystalline complexes are exposed in the easternmost range of the Bayan Tsagaan Mts. and the Khan Khayrkhan Crystalline Complex on the NE slopes of the Gichigeney Nuruu Mts. (Fig. 1).

2.1. Unegt Uul Crystalline Complex (UUC)

The exposures of UUC are restricted to a narrow belt in the Unegt Uul range lying directly in the tectonic mélange of the Bogd fault zone (Hanžl and Aichler 2007) (Fig. 2). The E–W trending branches of the master fault separate crystalline rocks and Permian volcanic rocks in the north from the Lower Palaeozoic marine sediments with limestone layers in the south. The rocks of UUC are represented mainly by deformed and metamorphosed biotite granites to leucogranites, aplitic granites and pegmatites. Gneisses, mica schists and amphibolites represent roof pendants of the granitic intrusions. Lenses of gabbros, ultramafic rocks, amphibolites and undifferentiated sediments are parts of a tectonic mélange in the eastern part of the belt.

Structural characteristics of the Unegt Uul Crystalline Complex reflect large-scale tectonic processes of brittle character. The E–W oriented fragmental faults of the Bogd fault system are the most distinct features. Faults are commonly accompanied by tens to a few hundred meters wide mylonitic zones of anastomozing character. Furthermore, E–W elongated Unegt Uul Crystalline Complex is transversely segmented by several NW–SE trending faults.

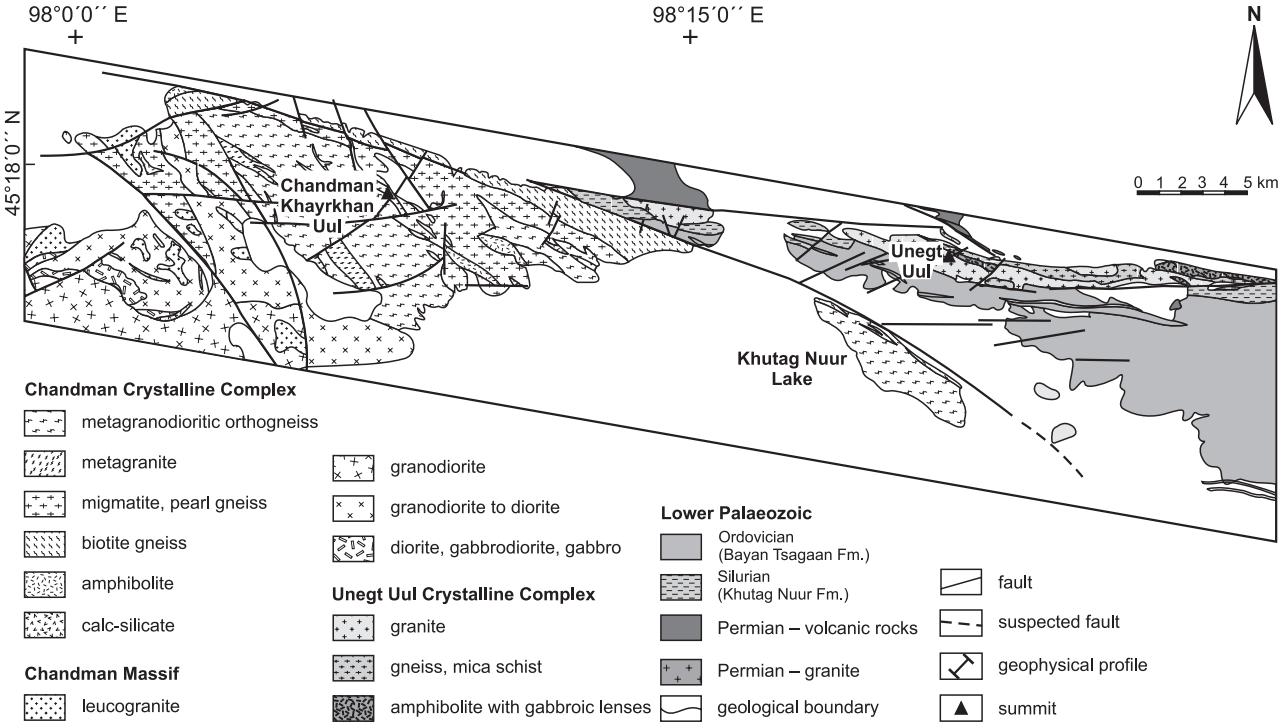

Fig. 2 More detailed geological map of the Chandman Khayrkhan and Unegt Uul crystalline complexes.

Ductile fabrics are represented by foliation and lineation in gneisses and amphibolites preserved as roof pendants to cataclastic granites. Subvertical tight folds with E–W trending axes are rare. Foliations are NW–SE trending with dips varying from 30–65° to NE or SW. Lineations have a crenulation character in mica schists and plunge to SE under 20–40° and are subparallel with fold axes.

2.2. Chandman Khayrkhan Crystalline Complex (CHC)

The CHC is situated in an E–W trending belt between the Chandman Sum and Khutag Nuur lake (Figs 1–2). It is exposed in tectonic blocks lining the Bogd fault from the S in the area of the Chandman Khayrkhan Uul and one of its branches north of Khutag Nuur.

The northern border of CHC is formed by the scarp of the Chandman rupture (Baljinnyam et al. 1993) of the Bogd fault. Boudins of limestones and sediments of the Lower Palaeozoic formations exposed there emphasize the fault line. The metamorphic complex is limited in the SW by intrusive rocks of the Chandman Massif; the southern continuation is covered by Quaternary sediments.

Migmatites, gneisses and orthogneiss of granitic to granodioritic composition alternate in WNW–ESE oriented irregular stripes and lenses. Amphibolite and calc-silicate lenses are rare. Rocks are penetrated by numerous thin dykes of aplites and pegmatites (Buriánek et al. in press). The conspicuous NWN–ESE trending foliation is moderately to steeply dipping to the south. The foliation planes bear metamorphic lineations plunging variably to NW or SE. Towards the SW, the degree of deformation in orthogneisses decreases; rocks acquire an appearance of metagranitoids and pass gradually into granitic rocks of the Chandman Massif. Granitoids of the Chandman Massif intruded the high-grade metamorphic rocks and both units were subsequently jointly deformed. Therefore the CHC represents wall rocks to the intrusion, which fact is reflected by a number of (deformed) pegmatite dykes pertaining to Chandman Massif penetrating the CHC.

2.3. Khan Khayrkhan Crystalline Complex (KKC)

The KKC is exposed as narrow, NW–SE trending tectonic slice along the NE slopes of the Gichigeney Nuruu range; the most extensive exposures are in the area of Khan Khayrkhan Uul (NW part of the Gichigeney Nuruu). The north-eastern as well as south-western boundary of this unit are formed by steep faults (Fig. 3). Carboniferous turbidites crop out in the SW, slightly metamorphosed volcanoclastic sediments of supposed Cambrian age (Rauzer et al. 1987) occur in the NE. A small tectonic slice of the

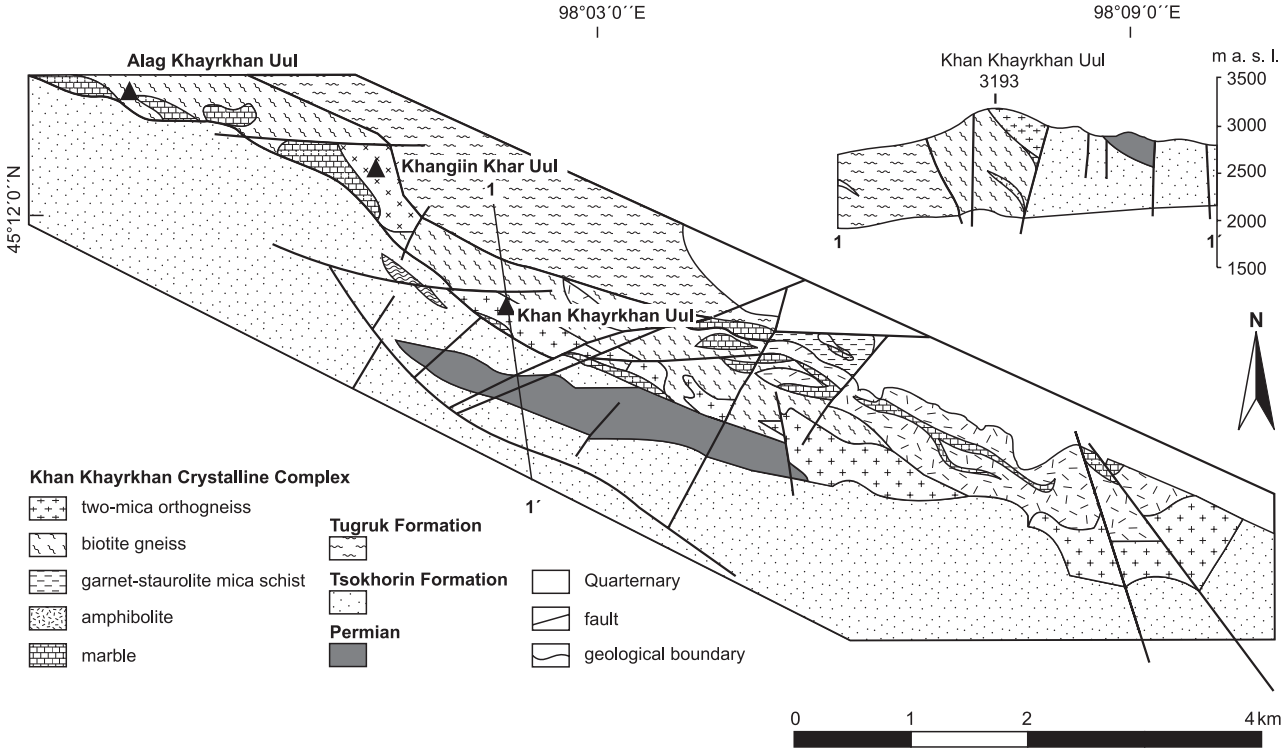

Fig. 3 More detailed geological map of the Khan Khayrkhan Crystalline Complex

KKC mapped in the area of the Darkhan Uul at the south-eastern termination of the mountain range is exposed between the Carboniferous turbidites and Devonian limestones. The KKC is characterised by varying lithologies. Fine-grained gneisses alternating with amphibolites occur on the NE slopes of the Khan Khayrkhan Uul. They are accompanied by intercalations of crystalline limestones and lenses of garnet-staurolite mica schists in the E part. The mountain range itself is built by fine- to medium-grained two-mica orthogneisses. The contact between orthogneisses and amphibolites is concordant.

Structures are characterized by a dominant foliation, which is NW–SE striking and steeply dipping to NE and SW. It corresponds to folding by large steep and tight folds confirmed by geological mapping (Hanžl and Aichler 2007). Linear structural elements – fold axes as well as lineations – are subhorizontal with prevailing WNW–ESE orientation.

The recrystallized limestones of the KKC contain also relics of fossil material. However, the fossils are poorly preserved and their determination may be problematic. Still, Middle to Late Ordovician age may be with certain doubts supposed for the belt of strongly re-crystallised carbonates forming rock cliffs at the summit of the Khan Khayrkhan Uul. The age is based on the rare remains of the questionable *Pluricollumnalia* (crinoid possessing a rather Ordovician character but indeterminable because of fairly high degree of metamorphic overprint – determination made by R. Prokop from National Museum, Prague). Nevertheless, strongly recrystallized limestones to marbles locally contain perceptible but entirely indeterminable echinoderms – possibly crinoid debris. From the residuum after maceration (tectonically confined outcrop of limestones with cherts), questionable sponge spicules were found but their poor preservation prohibited an exact determination (Hanžl and Aichler 2007).

3. Analytical techniques

Electron microprobe analyses were performed in the Joint Laboratory of Electron Microscopy and Microanalysis of the Masaryk University and the Czech Geological Survey (Brno) on the Cameca SX-50 instrument. Operating conditions were 15 kV accelerating voltage, and beam current of 80 nA. The obtained data were processed using THERMOCALC software (version 3.21; Powell and Holland, 1985; Holland and Powell, 1985; 1998; update February 2002) to calculate the P–T conditions and to reconstruct the metamorphic evolution of studied samples. Conventional thermometers (Thompson 1976; Lee and Holdaway 1977; Ferry and Spear 1978; Perchuk and Lavrent'eva 1983; Bhattacharya et al.1992; Ravna 2000) were also used for comparison.

Microprobe analyses for chemical Th-U-total Pb dating (CHIME) were carried out also in the Joint Laboratory of Electron Microscopy and Microanalysis in Brno. Operating conditions were 15 kV accelerating voltage, beam current 80 nA and a beam diameter of <1 μm for monazite and 5–10 μm for monazite alteration products. The monazite age was calculated using a method of Montel et al. (1996).

Isotope analyses for LA-ICP-MS (Laser Ablation-Inductive Coupled Plasma-Mass Spectrometry) U-Th-Pb dating of zircon and monazite were performed at the Institute of Geosciences, Goethe University Frankfurt, using a Thermo-Scientific Element II sector field ICP-MS coupled to a New Wave UP213 ultraviolet laser system (Gerdes and Zeh 2006, 2008). Laser spot-size varied from 20 to 40 μm and spot-selection was guided by internal structures as seen in cathodoluminescence (CL) images of the mounted and polished grains. Data were acquired in peak jumping mode over 900 mass scans during 20s background measurements followed by 30s sample ablation. A teardrop-shaped, low volume laser cell was used to enable precise detection of heterogeneous material during time resolved data acquisition. Raw data were corrected for background signal, common Pb, laser induced elemental fractionation, instrumental mass discrimination, and time-dependant elemental fractionation of Pb/Th and Pb/U using an Excel spreadsheet.

For the Sr and Nd isotopic study, the samples were dissolved using a combined HF-HCl-HNO_3 attack. Strontium was isolated by exchange chromatography techniques on PP columns with Sr.spec Eichrom resin and bulk REE were isolated on PP columns filled with TRU. spec Eichrom resin (Pin et al. 1994). The Nd was further separated on PP columns with Ln.spec Eichrom resin (Pin and Zalduegui 1997). Details of the procedure were published by Míková and Denková (2007). Isotopic analyses were performed on Finnigan MAT 262 thermal ionization mass spectrometer at Radiogenic Isotopes Laboratory of the Czech Geological Survey in dynamic mode using a double Re filament assembly. The $^{143}Nd/^{144}Nd$ ratios were corrected for mass fractionation to $^{146}Nd/^{144}Nd = 0.7219$, $^{87}Sr/^{86}Sr$ ratios assuming $^{86}Sr/^{88}Sr = 0.1194$. External reproducibility is given by results of repeat analyses of the La Jolla ($^{143}Nd/^{144}Nd = 0.511852 \pm 14$ (2σ), n = 23) and NBS 987 ($^{87}Sr/^{86}Sr = 0.710247 \pm 26$ (2σ), n = 25) isotopic standards. The Rb, Sr, Sm and Nd concentrations were obtained by ICP-MS in Acmelabs, Canada. The decay constants applied to age-correct the isotopic ratios were from Steiger and Jäger (1977 – Sr) and Lugmair and Marti (1978 – Nd). The initial ε_{Nd} values were obtained using Bulk Earth parameters of Jacobsen and Wasserburg (1980), the single- and two-stage Depleted Mantle Nd model ages (T_{Nd}^{DM}) were calculated after Liew and Hofmann (1988).

Samples representing main lithological types at least 2–4 kg in weight were used for whole-rock geochemical analyses. Major and trace elements were determined at ACME laboratories, Canada. Total abundances of the major oxides were analysed by ICP-emission spectrometry following a lithium metaborate/tetraborate fusion and dilute nitric digestion. Loss on ignition (LOI) is the weight difference after ignition at 1000 °C. The rare earth and most remaining trace elements were analysed by INAA and ICP-MS following a $LiBO_2$ fusion; precious and base metals by aqua regia digestion/ICP-MS.

4. Petrography

4.1. Unegt Uul Crystalline Complex

Fine-grained biotite granites to leucogranites with muscovite and igneous garnet are accompanied by dykes/bodies of aplites and pegmatites and occupy much of the UUC. They are exposed as an E–W elongated body with length *c.* 10 km no more than 1 km wide. Rocks are often deformed and cataclased, which is evident from brittle deformation of feldspar grains and strong undulatory extinction of quartz. Gneisses, mica schists and amphibolites form metamorphic wall rocks of granites. They occur as xenoliths in granitoid rocks as well as lenses and belts lining the northern margin of the granite body. The thickness of the individual septa shows a considerable variation but usually does not exceed a few tens of metres.

Fine-grained amphibolites with lenses of metagabbros and serpentinites often occur along, or within, the metagranite body. They are exposed in the northern foothill of the principal part of the Unegt Uul ridge and in the lock of the Khoid Ulaan Sair Valley. Amphibolites are commonly dark to black-green, fine-grained rocks, which alternate with greenish-grey amphibole-biotitic gneisses. The amphibolites exhibit lepidonematoblastic and nematogranoblastic texture and schistose or banded structure. They are composed of plagioclase, hornblende, quartz, biotite ± K-feldspar ± garnet. These minerals are often replaced by sericite, chlorite, epidote and iron oxides in altered domains. Apatite, titanite and opaque minerals are accessoric.

Plagioclase from amphibolites shows wide compositional variation from andesine to bytownite ($An_{34–81}$); plagioclases included in amphibole have an exclusively bytownite composition (An_{71}). On the other end of this spectrum, albites (An_8) are also present in some cases. Garnets from amphibolites (Fig. 4a–b) ($Alm_{55–65}$ $Grs_{24–36}$$Sps_{1–8}$$Prp_{3–12}$$Adr_{1–3}$) show zoning with slightly increasing or nearly constant *Prp* component contents and decreasing *Sps* contents from core to rim. Biotites (Fig. 4c) have X_{Fe} = 0.73–0.76 and Al^{IV} = 2.48–2.75. Amphiboles correspond mostly to ferrotschermakite (Leake et al. 1997) with X_{Mg} = 0.25–0.29 (Fig. 4d). The lenses of medium- to coarse-grained gabbro are confined to amphibolite bodies. These gabbroic rocks are composed of andesine to labradorite, hornblende, biotite, opaque minerals, titanite, epidote and accessoric zircon.

Lenses of metagabbros and serpentinites form a part of tectonic mélange and their relationships to metamorphic rocks and granites remain unclear.

Mica schists are lepidoblastic, medium-grained, crenulated rocks. The mineral assemblage of the studied sample includes quartz, plagioclase, muscovite ± biotite ± garnet. Modal composition of gneisses is rather similar, and the two rock types differ mainly in textural characteristics and presence of K-feldspar in the gneisses. The gneisses consist of quartz, orthoclase, plagioclase, biotite, muscovite and garnet. Petrographic types with amphibole are also present. The common accessories are represented by zircon, apatite and opaque minerals. Garnets from the mica schist and gneisses are chemically relatively homogenous, in both of the rock types *Alm* component predominates ($Alm_{64–79}$ $Grs_{1–9}$$Sps_{3–29}$ $Prp_{4–12}$) (Fig. 4a–b). In contrast to garnets from amphibolites of the UUC, garnets from mica schists show weak rimward increase in *Sps* and slight decrease in *Prp* components (Fig. 5). Plagioclase from mica schist is oligoclase ($An_{15–29}$). Biotites are enriched in Mg (X_{Fe} = 0.30–0.32) and slightly in Al^{IV} (2.60–2.69) compared to biotites from the amphibolite.

The migmatized gneisses are relatively rare; they show usually banded structure comprising light brown biotite-rich streaks alternating with light grey bands dominated by the quartz-feldspathic groundmass of quartz–plagioclase–K-feldspar composition. In addition, the quartzo-feldspathic bands contain garnet and sillimanite.

4.2. Chandman Khayrkhan Crystalline Complex

The CHC is built by orthogneiss, gneiss, migmatite and amphibolite with calc-silicate lenses. Orthogneisses forming bodies in migmatites mainly on the SE slopes of the Chandman Khayrkhan Uul and north of Khutag Nuur are deformed apophyses of the Variscan Chandman Massif (Economos et al. in print). They are medium-grained rocks, having granodioritic to granitic composition, with granoblastic, locally porphyroblastic texture. The fine-grained varieties form boudined dykes and small lenticular bodies in migmatites and granites on the SE slopes of the Chandman Khayrkhan Uul. The rocks have granular texture that gives a massive impression. Locally they are garnet bearing and, in some cases, the K-feldspar crystals can reach 1 mm in size.

The transition from orthogneisses to metagranites is marked by the occurrence of red porphyritic metagranite,

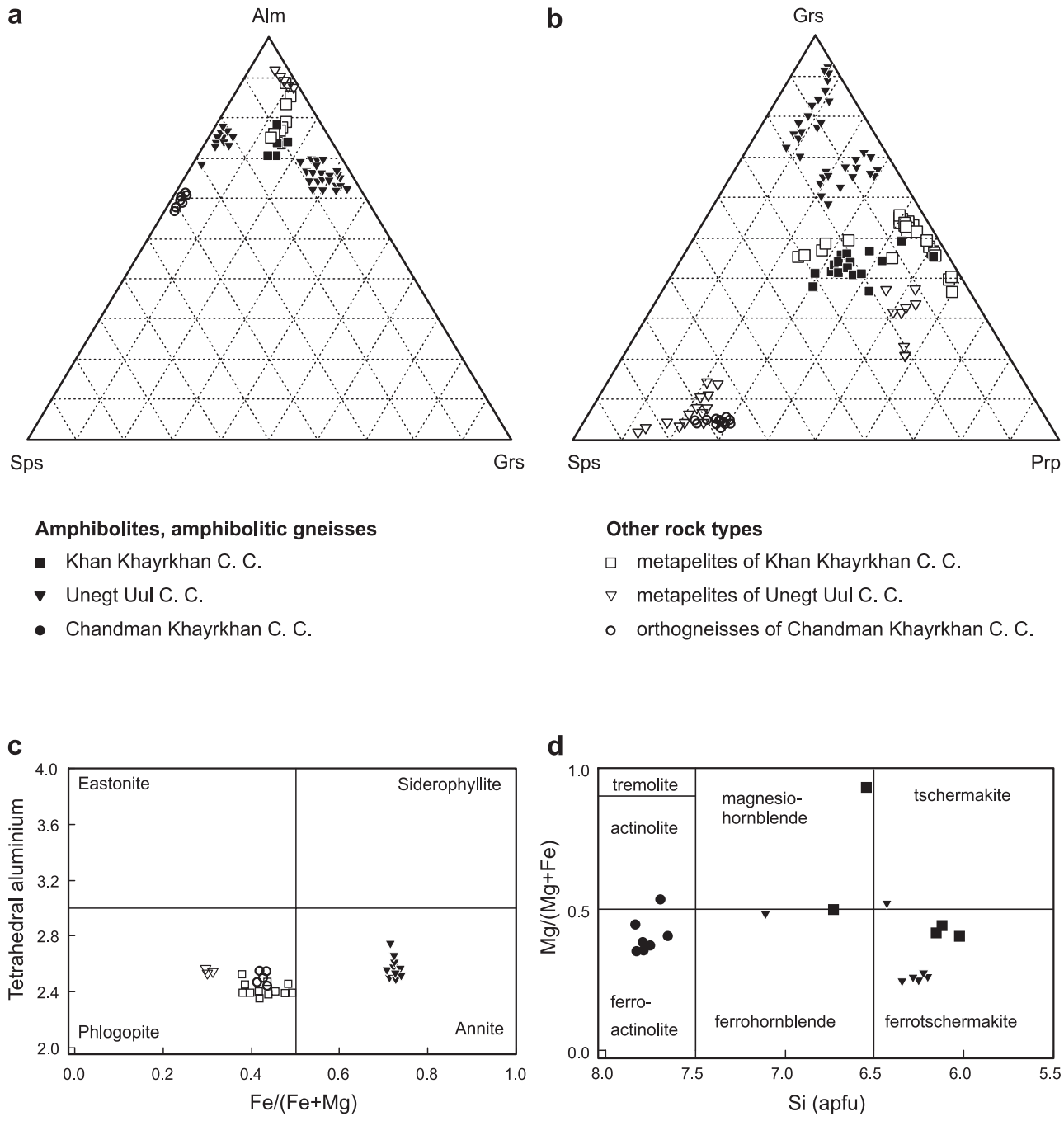

Fig. 4 Classification of rock forming minerals: **a, b** – garnet (mol. %), **c** – biotite (modified according to Guidotti 1984), **d** – amphibole (Leake et al. 1997). Plotted are chemical compositions of all analyzed minerals in the given rock type within individual crystalline complexes.

metagranodiorite to metadiorite, which are all present as bodies or boudins with ill-defined contacts against surrounding metagranodiorite and metadiorite. Red porphyritic metagranites are fine- to medium-grained rocks with plagioclase and biotite phenocrysts. The groundmass is equigranular and consists of plagioclase (30–40 vol. %), K-feldspar (20–30 %), quartz (15–20 %) and biotite (10–15 %). Plagioclase is subhedral and only locally displays growth zoning. Subhedral to anhedral K-feldspar and quartz are partly recrystallized. Accessory minerals include white mica, epidote, apatite and zircon. Biotite has been locally partially altered to chlorite and secondary epidote.

The metagranitoids are surrounded by biotite migmatite and pearl gneiss with anatectic textures, whereas the

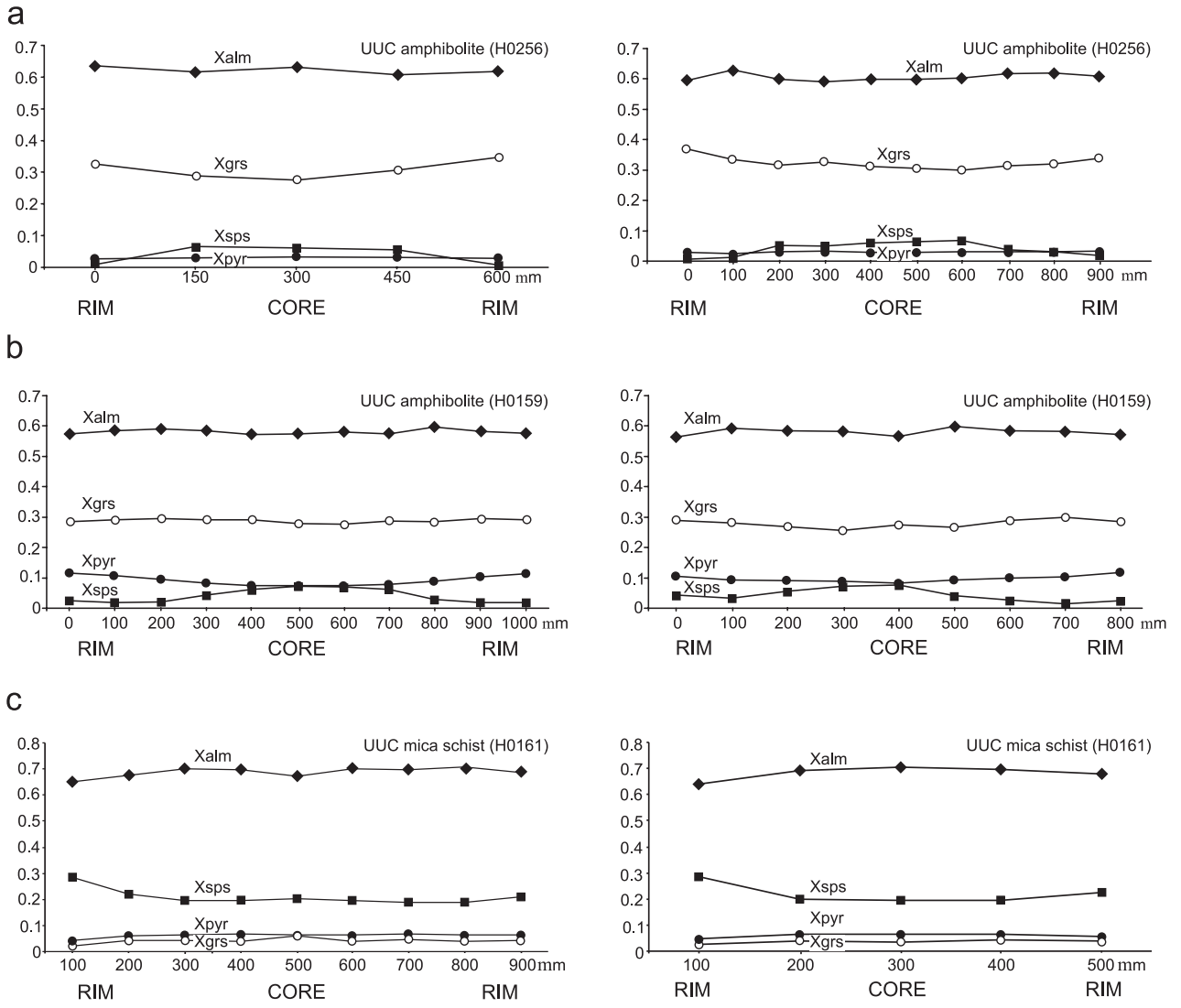

Fig. 5 Garnet profiles from the Unegt Uul Crystalline Complex amphibolite (a–b) and mica schist (c) samples.

migmatites represent the thermal aureole of the intrusion. Pearl gneisses occurring particularly in the N correspond to the deformed migmatites. The rocks are generally medium- to coarse-grained. Plagioclases are often present as porphyroblasts. The metasediments contain layers of locally migmatitized amphibolites up to several dm thick and consisting mainly of hornblende and plagioclase with minor quartz, biotite, epidote and titanite.

The feldspar-bearing pearl gneiss is typically strongly migmatitic and passes through the nebulitic and schlieren structure to truly anatectic rocks. Pearl gneisses consist of common biotite, plagioclase and quartz. Sometimes there are present muscovite, sillimanite and garnet (Fig. 4a–b). The garnet ($Alm_{51–54}$ $Sps_{30–36}$ $Prp_{11–14}$ $Grs_{0–3}$ $Adr_{0–3}$) shows a simple retrograde zoning characterised by concomitantly decreasing *Prp* and increasing *Sps* contents from core to rim. The *Grs* component shows a homogenous distribution throughout the garnet grains. Tourmaline is present as subhedral crystals (up to 1 cm across) at the boundary between melanosome and leucosome. Tourmalines are relatively homogeneous, sometimes with irregular zoning (Mg-rich cores). Biotite corresponds to phlogopite according to the Guidotti's classification (1984) (X_{Fe} = 0.40–0.42, Al^{IV} = 2.46–2.58 apfu – Fig. 4c). As accessoric minerals are present apatite and hematite. Migmatites also contain layers of calc-silicate rock up to 30 cm thick. On the eastern slope of the Chandman Khayrkhan Uul, there are exposed the largest bodies of biotite–amphibole gneiss to amphibolite with metagabbro and calc-silicate lenses. They form enclaves or layers (from several cm to 1 km long) surrounded by migmatites or metaigneous rocks. The calc-silicate rocks, amphibolites and mafic gneisses

show evidence of primary volcano-sedimentary origin. Medium- to fine-grained, commonly banded, granoblastic, nematoblastic or poikiloblastic rocks have varied contents of amphibole (30 to 70 vol. %). A retrograde metamorphic event is indicated by the amphibole composition. Minor biotite, ore minerals and titanite are locally present.

The metagabbro exposed in lenses is dark-grey to black, non-foliated, and very coarse-grained rock.

Calc-silicate rocks are a rare type forming small lenses (up to 10 metres) in amphibolites. They consist mainly of garnet and pyroxene accompanied by interstitial quartz and plagioclase. Amphibole and epidote are present in a calc-silicate layer embedded in the amphibolite. Their mineral composition documents retrogression. Amphiboles are replaced by younger actinolite and ferroactinolite (Fig. 4d) or overgrown by epidote ($Ps_{23–29}$), which sometimes forms independent, isometric grains. Calc-silicates also contain calcic plagioclase ($An_{89–93}$), quartz and secondary chlorite.

In the northernmost part of the unit along the Bogd fault occurs a belt of porphyritic biotite gneisses. They are dark grey rocks composed of plagioclase, biotite, quartz and sometimes K-feldspar or muscovite. Characteristic are deformed porphyroblasts of light feldspar up to 5 mm in size. The quartz-plagioclase ribbons, which rarely occur along foliation planes, indicate a local anatexis.

4.3. Khan Khayrkhan Crystalline Complex

The main rock types of the KKC are various ortho- and paragneisses. Most widespread are fine-grained orthogneisses exposed on the southern slope of the Khangiin Khar Uul and northern slope of the Khan Khayrkhan Uul. Gneisses alternate with amphibolite layers and common marble intercalations enclosing calc-silicate lenses. Some of the gneisses contain amphibole and pass into amphibole gneisses, usually associated with exposures of amphibolite. They are locally strongly deformed, become cataclastic to mylonitized with mortar structures.

Two-mica orthogneisses crop out on the southern slope of the Khan Khayrkhan mountain range. These orthogneisses are medium-grained, pink–grey rocks with augen structure. They consist of quartz, orthoclase, microcline, plagioclase of albite–oligoclase composition together with muscovite and biotite. Locally occur also garnet-sillimanite varieties. A layer of orthogneiss with 1–3 cm large nests containing muscovite pseudomorphs after sillimanite was also found.

The metabasic rocks include a number of different members – amphibole gneisses, amphibolite, metabasalts and metadiorites to metagabbros. The amphibole gneisses are banded, fine- to very fine-grained rocks of lepidogranoblastic textures, often with garnet porphyroblasts reaching a maximum size of several centimetres. The amphibolites are fine-grained rocks with lepidogranoblastic textures. They contain garnet porphyroblasts up to several cm across. Fine-grained matrix is composed of quartz, plagioclase, amphibole and biotite. Ilmenite, haematite and titanite are common accessories; zircon is scarce. The main ferromagnesian minerals are partly replaced by actinolite, chlorite, epidote and iron oxides. Amphibole has mostly ferrotschermakite composition (Leake et al. 1997) with X_{Mg} = 0.41–0.46 (Fig. 4d).

Garnet grains from amphibolite (Fig. 4a–b) dominated by almandine component ($Alm_{60–66}$ $Sps_{7–12}$ $Prp_{11–14}$ $Grs_{12–16}$ $Adr_{1–2}$) involve a moderate decrease in *Alm* component towards the rims. Relatively homogenous distribution of the *Prp* component shows a slight increase in the marginal parts and negligible increase in one of the internal zones. Nearly inverse pattern is shown by the *Grs* distribution (Fig. 6a). Plagioclases from amphibolites have andesine to labradorite compositions ($An_{41–58}$).

Garnet-staurolite mica schists crop out in a several tens of meters thick layer NW of the Tsakhir Bulagiin Uul. They exhibit granolepidoblastic to lepidoblastic texture and consist of fine- to very fine-grained matrix composed of a sericite–chlorite–biotite mixture; small grains of quartz, zoisite, and plagioclase are less common. Garnet

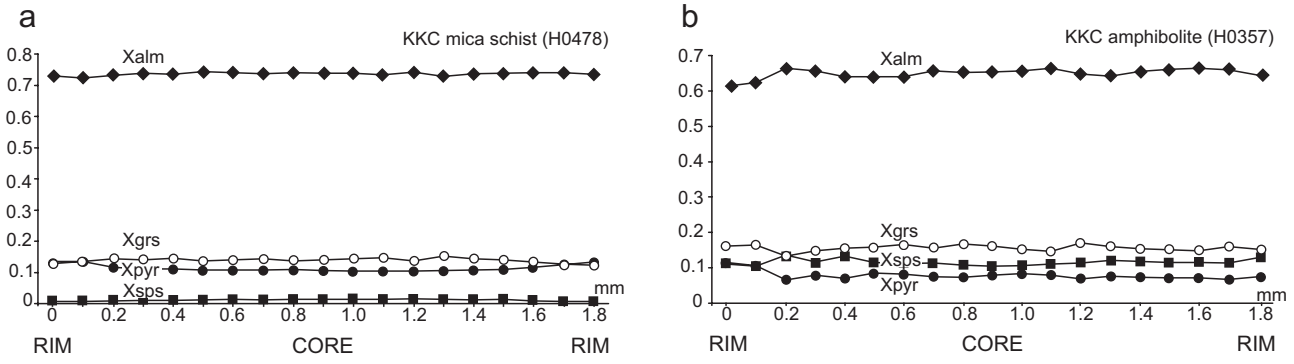

Fig. 6 Garnet profiles from the Khan Khayrkhan Crystalline Complex amphibolite (a) and mica schist (b) samples

and/or staurolite porphyroblasts, several cm across, float in the matrix. Kyanite porphyroblasts are also rarely present. Garnet porphyroblasts dominated by the almandine component contain linear trails of small quartz grains, aligned parallel to the foliation and documenting the late to post-deformational garnet growth. Garnet ($Alm_{67–73}$ $Sps_{0–9}$ $Prp_{7–14}$ $Grs_{8–13}$ $Adr_{2–3}$) (Fig. 4a–b) from the mica schist has zoning typical of a single-stage growth (e. g. Tracy 1982), with distinctive rimward increases in *Alm* and *Prp* compensated by antithetic deceases in *Grs* and *Sps* components (Fig. 6b). Biotite has nearly the same composition in both the studied rock types (mica schist and amphibolite): X_{Fe} = 0.39–0.52, Al^{IV} = 2.49–2.66 (Fig. 4c) Columnar crystals of staurolite, in some cases up to first cm in size, are intergrown by a large number of opaque minerals. In places they are strongly affected by retrogression, and often decomposed to biotite or mixture of quartz, biotite and iron oxides. They are also compositionally uniform (X_{Fe} = 0.86–0.89).

Plagioclase from mica schists has oligoclase composition ($An_{26–29}$) in one of the studied samples, and much more basic (andesine to bytownite, $An_{34–81}$) in the second one. The latter was sampled in close spatial relation with an amphibolite layer and such a high basicity of plagioclase likely reflects a preservation of primary composition of plagioclase from a tuffitic source. In some cases the plagioclases may show slight reverse zoning, whereby the core is more sodic than the marginal parts, and corresponds to the andesine (An_{37}).

5. Whole-rock geochemistry

The newly obtained whole-rock geochemical data from orthogneisses (metagranites) and amphibolites of the KKC and UUC are presented in Tables 1 and 2. They are complemented by Sr–Nd isotopic data from one KHC amphibolite and Nd data from an UUC gabbro. No samples of **Chandman Khayrkhan Crystalline Complex** were analysed in course of the present study. The data presented in the diagrams (Figs 7–8) are for comparison only and come from Chandman Massif (Economos et al. in print).

Metagranites of the Unegt Uul Crystalline Complex (Fig. 7a) usually show high to very high Ba contents (47–1002 ppm) and variable Rb/Sr ratios (0.1–6.1). The SiO_2 abundances range between 70 and 75 wt. %, A/CNK = 1.06–1.23 (Fig. 7b), potassium abundance is high (K_2O = 3.8–4.8 wt. %; Fig. 7c) and the total REE contents are very variable (62–329 ppm). Chondrite-normalised (Boynton 1984) REE patterns show slight LREE enrichment (La_N/Sm_N = 2.7–4.3), flat HREE (Gd_N/Yb_N = 1.1–1.2) and moderate to deep negative Eu anomalies (Eu/Eu* = 0.33–0.61) (Fig. 7e). They fit the field of syn-collisional, within plate and volcanic arc associations in the Rb vs. Ta + Yb diagram of Pearce (1984) (Fig. 7d).

Amphibolites of the Unegt Uul Crystalline Complex are tholeiitic with SiO_2 = 48.6–51.1 wt. % and K_2O/Na_2O = 0.1–1.0. Amphibolites correspond to MORB in geotectonic discrimination diagram of Meschede (1986) (Fig. 8b). Compared to N-MORB (Sun and McDonough 1989), the amphibolites are somewhat enriched in lithophile elements (Fig. 8a). Still, the REE contents are very low (34–43 ppm) and chondrite-normalized REE patterns flat as demonstrated by low LREE/HREE and LREE/MREE ratios (La_N/Yb_N = 1.4, La_N/Sm_N = 1.0–1.2; Fig. 8c).

Exact age of the gabbro sample (D0873), which comes from a tectonic mélange, is not at all clear. Fortunately the age-corrected Nd isotopic composition does not vary greatly with time and thus it in any case demonstrates a large proportion of the crustal material (ε_{Nd}^{900} = -4.0), precluding direct derivation from the Earth's mantle.

Granitic orthogneisses of the **Khan Khayrkhan Crystalline Complex** are medium-K calc-alkaline, slightly metaluminous to peraluminous rocks (A/CNK = 0.9–1.3; K_2O/Na_2O = 0.4–1.2). Trace-element signatures of the metagranitic rocks indicate a volcanic-arc character *sensu* Pearce et al (1984). Chondrite-normalised patterns show well fractionated LREE and flat trend for the HREE (La_N/Yb_N = 6.5–11.5, La_N/Sm_N = 3.89–6.43). The Eu anomaly is variably negative to negligible (Eu/Eu* = 0.5–1.0). (Fig. 7a–d, f)

Amphibolites from the **Khan Khayrkhan Crystalline Complex** are tholeiitic to calc-alkaline with SiO_2 = 43.1–47.8 wt. % and very variable K_2O/Na_2O ratios (K_2O/Na_2O = 0.05–1.80). Chondrite-normalized REE patterns show a fair fractionation as demonstrated by LREE/HREE and LREE/MREE ratios (La_N/Yb_N = 3.0–6.4, La_N/Sm_N = 1.6–2.7). They are strongly enriched in lithophile and weakly in HFS elements compared with N-MORB (Sun and McDonough 1989) (Fig. 8b). Amphibolite samples fit into fields of within-plate basalt in the discrimination diagram of Meschede (1986) (Fig. 8a).

The trace-element composition of the amphibolite H0477 resembles EMORB (Fig. 8a–b). Accordingly, the Sr–Nd isotopic signature is primitive, in line with its likely derivation from a moderately depleted mantle source in Cambrian times (ε_{Nd}^{550} = +8.4, $^{87}Sr/^{86}Sr_{550}$ = 0.7040, T_{Nd}^{DM} = 0.56 Ga).

6. Metamorphic conditions

6.1. Unegt Uul Crystalline Complex

Three samples from the UUC have been studied to estimate metamorphic conditions of the unit: a mica schist

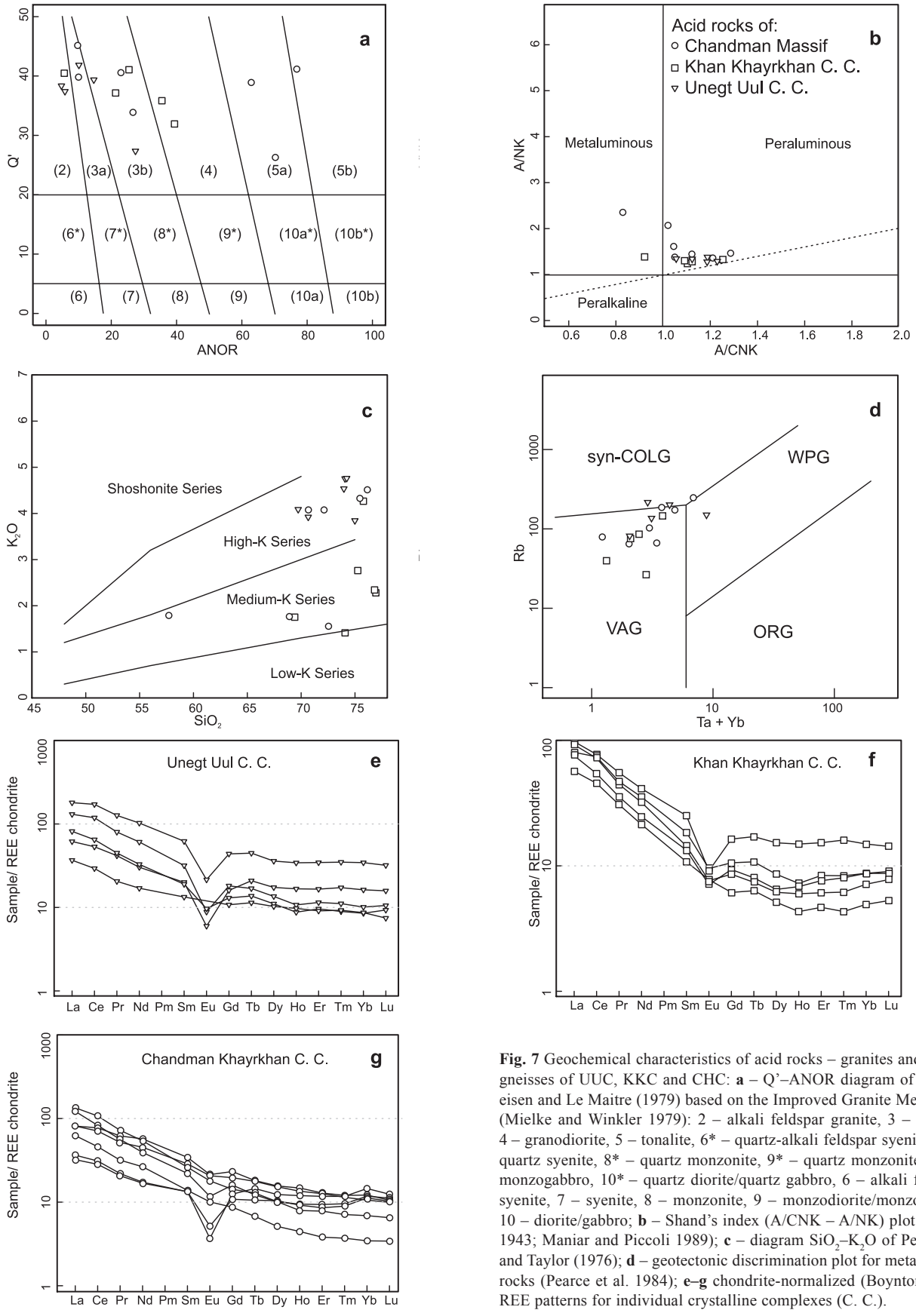

Fig. 7 Geochemical characteristics of acid rocks – granites and orthogneisses of UUC, KKC and CHC: **a** – Q'–ANOR diagram of Streckeisen and Le Maitre (1979) based on the Improved Granite Mesonorm (Mielke and Winkler 1979): 2 – alkali feldspar granite, 3 – granite, 4 – granodiorite, 5 – tonalite, 6* – quartz-alkali feldspar syenite, 7* – quartz syenite, 8* – quartz monzonite, 9* – quartz monzonite/quartz monzogabbro, 10* – quartz diorite/quartz gabbro, 6 – alkali feldspar syenite, 7 – syenite, 8 – monzonite, 9 – monzodiorite/monzogabbro 10 – diorite/gabbro; **b** – Shand's index (A/CNK – A/NK) plot (Shand 1943; Maniar and Piccoli 1989); **c** – diagram SiO_2–K_2O of Peccerillo and Taylor (1976); **d** – geotectonic discrimination plot for metagranitic rocks (Pearce et al. 1984); **e–g** chondrite-normalized (Boynton 1984) REE patterns for individual crystalline complexes (C. C.).

Tab. 1 Whole-rock analyses (major elements in wt. %, trace elements in ppm) for acid rocks from the eastern Mongolian Altay.

Sample	**H0168**	**H0267A**	**H0332**	**H0333**	**H0335**	**R0221**	**Z0992**	**AB6-8**	**D0816**
Sheet_no	L-47-101A	L-47-101B	L-47-101A	L-47-101A	L-47-101A	L-47-101A	L-47-101A	L-47-100	L-47-101V
E_coord. (°)	98.22329	98.37318	98.16809	98.19587	98.21791	98.08679	98.17676	97.96672	45.21626
N_coord. (°)	45.27573	45.23777	45.26511	45.26924	45.28201	45.29015	45.27202	98.15597	45.15311
Rock	orthogneiss	orthogneiss	orthogneiss	orthogneiss	orthogneiss	orthogneiss	orthogneiss	orthogneiss	orthogneiss
Formation	CHC	CHC	CHC	CHC	CHC	CHC	CHC	KKC	KKC
SiO_2	75.48	72.56	57.72	76.12	72.12	68.89	70.64	69.30	74.08
Al_2O_3	14.00	14.23	15.43	13.43	13.19	14.63	14.16	13.45	13.86
Fe_2O_3	1.05	2.49	8.39	1.15	2.00	4.62	2.92	2.56	2.01
MgO	0.13	0.71	4.14	0.19	0.34	1.86	0.69	1.05	0.62
CaO	0.66	2.63	6.63	0.68	1.47	3.99	1.78	2.67	0.82
Na_2O	3.45	4.35	2.82	2.63	2.85	3.14	3.56	4.76	5.81
K_2O	4.32	1.55	1.78	4.51	4.07	1.76	4.07	1.75	1.41
TiO_2	0.05	0.27	1.20	0.08	0.18	0.46	0.43	0.24	0.27
P_2O_5	0.08	0.10	0.46	0.08	0.05	0.14	0.13	0.06	0.06
MnO	0.10	0.05	0.13	0.04	0.03	0.07	0.03	0.06	0.06
LOI	0.60	0.60	0.80	0.90	1.00	0.40	1.40	3.90	1.00
TOT_C	0.01	0.01	0.01	0.01	0.06	0.01	0.10	0.83	0.04
Total	99.92	99.54	99.52	99.81	97.30	99.97	99.82	99.81	100.00
Sc	4	3	18	4	3	11	4	4	3
Ba	119.2	296.6	404.4	174.3	733.9	249.9	1305.0	559.7	276.4
Be	4	2	2	3	1	3	2	1	2
Co	0.8	3.9	27.6	1.0	2.6	12.2	5.5	4.0	2.9
Cs	8.6	3.9	1.9	4.4	9.1	9.3	1.7	1.3	0.3
Ga	21.4	20.0	20.8	17.8	17.0	21.4	15.7	12.8	13.9
Hf	2.4	4.3	5.4	1.9	4.4	6.2	6.8	3.3	5.5
Nb	32.0	7.0	14.9	19.1	11.0	11.5	9.0	4.6	10.7
Rb	244.9	78.8	66.9	173.3	185.3	102.8	65.1	39.9	26.8
Sn	2	2	3	2	2	3	1	1	2
Sr	28.6	312.8	382.1	50.3	159.8	183.2	278.0	156.1	161.2
Ta	3.8	0.5	0.9	2.5	1.3	0.8	0.6	0.3	1.0
Th	6.7	10.0	4.4	7.2	32.1	8.1	6.5	8.2	9.8
U	1.3	1.4	1.2	1.6	2.5	1.0	1.3	1.8	1.5
V	–	26	173	6	14	71	29	28	16
W	0.5	0.2	0.1	2.4	0.7	0.2	0.2	0.4	0.7
Zr	48.6	148.7	226.7	45.5	147.0	194.4	267.9	98.1	166.2
Y	25.8	9.7	29.0	21.9	21.1	25.2	17.9	10.4	17.9
Mo	0.2	0.2	0.3	0.2	0.2	0.2	0.2	0.4	0.3
Cu	6.3	7.9	53.0	6.9	7.6	20.2	6.1	15.2	10.8
Pb	1.7	2.7	1.1	2.8	6.0	1.6	3.2	6.6	1.8
Zn	9	48	61	13	25	74	35	39	31
Ni	2.2	5.1	49.9	2.1	3.0	32.8	4.4	6.6	3.6
As	0.5	0.5	0.8	0.6	0.6	–	0.5	3.1	0.8
Cd	0.1	–	–	–	0.1	0.1	–	–	–
Sb	–	–	–	–	0.1	–	–	–	0.1
Bi	0.1	–	–	0.2	0.1	0.1	–	0.1	0.1
Au	1.4	1.0	1.1	0.9	–	17.1	4.3	–	0.8
Tl	0.1	0.3	0.3	0.1	0.3	0.5	0.1	–	–
La	10.0	19.4	25.2	11.3	37.8	25.2	41.7	17.6	24.9
Ce	22.9	37.2	62.5	25.1	67.0	57.3	86.7	36.7	59.8
Pr	2.52	3.88	7.55	2.68	6.87	6.32	8.83	3.75	5.73
Nd	10.1	15.9	34.3	10.4	23.6	27.2	32.5	12.8	21.2
Sm	2.6	2.7	6.7	2.6	4.3	5.6	5.1	2.1	3.6
Eu	0.27	0.74	1.57	0.38	0.86	1.52	1.32	0.57	0.70
Gd	3.23	2.25	6.02	2.80	4.14	5.08	3.69	1.59	2.74
Tb	0.69	0.32	0.86	0.50	0.58	0.84	0.61	0.30	0.51
Dy	3.97	1.65	5.03	3.35	3.23	4.92	3.26	1.65	2.76
Ho	0.86	0.32	1.06	0.66	0.68	0.97	0.57	0.31	0.52
Er	2.46	0.80	2.70	1.80	1.97	2.65	1.64	0.98	1.76
Tm	0.38	0.12	0.39	0.29	0.31	0.37	0.23	0.14	0.27
Yb	3.04	0.72	2.54	2.35	2.46	2.21	1.44	1.03	1.82
Lu	0.40	0.11	0.34	0.33	0.36	0.32	0.21	0.17	0.29
∑ REE	63.42	86.11	156.76	64.54	154.16	140.50	187.80	79.69	126.60

Tab. 1 continued Whole-rock analyses (major elements in wt. %, trace elements in ppm) for acid rocks from the eastern Mongolian Altay.

Sample	**H0352**	**R0196**	**R0237**	**A1000-2**	**D0713**	**D0714**	**H0165**	**H0272**	**H1291**
Sheet_no	L-47-101A	L-47-101A	L-47-101A	L-47-101B	L-47-101G	L-47-101G	L-47-101A	L-47-101B	L-47-101A
E_coord. (°)	98.03787	98.00885	98.07759	98.36456	98.41703	98.44172	98.24330	98.27132	98.24266
N_coord. (°)	45.18757	45.20836	45.17450	45.28449	45.27529	45.27385	45.29260	45.29054	45.29318
Rock	orthogneiss	orthogneiss	orthogneiss	granite	granite	granite	rhyolite	granite	granite
Formation	KKC	KKC	KKC	UUC	UUC	UUC	UUC	UUC	UUC
SiO_2	76.78	75.24	75.76	74.07	69.72	74.05	70.13	74.99	70.66
Al_2O_3	12.92	13.89	13.78	13.44	15.50	13.23	14.22	14.23	13.14
Fe_2O_3	1.27	1.63	1.23	1.89	1.73	2.07	3.31	0.98	5.82
MgO	0.27	0.22	0.11	0.52	0.62	0.48	0.78	0.08	0.47
CaO	0.95	0.91	0.32	0.87	1.78	0.98	1.05	0.30	0.40
Na_2O	4.58	4.71	3.53	2.79	4.30	2.95	3.51	4.18	3.71
K_2O	2.34	2.77	4.27	4.75	4.08	4.76	5.14	3.84	3.92
TiO_2	0.17	0.18	0.08	0.26	0.25	0.22	0.46	0.02	0.56
P_2O_5	0.04	0.04	0.02	0.20	0.05	0.04	0.11	0.02	0.14
MnO	0.02	0.03	0.02	0.02	0.03	0.03	0.04	0.01	0.08
LOI	0.50	0.60	1.20	1.00	1.80	1.10	1.20	1.00	1.00
TOT_C	0.02	0.03	0.02	0.05	0.27	0.04	0.15	0.03	0.03
Total	99.84	100.22	100.32	99.81	99.86	99.91	99.95	99.65	99.90
Sc	2	2	2	4	4	3	5	4	10
Ba	441.0	521.0	479.0	495.6	1002.0	759.8	717.2	47.0	507.1
Be	3	1	1	2	2	2	2	3	3
Co	1.8	1.6	1.0	2.2	2.4	2.9	5.8	0.8	4.0
Cs	1.1	1.7	2.1	12.3	2.1	2.4	2.7	5.7	1.9
Ga	14.7	15.7	15.1	17.9	14.9	15.4	18.4	21.2	24.7
Hf	2.9	3.1	3.1	3.7	3.9	4.7	6.0	1.5	13.4
Nb	7.2	7.9	8.9	9.4	5.1	8.6	10.1	10.3	24.0
Rb	75.8	85.1	146.5	205.8	80.7	137.1	181.5	218.3	151.6
Sn	1	–	5	3	2	3	4	4	6
Sr	86.6	110.5	86.5	126.4	593.2	241.3	118.5	36.1	81.6
Ta	0.6	0.6	0.7	1.0	0.3	1.0	1.0	1.1	1.7
Th	12.0	8.5	15.9	11.0	12.8	29.2	21.0	10.7	31.8
U	1.4	1.3	6.7	4.1	2.4	4.1	5.3	4.4	4.0
V	11	11	–	17	24	26	30	–	28
W	5.2	0.7	0.4	2.8	0.5	0.2	1.2	1.3	0.6
Zr	83.3	118.2	80.8	112.0	146.8	108.2	188.0	31.4	472.0
Y	14.1	16.2	31.0	38.2	23.0	26.0	31.2	22.3	68.9
Mo	0.4	0.7	7.0	0.2	0.3	1.0	0.3	0.2	0.8
Cu	8.4	5.3	6.8	4.1	7.5	10.6	26.5	8.4	17.9
Pb	3.4	2.2	2.8	5.2	14.0	6.7	24.9	8.8	12.5
Zn	16	17	26	23	25	31	45	12	129
Ni	2.5	4.3	2.1	4.6	3.7	3.7	5.6	1.9	4.1
As	–	1.2	0.9	5.0	–	–	0.8	2.7	0.7
Cd	0.1	–	–	–	0.1	–	0.1	–	0.1
Sb	–	–	–	0.2	–	–	–	–	–
Bi	–	–	0.1	0.1	0.1	0.2	0.2	0.6	0.1
Au	–	–	–	1.0	0.7	–	0.8	1.1	0.9
Tl	0.1	0.1	0.1	0.6	–	–	–	0.1	0.1
La	28.6	23.4	30.3	19.1	25.3	40.5	43.2	11.4	55.8
Ce	58.2	43.9	62.4	43.1	52.4	95.9	89.7	23.7	138.8
Pr	5.44	4.33	6.74	5.09	5.48	9.77	9.25	2.51	15.46
Nd	19.2	14.8	24.7	18.2	19.7	36.5	39.0	10.2	61.6
Sm	2.8	2.6	4.9	3.9	3.7	6.2	6.4	2.6	12.1
Eu	0.56	0.52	0.67	0.44	0.71	0.65	0.95	–	1.58
Gd	2.22	2.42	4.23	4.15	3.37	4.70	6.02	2.79	11.35
Tb	0.35	0.38	0.81	0.99	0.65	0.80	0.87	0.54	2.12
Dy	1.98	2.09	4.91	5.59	3.56	4.37	5.04	3.31	11.57
Ho	0.43	0.49	1.07	1.20	0.63	0.77	1.02	0.70	2.46
Er	1.28	1.60	3.21	3.48	2.02	2.41	2.84	1.91	7.25
Tm	0.20	0.26	0.52	0.56	0.29	0.36	0.44	0.30	1.13
Yb	1.49	1.82	3.12	3.40	1.78	2.11	2.98	1.81	7.20
Lu	0.25	0.28	0.46	0.51	0.30	0.34	0.42	0.24	1.03
∑ REE	123.00	98.89	148.04	109.71	119.89	205.38	208.13	61.96	329.45

Tab. 2 Whole-rock analyses (major elements in wt. %, trace elements in ppm) for basic rocks from the eastern Mongolian Altay.

Sample	**H0333B**	**H0693**	**H0477**	**H1300A**	**H1300B**	**D0711**	**D0715**	**D0873**
Sheet_no	L-47-101A	L-47-101A	L-47-101A	L-47-101V	L-47-101V	L-47-101G	L-47-101G	L-47-101B
E_coord. (°)	98.19587	98.11516	98.09348	98.00317	98.00317	98.39088	98.43877	98.46475
N_coord. (°)	45.26924	45.17224	45.17784	45.23340	45.23340	45.27602	45.27262	45.27620
Rock	amphibolite	metagabbro	amphibolite	amphibolite	amphibolite	amphibolite	amphibolite	gabbro
Formation	CHC	KKC	KKC	KKC	KKC	UUC	UUC	UUC
SiO_2	43.24	46.97	43.10	46.80	47.84	48.60	51.13	48.13
Al_2O_3	13.64	15.65	17.64	16.43	18.11	14.18	14.08	16.05
Fe_2O_3	14.49	12.58	13.25	11.81	12.47	12.59	11.63	13.00
MgO	7.50	8.97	3.44	6.83	4.67	8.44	7.29	7.96
CaO	15.41	9.17	12.45	12.11	8.85	12.09	10.44	9.39
Na_2O	0.53	3.22	0.95	1.69	4.04	1.75	2.34	1.35
K_2O	0.35	0.17	1.73	0.28	0.21	0.26	0.90	1.07
TiO_2	2.65	1.70	2.07	2.12	2.11	0.87	0.88	1.36
P_2O_5	0.28	0.15	0.43	0.32	0.36	0.07	0.08	0.07
MnO	0.20	0.18	0.24	0.19	0.15	0.18	0.19	0.21
Cr_2O_3	0.04	0.03	0.05	0.03	0.03	0.04	0.04	0.02
LOI	1.00	1.00	3.90	1.20	1.10	0.90	1.00	1.20
TOT_C	0.04	0.05	0.95	0.02	0.05	0.08	0.06	0.03
Total	99.36	99.81	99.26	99.81	99.96	99.99	100.02	99.82
Sc	44	41	29	34	39	40	38	41
Ba	93.6	20.8	798.0	37.8	100.6	49.5	91.6	132.1
Be	2	1	2	1	1	1	1	2
Co	62.4	48.1	39.5	40.3	47.0	51.5	43.0	54.1
Cs	0.6	–	1.4	0.4	0.1	0.9	1.2	0.8
Ga	23.4	18.1	24.7	18.9	19.1	16.2	16.3	20.1
Hf	5.5	2.5	5.6	3.5	3.6	1.7	1.8	3.5
Nb	19.8	2.3	40.4	21.9	19.2	2.6	3.9	24.5
Rb	4.3	1.0	40.3	7.9	2.5	10.4	20.2	50.6
Sn	2	–	3	1	1	1	1	2
Sr	508.2	518.0	332.8	449.7	281.0	252.2	153.7	311.3
Ta	1.2	0.2	2.7	1.2	1.2	0.2	0.3	1.0
Th	1.7	–	3.4	1.8	0.8	0.6	1.8	5.1
U	1.6	0.2	1.2	0.5	0.4	0.1	0.7	0.8
V	394	323	244	240	287	335	312	308
W	1.8	0.4	1.9	0.4	0.1	–	0.4	3.8
Zr	206.7	96.6	219.5	139.2	138.1	51.3	56.6	116.2
Y	47.4	31.9	43.4	28.5	31.9	18.1	21.4	26.6
Mo	0.2	0.2	0.7	0.2	0.8	–	0.2	0.1
Cu	5.4	36.4	66.5	65.2	91.3	96.7	74.9	1.9
Pb	5.9	0.3	2.4	0.6	0.3	0.9	2.4	4.3
Zn	20	19	73	15	34	14	20	27
Ni	30.5	26.7	74.5	17.5	32.3	20.9	23.4	25.0
As	–	0.7	0.9	–	–	–	–	–
Cd	–	–	0.1	–	–	–	–	–
Sb	0.1	0.1	0.1	–	–	–	–	–
Bi	2.4	–	–	–	–	–	0.1	0.3
Au	–	0.5	1.0	–	0.7	0.7	1.3	1.4
Tl	–	–	0.1	–	–	–	–	–
La	17.4	4.2	32.6	14.8	12.8	3.3	4.9	18.2
Ce	44.5	12.6	71.7	35.5	32.3	9.1	12.4	43.1
Pr	5.77	2.14	8.15	4.53	4.36	1.34	1.70	5.16
Nd	28.6	10.5	36.9	21.7	19.5	7.3	8.0	21.7
Sm	7.1	3.7	7.5	4.9	4.8	2.1	2.5	4.8
Eu	2.29	1.54	2.63	1.68	1.50	0.77	0.76	1.20
Gd	8.55	4.69	7.33	5.05	5.28	2.53	2.91	5.13
Tb	1.28	0.97	1.19	0.88	0.95	0.49	0.59	0.88
Dy	8.15	5.40	6.98	5.04	5.14	3.27	3.58	4.65
Ho	1.74	1.15	1.43	1.05	1.11	0.57	0.66	0.83
Er	4.59	3.44	3.89	2.97	3.26	1.93	2.05	2.64
Tm	0.60	0.47	0.55	0.41	0.47	0.25	0.30	0.39
Yb	4.48	2.73	3.44	2.71	2.87	1.55	1.84	2.42
Lu	0.64	0.47	0.58	0.39	0.42	0.26	0.30	0.35
∑ REE	135.69	54.00	184.87	101.61	94.76	34.76	42.49	111.45

representing a roof pendant to the Unegt Uul metagranite and two amphibolites, which are likely tectonic fragments incorporated into the UUC by the activity of the Bogt fault.

The P–T conditions were calculated for marginal parts of the mineral grains, which seem to be well equilibrated. Additionally, wherever possible, independent estimates were obtained for central parts of garnet grains taking the included minerals into account. The aim was to estimate P–T conditions for the early and late stages of metamorphism.

The amphibolites are represented by two garnet-bearing samples H0256 and H0159. The sample H0256 consists of amphibole, garnet, plagioclase and biotite; titanite and opaque minerals are accessoric. Amphibole corresponding to ferrotschermakite (Leake et al. 1997) has X_{Mg} = 0.24 in the centres of the crystals and slightly higher X_{Mg} = 0.25 in the marginal parts. Garnet grains show zoning from Alm_{61} Sps_3 Prp_3 Grs_{31} in cores to Alm_{61} $Sps_{0.5}$ Prp_{2-3} Grs_{34} at the rims (Fig. 5a). Plagioclase has labradorite composition ($An_{60–62}$). Biotite in matrix (Al^{IV}= 2.75 and X_{Fe}=0.73) differs slightly from that included in garnet grains (Al^{IV}= 2.48 and X_{Fe}=0.74).

The sample H0159 contains garnet with compositional zoning from Alm_{57} Sps_7 $Prp_{7–8}$ Grs_{27} in the central parts to Alm_{56} Sps_{1-2} Prp_{11} Grs_{28-29} in the rims (Fig. 5b). Plagioclases are labradorite ($An_{53–54}$). Amphiboles correspond to ferrotschermakite with X_{Mg} = 0.39.

The metamorphic conditions calculated using THERMOCALC (Powell and Holland 1985) from amphibolites suggest a prograde growth at progressively increasing temperature, the central parts together with included grains giving T = 613 ± 90 °C; P = 6.4 ± 1.1. Marginal parts yield conditions of 761 ± 79 °C; 6.2 ± 1.4 kbar, 753 ± 87 °C; 6.4 ± 1.6 kbar and T = 655 ± 46 °C and P = 7.5 ± 0.9 kbar (Tab. 3, Figs 9a, 10).

The conventional garnet–amphibole thermometer of Ravna (2000), also used for estimating the metamorphic conditions, shows slightly lower temperatures then THERMOCALC calculations. The temperatures calculated for the rims in the sample H0256 yield values of 753 and 687 °C. The temperatures calculated for the sample H0159 from the central parts of mineral grains correspond to 490–554 °C, for marginal parts to 561 °C (Tab. 5).

The mica schists are represented by the sample H0161. Its mineral association comprises quartz, muscovite, biotite, garnet and plagioclase; zircon and apatite are accessoric. The garnet zoning ranges between $Alm_{67–69}$

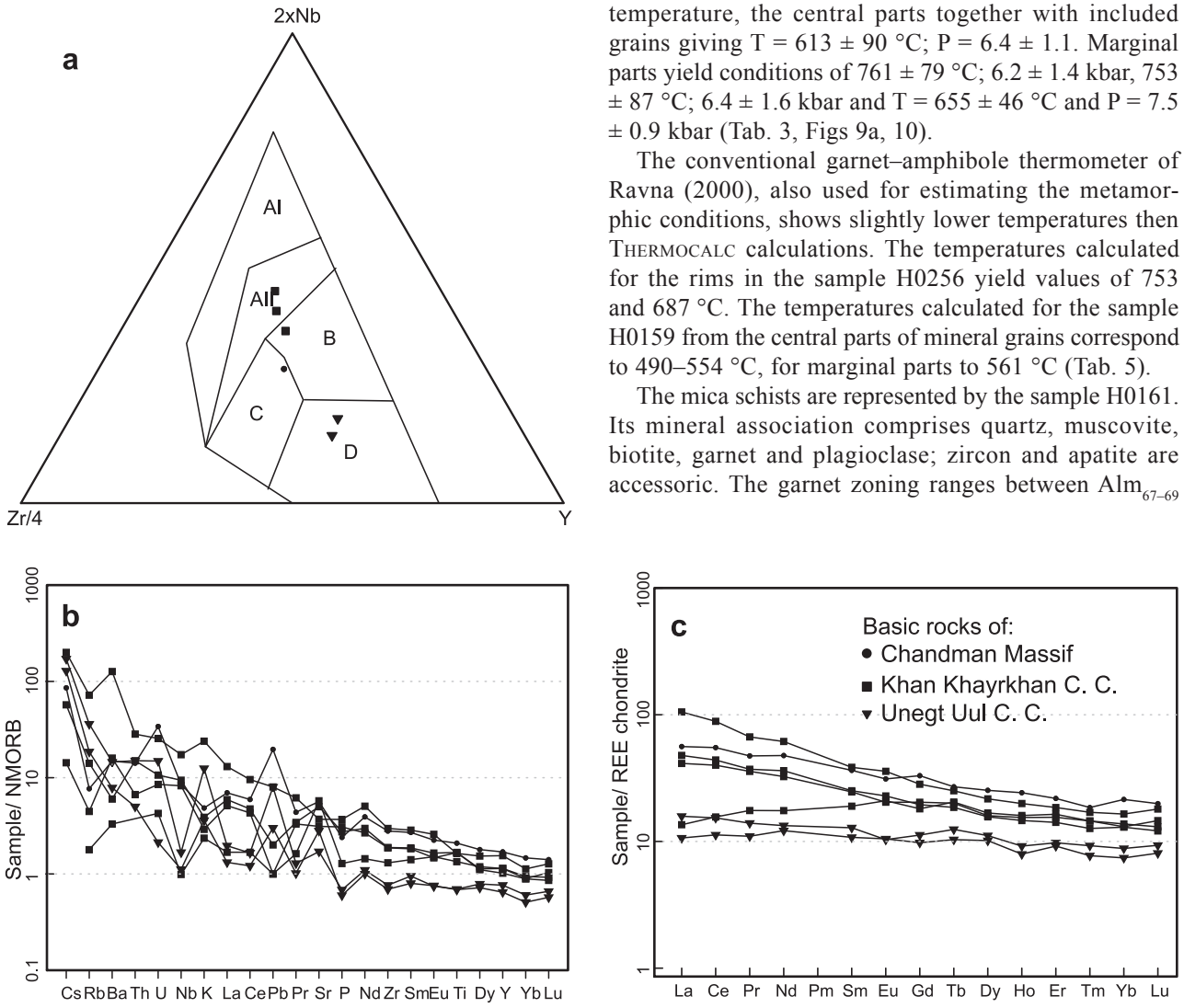

Fig. 8 Geochemical characteristics of the basic rocks from the individual crystalline complexes **a** – ternary diagram Zr/4–2×Nb–Y for geotectonic discrimination of basaltic rocks (Meschede 1986), AI – Within-plate alkali basalt, AII – Within-plate alkali basalt, Within-plate tholeiite, B – Enriched Mid-ocean ridge basalt, C – Volcanic arc basalt, D – Normal Mid-ocean ridge basalt ; **b** – trace-element multielement plots (normalized to N-MORB after Sun and McDonough 1989); **c** – characteristic REE patterns (normalized to average chondrite composition after Boynton 1984).

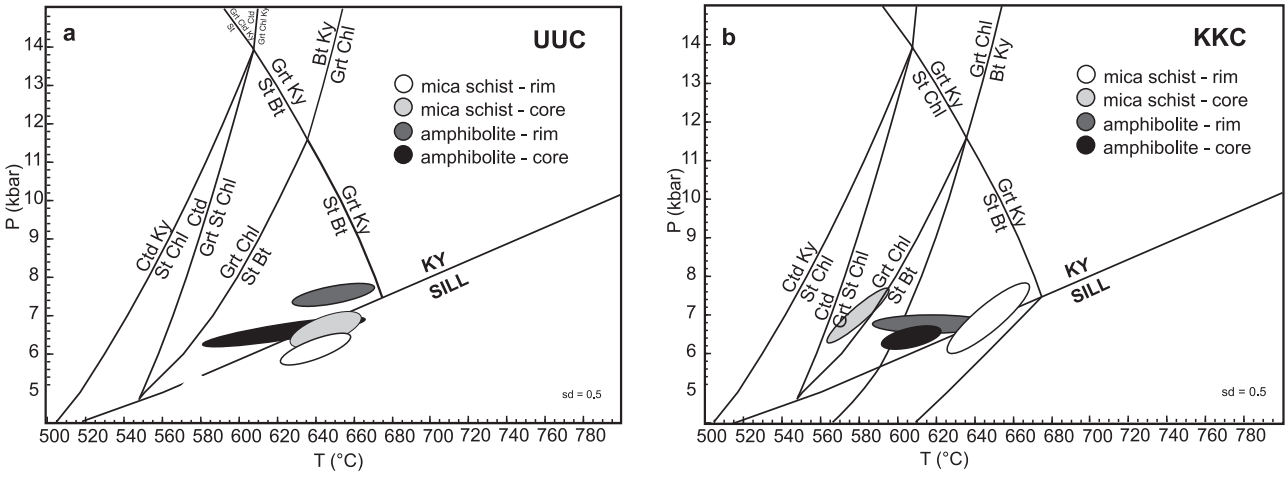

Fig. 9 P–T grid for samples of amphibolitic rocks and metapelites from **a** – Unegt Uul Crystalline Complex; **b** – Khan Khayrkhan Crystalline Complex.

Sps_{20} Prp_{6} $Grs_{3–6}$ in the cores and Alm_{66} Sps_{25} Prp_{5} Grs_{2} in the rims (Fig. 5c). In contrast to the garnet grains in the amphibolites of the same unit, they show more retrograde character documented by rimward increase in *Sps* and decrease in *Prp* components. Plagioclases show also slightly different character in centres of the grains, where they have An_{28}. The marginal parts of plagioclases correspond to An_{24}.

The P–T estimates computed from mica schist seem to be relatively constant for the central and marginal parts of the mineral grains, which suggests a likely faster mineral growth at T ranging from 639 ± 30 to 657 ± 33 °C and P from 6 ± 1.2 to 6.7 ± 1.2 kbar (Tab. 3, Figs 9a, 10).

For the comparison, the garnet–biotite thermometers were also used for calculating temperatures in mica schists. Five different thermometers were employed (Thompson 1976; Lee and Holdaway 1977; Ferry and Spear 1978; Perchuk and Lavrent'eva 1983; Bhattacharya et al. 1992). The results differ in order of tens of degrees, as summarized in Tab. 4.

The temperatures in mica schists at 6 kbar reach 516–622 °C in marginal parts of the garnet grains and span 508–665 °C in the cores. These are in agreement with THERMOCALC results, showing no significant temperature differences between cores and rims.

6.2. Chandman Khayrkhan Crystalline Complex

The widespread migmatitization probably bears witness to peak metamorphic conditions. The migmatitization may be related to the pre-intrusive metamorphic event or it may be a result of periplutonic metamorphism linked with the high-T regime during granite emplacement of the Chandman Massif.

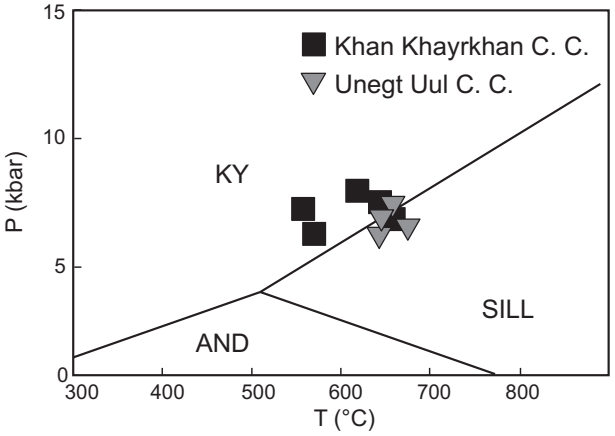

Fig. 10 Correlation of calculated P–T conditions of samples from Unegt Uul Crystalline Complex and Khan Khayrkhan Crystalline Complex units.

Subsequently the rocks of the CHC were strongly affected by a younger retrograde metamorphic event. Mineral assemblage in the calc-silicate rocks (Ep + Act + Pl) is probably a product of retrograde metamorphism under the lower amphibolite to greenschist-facies conditions (< 600 ºC for 5 kbar – Thompson and Norton 1968). Mineral assemblage observed in the studied rocks however precludes a more accurate P–T calculation.

6.3. Khan Khayrkhan Crystalline Complex

Metamorphism in the Khan Khayrkhan Crystalline Complex was studied on samples of mica schists and garnet-bearing amphibolites.

Mica schists are represented by samples H0478 and H0477. Sample H0478 comprises mineral assemblage Grt + Bt + St + Pl. Garnet zoning (Fig. 6a) varies from

Tab. 3 Results of P–T calculations using THERMOCALC. The results falling outside the sigfit limit are shown in grey.

Sample	Position	Unit	Rock	av T°C	sd (T)	P (kbar)	sd (P)	corr	**sigfit**	fit for 95% confidence
H0256	core	UUC	amphibolite	613	90	6.4	1.1	0.888	1.20	1.54
H0256	rim	UUC	amphibolite	761	79	6.2	1.4	0.192	1.30	1.45
H0256	rim	UUC	amphibolite	753	87	6.4	1.6	0.056	1.34	1.45
H0159	rim	UUC	amphibolite	655	46	7.5	0.9	0.592	1.10	1.45
H0161	core	UUC	mica schist	647	31	6.7	1.2	0.724	0.44	1.61
H0161	core	UUC	mica schist	657	33	6.6	1.4	0.693	0.81	1.61
H0161	rim	UUC	mica schist	639	30	6.0	1.2	0.730	0.65	1.61
H0478	core	KKC	mica schist	559	33	7.4	1.6	0.944	0.11	1.73
H0478	rim	KKC	mica schist	608	36	7.9	1.5	0.947	0.90	1.61
H0478	rim	KKC	mica schist	639	22	7.5	0.8	0.235	0.41	1.61
H0477	core	KKC	mica schist	651	47	7.2	2.9	0.929	0.40	1.73
H0477	rim	KKC	mica schist	636	47	7.9	3.1	0.933	0.24	1.73
H0357	rim	KKC	amphibolite	575	24	6.2	1.6	0.183	1.71	1.42
H0357	rim	KKC	amphibolite	578	69	6.4	1.5	0.533	1.34	1.54
H0478B	rim	KKC	amphibolite	683	97	6.7	2.4	0.614	1.68	1.61
H0478B	core	KKC	amphibolite	587	109	6.2	2.6	-0.119	2.16	1.54

composition Alm_{73} Sps_{0-1} $Prp_{10–11}$ Grs_{14} in cores to Alm_{72} Sps_{1} $Prp_{14–15}$ $Grs_{11–12}$ in rims. Biotite has Al^{IV} = 2.42 and X_{Fe} = 0.50–0.51 in contact with garnet, the values of Al^{IV}= 2.38 and X_{Fe}=0.46–0.47 are characteristic of biotites from matrix and Al^{IV} = 2.5 with X_{Fe} = 0.43–0.45 have biotites in contact with staurolite. Staurolite is Fe staurolite with X_{Fe} = 0.87–0.89. Plagioclase corresponds to andesine (An_{37}). Alumosilicate kyanite is present in comparable mica schist samples which, unfortunately, were not analysed.

Sample H0477 has mineral assemblage Mu + Bt + St + Pl. Plagioclase is oligoclase with $An_{24–27}$, X_{Fe} in staurolite is 0.86–0.89; biotites have Al^{IV} = 2.42–2.46 and X_{Fe} = 0.46–0.50.

THERMOCALC P–T calculations for the samples of mica schists yielded conditions varying from *c.* 559 ± 33 to 651 ± 47 °C and from 7.2 ± 2.9 to 7.4 ± 1.6 kbar for the central parts of garnet porphyroblasts and from 636 ± 47 °C to 639 ± 22 °C and from 7.5 ± 0.8 to 7.9 ± 1.5 kbar for the rims. The peak metamorphic assemblage was Bt + Ms + Grt ± St ± Ky. However, these P–T conditions seem to be rather high for mentioned mineral assemblage. Similar conditions were obtained also using garnet–biotite thermometer, which yielded temperatures from 654 to 715 °C for the rims of mineral grains, setting P = 6 kbar (Tab. 4).

Amphibolite samples H0357 and H0478B were also used for P–T calculations. Mineral association of H0357 includes ferrotschermakite (X_{Mg}=0.42–0.49), biotite (Al^{IV}= 2.52–0.60 and X_{Fe}=0.43–0.55), garnet (with compositional zoning from Alm_{65} Sps_{8} Prp_{10} Grs_{15} in cores to Alm_{64} Sps_{7} Prp_{12} Grs_{15} at the rims) and labradorite ($An_{52–65}$).

Tab. 4 Results of P–T calculations using garnet–biotite thermometers according to Thompson (1976), Lee and Holdaway (1977), Ferry and Spear (1978), Perchuk and Lavrent'eva (1983) and Bhattacharya et al. (1992).

Sample	**Position**	**Unit**	**Rock**	**Temperature °C**					
				P (kbar)	Bhatacharya et al. (1992)	Ferry and Spear (1978)	Perchuk and Lavrent´eva (1983)	Thompson (1976)	Lee and Holdaway (1977)
H0161	rim	**UUC**	micaschist	6	544	612	602	626	602
H0161	rim	**UUC**	micaschist	6	516	581	585	602	581
H0161	core	**UUC**	micaschist	6	570	658	626	665	633
H0478	rim	**KKC**	micaschist	6	682	715	654	703	668

Mineral assemblage of the sample H0478B is fairly similar and involves garnet, amphibole and plagioclase. Garnet zoning varies from Alm_{73} Sps_{3} Prp_{9} Grs_{10} in central part of grains to Alm_{72} $Sps_{0.8}$ Prp_{13} Grs_{11} in the rim. Composition of amphibole slightly differs in the cores (X_{Mg} = 0.40) from the rims (X_{Mg} = 0.37). Plagioclase with normal zoning from this sample corresponds to andesine (An_{35}).

Metamorphic conditions estimated from amphibolites indicate an evolution similar to that of mica schists. Results of THERMOCALC calculations for amphibolite H0478B correspond to T = 587 ± 109 °C and P = 6.2 kbar for the mineral cores, slightly higher conditions 683 ± 97 °C and 6.7 ± 2.4 kbar were calculated for the rims. Using THERMOCALC, the sample H0357 yielded temperatures of 575 and 578 °C at pressures of 6.2 and 6.4 kbar for the marginal parts of measured mineral grains. Garnet–amphibole thermometer (Ravna 2000) gave T = 617 and 514 °C (Tab. 5). Both temperatures correspond to the marginal parts of the mineral grains.

The contrast between P–T conditions estimated from central and marginal parts of the grains as well as (although indistinctive) zoning in *Prp* and *Sps* components across the garnet grains provide an evidence for prograde metamorphism (Tab. 3, Figs. 9b, 10).

7. Dating

7.1. Unegt Uul Crystalline Complex

Two grains of slightly cloudy zircon, with rectangular shape (*c.* 80 × 160 μm), have been recovered from leucogranite H0057. The grain zr1 is characterized by a sector zoning with only relict oscillatory banding (Fig. 11a), while in zr2 the fine oscillatory zoning, with darker core and lighter mantle, is well preserved. Four LA-ICP-MS spots on each grain give contrasting results (Tabs 6, 9); zr1 analyses define an upper intercept of 329 ± 33 Ma, which is consistent with the concordia age of 337 ± 6 Ma (Early Carboniferous) from two concordant spots. In contrast all analyses from zr2 yield a concordia age of 518 ± 5 Ma (Early Cambrian). The contrasting ages are difficult to interpret given the small number of analyzed grains and that the leucogranite shows no clear signs of a metamorphic overprint. The age of *c.* 518 Ma most likely dates the time of zr2 crystallization, which could be related to the leucogranite formation. The meaning of the *c.* 337 Ma age remains, however, unclear.

7.2. Chandman Khayrkhan Crystalline Complex

These metamorphic rocks have not been successfully dated in the frame of the project, the data obtained from this part of the studied area come from granitoid rocks of the Chandman Massif only. The monazite from granite was dated using the CHIME technique. Only one monazite grain could be measured and thus it is essential to consider the credibility of such an individual measurement. The measured monazite was yellowish short prismatic with length of 80–120 μm. No metamictization effects have been observable under CL. The data obtained point to an age of 332 ± 29 Ma (MSWD = 0.20), which corresponds to Late Carboniferous.

The LA-ICP-MS U-Pb dating of zircons from the Chandman granite yields concordia age of 345 ± 2 Ma (2σ) (Tabs 7, 9; Fig. 11b). Together with 6 discordant analyses they define a discordia with intercepts at 354 ± 26 and 154 ± 160 Ma or with an upper intercept of

Tab. 5 Results of P–T calculations using garnet–amphibole thermometer according to Ravna (2000)

sample	unit	mineral	position	#Fe^{+2}	#Mn	#Mg	#Ca	$K_{D(Fe^{2+}/Mg)}^{Grt\text{-}Amp}$	X_{Ca}^{Grt}	X_{Mn}^{Grt}	Temperature
H0159	UUC	Grt	rim × rim	1,73	0,08	0,35	0,86	5,739	0,285	0,025	*T* (°C)
H0159	UUC	Amp	rim × rim	2,13	0,04	2,46	1,98				561,29
H0159	UUC	Grt	core × core	1,78	0,06	0,35	0,89	5,839	0,291	0,018	*T* (°C)
H0159	UUC	Amp	core × core	2,13	0,04	2,46	1,98				554,10
H0159	UUC	Grt	core × core	1,74	0,23	0,25	0,85	7,924	0,275	0,076	*T* (°C)
H0159	UUC	Amp	core × core	2,11	0,03	2,44	1,93				490,56
H0256	UUC	Grt	rim × rim	1,98	0,07	0,12	1,87	4,857	0,465	0,016	*T* (°C)
H0256	UUC	Amp	rim × rim	3,13	0,02	0,92	1,80				753,58
H0256	UUC	Grt	rim × rim	1,95	0,05	0,10	1,88	5,718	0,471	0,013	*T* (°C)
H0256	UUC	Amp	rim × rim	3,03	0,02	0,93	1,80				687,93
H0357	KKC	Grt	rim × rim	2,02	0,20	0,41	0,41	3,931	0,134	0,066	*T* (°C)
H0357	KKC	Amp	rim × rim	2,08	0,02	1,67	1,71				617,41
H0357	KKC	Grt	rim × rim	1,99	0,24	0,35	0,45	5,506	0,149	0,079	*T* (°C)
H0357	KKC	Amp	rim × rim	2,13	0,05	2,08	1,74				514,56

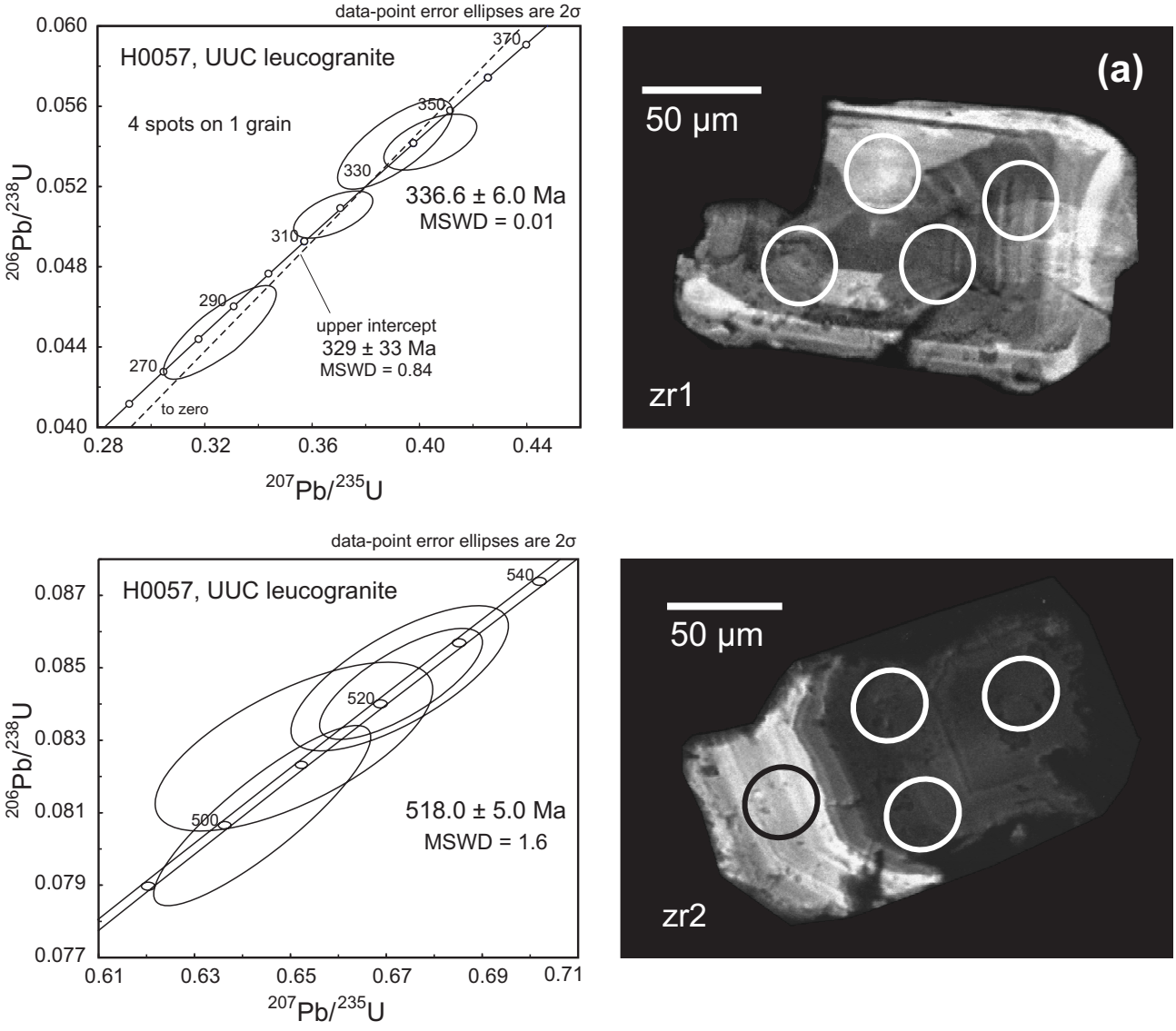

Fig. 11a Position of analyzed points in zircon grains and calculated concordia ages for Unegt Uul Crystalline Complex.

346 ± 12 Ma when forced through zero. The age of 345 ± 2 Ma (Early Carboniferous) is therefore interpreted as the best estimate for the time of granite crystallization.

7.3. Khan Khayrkhan Crystalline Complex

Zircons from the sample R0237 (leucocratic orthogneiss) are clear to cloudy, yellowish, and short to long prismatic with aspect ratios of 1:1 to 3:1 and length of 150–350 μm (Fig. 11c). Twenty-six U-Pb spot analyses were carried out on 24 grains. The U contents range from 100 to *c.* 2000 ppm, while the Th/U ratios vary only from 0.40 to 1.00. Cracks are abundant in most grains. Oscillatory zoning predominates in the CL images. It is well-defined in the outer domains while the inner parts of various grains are characterized by chaotic zoning, an almost uniform grey luminescence, or a combination of both. This is consistent with multiphase zircon growth, in which the earlier zoning was variously obliterated due to a later crystallization event. The latter was dated by 24 spots, which define a discordia with intercepts at 362 ± 17 Ma and around zero. Only 10 of the spots yield concordant results with a concordia age of 363 ± 3 Ma (Tabs 8–9). The high percentage of discordant analyses relates to Pb-loss due to radiation damage. This is supported by a clear correlation between the degree of discordance and the U content (r^2 = 0.60). Two spots yielded older, apparently concordant U-Pb ages of around 529 and 591

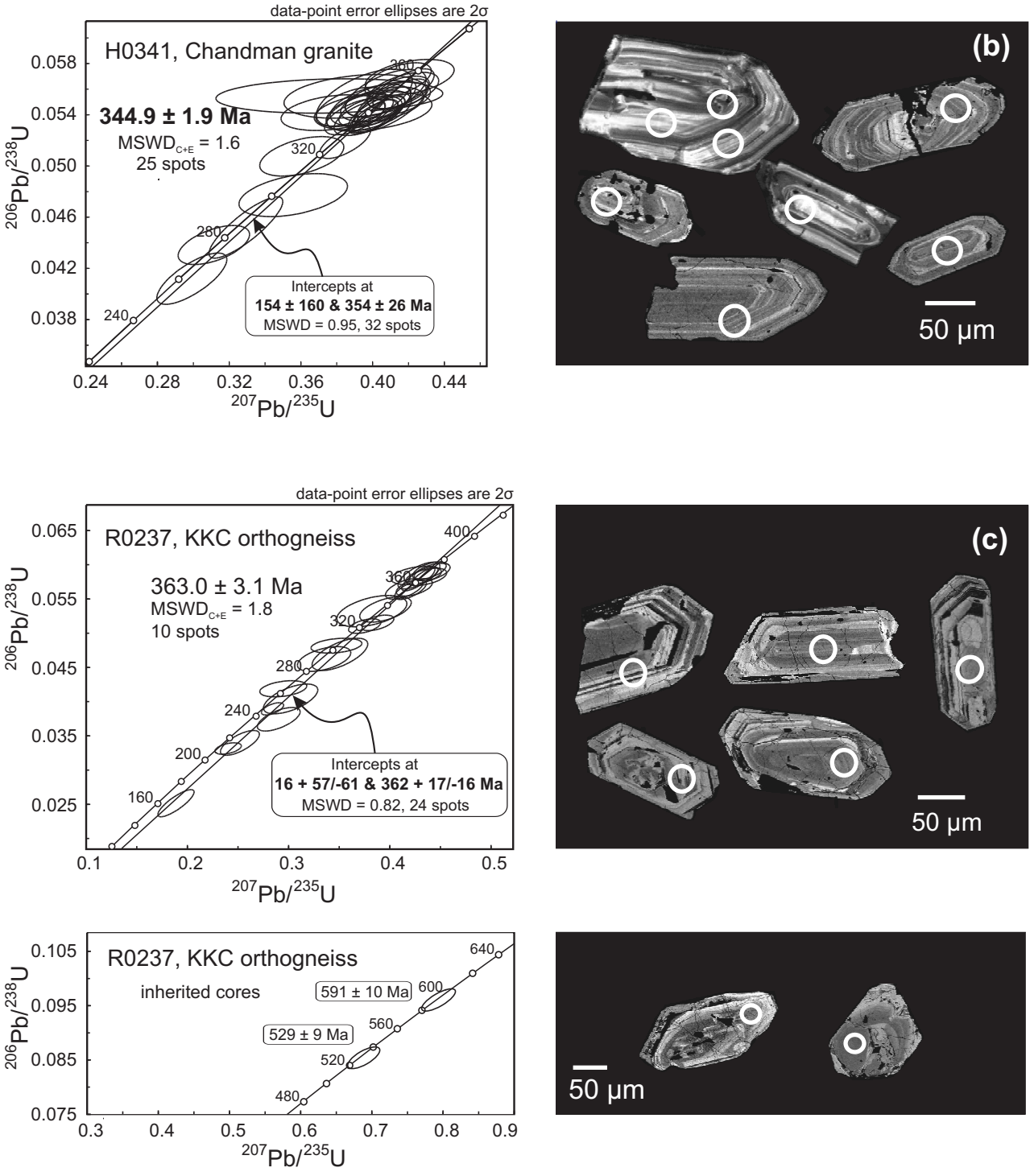

Fig. 11b, c Position of analyzed points in zircon grains and calculated concordia ages for b – Chandman Massif; c – Khan Khayrkhan Crystalline Complex.

Ma, respectively. Thus in most analyzed grains inherited domains have been fully reset during re-crystallization or were not present. The age of 363 ± 3 Ma (the latest Devonian) is interpreted as the time of granite crystallization, while the cores probably record Cambrian inheritance in the granite protolith.

Tab. 6 LA-ICP-MS U, Pb and Th isotope data of dated zircon grains from sample H0057, Unegt Uul Crystalline Complex.

No.	Isotope ratios[c]												Ages (Ma)					
	^{207}Pb[a] (cps)	U[b] (ppm)	Pb[b] (ppm)	Th[b] U	$^{206}Pb/^{204}Pb$	$^{206}Pb^*/^{238}U$	±2σ (%)	$^{207}Pb^*/^{235}U$	±2σ (%)	$^{207}Pb^*/^{206}Pb^*$	±2σ (%)	rho[d]	$^{207}Pb/^{235}U$	±2σ	$^{206}Pb/^{238}U$	±2σ	$^{207}Pb/^{206}Pb$	±2σ
sample H0057, leucogranite																		
zr1-a	837	186	13.1	1.60	1589	0.05411	3.4	0.3917	4.5	0.05250	3.0	0.75	340	12	336	30	307	67
zr1-b	2702	155	10.0	1.52	5030	0.05055	1.9	0.3689	3.3	0.05292	2.6	0.59	318	6	319	21	325	60
zr1-c	1989	172	11.7	1.42	3605	0.05341	2.2	0.3988	3.6	0.05415	2.9	0.60	335	7	341	25	377	65
zr1-d	932	93	5.1	1.03	1719	0.04472	4.3	0.3263	5.3	0.05292	3.1	0.81	282	12	287	31	325	71
zr2-a	12517	390	36	0.94	184	0.08281	2.4	0.6522	3.7	0.05712	2.8	0.65	513	12	510	38	496	62
zr2-b	14545	872	85	0.90	24734	0.08451	1.6	0.6745	2.1	0.05788	1.4	0.75	523	8	523	22	525	31
zr2-c	10150	637	60	0.88	7558	0.08097	2.6	0.6456	3.0	0.05783	1.4	0.88	502	13	506	30	523	31
zr2-d	5204	566	50	0.41	8595	0.08471	2.1	0.6739	2.8	0.05770	1.9	0.73	524	11	523	30	518	42
Plesovi[e]	6982	732	37	0.12	11233	0.05397	1.5	0.3972	1.6	0.05338	0.5	0.74	339	5	340	5	345	11

[a] within-run background-corrected mean ^{207}Pb signal in counts per seconds. [b] U and Pb content and Th/U ratio were calculated relative to GJ-1 reference and are accurate to approximately 10 % due to heterogeneity of the GJ-1 zircon. [c] corrected for background, mass bias, laser induced U-Pb fractionation and common Pb using Stacey and Kramers (1975) model Pb composition. $^{207}Pb/^{235}U$ calculated using $^{207}Pb/^{206}Pb/(^{238}U/^{206}Pb \times 1/137.88)$. Uncertainties are propagated by quadratic addition of within-run precision (2SE) and the reproducibility of GJ-1 (2SD). [d] Rho is the error correlation defined as $err^{206}Pb/^{238}U/err^{207}Pb/^{235}U$. [e] mean and standard deviation (2σ) of 14 analyses of the Plešovice reference zircon (338 ± 1 Ma; Sláma et al. 2008).

8. Discussion

8.1. Metamorphic development

The Altay orogen as a part of Central Asian Orogenic Belt extends from Russia and East Kazakhstan in the west, through Northern China to south-eastern Mongolia in the east. It is composed of Proterozoic to Palaeozoic volcanosedimentary rocks accreted between the Siberian and Tarim continental blocks. The metamorphic rocks in the Mongolian Altay, known only from the Tseel Terrane (Badarch et al. 2002), amalgamated to the SW rim of the Gobi Altay Terrane (see Introduction to this Volume) and the Neoproterozoic metamorphic complex consisting of amphibolite- to granulite-facies metasedimentary and meta-igneous rocks thrusted over the ophiolite in Dariv Range (Dijkstra et al. 2006). In the easternmost Mongolian Altay, three newly described MP-MT metamorphic units – Unegt Uul, Khan Khayrkhan and Chandman Khayrkhan crystalline complexes were tectonically incorporated into geological structures of the Palaeozoic volcanosedimentary complexes of the Gobi-Altay Terrane along its northern margin.

Apparently, despite their close spatial association contrasting metamorphic conditions and geochronological data reveal that the evolution of the three studied crystalline units exhibits distinct features.

The leucogranites and orthogneisses of **Unegt Uul Crystalline Complex** are exposed in a tectonic mélange along the Cenozoic Bogd fault, with dominating strike-slip component of shearing. There were observed no geological relations with adjacent Palaeozoic rocks. Nevertheless, despite the fact that the granite dating detected two contrasting ages, the studied zircons show no signs of polyphase development or of metamorphic overprint. The leucogranite formation took place at 518 ± 5 Ma, which indicates pre-Variscan evolution and corresponds well with ages of Cambrian granites in the Lake Zone Terrane (Hanžl and Aichler eds. 2007). Significance of the measured ages of *c.* 377 Ma remains unclear.

Mineral association in metamorphic rocks of the UUC points to a simple MP–MT event. The P–T conditions in mica schist were estimated to *c.* 640–660 °C and 6–6.7 kbar. The metamorphic conditions estimated from amphibolitic rocks correspond to average temperatures of *c.* 610–760 °C and pressures of 6.2–7.5 kbar.

The exposures of the **Chandman Khayrkhan Crystalline Complex** are spatially related to the Chandman granite Massif, intrusion of which has been dated at 345 ± 2 Ma. Although the metamorphic evolution preceding this granite intrusion remains unconstrained, the character of metamorphism (strong migmatitization), together with the geochemical signature of the granitic plutons themselves points to an evolution within the continental crust realm.

The rocks of **Khan Khayrkhan Crystalline Complex** are systematically exposed in tectonic slices between the unmetamorphosed Lower Carboniferous flysh in the SW and weakly metamorphosed Lower Palaeozoic volcanosedimentary complex in the N. The peak metamorphic assemblage was Bt + Ms + Grt ± St ± Ky and the calculated conditions correspond to temperatures of *c.* 560–650 °C and pressures of 7.2–7.4 kbar for the central parts and *c.* 630–660 °C and 7.5–7.9 kbar for marginal parts of mineral grains in mica schists. Temperatures of *c.* 580 °C and pressures of 6.2 kbar for the central parts

Tab. 7 LA-ICP-MS U, Pb and Th isotope data of dated zircon grains from sample HO341, Chandman Massif.

No.	Isotope ratios[c]												Ages (Ma)					
	^{207}Pb[a] (cps)	U[b] (ppm)	Pb[b] (ppm)	Th/U[b]	$^{206}Pb/^{204}Pb$	$^{206}Pb^*/^{238}U$	±2σ (%)	$^{207}Pb^*/^{235}U$	±2σ (%)	$^{207}Pb^*/^{206}Pb^*$	±2σ (%)	rho[d]	$^{207}Pb/^{235}U$	±2σ	$^{206}Pb/^{238}U$	±2σ	$^{207}Pb/^{206}Pb$	±2σ
sample HO341																		
zr28	3175	109	7	0.63	1322	0.05547	2.0	0.3759	14	0.0492	6.8	0.14	324	45	348	7	155	319
zr26	3469	118	7	0.39	7032	0.05424	2.1	0.3930	3.9	0.0526	1.6	0.55	337	13	340	7	310	73
zr25	94337	293	39	1.00	3593	0.05423	1.8	0.3988	3.6	0.0533	1.6	0.51	341	12	340	6	343	70
zr26	4595	157	9	0.46	3941	0.05575	1.9	0.4145	3.4	0.0539	1.4	0.55	352	12	350	6	368	64
zr20	1572	45	3	0.46	2843	0.05569	2.7	0.4073	4.5	0.0530	1.8	0.60	347	16	349	9	331	82
zr19	6920	218	13	0.70	12675	0.05432	2.4	0.3978	4.9	0.0531	2.1	0.49	340	17	341	8	334	96
zr18	19926	367	24	0.73	488	0.05463	2.3	0.3878	4.1	0.0515	1.7	0.55	333	14	343	8	263	78
zr17	7120	212	13	0.78	7122	0.05405	2.2	0.4022	3.2	0.0540	1.2	0.68	343	11	339	7	369	53
zr16	11453	352	20	0.61	18191	0.05188	2.0	0.3846	3.0	0.0538	1.1	0.68	330	10	326	7	361	50
zr14	13029	261	16	0.55	641	0.05532	3.3	0.3954	5.5	0.0518	2.2	0.60	338	19	347	12	279	101
zr11	10823	320	19	0.66	1905	0.05417	2.1	0.3779	6.3	0.0506	2.9	0.34	326	20	340	7	223	136
zr10	14243	421	21	0.72	2694	0.04120	4.0	0.2992	5.3	0.0527	1.8	0.74	266	14	260	10	315	81
zr7	9658	292	17	0.50	17693	0.05464	2.3	0.4057	3.2	0.0539	1.1	0.72	346	11	343	8	365	49
zr6	17020	389	23	0.61	505	0.05428	2.3	0.4003	6.7	0.0535	3.2	0.34	342	23	341	8	349	143
zr8	7671	241	14	0.51	11688	0.05400	2.1	0.4036	2.9	0.0542	1.0	0.74	344	10	339	7	380	44
zr3	26530	447	29	0.87	1005	0.05544	2.5	0.3903	8.3	0.0511	4.0	0.30	335	28	348	9	244	183
zr1a	6152	180	10	0.50	10443	0.05472	3.1	0.4100	4.3	0.0543	1.5	0.72	349	15	343	11	385	66
zr1b	28833	294	18	0.53	749	0.05385	2.2	0.3902	3.5	0.0526	1.4	0.61	334	12	338	7	310	64
zr42a	24735	264	16	0.48	3466	0.05671	1.9	0.4142	3.7	0.0530	1.5	0.53	352	13	356	7	328	70
zr42b	12942	341	21	0.44	6607	0.05692	2.0	0.4207	4.8	0.0536	2.2	0.42	357	17	357	7	354	99
zr42c	22104	255	16	0.58	841	0.05517	2.1	0.4084	4.8	0.0537	2.2	0.43	348	17	346	7	358	97
zr38	11954	367	19	0.54	4559	0.04773	2.9	0.3557	7.0	0.0541	3.2	0.41	309	21	301	9	374	142
zr41	10428	280	15	0.50	1247	0.05075	2.5	0.3605	5.3	0.0515	2.4	0.47	313	17	319	8	264	108
zr40	26694	315	20	0.66	961	0.05589	2.1	0.4168	3.9	0.0541	1.7	0.53	354	14	351	7	375	75
zr36	20469	277	16	0.54	1299	0.05477	2.4	0.3988	4.6	0.0528	2.0	0.52	341	16	344	8	321	89
zr33	18309	265	15	0.43	2822	0.05384	2.0	0.4005	2.8	0.0539	1.0	0.73	342	10	338	7	369	43
zr31a	17359	218	13	0.44	1072	0.05481	2.0	0.4053	4.7	0.0536	2.1	0.43	346	16	344	7	356	95
zr31b	8072	256	15	0.45	14737	0.05505	2.4	0.4077	3.3	0.0537	1.2	0.71	347	11	345	8	359	52
zr32a	32632	453	27	0.51	9002	0.05602	2.3	0.4172	3.3	0.0540	1.2	0.68	354	12	351	8	372	55
zr32b	26341	357	21	0.59	813	0.05380	2.2	0.3963	3.7	0.0534	1.5	0.58	339	13	338	7	347	68
zr49	49539	277	17	0.72	194	0.04519	4.3	0.3293	5.1	0.0529	1.4	0.85	289	15	285	12	322	62
zr50	6064	405	17	0.65	12167	0.04382	2.8	0.3115	5.2	0.0515	2.2	0.54	275	14	276	8	265	101

and *c.* 570–680 °C and 6.2–6.7 kbar for marginal parts of mineral grains were estimated from amphibolites. This suggests prograde stage of metamorphism during grains growth. This assumption is also in agreement with garnet zoning, whereby the content of *Prp* increases and *Sps* decreases from core to rim.

In the late stage of metamorphic development the metamorphosed volcanosedimentary sequence was intruded by a granitic body. The low temperature contrast and, consequently, heat interchange during syn-metamorphic intrusion prevented growth of contact metamorphic minerals. However, the nests of decomposed alumosilicates may be a relict of a former contact-metamorphic mineral assemblage.

Main magmatic event – formation of the granitic protolith to the orthogneiss – corresponded to the latest Devonian (363 ± 3 Ma). In addition, ages of *c.* 529 and 591 Ma were also obtained in zircon cores from Khan Khayrkhan Crystalline Complex. These may be interpreted as inherited components and point to the presence of pre-Variscan continental crust. Besides the isotopic dating, the palaeontological finds may support the Middle to Late Ordovician age for the sedimentation of the recrystallized limestones in the KKC.

There is some contrast between the chemically relatively evolved granites (slightly metaluminous to peraluminous, medium-K calc-alkaline) of volcanic-arc character and the occurrence of within-plate basalts with tholeiitic affinity and primitive, depleted-mantle like isotopic composition (ε_{Nd}^{550} = +8.4, $^{87}Sr/^{86}Sr_{550}$ = 0.7040, T_{Nd}^{DM} = 0.56 Ga).

Tab. 8 LA-ICP-MS U, Pb and Th isotope data of dated zircon grains from sample RO237, Khan Khayrkhan Crystalline Complex.

No.	Isotope ratios[c]												Ages (Ma)					
	$^{207}Pb^{a}$ (cps)	U^{b} (ppm)	Pb^{b} (ppm)	$\frac{Th^{b}}{U}$	$\frac{^{206}Pb}{^{204}Pb}$	$\frac{^{206}Pb^{*}}{^{238}U}$	±2σ (%)	$\frac{^{207}Pb^{*}}{^{235}U}$	±2σ (%)	$\frac{^{207}Pb^{*}}{^{206}Pb^{*}}$	±2σ (%)	rho[d]	$\frac{^{207}Pb}{^{235}U}$	±2σ	$\frac{^{206}Pb}{^{238}U}$	±2σ	$\frac{^{207}Pb}{^{206}Pb}$	±2σ
sample RO237																		
zr6	133059	1336	93	0.41	182	0.0510	1.7	0.3751	3.5	0.0533	3.0	0.49	323	11	321	5	342	69
zr7	7732	265	16	0.68	12128	0.0535	2.8	0.3957	5.3	0.0537	4.4	0.54	339	18	336	10	357	100
zr35	12676	242	14	0.63	631	0.0469	4.1	0.3507	6.4	0.0542	4.9	0.64	305	20	296	12	380	111
zr14	421031	1450	136	1.00	51	0.0252	6.4	0.1887	7.7	0.0544	4.3	0.83	176	14	160	10	388	97
zr15a	20099	420	24	0.65	217	0.0482	1.8	0.3473	5.9	0.0523	5.6	0.31	303	18	303	6	298	128
zr15b	302113	1631	137	0.85	88	0.0419	2.3	0.2947	6.4	0.0510	6.0	0.36	262	17	264	6	243	139
zr12	621753	1981	211	0.72	158	0.0332	2.0	0.2402	4.4	0.0526	4.0	0.46	219	10	210	4	310	90
zr18	74553	868	54	0.56	287	0.0515	1.8	0.3876	3.5	0.0546	3.0	0.52	333	12	324	6	395	67
zr19a	19487	628	37	0.38	34269	0.0583	1.9	0.4345	2.4	0.0541	1.5	0.77	366	9	365	7	374	35
zr19b	6008	186	11	0.38	9994	0.0591	1.8	0.4391	3.1	0.0538	2.5	0.57	370	11	370	7	365	57
zr20	218534	1487	106	0.57	129	0.0389	1.9	0.2841	3.2	0.0529	2.5	0.59	254	8	246	5	324	58
zr27	3230	116	8	0.98	6789	0.0565	2.2	0.4143	3.7	0.0532	3.0	0.59	352	13	354	8	338	67
zr28	466679	472	140	0.66	128	0.0584	2.7	0.4288	3.9	0.0532	2.8	0.69	362	14	366	10	339	65
zr29	6864	152	15	0.72	11295	0.0855	1.8	0.6889	2.5	0.0584	1.8	0.70	532	13	529	9	546	39
zr30	11169	319	21	0.74	1259	0.0582	1.8	0.4361	3.8	0.0543	3.3	0.46	367	14	365	6	384	75
zr31	11659	406	24	0.43	19515	0.0563	2.0	0.4205	3.1	0.0541	2.3	0.67	356	11	353	7	377	51
zr32	123561	1349	81	0.61	526	0.0404	4.4	0.3020	7.3	0.0542	5.8	0.61	268	19	255	11	380	130
zr33	14379	298	20	0.59	15780	0.0579	2.5	0.4282	3.1	0.0536	1.9	0.79	362	11	363	9	354	44
zr1	12890	237	26	0.88	19940	0.0960	1.7	0.7931	2.4	0.0599	1.7	0.70	593	14	591	10	600	38
zr2	226195	900	100	0.48	155	0.0532	3.5	0.3822	7.4	0.0521	6.5	0.47	329	24	334	12	289	149
zr8	19892	1196	48	0.54	182	0.0340	4.4	0.2519	6.2	0.0538	4.5	0.70	228	14	215	9	362	101
zr9	98063	1010	67	0.65	223	0.0462	3.2	0.3351	6.4	0.0526	5.6	0.50	293	19	291	9	310	127
zr23	52193	706	39	0.87	202	0.0374	3.8	0.2903	6.0	0.0562	4.6	0.63	259	15	237	9	462	102
zr24	5008	176	11	0.79	7606	0.0567	1.8	0.4242	3.4	0.0543	2.9	0.53	359	12	355	6	382	66
zr26	3260	98	6	0.34	3861	0.0584	1.9	0.4261	4.8	0.0529	4.4	0.39	360	17	366	7	324	99
zr4	35499	604	38	0.48	8021	0.0589	1.8	0.4418	3.3	0.0544	2.8	0.53	372	12	369	6	386	63

Tab. 9 Summarized LA-ICP-MS U, Pb and Th isotope ages from Unegt Uul Crystalline Complex, Chandman Massif and Khan Khayrkhan Crystalline Complex.

sample	rock	unit	LI (Ma)	UI (Ma)	AVG (Ma)	map (Ma)	dated event
H0057	granite	UUC		329 ± 33	336 ± 6.0	330	?
H0057	granite	UUC			518 ± 5.0	518	granite crystallization
H0341	granodiorite	GCH	154 ± 160	354 ± 26	344 ± 1.9	345	granite emplacement
R0237	orthogneiss	KKC	160 +57/-61	362 +17/-16	363 ± 3.1	363	granite emplacement
R0237	orthogneiss	KKC		529 ± 9	529 ± 9	530	inheritance
R0237	orthogneiss	KKC		591 ± 10	591 ± 10		inheritance

8.2. Geological interpretation

The southern domains of Mongolia are represented by the Silurian to Carboniferous accretionary complexes and arc-related volcanoclastic rocks (Lamb and Badarch 1997). This characteristic can be also applied to the Gobi-Altay Terrane in the Chandman area. The whole sequence is built by very low grade Ordovician to Devonian sedimentary–volcanosedimentary complex representing relatively deep-basin sediments. This Ordovician and Silurian sedimentation was characterized by an episodic influx of clastic and bioclastic material to the basins towards the Devonian and Carboniferous (Hanžl and Aichler 2007). Within these sedimentary sequences are tectonically incorporated crystalline units of different lithological and metamorphic character. The whole assemblage was intruded by Variscan granitoid rocks of I-type (CHC) and S-type (KKC) affinity during a relatively short time interval between 363 and 354 Ma, respectively 332 Ma.

The spatial and temporal relations suggest the contemporary evolution of the Chandman Khayrkhan and Khan Khayrkhan crystalline units in Late Palaeozoic. However, their position in the frame of orogenic belt was different. The intrusion of the protolith to the Khan Khayrkhan orthogneisses was probably related to an earlier phase of Variscan metamorphism in a volcanic-arc environment. The emplacement of the Chandman Massif followed the peak of Variscan metamorphism in the frame of accretion (collision) of an evolved volcanic arc or a microcontinent.

Both units were accreted together with the Palaeozoic sequences between the Lake Zone Terrane in the N and Tseel Terrane in the S. The more precise interpretation is hampered by Cenozoic imbrication in restraining bends evolved in the Northern Gobi-Altay fault zone.

Noticeable is the temporal (and partly lithologic) analogy with the Tseel Terrane (see Introduction to this Volume). The Tseel Terrane is a complex of Early Devonian volcanic-arc rocks with zircon age of *c.* 400 Ma that were subsequently metamorphosed to amphibolite-facies migmatitic amphibolites and gneisses (Windley et al. 2007). The zircon age from gneisses corresponds to 360.5 ± 1.1 Ma and the Tseel Terrane is interpreted as the root of an arc system (Kröner et al. 2007).

The Unegt Uul Crystalline Complex has a lithologic character as well as a metamorphic and structural evolution completely different from the remaining two units. Geochemical characteristics with geochronological data resemble closely the Burdnii Gol Massif (Hanžl et al. 2007), which belongs to the Lake Zone Terrane. Consequently, the Unegt Uul Crystalline Complex may also show a genetic link to the Lake Zone Terrane and be independent of the Gobi-Altay Terrain. Instead it may represent a rock slice incorporated into the Gobi-Altay Zone tectonically along the Bogd fault.

9. Conclusions

Metamorphic domains exposed in tectonic slices among the Palaeozoic volcanosedimentary sequences were newly described in the Gichigeney Nuruu Mountains (eastern Mongolian Altay) and Unegt Uul range (western Gobi Altay). The area is situated along the northern margin of the Gobi Altay Terrane, close to boundary with the Lake Zone Terrane. Unegt Uul, Chandman Khayrkhan and Khan Khayrkhan crystalline complexes were defined on the basis of distinct geological position, lithology, metamorphic conditions and age.

Unegt Uul Crystalline Complex represents a tectonic mélange closely associated with the Bogd Fault system. The Complex consists of prevailing granites to leucogranites with mica schists representing the roof pendants of the granitic intrusions and tectonically assembled fragments of basic rocks. The metamorphic conditions estimated for the amphibolites correspond to *c.* 610 °C and 6 kbar in the cores and *c.* 650–760 °C and 6–7 kbar in the marginal parts of the mineral grains. Mica schists yielded T = *c.* 640–660 °C and P = 6.0–6.7 kbar.

Chandman Khayrkhan Crystalline Complex is a metamorphic unit markedly affected by the Chandman granite intrusion. It is represented by orthogneisses and migmatites with lenses of amphibolite and sporadic calc-silicate bodies. The metamorphic development featured a HT event with subsequent retrogression under amphibolite-facies conditions perceptible from the mineral association of the calc-silicate rocks. The monotonous mineral assemblages of the rocks hamper any more specific determination of the P–T metamorphic conditions.

Khan Khayrkhan Crystalline Complex is a narrow tectonic slice sandwiched in between the Lower and Upper Palaeozoic sedimentary sequences represented by orthogneisses with lenses and layers of amphibolites, mica schists, paragneisses and recrystallized limestones. The P–T conditions correspond to *c.* 560– 650 °C and 6.2–7.4 kbar for the central parts and *c.* 630–680 °C, 6.4–8 kbar for marginal parts of mineral grains.

Laser ablation ICP-MS U-Pb dating suggests a formation of the UUC leucogranites at *c.* 518 Ma. Intrusion of granitic protolith to the KKC orthogneiss took place at 363 ± 3 Ma, while inherited zircon cores point to earlier zircon crystallization events at *c.* 529 and 591 Ma. The rocks of CHC remain undated, the only time information having been provided by dating of the Chandman Massif granites themselves (345 ± 2 Ma). These data confirm the Variscan tectonometamorphic activity inside the Gobi-Altay and Lake Zone terranes in the Southern Domain of Mongolia.

Acknowledgements. The presented data have been gathered within the framework of the project Zamtyn Nuruu-50 funded by the International Development Cooperation of the Czech Republic. It could not materialize without neither the logistic support by J. Holák a Z. Novotný for the technical background provided by Mongolian drivers and students. We are indebted to V. Erban from the Radiogenic Isotopes Lab of the Czech Geological Survey, who acquired the Sr–Nd isotopic data and to R. Čopjaková with R. Škoda from the Joint Electron Microanalysis Laboratory of the Masaryk University and the Czech Geological Survey in Brno, who were responsible for microprobe analysis and CHIME monazite dating. We are also grateful to M. Janák and A. Proyer for helpful reviews. Last but not least, the careful editorial handling by W. S. Faryad helped us to improve significantly the ideas expressed in this text.

Electronic supplementary material. The Tabs 1–2, as well as GPS coordinates of the studied samples, are available online at the Journal web site (http://dx.doi.org/10.3190/jgeosci.027).

References

Badarch G, Tomurtogoo O (2001) Tectonostratigraphic Terranes of Mongolia. Gondwana Research 4: 143–144

Badarch G, Cunningham WD, Windley BF (2002) A new terrane subdivision for Mongolia: implications for the Phanerozoic crustal growth of central Asia. J Asian Earth Sci 20: 87–100

Baljinnyam I, Bayasgalan A, Borisov BA, Cisternas A, Dem'yanovich MG, Ganbaatar L, Kochetkov VM, Kurushin RA, Molnar P, Philip H, Vashchilov YY (1993) Ruptures of major earthquakes and active deformation in Mongolia and its surroundings: Geol Soc Am Memoir 181: pp 1–62

Bayasgalan A (1999) Active tectonics of Mongolia. Unpublished PhD. Thesis, Trinity College Cambridge, pp 1–180

Batchelor RA, Bowden P (1985) Petrogenetic interpretation of granitoid rock series using multicationic parameters. Chem Geol 48: 43–55

Bhattacharya A, Mohanty L, Maji A, Sen SK, Raith M (1992) Non-ideal mixing in the phlogopite–annite binary: constraints from experimental data on Fe-Mg partitioning and a reformulation of the biotite-garnet thermometer. Contrib Mineral Petrol 111: 87–93

Boynton WV (1984) Cosmochemistry of the rare earth elements: meteorite studies. In: Henderson P (ed) Rare Earth Element Geochemistry. Elsevier, Amsterdam, pp 63–114

Buchan C, Pfander J, Kröner A (2002) Timing of accretion and collisional deformation in the Central Asian Orogenic Belt: implications of granite geochronology in the Bayankhongor ophiolite zone. Chem Geol 192: 23–45

Buriánek D, Hanžl P, Hrdličková K (in press) Tourmaline in migmatites, pegmatites and quartz veins of the Chandman Massif (Gobi Altay, Western Mongolia), example of fractionation of anatectic melt. Mongolian Geoscientist

Cunningham WD, Dijkstra A, Howard J, Quarles A, Badarch G (2003) Active intraplate strike-slip faulting and transpressional uplift in the Mongolian Altai. In: Storti F, Holdsworth RE, Salvini F (eds) Intraplate Strike-slip Deformation Belts. Geol Soc London Spec Pub 210: pp 65–87

Dergunov AB (ed) (2001) Tectonics, Magmatism, and Metallogeny of Mongolia. Routledge, London, pp 1–288

Dijkstra AH, Brouwer FM, Cunningham WD, Buchan C, Badarch G, Mason PRD (2006) Late Neoproterozoic proto-arc ocean crust in the Dariv Range, Western Mongolia: a supra-subduction zone end-member ophiolite. J Geol Soc, London 163: 363–373

Economos R, Hanžl p, Hrdličková K, Buriánek D, Said LO, Gerdes A (in press) Geochemical and structural constraints on the magmatic history of the Chandman Massif of the eastern Mongolian Altay Range, SW Mongolia. J Geosci

Ferry JM, Spear FS (1978) Experimental calibration of the partitioning of Fe and Mg between biotite and garnet. Year Book – Carnegie Institution of Washington 76: 579–581

Gerdes A, Zeh A (2006) Combined U-Pb and Hf isotope LA-(MC-) ICP-MS analyses of detrital zircons: comparison with SHRIMP and new constraints for the provenance and age of an Armorican metasediment in Central Germany. Earth Planet Sci Lett 249: 47–62

Gerdes A, Zeh A (2008) Zircon formation versus zircon alteration – new insights from combined U-Pb and Lu-Hf in-situ La-ICP-MS analyses of Archean zircons from the Limpopo Belt. Chem Geol, doi 10.1016/j.chemgeo.2008.03.005

Guidotti CV (1984) Micas in metamorphic rocks. In: Bailey SW (ed) Micas. Mineralogical Society of America and Geochemical Society Reviews in Mineralogy and Geochemistry 13, Washington, pp 357–467

Hanžl p, Buriánek D, Hrdličková K, Aichler J, Gerdes A, Byambasuren D (2007) Granitoid massifs of the Zamtyn Nuruu area, SW Mongolia. In: Breiter K (ed) Proceedings of the 3rd Meeting of the Czech Geological Society, Volary, 19–22 September 2007, pp 27 (in Czech)

Hanžl P, Aichler J (eds) (2007) Geological Survey of the Mongolian Altay at a scale 1:50,000 (Zamtyn Nuruu – 50), Final Report, pp 1–389

Helo C, Hegner E, Kröner A, Badarch G, Tomurtogoo O, Windley BF, Dulski P (2006) Geochemical signature of Paleozoic accretionary complexes of the Central Asian Orogenic Belt in South Mongolia: constraints on arc environments and crustal growth. Chem Geol 227: 236–257

Holland TJB, Powell R (1985) An internally consistent thermodynamic dataset with uncertainties and correlations: 2. Data and results. J Metamorph Geol 3: 343–370

Holland TJB, Powell R (1998) An internally consistent thermodynamic data set for phases of petrological interest. J Metamorph Geol 16: 309–343

Jacobsen SB, Wasserburg GJ (1980) Sm–Nd isotopic evolution of chondrites. Earth Planet Sci Lett 50: 139–155

Jahn BM, Capdevila R, Liu D, Vernon A, Badarch G (2004) Sources of Phanerozoic granitoids in the transect Bayanhongor–Ulaan Baatar, Mongolia: geochemical and Nd isotopic evidence, and implications for Phanerozoic crustal growth. J Asian Earth Sci 23: 629–653

Kepezhinskas PK, Kepezhinskas KB, Pukhtel IS (1991) Lower Paleozoic oceanic crust in Mongolian Caledonides; Sm-Nd isotope and trace element data. Geophys Res Lett 18: 1301–1304

Khain EV, Bibikova EV, Kröner A, Zhuravlev DZ, Sklyarov EV, Fedotova AA, Kravchenko-Berezhnoy IR (2002) The most ancient ophiolite of the Central Asian fold belt: U-Pb and Pb-Pb zircon ages for the Dunzhugur Complex, Eastern Sayan, Siberia, and geodynamic implications. Earth Planet Sci Lett 199: 311–325

Khain EV, Bibikova EV, Salnikova EB, Kröner A, Gibsher AS, Didenko AN, Degtyarev KE, Fedotova AA (2003) The Palaeo-Asian ocean in the Neoproterozoic and Early Palaeozoic: new geochronologic data and palaeotectonic reconstructions. Precambr Res 122: 329–358

Kovach VP, Jian P, Yarmolyuk VV (2005) Magmatism and geodynamics of early stages of the Paleoasian ocean formation: geochronological and geochemical data on ophiolites of the Bayan-Khongor zone. J Earth Sci 404: 1072–1077

Kozakov IK, Liu D, Terenteva LB, Lebedev VI, Kovalenko VI (2005) Magmatism and geodynamics of early stages of the Paleoasian Ocean formation: geochronological and geochemical data on ophiolites of the Bayan-Khongor Zone. J Earth Sci 404: 1072–1077

Kröner A, Windley BF, Badarch G, Tomurtogoo O, Hegner E, Jahn BM, Gruschka S, Khain EV, Demoux A, Wingate MTD (2007). Accretionary growth and crust-formation in the Central Asian Orogenic Belt and comparison with the Arabian-Nubian shield. In: Hatcher RD Jr, Carlson MP, McBride JH, Martínez Catalán JR (eds), 4-D Framework of Continental Crust. Geol Soc Am Memoir 200: pp 181–209.

Lamb MA, Badarch G (1997) Paleozoic sedimentary basins and volcanic-arc systems of southern Mongolia: new stratigraphic and sedimentologic constraints. Int Geol Rev 39: 542–576

Leake BE, Woolley AR, Arps CES, Birch WD, Gilbert MC, Grice JD, Hawthorne FC, Kato A, Kisch HJ, Krivovichev VG, Linthout K, Laird J, Mandarino JA, Maresch WV, Nickel EH, Rock NMS, Schumacher JC, Smith DC, Stephenson NCN, Ungaretti L, Whittaker EJW, Youshi G (1997) Nomenclature of amphiboles: report of the Subcommittee on amphiboles of the International Mineralogical Association, Commission on new minerals and mineral names. Amer Miner 82: 1019–1037

Lee SM, Holdaway MJ (1977) Significance of Fe-Mg cordierite stability relations on temperature, pressure, and water pressure in cordierite granulites. In: Heacock JG (ed) The Earth's Crust; Its Nature and Physical Properties. Geophys Monograph 20, AGU Washington pp 79–94

Liew TC, Hofmann AW (1988) Precambrian crustal components, plutonic associations, plate environment of the Hercynian Fold Belt of Central Europe: indications from a Nd and Sr isotopic study. Contrib Mineral Petrol 98: 129–138

Lugmair GW, Marti K (1978) Lunar initial $^{143}Nd/^{144}Nd$: differential evolution line of the lunar crust and mantle. Earth Planet Sci Lett 39: 349–357

Maniar PD, Piccoli PM (1989) Tectonic discrimination of granitoids. Geol Soc Am Bull 101: 635–643

Marinov NA, Zonenshain LP, Blagonravov VA (eds) (1973) Geologija Mongolskoi narodnoi respubliky. Nedra, Moscow, pp 1–582 (in Russian)

Meschede M (1986) A method of discriminating between different types of mid-ocean ridge basalts and continental tholeiites with the Nb–Zr–Y diagram. Chem Geol 56: 207–218

Mielke P, Winkler HGF (1979) Eine bessere Berechnung der Mesonorm für granitische Gesteine. Neu Jb Mineral, Mh 471–480

Míková J, Denková P. (2007) Modified chromatographic separation scheme for Sr and Nd isotope analysis in geological silicate samples. J Geosci 52: 221–226

Molnar P, Tapponnier P (1975) Cenozoic tectonics of Asia: effects of a continental collision: features of recent continental tectonics in Asia can be interpreted as results of the India–Eurasia collision. Science 189: 419–426

Montel JM, Foret S, Veschambre M, Nicollet C, Provost A (1996) Electron microprobe dating of monazite. Chem Geol 131: 37–53

Mossakovsky AA, Ruzhentsev SV, Samygin SG, Kheraskova TN (1994) Central Asian fold belt; geodynamic evolution and formation history. Geotectonics 27: 445–474.

Pearce JA, Harris NW, Tindle AG (1984) Trace element discrimination diagrams for the tectonic interpretation of granitic rocks. J Petrol 25: 956–983

Peccerillo A, Taylor SR (1976) Geochemistry of Eocene calc-alkaline volcanic rocks from the Kastamonu area, Northern Turkey. Contrib Mineral Petrol 58: 63–81

Perchuk LL, Lavrenteva IV (1983) Experimental investigation of exchange equilibria in the system cordierite-garnet-biotite. In: Saxena SK (ed) Kinetics and Equilibrium in Mineral Reactions. Springer-Verlag, Berlin, pp 199–239

Pin C, Zalduegui JFS (1997) Sequential separation of light rare-earth elements, thorium and uranium by miniaturized extraction chromatography: application to isotopic analyses of silicate rocks. Anal Chim Acta 339: 79–89

Pin C, Briot D, Bassin C, Poitrasson F (1994) Concomitant separation of strontium and samarium-neodymium for isotopic analysis in silicate samples, based on specific extraction chromatography. Anal Chim Acta 298: 209–217

Powell R, Holland TJB (1985) An internally consistent thermodynamic dataset with uncertainties and correla-

tions: 1. Method and a worked example, J Metamorph Geol 3: 327–342

Rauzer AA, Zhanchiv DI, Golyakov VI, Ykhina IF, Ivanov IG, Tsukernik AB, Afonin VV, Smirnov IG, Bykhover VI, Kravtsev AV, Baatarkhuyag A, Skoryukin MI, Khodikov IV, Mantsev NV, Okaemov SV, Mischin VA, Enkhsajkhan T (1987) Report on results of geological mapping on scale 1:200,000 in the south-western part of Mongolian Altay in 1983–1986, Mongolian National Republic. Tekhnoexport, Moscow, pp 1–352 (in Russian)

Ravna EK (2000) Distribution of Fe^{2+} and Mg between coexisting garnet and hornblende in synthetic and natural systems: an empirical calibration of the garnet–hornblende Fe–Mg geothermometer. Lithos 53: 265–277

Sengör AC, Natalin BA, Burtman VS (1993) Evolution of the Altaid tectonic collage and Paleozoic crustal growth in Eurasia. Nature 364: 299–306

Shand SJ (1943) Eruptive Rocks. Their Genesis, Composition, Classification, and Their Relation to Ore-Deposits with a Chapter on Meteorite. 2nd Edition. John Wiley & Sons, New York, pp 1–444

Sláma J, Košler J, Condon D J, Crowley J L, Gerdes A, Hanchar J M, Horstwood M S A, Morris G A, Nasdala L, Norberg N, Schaltegger U, Schoene B, Tubrett M N, Whitehouse M J (2008) Plešovice zircon – a new natural reference material for U-Pb and Hf isotopic microanalysis. Chem Geol 249: 1–35

Stacey J, Kramers J (1975) Approximation of terrestrial lead isotope evaluation by a two-stage model. Earth Planet Sci Lett 26: 207–221

Steiger RH, Jäger E (1977) Subcommission on Geochronology; convention on the use of decay constants in geo- and cosmochronology. Earth Planet Sci Lett 36: 359–362

Streckeisen A, Le Maitre RW (1979) A chemical approximation to the modal QAPF classification of the igneous rocks. Neu Jb Mineral, Abh 136: 169–206

Sun SS, McDonough WF (1989) Chemical and isotopic systematics of oceanic basalts: implications for mantle composition and processes. In: Saunders AD, Norry MJ (eds) Magmatism in Ocean Basins. Geol Soc London Spec Pub 42: pp 313–345

Thompson AB (1976) Mineral reactions in pelitic rocks: II. Calculation of some P-T-X (Fe-Mg) phase relations. Amer J Sci 276: 425–454

Thompson JB Jr, Norton SA (1968) Paleozoic regional metamorphism in New England and adjacent areas. In: Zen E, White WS, Hadley JB, Thompson JB (eds) Studies of Appalachian Geology, Northern and Maritime. Interscience Publishers, New York, pp 319–327

Tracy RJ (1982) Compositional zoning and inclusions in metamorphic minerals. In: Ferry JM (ed) Characterization of Metamorphism Through Mineral Equilibria. Rev Mineral Geochem 10: 355–397

Vassallo R, Ritz J, Braucher R, Jolivet M, Carretier S, Larroque C, Chauvet A, Sue C, Todbileg M, Bourles D (2007) Transpressional tectonics and stream terraces of the Gobi-Altay, Mongolia. Tectonics 26, TC5013, doi:10.1029/2006TC002081.

Windley BF, Kröner A, Guo J, Qu G, Li Y, Zhang C (2002) Neoproterozoic to Paleozoic geology of the Altai orogen, NW China: new zircon age data and tectonic evolution. J Geol 110: 719–737

Windley BF, Dmitriy A, Wenjiao X, Kröner A, Badarch G (2007) Tectonic models for accretion of the Central Asian Orogenic Belt. J Geol Soc, London 164: 31–47

Xiao XC, Tang YQ, Feng YM, Zhu BQ, Li JY, Zhao M (1992) In: Tectonic Evolution of the Northern Xinjiang and Its Adjacent Region, Geological Publishing House, Beijing (1992), pp 1–180 (in Chinese, with English abstract)

Yarmolyuk VV, Kovalenko VJ (2001) Middle Palaeozoic continental margin magmatism of Mongolia. In: Dergunov AB (ed) Tectonics, Magmatism, and Metallogeny of Mongolia. Routledge, London, pp 95–127

Journal of Geosciences, 53 (2008), 167–180 DOI: 10.3190/jgeosci.026

Original paper

The Early Cretaceous volcanic activity in the western part of the Gobi-Altay rift (Shiliin Nuruu, SW Mongolia)

David BURIÁNEK[1*], Pavel HANŽL[1], Vojtěch ERBAN[1], Helena GILÍKOVÁ[1], Khasbar BOLORMAA[2]

[1] *Czech Geological Survey, Klárov 3, 118 21 Prague 1, Czech Republic; david.burianek@geology.cz*
[2] *Geological Investigation Center, Songino Khayrkhan District, PO Box 37/307, Ulaanbaatar, Mongolia*
[*] *Corresponding author*

The Cretaceous continental sedimentation in SW Mongolia was commonly accompanied by volcanic activity. Bimodal association of the Cretaceous Khulsan Gol Formation is represented mostly by calc-alkaline and rare alkaline volcanic rocks (basaltic andesite, trachybasalt to trachyandesite lavas or tuffs with lahars). The lavas were extruded mainly subaerially, although locally there is a subaqueous component present corresponding to final phases of Mesozoic sedimentation in the Gobi-Altay rift zone. Variations in chemical and isotopic composition reflect crustal assimilation coupled with fractional crystallization of parental magma generated by melting of lower lithosphere and/or uppermost asthenospheric mantle. These within-plate volcanic rocks can be explained as initial stages of Cenozoic magmatic activity in the Mongolia.

Keywords: Cretaceous; calc-alkaline volcanites; Gobi-Altay; Sr-Nd isotopes; petrogenesis; Mongolia
Received: 8 April 2008; accepted 11 June 2008; handling editor: E. Jelínek

The online version of this article (doi: 10.3190/jgeosci.026) contains supplementary electronic material.

1. Introduction

Volcanic activity in Mongolia has continued almost without interruption for the past 160 Ma, being concentrated within two periods, namely the Early Mesozoic and the Late Mesozoic–Cenozoic (Yarmolyuk and Kovalenko 2001).

The Early Mesozoic (Triassic–Early Jurassic) igneous period was largely influenced by continental collision during the closure of Mongolsk–Ochotsk marine basin (in the NE part of today's Mongolia). System of troughs infilled with terrigenous, coal-bearing molasse developed during the Triassic–Jurassic (Yanshin 1976) and they are interpreted as foreland basins. However, relations to strike-slip faulting could not be excluded (Hendrix et al. 1996). Extensional tectonics was accompanied by Early Mesozoic granitoid intrusions in eastern Mongolia. The only terrigenous sediments of this age are preserved in western Mongolia (Yarmolyuk and Kovalenko 2001).

Late Mesozoic–Cenozoic igneous period was related to extensional tectonics, which is one of the most striking features in the N and NE parts of the North China Block and the S part of the Variscan Central Asian Orogenic Belt (e.g. Hendrix et al. 1992). Foreland-style basins (Graham et al. 2001), rift zones (Yanshin 1976), system of grabens and graben–synclines were formed in the Late Mesozoic times (Late Jurassic–Early Cretaceous). The tectonic depressions formed the sites of formation of lava plateaux, as well as volcanic ring structures and subvolcanic intrusions composed of rhyolites, granitoids and basaltoids (Yarmolyuk and Kovalenko 2001).

The end of the Early Cretaceous saw the progressive cessation of tectonic processes throughout the whole of Mongolia and the Late Cretaceous–Palaeogene is a period of development similar to a platform evolution (Yanshin 1976). Within-plate magmatic activity in the southwestern Mongolia started during Mesozoic and culminated in the Cenozoic (Barry et al. 2003). The majority of the Late Mesozoic volcanic rocks tend to be localised within the Gobi-Altay rift (Yarmolyuk 1986). The Gobi-Altay rift zone can be divided into three segments: eastern, central and western, which to some extent differ in their subsequent history of magmatism. Eastern segment is Late Jurassic to Middle Cretaceous, central one is Late Jurassic to Late Cretaceous and western is Early to Late Cretaceous (Yarmolyuk and Kovalenko 2001).

Numerous basaltic lava sheets and body of lahar with prevailing acid fragments (rhyolite, granitoids) belonging to the western part of the Gobi-Altay rift zone are well exposed in the area of Shillin Nuruu and Khar Argalantyn Nuruu Mts. They are part of the Upper Jurassic to Lower Cretaceous continental sediments preserved in the separate block along the southern rim of Valley of Lake west of the Boon Tsagaan Nuur, Gobi Altay Aymag (SW Mongolia).

The interpretation of textural features in the Late Cretaceous volcanic rocks, their close relation to palaeontologically dated sediments, as well as newly obtained

whole-rock geochemical and isotopic data contribute to understanding of the origin of volcanic rocks in the intracontinental rift environment.

2. Geology

The Upper Jurassic–Lower Cretaceous sediments west of lake Boon Tsagaan Nuur are exposed along the southern margin of intermontane depression Ulaan Shalyn Khooloi, which separates the Neoproterozoic to Lower Palaeozoic complexes of the Lake Zone in the south from the Proterozoic metamorphic rocks of the Byadrag Terrane in the north.

Most of the Upper Mesozoic sequences in the area are exposed in a flat syncline in the Shiliin Nuruu Mts. and at Samoadanba Uul Mt. (Fig. 1). Minor exposures are bound to the slopes of the Erdene Uul Mt. in the west and in surroundings of river Khulsni Gol in the east. The syncline is built by continental sediments and terrestrial volcanic rocks developed in the western part of the Late Mesozoic Gobi-Altay rift zone (Yarmolyuk 1983, 1986; Kovalenko et al. 1995). There are preserved transgressive contacts of Upper Jurassic–Lower Cretaceous sediments with the underlying Precambrian–Palaeozoic sequences. Nevertheless, there are often rather gradual depositional transitions (Fig. 2) between the individual Mesozoic formations (Hanžl et al. 2007): Toromkhon, Undurukhin, Anday Khudag and Khulsan Gol (e.g. Sinica 1993).

The Upper Jurassic **Toromkhon Fm.** consists of poorly to extremely poorly sorted, usually red conglomerates, breccias and sandy conglomerates. They were interpreted as sediments of proximal part of alluvial fans (Gilíková et al. 2007).

The Lower Cretaceous **Undurukhin Fm.** was described in the area of the Lake Zone and Mongolian Altay by Ivanov in Rauzer et al. (1987) based on previous studies of the Mongolian Mesozoic basin undertaken by Martinson (1982). The sediments of the Undurukhin Fm. (Berriasian to Valanginian) form cycles up to 13 m thick consisting of conglomerates grading upwards into sandstones, mudstones and marls. They rest locally unconformably upon the pre-Mesozoic basement. Contact with the Toromkhon Fm. in the footwall is transitional with local wash-outs. The formation was presumably deposited in a fluvial and shallow lacustrine environment

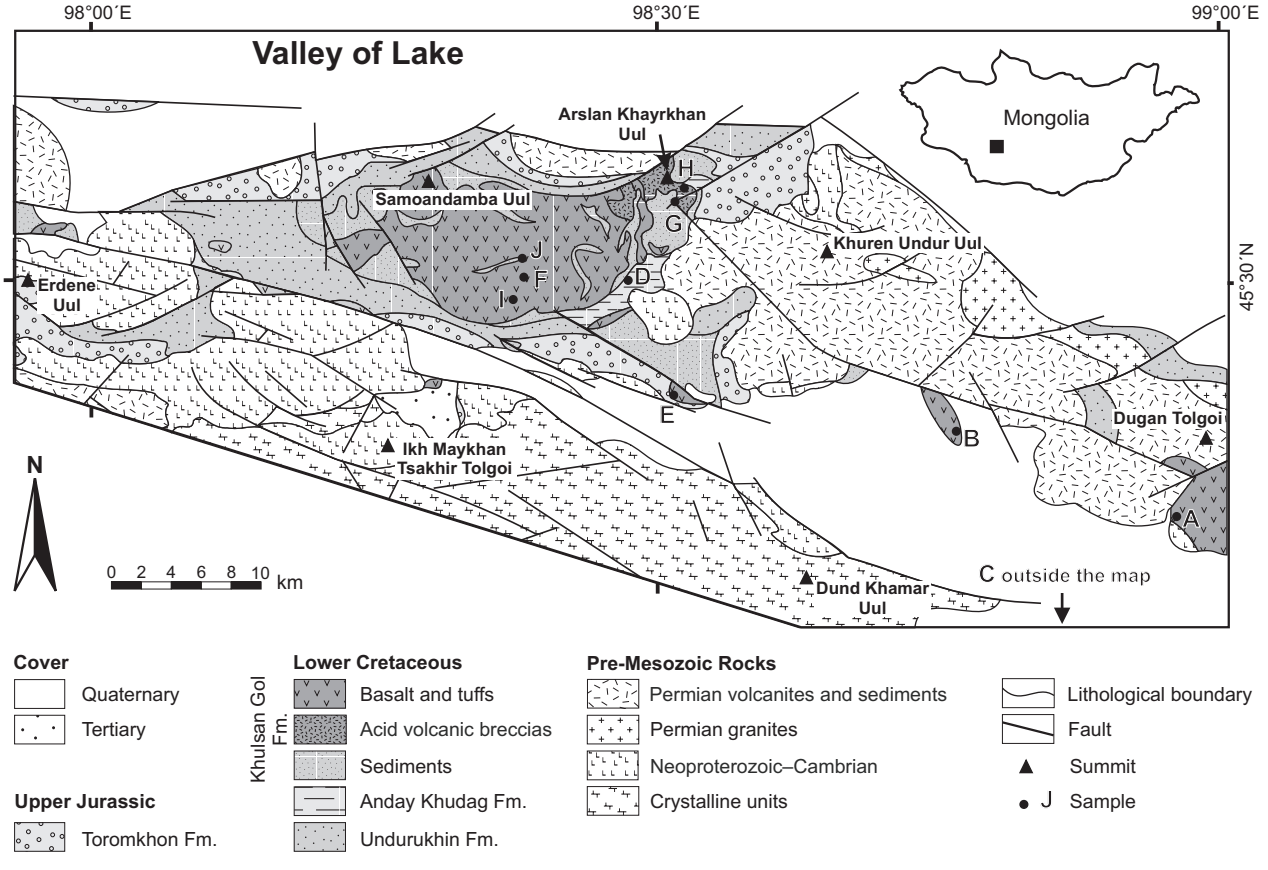

Fig. 1 Simplified geological outline of the Shiliin Nuruu area based on new geological mapping (Hanžl et al. 2007). Geochemical samples labelled by their ID (same as in tables).

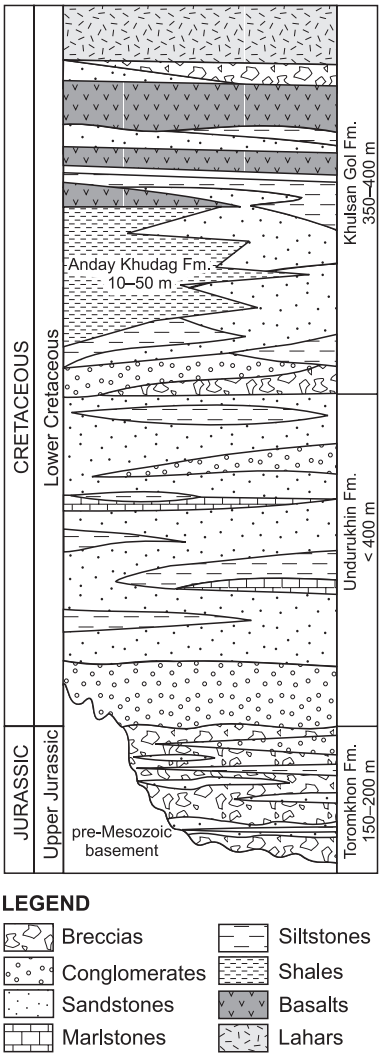

Fig. 2 Summary stratigraphic column for the studied area modified from Hanžl et al. (2007).

(Gilíková et al. 2007). According to petrography, the sediments of the Undurukhin Fm. were derived mainly from Permian volcanic rocks.

The **Anday Khudag Fm.** (Hauterivian to Barremian) is characterized by variable and commonly small thickness (first tens of metres). The sediments of the formation are mostly exposed as a finer facies (mudstones and siltstones with fine-grained conglomerates and sandstones on the base) inside the Khulsan Gol Formation.

The **Khulsan Gol Fm.** (Aptian–Albian) has a volcanosedimentary character and represents the uppermost part of the Mesozoic sequence in this segment of the Gobi-Altay rift. The thickness of the Khulsan Gol Fm. is estimated to 350–400 m in the area of the Arslan Khayrkhan Uul Mt. The main constituents are sandstones alternating with marlstones and mudstones, accompanied by sporadic intercalations of coal, conglomerates and breccias. Shallow lacustrine environment is supposed to have prevailed during deposition of the formation; the accumulations of bivalves in the sandstones probably indicate storm events. The conglomerates, breccias, and massive sandstones are sediments of alluvial fan. The most usual direction of the material transport was from north to south. According to petrography, the sediments of the Khulsan Gol Fm. were derived mainly from the Permian volcanic and plutonic rocks. The evolution of the sedimentary basin was terminated by volcanic activity documented by basaltic lava flows and sills with thickness up to 30 meters. Lahar and coarse-grained volcanic breccia layers are composed of acid to intermediate rocks (rhyolite, granitoids). They are up to 100 m thick and are exposed in the uppermost part of the Khulsan Gol Fm. in the Arslan Khayrkhan Uul Mt. Basalts rarely enclose xenoliths of sediments; mantle and lower crustal xenoliths are missing. Marlstones and mudstones are baked on the contacts with basaltic flow, forming zones only several centimetres thick. No structures similar to a volcano morphology were found in the area; the character of lavas instead resembles plateau basalts.

3. Analytical methods

Whole-rock samples were collected in the frame of the Development cooperation project of the Czech Republic "Geological mapping of the Mongolian Altay at a scale of 1 : 50,000". Nine were sampled in the area of the Shilin Nuruu (Fig. 1); one was located on the SE slopes of the Gichigeney Nuruu Mts. *c.* 60 km S of the Arslan Khayrkhan Uul.

The only wet major-element whole-rock geochemical analyses performed under standard conditions (Hanžl et al. 2007) at the Central Geological Laboratory in Ulaanbaatar are available for two samples. Eight rock powders were analysed in the Acme Analytical Laboratories, Vancouver, Canada. Major-element contents were determined using ICP ES and trace elements by ICP MS. The whole-rock analyses were interpreted by the GCDkit software (Janoušek et al. 2006).

Strontium and neodymium isotope analyses were performed at the Radiogenic Isotope Laboratory of the Czech Geological Survey. Samples were dissolved using a combined HF–HCl–HNO_3 attack. Sr and bulk REE were separated by cation-exchange chromatography using BioRad AG-W X8 resin loaded into quartz columns. Nd was further separated on quartz columns with Biobeads S-X8 coated with HDEHP (Richard et al. 1976). Isotopic composition was analysed on Finnigan MAT 262 thermal ionization mass spectrometer in dynamic mode using a double Re filament assembly for both Sr and Nd. The NBS 987 reference material yielded a long-time average

$^{87}Sr/^{86}Sr$ of 0.710244 (1σ = 0.000013, 27 values), while the Nd La Jolla average $^{143}Nd/^{144}Nd$ was 0.511852 (1σ = 0.000007, 25 values). The decay constants applied to age-correct the isotopic ratios are from Steiger and Jäger (1977) (Sr) and Lugmair and Marti (1978) (Nd). The ε_i^{Nd} values were obtained using Bulk Earth parameters of Jacobsen and Wasserburg (1980).

Electron microprobe analyses (EMPA) were performed on the instrument Cameca SX-50, in the Joint Laboratory of Electron Microscopy and Microanalysis of the Masaryk University and the Czech Geological Survey (Brno, Czech Republic) by analysts R. Čopjaková and R. Škoda. Wavelength-dispersion mode with a beam diameter of 4–5 μm, an accelerating potential of 15 kV and sample current of 20 nA were used for Si, Al, Ti, Fe, Mn, Mg, Ca, Na and K. Higher current of 40 nA was employed for Zn, F and P; counting time was 20 s for all elements. The following standards were used (K X-ray lines): diopside (Si, Ca), kyanite (Al), fayalite (Fe), rutile (Ti), pyrope (Mg), spessartine (Mn), albite (Na), orthoclase (K), fluorapatite (P, F) and gahnite (Zn).

4. Geology and petrology of volcanic rocks

Cretaceous volcanic rocks in the Shiliin Nuruu are stratigraphically related to the uppermost part of the Khulsan Gol Fm. Three groups of volcanic rocks were distinguished here according to volcanic character and petrography: 1 – massive basalt to basaltic andesite lava sheets and sills; 2 – basaltic to trachyandesitic tuffs; 3 – volcanic breccias, lahars.

4.1. Basalt to basaltic andesite

Lava sheets and sills composed of massive basalt to basaltic andesite are the most common volcanic forms. At least three main lava flows alternate with siltstones, marlstones and sandstones in the studied area. Thickness of individual lava flows reaches up to 30 m; the sills are up to 20 m thick. The basalts are massive, often with columnar jointing (Fig. 3a–b). The flows of basalt into

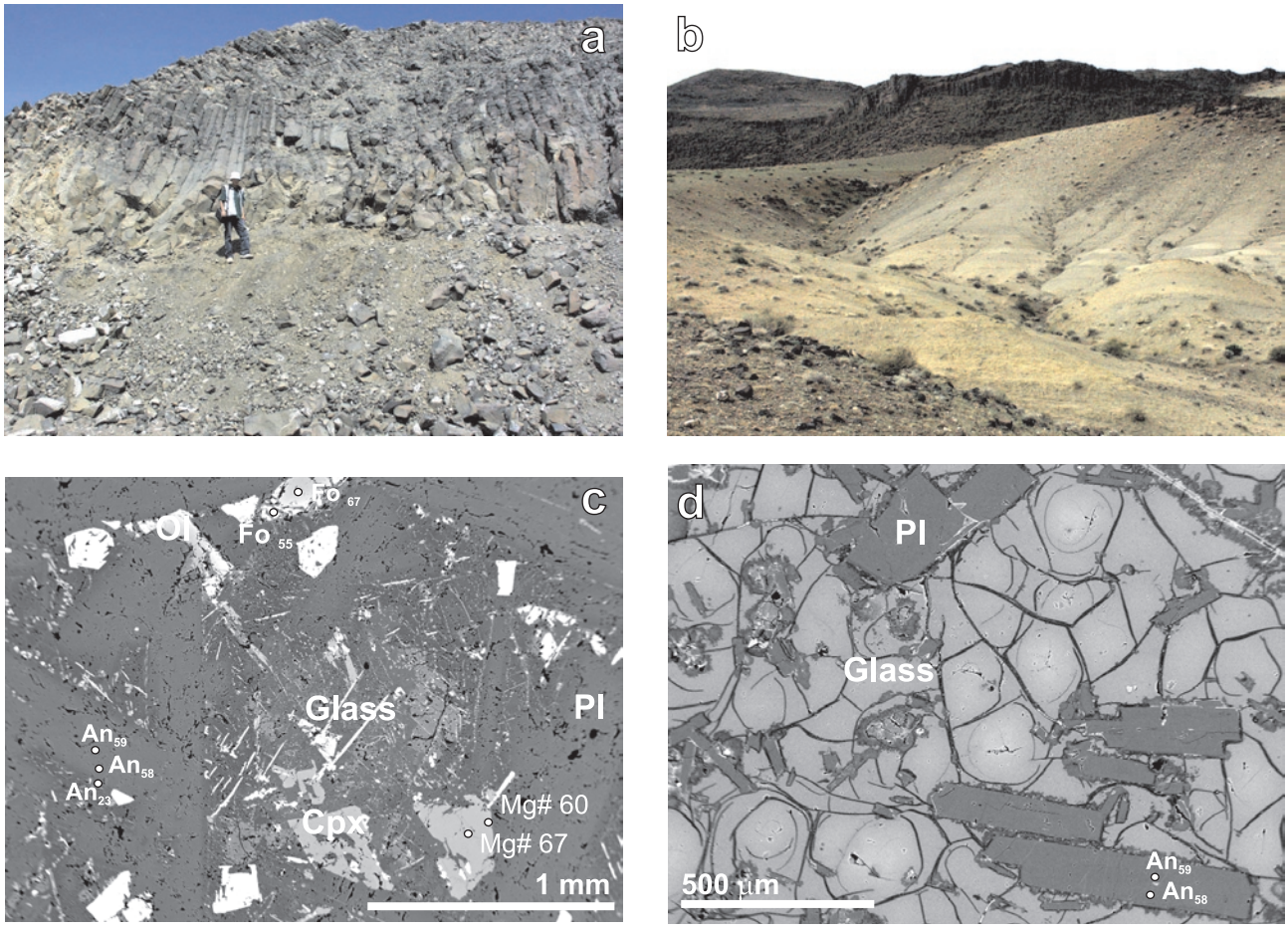

Fig. 3 Outcrop photographs (a–b), a BSE photo (c) and a photomicrograph (d) from Shiliin Nuruu area: **a, b** – basalt lava flows in hanging wall of sandstones of the Khulsan Gol Fm.; **c –** intersertal texture in the basalt. Interstices between plagioclase, pyroxene and olivine grains are filled by glass and secondary minerals; **d –** vitrophyric basalt; plagioclase xenocrysts set in glass matrix with perlitic cracking (*An* – anorthite component in plagioclase, *Fo* – forsterite component in olivine, Mg# – atomic 100×Mg/(Fe^{2+} + Fe^{3+} + Mn + Mg) in clinopyroxene).

water-rich sediments are documented by the disintegration of lavas into blocks, the occurrence of rare pillow lavas and the presence of marlstone tongues penetrating basalt flows. Flow textures with ropy crust are locally preserved in this type of basalts rich in fluids. They have the same petrographic composition as massive basalts but their matrix is finer and the abundance of devitrified volcanic glass therein greater. The amygdales and cavities up to 40 cm in size are empty or filled with calcite and quartz crystals, chlorite, chalcedony and agate. Zeolites and pyrite are subordinate minerals.

Basalts to basaltic andesites are dark grey to black, fine- to medium-grained rocks. The igneous textures are ophitic, intersertal or porphyritic with fine-grained ophitic to subtrachytic or intersertal matrix (Fig. 3c). The groundmass consists of plagioclase [45–60 mod. (modal mineral proportion) %], interstitial glass (0–30 mod. %) and sometimes clinopyroxene (0–25 mod. %) and/or olivine (0–10 mod. %) and opaque minerals (up to 5 mod. %). Some clinopyroxene phenocrysts are poikilitic enclosing plagioclase laths. Amphibole is a minor mineral. Hematite and Ti-magnetite as typical accessory phases are often partially maghemitized. Basalts with vitrophyric texture are present locally (Fig. 3d). In this case the brown glass with perlite-like cracking encloses long laths of plagioclase (0.05–0.10 mm) and euhedral opaque minerals. Minerals of the epidote and serpentinite groups, clay minerals and chlorite are secondary.

Typical olivine-clinopyroxene basaltic andesites with vitrophyric texture were studied using electron microprobe. Pyroxene phenocrysts and microlites are classified as augite (Morimoto et al. 1988). The clinopyroxenes are characterised by Mg# (atomic 100*Mg/(Fe^{2+} + Fe^{3+} + Mn + Mg)) in the range 57–67 (Tab. 1). Clinopyroxene crystals also display a trend of decreasing Mg and Ca and increasing of Fe rimwards. Olivine phenocrysts and microlites are zoned (Tab. 1), with cores typically $Fo_{46–57}$ and Mg-rich rims ($Fo_{63–70}$). Plagioclase forms phenocrysts

Tab. 1 Representative chemical compositions of ferromagnesian minerals in the basalts [wt. % and apfu based on 6 O (pyroxene) and 4 O (olivine)].

Sample	C (Px)	C (Px)	E (Px)	E (Px)	E (Ol)	E (Ol)
Analysis	H1217/2	H1217/5	H0189/8	H0189/2	H0189/1	H0189/5
SiO_2	46.71	49.83	48.92	48.82	37.11	35.37
TiO_2	2.31	0.94	1.47	1.75	0.03	0.11
Al_2O_3	3.72	1.31	2.67	2.65	0.04	0.02
Cr_2O_3	0.03	0.00	0.06	0.04	0.01	0.00
NiO	–	–	–	–	0.13	0.06
FeO	10.24	11.63	6.82	9.88	28.93	36.53
Fe_2O_3	3.91	2.94	4.47	2.41	–	–
MnO	0.30	0.50	0.26	0.34	0.47	0.69
MgO	10.66	12.26	12.87	12.51	33.06	27.12
CaO	20.42	18.80	20.98	19.94	0.26	0.29
Na_2O	0.48	0.50	0.62	0.41	–	–
K_2O	0.00	0.01	0.01	0.01	–	–
Total	98.78	98.73	99.15	98.75	100.03	99.75
Si^{4+}	1.808	1.919	1.857	1.870	1.001	0.992
Ti^{4+}	0.067	0.027	0.042	0.050	0.001	0.002
Al^{3+}	0.170	0.060	0.119	0.120	0.001	0.001
Cr^{3+}	0.001	0.000	0.002	0.001	0.000	0.000
Ni^{2+}	–	–	–	–	0.003	0.001
Fe^{2+}	0.331	0.375	0.216	0.316	0.652	0.857
Fe^{3+}	0.114	0.085	0.128	0.069	–	–
Mn^{2+}	0.010	0.016	0.008	0.011	0.011	0.016
Mg^{2+}	0.615	0.704	0.728	0.714	1.329	1.135
Ca^{2+}	0.847	0.776	0.853	0.818	0.008	0.009
Na^{+}	0.036	0.037	0.046	0.030	–	–
K^{+}	0.000	0.001	0.000	0.000	–	–
Mg#	57.5	59.7	67.4	64.3	66.7	56.5

or glomerocrysts up to 2 mm across and small subhedral laths in the groundmass. The slightly oscillatory zoned plagioclase belongs mostly to labradorite ($An_{58–59}$); only narrow rims of the plagioclase laths could be classified as oligoclase ($An_{23–28}$). The content of the SrO is ~ 0.2 wt. % and K_2O ~ 0.2 wt. % in the core and 0.9–1.0 wt. % in the rim (Tab. 2). Interstitial glass of picrobasaltic composition (SiO_2 ~ 44 wt. %) is partially replaced by chlorite and smectite. Plagioclase phenocrysts ($An_{58–59}$) in the basaltic andesite with vitrophyric texture are slightly oscillatory zoned and coexist with picrobasaltic glass (SiO_2 ~ 44 wt. %).

4.2. Basaltic to trachyandesitic tuffs

Basaltic tuffs and *aa* lavas are subordinate members of the volcanic complex. They are made of massive or vesicular basalt fragments with oval volcanic bombs up to 50 cm in size. No gradation or preferential orientation of clasts was observed. Fine-grained ash tuffs are exposed only as rare, several cm thick layers and laminae in the siltstones.

Basaltic tuffs consist of four principal components: ash- to lapilli-size volcanic material, lithic clasts, altered matrix, volcanic bombs and lithic clasts (up to 50 cm). The matrix includes fine-grained vitric ash, clay and calcite. The lapilli and crystal fragments are generally unaltered, only plagioclase fragments are rarely partially sericitized and carbonatized. The basalt bombs and clasts are predominantly massive to moderately vesicular. Petrographic character is very similar to massive basalts to basaltic andesites described above; the rocks are dominated by glass, plagioclase and/or clinopyroxene. Volcanic bombs have ophitic and subophitic textures in core and intersertal textures in the rim. Rare, small subangular lithic fragments are represented by siltstones and marlstones.

4.3. Volcanic breccias, lahars

Volcanic breccias, lahars and tuffaceous conglomerates with volcanic fragments of acid to intermediate composition are exposed as the uppermost member of the Khulsan Gol Fm. These rocks are restricted to the vicinity of the

Tab. 2 Representative plagioclase compositions (wt. % and apfu based on 8 oxygens).

Sample	C	C	C	C	D	D
Analysis	H1217/13	H1217/14	H1217/15	H1217/17	K0095/3	K0095/4
SiO_2	54.36	54.12	63.01	61.26	53.47	53.66
P_2O_5	0.00	0.02	0.03	0.03	0.01	0.01
Al_2O_3	27.91	27.77	22.24	22.72	28.77	28.68
FeO	0.57	0.63	0.66	0.99	0.51	0.53
CaO	11.96	11.61	4.57	5.64	11.95	11.83
Na_2O	4.46	4.45	7.56	7.24	4.45	4.56
K_2O	0.23	0.23	0.96	0.91	0.27	0.24
BaO	0.00	0.03	0.17	0.12	0.00	0.01
SrO	0.17	0.22	0.20	0.17	0.18	0.22
Total	99.49	98.83	99.03	98.79	99.43	99.50
Si^{4+}	2.465	2.466	2.805	2.746	2.429	2.435
Al^{3+}	1.491	1.492	1.167	1.200	1.541	1.534
Fe^{3+}	0.022	0.024	0.025	0.037	0.019	0.020
T-site	3.978	3.982	3.996	3.984	3.989	3.988
K^+	0.014	0.013	0.055	0.052	0.016	0.014
Na^+	0.392	0.393	0.653	0.629	0.392	0.401
Ca^{2+}	0.573	0.560	0.215	0.268	0.574	0.568
Ba^{2+}	0.000	0.001	0.008	0.002	0.000	0.000
Sr^{2+}	0.005	0.006	0.005	0.004	0.005	0.006
O-site	1.153	1.219	1.294	1.236	1.159	1.213
Mol per cent						
An	59	58	23	29	58	58
Ab	40	41	71	66	40	41
Or	1	1	6	5	2	1

Arslan Khayrkhan Uul. Breccias form tabular bodies up to 100 m thick. These lack bedding and cover sediments of the Khulsan Gol Fm. (including the basaltic andesite sheets) as well as marlstones of the Anday Khudag Fm. The angular to subangular character of the fragments and the absence of bedding in the strongly consolidated breccia point to an origin related to debris flow and these rocks are described here as lahar.

The fragments are composed of red granites, various types of porphyries, rhyolites, dacites and rare andesites. They are angular to subangular with size reaching up to 2 m. Matrix is reddish grey with tuffaceous ash- to lapilli-size and consists of glass (rarely devitrified), feldspars, quartz and subordinate biotite with epidote. Matrix is locally chloritized, carbonatized and silicified. Dacite to rhyolite clasts are composed of quartz-feldspathic matrix often with glass and feldspar phenocrysts (of both K-feldspar and plagioclase). Minor minerals include muscovite, rare apatite, biotite and/or pyroxene. Chloritization of biotite and sericitization of plagioclase are common. Subangular to angular granite-like clasts are composed of equigranular fine- to medium-grained or porphyritic rocks with granitic texture. The main minerals are quartz (15–20 mod. %), K-feldspar (35–40 mod. %), plagioclase (30–35 mod. %), biotite (3–5 mod. %) and locally muscovite. Euhedral to subhedral plagioclases with oscillatory zoning are intensely sericitized in their cores. Subhedral K-feldspar commonly contains microcline lamellae. Small biotite crystals frequently enclosed in feldspars are partially replaced by chlorite. Apatite, monazite, zircon and secondary epidote occur as accessory phases.

5. Whole-rock geochemistry and Sr–Nd isotopic compositions

The volcanic rocks of the Khulsan Gol Fm. show bimodal composition with strongly prevailing basic members. Basic to intermediate rocks are represented by nine, and acid rocks by a single analysed sample. Most of them are characterized by both major- and trace-element analyses; major-element data only are available from two samples (Tab. 3). Alteration played a substantial role in modification of the geochemistry in some lavas. Commonly is the degree of alteration assessed by the loss on ignition (LOI). For the purpose of determining the primary unaltered geochemical character, samples with >2 wt. % LOI were excluded from consideration, but are shown for comparison together with fresh samples in Fig 4. These samples indeed show a petrographic evidence for alteration such as the presence of newly-formed chlorite, iddingsite and sericite.

Tab. 3 Whole-rock geochemical data (major and minor elements) for volcanic rocks from the Khulsan Gol Fm. (wt. %).

Sample	A	B	C	D	E	F	G	H	I	J
Analysis	D0735	H0953	H1217	K0095	H0189	H0516	H0542	H0545	H0079	H0082
Rock	basaltic andesite	basalt	basalt	basalt	basalt	basaltic andesite	trachy-andesite	porphyry	trachy-andesite	basaltic andesite
Type occur.	lava sheet	lava sheet	lava sheet	lava sheet	lava sheet	lava sheet	tuff	lahar	lava sheet	lava sheet
E_coord. (°)	98.958	98.762	98.493	98.475	98.517	98.381	98.518	98.525	98.356	98.391
N_coord. (°)	45.356	45.408	45.003	45.5	45.43	45.484	45.547	45.559	45.474	45.499
Laboratories*	ACME	ACME	ACME	ACME	ACME	ACME	ACME	ACME	CGL	CGL
SiO_2	53.13	51.34	49.09	51.08	51.60	53.71	57.48	71.19	52.99	52.83
Al_2O_3	16.28	17.20	14.66	16.39	15.81	15.60	16.66	14.36	17.72	18.90
Fe_2O_3	9.73	10.70	13.20	10.23	10.68	9.04	7.64	2.45	4.30	2.90
FeO	–	–	–	–	–	–	–	–	4.29	6.56
MgO	5.24	5.19	4.11	4.60	5.95	3.76	2.51	0.54	3.86	4.45
CaO	7.01	7.49	7.05	7.56	7.44	6.82	5.12	1.36	6.02	6.37
Na_2O	4.06	4.13	3.25	3.97	3.73	3.88	4.80	4.40	3.93	3.93
K_2O	1.03	0.98	1.93	0.60	0.70	0.80	1.81	4.05	2.02	0.88
TiO_2	1.25	1.23	2.69	1.25	1.42	1.34	1.21	0.34	1.63	1.49
P_2O_5	0.29	0.28	1.56	0.33	0.46	0.61	0.51	0.09	–	–
MnO	0.14	0.15	0.17	0.13	0.13	0.14	0.15	0.04	0.10	0.10
Cr_2O_3	0.02	0.01	0.01	0.01	0.02	0.01	0.00	0.00	–	–
LOI	1.6	1.2	2.0	3.5	1.8	3.7	1.6	0.9	3.4	2.3
Total	99.78	99.9	99.72	99.65	99.74	99.41	99.49	99.72	100.26	100.71

* Laboratories: ACME = Acme Analytical Laboratories, Vancouver, Canada and CGL = Central Geological Laboratory in Ulaanbaatar, Mongolia

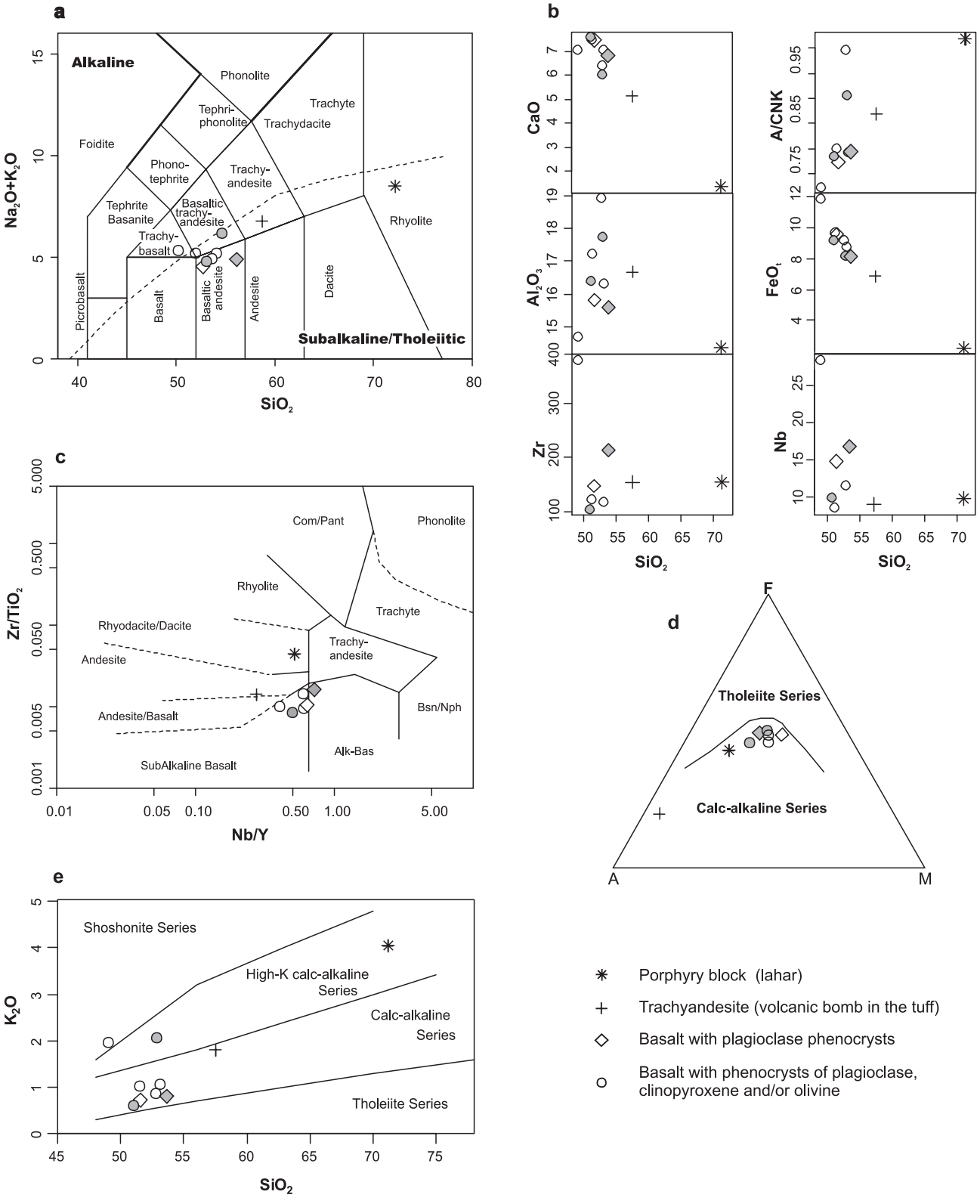

Fig. 4 Chemical composition of the volcanic rocks from the Khulsan Gol Fm.: **a** – Total alkali-silica diagram – TAS (Le Maitre et al. 2002); **b** – Variation diagrams SiO_2 vs. CaO, A/CNK, Al_2O_3, FeO_t, Zr and Nb, **c** – Zr/TiO_2 versus Nb/Y diagram (Winchester and Floyd 1977), **d** – AFM diagram (Irvine and Baragar 1971), **e** – SiO_2–K_2O diagram (Peccerillo and Taylor 1976). Gray-filled symbols represent altered rocks with more than 2 wt. % of LOI.

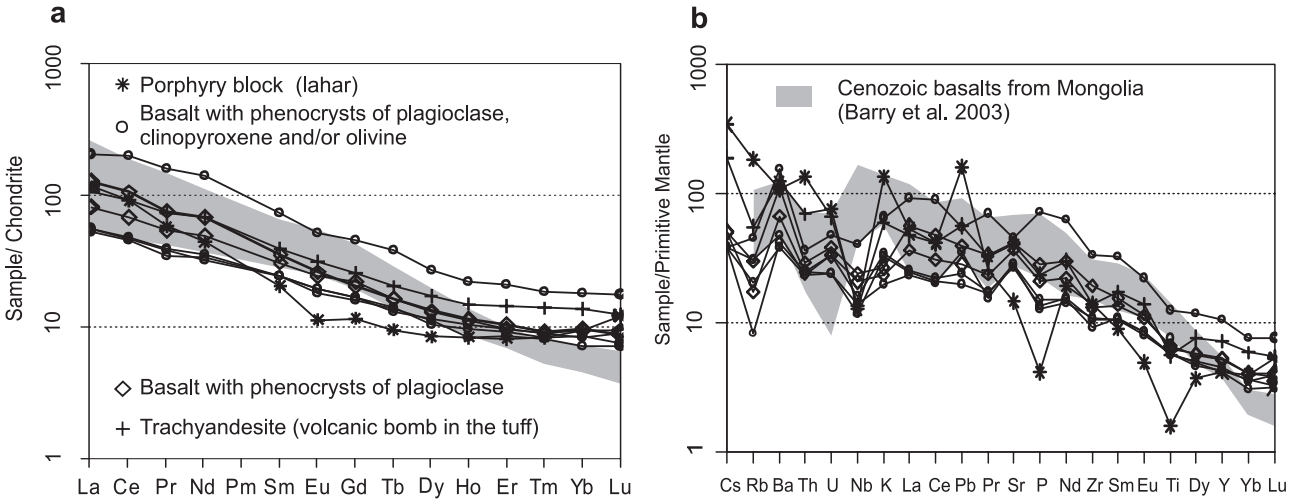

Fig. 5 Chemical composition of the volcanic rocks from the Khulsan Gol Fm.: **a** – Chondrite-normalized REE plot (Boynton 1984). **b** – Primitive-mantle normalized trace-element multielement diagram (Sun and McDonough 1989). Field for Cenozoic basalts from Mongolia (Barry et al. 2003) is shown for comparison.

The **basic–intermediate rocks** of the Khulsan Gol Fm. (SiO_2 = 49.0–57.5 wt. %) contain moderate MgO concentrations (2.5–6 wt. %). Variations of selected major and trace elements relative to SiO_2 are shown in Fig. 4b.

In the TAS classification (Le Maitre et al. 2002, Fig. 4a) they correspond to subalkaline basaltic andesite or basaltic trachyandesite, one sample fits into field of alkaline trachybasalt and another to trachyandesite. In the Zr/TiO_2 versus Nb/Y diagram (Winchester and Floyd 1977) the lavas correspond mainly to subalkaline basalt (Fig. 4c).

The AFM diagram (Irvine and Baragar 1971, Fig. 4d) characterises the majority of the samples as calc-alkaline. In the SiO_2–K_2O plot (Peccerillo and Taylor 1976, Fig. 4e), most rocks seem to belong to the normal calk-alkaline series (K_2O = 0.6–2.0 wt. %). The K_2O/Na_2O ratios are usually low (0.1–0.6).

Chondrite-normalized REE patterns are mutually comparable (Fig. 5a), with gently decreasing trend from LREE to HREE (La_N/Yb_N = 6–13) and no Eu anomalies. Individual patterns are subparallel, with differences in total REE contents (96–377 ppm).

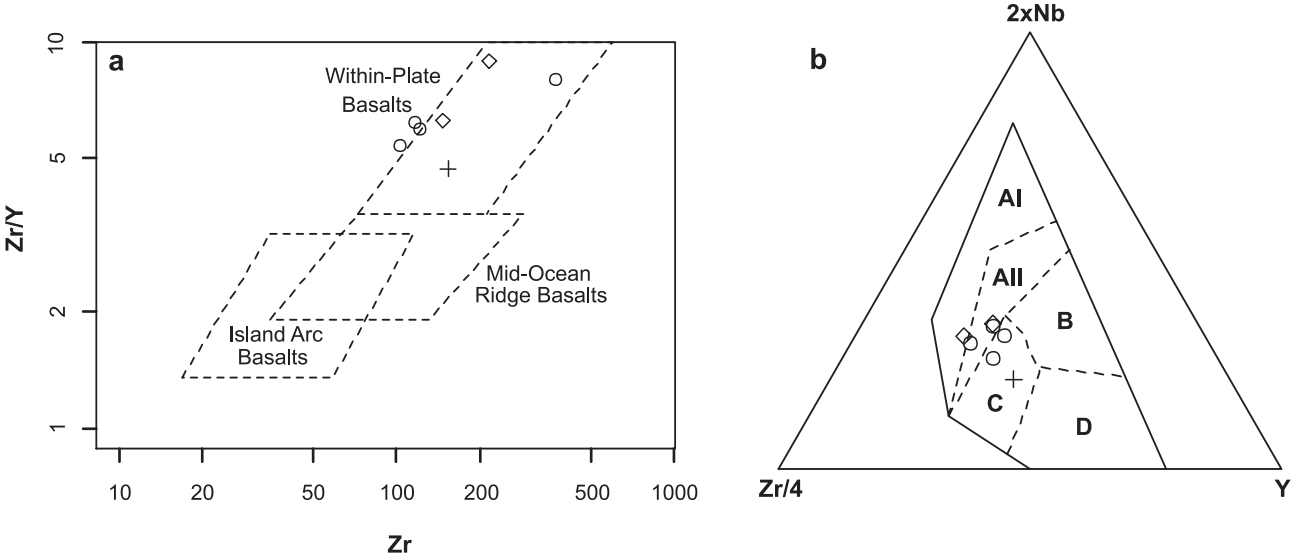

Fig. 6 Geotectonic discriminant diagrams: **a** – Zr–Zr/Y classification plot (Pearce and Norry 1979) and **b** – discrimination diagram Zr/4–2×Nb–Y (Meschede 1986); AI–AII = Within-Plate Alkaline Basalts, AII–C = Within-Plate Tholeiites, B = P-type Mid-Ocean Ridge Basalts, D = N-type Mid-Ocean Ridge Basalts, C–D = Volcanic Arc Basalts. Symbols as in Fig. 4.

The primitive- mantle normalised spider diagram (Fig 5b) shows strong enrichment in LIL elements; negative anomalies in Rb and Nb are also characteristic. On the other hand, Ba forms strong positive anomalies. Rocks plot as within-plate basalts in the various geotectonic discrimination diagrams (e.g., Fig. 6a–b).

Acid sample of a porphyry block from volcanic breccia (SiO_2 = 71.2 wt. %) can be classified as rhyolite/granite (Fig. 4a). Its K_2O is high, fitting to high-K calc-alkaline series (4.1 wt. %), as is its K_2O/Na_2O ratio (0.9). The REE pattern features a strong fractionation of LREE (La_N/Yb_N = 13) with a negative Eu anomaly (Eu/Eu*= 0.7). Acid porphyry is, in comparison with more basic rocks, enriched in Cs, Rb, Th, U, K, and Pb as well as strongly depleted in Ti and P.

The basaltic andesites have a less radiogenic strontium ($^{87}Sr/^{86}Sr_{110}$ = 0.7047 and 0.7049) and more radiogenic neodymium (ε^{Nd}_{110} = +1.8 and +0.5) than the porphyry block from the volcanic breccia ($^{87}Sr/^{86}Sr_{110}$ = 0.7078 and ε^{Nd}_{110} = -0.8) (Tab. 4).

6. Discussion

The Mesozoic volcanites of the Khulsan Gol Fm. in the Shillin Nuruu area are represented by basaltic andesite, trachybasalt to trachyandesite lavas with subordinate tuffs and lahars. The relation with palaeontologically documented sediments points to its uppermost Early Cretaceous age (Aptian–Albian). The lavas were extruded subaerially, although also sills are locally present. The rare pillow lavas and the presence of vitrophyric basaltic glass document lava flows into subaqueous environment.

The fairly evolved composition of the basaltic rocks (i.e. low MgO, Ni and Cr) is far from being in equilibrium with mantle minerals. The decreasing Ni and MgO contents indicate fractionation of olivine. A positive correlation of SiO_2 with Al_2O_3 and negative with CaO and FeO_t suggest that clinopyroxene could have been an important fractionating phase in the evolution of the magma. The lithophile elements (e.g., Pb, K, and Ba) are progressively enriched, while the HFSE tend to be increasingly depleted.

The role for crustal contamination can be assessed using trace elements. Studied basic–intermediate rocks show wide range of Ce/Pb ratios (15–41) much more similar to mantle (ratios for most mantle compositions are ~25 and primitive mantle ~9; Hofmann et al. 1986) than to the crustal compositions (Ce/Pb < 5). On the other hand, La/Nb ratios (1.5–3.7) are higher than in Cenozoic Mongolian basalts (Barry et al. 2003) (Fig. 7b), providing an evidence for crustal contamination (La/Nb ~1.5 for upper crust and ~4.5 lower crust; Taylor and McLennan 1985).

The Sr and Nd isotope compositions of selected rock samples plot close to the Bulk Silicate Earth (Hart and Zindler 1986, Fig. 7a), which is a feature typical also of younger Mongolian basalts (Barry et al. 2003). For the basaltic samples, the time-integrated shift in the Sr isotopic value can be considered as negligible due to low Rb/Sr values (0.01–0.03). The change in Nd isotopes is more significant, but still small enough to be within the limits typical for BSE rocks (Sm/Nd = 0.17–0.24). Although the isotopic composition of the studied basaltic andesites does not show clear evidence for the crustal contamination, the influence of such process also cannot be excluded. As the isotopic composition of locally documented crustal xenoliths and of the studied acid porphyry are fairly primitive, the shift in isotopic composition resulting from reasonable extent of crustal contamination would be only limited.

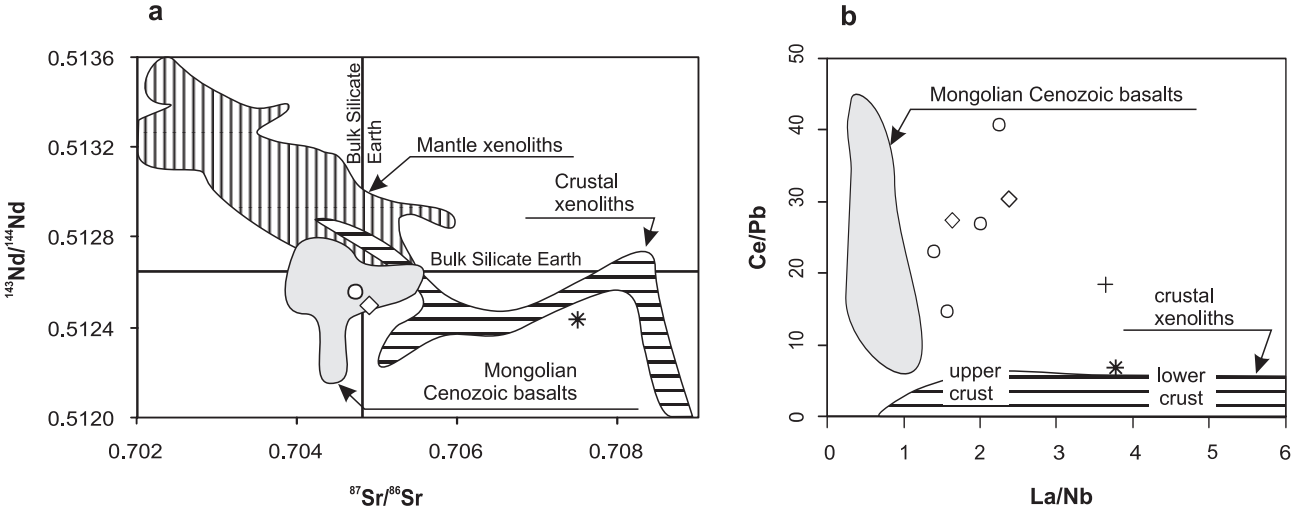

Fig. 7 Plots of $^{143}Nd/^{144}Nd$ versus $^{87}Sr/^{86}Sr$ (a) and Ce/Pb versus La/Nb plot (b) for Mesozoic volcanic rocks from Khulsan Gol Fm. Symbols as in Fig. 4. The fields for Mongolian Cenozoic basalts (gray), mantle (vertical hatching) and crustal (horizontal hatching) xenoliths are from Barry et al. (2003). Studied Cretaceous samples are age-corrected to 110 Ma and Cenozoic samples of Barry et al. (2003) to 33 Ma.

Tab. 4 Whole-rock trace-element chemical compositions (ppm) and Sr-Nd isotopic data for the volcanic rocks from the Khulsan Gol Fm.

Sample	A	B	C	D	E	F	G	H
Analysis	D0735	H0953	H1217	K0095	H0189	H0516	H0542	H0545
Sc	16	17	21	17	18	15	17	3
Ba	329.3	266.2	1073.5	294.8	467.9	775.9	867.8	762.2
Be	1	1	3	1	1	2	3	3
Co	32.3	35.3	30.7	33.9	37.7	27.3	13.0	3.7
Cs	0.3	0.3	0.3	0.3	0.4	0.4	1.5	2.7
Ga	20.2	21.6	21.1	21.2	22.9	20.9	22.4	17.8
Hf	3.3	3.0	8.7	2.5	3.6	5.4	4.7	4.9
Nb	11.5	8.5	28.5	9.8	14.8	16.9	9.0	9.7
Rb	19.8	12.9	28.6	5.2	11.0	18.9	35.0	117.6
Sn	1	1	2	1	1	1	2	1
Sr	560.1	599.6	941.9	599.7	772.1	871.3	857.3	308.5
Ta	0.7	0.5	1.6	0.6	0.8	0.9	0.4	0.9
Th	2.0	2.0	3.1	2.1	2.1	2.5	5.9	11.4
U	0.7	0.5	1.0	0.5	0.7	0.8	1.6	1.4
V	186	185	202	189	180	160	116	23
W	0.5	0.9	0.5	0.4	0.4	0.4	0.5	0.6
Zr	117.3	122.2	377.7	103.6	146.1	214.5	153.6	154.9
Y	19.0	20.7	47.7	19.4	23.3	24.0	32.7	19.0
Mo	0.7	0.6	0.8	1.0	0.7	0.7	1.2	0.7
Cu	56.4	81.6	28.7	81.8	68.6	50.3	18.4	8.3
Pb	1.7	1.4	3.9	2.5	2.0	2.8	4.0	11.5
Zn	77	81	124	89	84	95	48	31
Ni	82.0	71.2	25.4	80.6	89.5	63.5	7.7	3.9
La	17.4	17.1	63.3	16.2	25.2	39.1	33.0	36.8
Ce	39.0	37.6	158.9	36.5	54.7	85.2	73.8	73.6
Pr	4.81	4.61	19.56	4.26	6.53	9.23	8.95	7.06
Nd	21.1	19.3	84.3	20.2	29.7	40.8	40.8	26.4
Sm	4.7	4.7	14.3	4.8	6.0	6.9	7.6	4.0
Eu	1.34	1.44	3.74	1.43	1.80	1.91	2.30	0.83
Gd	4.10	4.35	11.81	4.33	5.71	5.31	6.58	3.00
Tb	0.65	0.62	1.81	0.66	0.78	0.77	0.96	0.45
Dy	3.58	3.68	8.65	3.37	4.16	4.25	5.55	2.71
Ho	0.60	0.75	1.59	0.69	0.80	0.82	1.07	0.60
Er	1.78	2.05	4.36	1.92	2.02	2.21	3.03	1.70
Tm	0.26	0.29	0.60	0.27	0.29	0.30	0.45	0.27
Yb	1.49	1.75	3.76	1.77	1.97	2.01	2.88	1.95
Lu	0.23	0.29	0.56	0.24	0.30	0.28	0.40	0.39
Ce/Pb	22.94	26.86	40.74	14.60	27.35	30.43	18.45	6.40
La/Nb	1.51	2.01	2.22	1.65	1.70	2.31	3.67	3.79
$^{87}Rb/^{86}Sr$	–	–	–	0.02509	–	0.06277	–	1.10351
$^{87}Sr/^{86}Sr$	–	–	–	0.704776	–	0.705013	–	0.709540
2 s.e. Sr	–	–	–	0.000009	–	0.000013	–	0.000011
$^{147}Sm/^{144}Nd$	–	–	–	0.14366	–	0.10224	–	0.09160
$^{143}Nd/^{144}Nd$	–	–	–	0.512691	–	0.512595	–	0.512520
2 s.e. Nd	–	–	–	0.000006	–	0.000007	–	0.000008
$(^{87}Sr/^{86}Sr)_{110}$	–	–	–	0.704737	–	0.704915	–	0.707815
$(^{143}Nd/^{144}Nd)_{110}$	–	–	–	0.512588	–	0.512521	–	0.512454
ε_{110}^{Nd}	–	–	–	+1.78	–	+0.49	–	-0.83

Crustal contamination can be documented also by the chemistry of porphyry clast from the lahar. This clast is very close to chemical composition of the adjacent Permian granites exposed in the footwall of the Mesozoic sequence. Their Sr–Nd isotopic signature is also not very far from that of Bulk Earth; $^{87}Sr/^{86}Sr_{285}$ ratios are 0.7043 to 0.7048, and ε_{285}^{Nd} values are +1.3 to +0.7 according Hanžl et al. (2007). The significant part of the lithic clasts in acid volcanic breccia thus may represent recycled material from the underlying Permian plutonic complex.

Widespread intraplate volcanism has occurred throughout Mongolia from Early Mesozoic through Miocene (Whitford-Stark 1987) up to Pleistocene–Holocene (Yarmolyuk and Kovalenko 2001) and can be subdivided into several stages.

The *Early Mesozoic* volcanic history was related with the largest Mesozoic rift structure in the northern Mongolia–western Transbaikalia (Vorontsov et al. 2007). The subalkaline to alkaline trachybasaltic andesites with subordinate basalts and trachytes documented by these authors were characterised by higher contents of K_2O (2.38–3.85 wt. %), Rb (30–101 ppm), Ba (842–2800 ppm), Th (4.1–12.8 ppm) and Pb (17.4–29.8 ppm) compared to the studied rock samples from the Shillin Nuruu area. Geochemical and isotopic data suggest that the basic rocks of the bimodal volcanic association are most likely products of melting of a geochemically variable mantle source (Vorontsov et al. 2007).

The *Late Mesozoic–Cenozoic* igneous rocks in the southern Mongolia adjacent to the Khangay Mts. are linked with a South Khangay hot spot (Yarmolyuk et al. 1994). Development and Cenozoic uplift of the Mongolian Plateau represented by Khentey and Khangay domes as well as basin and range topography are related to interaction of a mantle plume with the overlying lithosphere (Windley and Allen 1993). The several stages in development of the Khangay Mts. region were recognized (Yarmolyuk and Kovalenko 2001). The Late Jurassic period was represented by highly alkaline rocks and corresponded with the formation of the Khangay igneous province. Early Cretaceous stage was characterised by subalkaline basalts followed by acid rocks. At the Early Cretaceous stage (118–105 Ma), subalkaline basalts to andesitic basalts were dominant.

Geochemical and isotopic data indicate close relationship of samples studied in course of the present work with Early Cretaceous trachybasalts and trachybasaltic andesites in the eastern part of the Gobi-Altay rift zone in the Arts-Bogd area (Samoilov et al. 1998). These basic rocks ($Na_2O + K_2O$ = 6–9 wt. %) show isotopic composition ($^{87}Sr/^{86}Sr_{130}$ = 0.7049–0.7059) similar to the studied rocks from the Shillin Nuruu area. Chondrite-normalized REE patterns display analogous trends (La_N/Yb_N = 11–19) with no Eu anomalies. The total REE contents (221–498 ppm) are slightly higher than in basic rocks from the Shillin Nuruu area. The evolution of basaltic magmatism in the Gobi-Altay rift was related to the Khangay mantle hotspot (Samoilov et al. 1998). High heat flow, rifting and magmatism in the central part of Mongolia during the Late Mesozoic and Cenozoic times were presumably associated with this diapiric upwelling of a mantle asthenosphere (Windley and Allen 1993).

On the other hand, according to Barry et al. (2003), Cenozoic volcanism in Mongolia belongs to a large igneous province extending from NE China to Lake Baikal. Alkaline to calc-alkaline basaltic to trachyandesitic volcanic rocks (K_2O = 1.8–4.1 wt. %), form numerous small volcanic complexes distributed mainly throughout the central Mongolia. Chondrite-normalised REE patterns are very similar to those shown in Fig. 5b except for slight depletion in the Tm, Yb and Lu. The Sr–Nd isotopic compositions of the studied samples resemble the Mongolian Cenozoic basalts (Fig. 7a), whose genesis was explained by partial melting of metasomatically-enriched lower lithospheric mantle (Barry et al. 2003).

The spatial relationship and geochemical similarity with the younger Cenozoic basalts in Mongolia suggests that the volcanites in the Shiliin Nuruu area could have been also associated with extension and thinning of the lithosphere along eastern margin of the Euroasian plate in the eastern China (Northrup et al. 1995). Calc-alkaline magmatism is common in this geotectonic environment (e.g. Hawkesworth et al. 1995). However, Liu et al. (2004) suggested that both the Indo-Eurasian collision and subduction of the Pacific Plate played important roles in the Cenozoic rifting and volcanism. The evolution after Indo-Asian collision may have driven lateral extrusion of the mantle asthenosphere and lithospheric thinning. Lateral mantle flow would help to explain many features of the Khangay mantle plume, asthenospheric upwelling under eastern China and related magmatic activity including volcanism in the Shillin Nuruu area.

7. Conclusions

The evolution of the Mesozoic intracontinental basin in western Mongolia filled by continental sediments was accompanied by a volcanic activity. One of the extension-related structures was the Gobi-Altay rift, parts of which are preserved today only in sunken blocks along the northern slopes of the Gobi-Altay range. The western part of the Gobi-Altay rift is represented by a syncline in the area of the Shiliin Nuruu and smaller blocks surrounding the Khar Argalantyn Mts. The E–W oriented syncline is formed by the Upper Jurassic to Lower Cretaceous continental sediments. The extensional evolution of this basin culminated by huge volcanic activity in the Early Cretaceous.

Bimodal volcanic sequence consists of basaltic lava sheets and small amounts of acid effusive rocks. The basaltic to andesitic lavas (SiO_2 = 49–58 wt. %) extruded mainly subaerially, and only locally in a subaqueous environment. Volcanic rocks associated with continental rifting could have been related to the evolution of the so-called southern Khangay hot spot and reflect lithospheric thinning and extension. Variations in chemical composition reflect major role for fractional crystallization driven mainly by clinopyroxene and, to a lesser extent, olivine. The parental magma was presumably generated by melting of metasomatically enriched lower lithospheric and/or uppermost asthenospheric mantle. However trace-element and Sr-Nd isotope compositions of some lavas provide an evidence for crustal contamination.

Volcanism in the Shiliin Nuruu area had a character distinct from that of the Early Mesozoic rift in the northern Mongolia, as indicated by within-plate geochemical features resembling the Cenozoic Mongolian basic volcanites. Geochemical and isotopic (Sr, Nd) similarity with Cenozoic volcanic rocks implies that bimodal volcanism of Shiliin Nuruu could have represented initial stages of this Cenozoic magmatic activity in Mongolia.

Acknowledgements. The fieldwork was undertaken during the project 'Geological survey of the Mongolian Altay on the scale 1 : 50,000' within the frame of the Program of the Development Cooperation Project of the Czech Republic. We are grateful to Mongolian staff of the expedition for participating in the fieldwork. We are indebted to J. Holák and Z. Novotný for technical backing of the geological survey.

Electronic supplementary material. The tables 3 and 4, as well as GPS coordinates of the studied samples, are available online at the Journal web site (http://dx.doi.org/10.3190/jgeosci.026).

References

Barry TL, Saunders AD, Kempton PD, Windley BF, Pringle MS, Dorjnamjaa D, Saandar S (2003) Petrogenesis of Cenozoic basalts from Mongolia: evidence for the role of asthenospheric versus metasomatized lithospheric mantle sources. J Petrol 44: 55–91

Boynton WV (1984) Cosmochemistry of the rare earth elements: meteorite studies. In: Henderson P (ed) Rare Earth Element Geochemistry. Elsevier, Amsterdam, pp 63–114

Gilíková H, Budil P, Otava J, Hanžl P, Buriánek D (2007) Mesozoic. In: Hanžl P (ed) Geological survey of the Mongolian Altay at a scale of 1 : 50,000 (Zamtyn Nuruu - 50), Unpublished manuscript, Geological Information Centre, MRPAM, Ulaanbaatar

Graham SA, Hendrix MS, Johnson CL, Badamgarav D, Badarch G, Amory J, Porter M, Barsbold R, Webb LE (2001) Sedimentary record and tectonic implications of late Mesozoic rifting, southeast Mongolia. Geol Soc Am Bull 113: 1560–1579

Hanžl P, Aichler J, Bolormaa K, Byambasuren D, Budil P, Buriánek D, Hrdličková K, Erban V, Gerdes A, Gilíková H, Holák J, Janoušek V, Kosmák V, Krejčí Z, Malec J, Mašek D, Maštera L, Metelka V, Novotný Z, Otava J, Rejchrt M, Rukavičková L, Sidorinová T, Skácelová Z, Táborský Z, Tsend-Ayush T, Valtr V, Večeřa J, Vít J (2007) Geological survey of the Mongolian Altay at a scale of 1 : 50,000 (Zamtyn Nuruu – 50), Unpublished manuscript, Geological Information Centre, MRPAM, Ulaanbaatar, pp 1–376

Hart SR, Zindler A (1986) In search for bulk-earth composition. Chem Geol 57: 247–267

Hawkesworth C, Turner S, Gallagher K, Hunter A, Bradshaw T, Rogers N (1995) Calc-alkaline magmatism, lithospheric thinning and extension in the Basin and Range. J Geophys Res 100: 271–286

Hendrix MS, Graham SS, Carroll AR, Sobel ER, Mc Knight CL, Schulein BJ, Wang Z (1992) Sedimentary record and climatic implications of recurrent deformation in the Tianshan: evidence from Mesozoic strata of the north Tarim, south Junggar and Turpan basins, northwest China. Geol Soc Am Bull 104: 53–79

Hendrix MS, Graham SA, Amory JY, Badarch G (1996) Noyon Uul syncline, southern Mongolia: Lower Mesozoic sedimentary record of the tectonic amalgamation of central Asia. Geol Soc Am Bull 108: 1256–1274

Hofmann AW, Jochum KP, Seufert M, White WM (1986) Nb and Pb in oceanic basalts: new constraints on mantle evolution. Earth Planet Sci Lett 79: 33−45

Irvine TN, Baragar WRA (1971) A guide to chemical classification of the common volcanic rocks. Can J Earth Sci 8: 253–248

Jacobsen SB, Wasserburg GJ (1980) Sm–Nd isotopic evolution of chondrites. Earth Planet Sci Lett 50: 139–155

Janoušek V, Farrow CM, Erban V. (2006) Interpretation of whole-rock geochemical data in igneous geochemistry: introducing Geochemical Data Toolkit (GCDkit). J Petrol 47: 1255–1259

Kovalenko VI, Yarmolyuk VV, Bogatikov OA (1995) Magmatism, Geodynamics and Metallogeny of Central Asia. Miko Commercial Herald Publishers, Moscow, pp 1–272

Le Maitre RW, Streckeisen A, Zanettin B, Le Bas MJ, Bonin B, Bateman P, Bellieni G, Dudek A, Efremova S, Keller J, Lamere J, Sabine PA, Schmid R, Sorensen H, Woolley AR, (2002) Igneous Rocks: A Classification and Glossary of Terms, Recommendations of the International Union of Geological Sciences, Subcommission of

the Systematics of Igneous Rocks. Cambridge University Press, Cambridge, pp 1–236

Liu M, Cui X, Liu F (2004) Cenozoic rifting and volcanism in eastern China: a mantle dynamic link to the Indo–Asian collision? Tectonophysics 393: 29–42

Lugmair GW, Marti K (1978) Lunar initial $^{143}Nd/^{144}Nd$: differential evolution line of the lunar crust and mantle. Earth Planet Sci Lett 39: 349–357

Martinson GG (1982) Mesozoic lake's pools of Mongolia. Nauka, Leningrad, pp 1–210 (in Russian)

Meschede M (1986) A method discriminating between different types of mid-ocean ridge basalts and continental tholeiites with Nb-Zr-Y diagram. Chem Geol 56: 207–218

Morimoto N (1988) Nomenclature of pyroxenes. Mineral Mag 52: 535–550

Northrup CJ, Royden LH, Burchfiel BC (1995) Motion of the Pacific plate relative to Eurasia and its potential relation to Cenozoic extension along the eastern margin of Eurasia. Geology 23: 719–722

Pearce JA, Norry MJ (1979) Petrogenetic implications of Ti, Zr, Y, and Nb variations in volcanic rocks. Contrib Mineral Petrol 69: 33–47

Peccerillo A, Taylor SR (1976) Geochemistry of Eocene calc-alkaline volcanic rocks from the Kastamonu area, northern Turkey. Contrib Mineral Petrol 68: 61–81

Rauzer AA, Zhanchiv DI, Golyakov VI, Ykhina IF, Ivanov IG, Tsukernik AB, Afonin VV, Smirnov IG, Bykhover VI, Kravtsev AV, Baatarkhuyag A, Skoryukin MI, Khodikov IV, Mantsev NV, Okaemov SV, Mischin VA, Enkhsajkhan T (1987) Report on results of geological mapping on scale 1:200,000 in the south-western part of Mongolian Altay in 1983–1983, Mongol. National. Rep. Tekhnoexport, Moscow, pp 1–352 (in Russian)

Richard P, Shimizu N, Allégre, CJ (1976) $^{143}Nd/^{146}Nd$, a natural tracer: an application to oceanic basalts. Earth Planet Sci Lett 31: 269–278

Samoilov VS, Yarmolyuk VV, Kovalenko VI, Ivanov VG, Pokhoľchenko YA (1998) Geochemical and isotopic characteristics and magma sources of the Early Cretaceous trachybasalts of the Gobi-Altai rift zone: an example of grabens in the Arts-Bogdo range. Geochem Int 12: 1203–1216

Sinica SM (1993) Jurassic and Lower Cretaceous of central Mongolia. In: The works combined Russian-Mongolian paleontology expedition, vol 42. pp 1–236 (in Russian)

Steiger RH, Jäger E (1977) Subcommission on Geochronology; convention on the use of decay constants in geo- and cosmochronology. Earth Planet Sci Lett 36: 359–362

Sun SS, McDonough WF (1989) Chemical and isotopic systematics of oceanic basalts: implications for mantle composition and processes. In: Saunders AD, Norry M (eds) Magmatism in Ocean Basins. Geol Soc London Spec Pub 42, pp 313–345

Taylor SR, McLennan SM (1985) The Continental Crust: Its Composition and Evolution. Blackwell, Oxford, pp 1–312

Vorontsov AA, Yarmolyuk VV, Lykhin DA, Dril SI, Tatarnikov SA, Sandimirova GP (2007) Magmatic sources and geodynamics of the Early Mesozoic Northern Mongolia–Western Transbaikalia rift zone. Petrology 15: 35–57

Whitford-Stark JL (1987) A Survey of Cenozoic volcanism on mainland Asia. Geol Soc Am, Special Paper 213, pp 1–74

Winchester JA, Floyd PA (1977) Geochemical discrimination of different magma series and their differentiation products using immobile elements. Chem Geol 20: 325–343

Windley BF, Allen MB (1993) Mongolian plateau: evidence for a Late Cenozoic mantle plume under central Asia. Geology 21: 295–298

Yanshin AL (1976) Map of Mesozoic and Cenozoic tectonics of the Mongolian People's Republic: U.S.S.R. Academia Sciences, Moscow, 4 sheets, scale 1 : 1,5,000,000

Yarmolyuk VV (1983) Late Paleozoic Volcanism of the Continental Rift Structures of Central Asia. Nauka, Moscow, pp 1–198 (in Russian)

Yarmolyuk VV (1986) Characteristics of structural position of continental rift structures in Mongolia. Izv Akad Nauk SSSR, Ser geol 9: 3–15 (in Russian)

Yarmolyuk VV, Kovalenko VI (2001) The Mesozoic–Cainozoic of Mongolia. In: Dergunov AB (ed) Tectonics, Magmatism, and Metallogeny of Mongolia, Taylor & Francis Group, London, pp 203–244

Yarmolyuk VV, Ivanov VG, Kovalenko VI, Samoilov VS (1994) Dynamics of formation and magmatism of the Late Mesozoic–Cenozoic southern Khangai mantle hot spot, Mongolia. Geotektonika 5: 28–45

Journal of Geosciences, 53 (2008), 181–191 DOI: 10.3190/jgeosci.024

Original paper

Mud volcanoes in the Khar Argalantyn Nuruu, NW Gobi Altay, Mongolia as manifestation of recent seismic activity

Lenka RUKAVIČKOVÁ[1,*], Pavel HANŽL[2]

[1] *Czech Geological Survey, Geologická 6, 152 00 Prague 5, Czech Republic; lenka.rukavickova@geology.cz*
[2] *Czech Geological Survey, Leitnerova 22, 602 00 Brno, Czech Republic*
[*] *Corresponding author*

A group of mud volcanoes was discovered in the NW part of the Gobi Altay on a northern foothill of the Khar Argalantyn Nuruu Mts. Several mud cones and mud mounds with elevation up to 0.8 m, as well as pools with muddy water and mud outflows were encountered. Jurassic to Quaternary sedimentary successions provide the source for the mud volcanoes. Jurassic sediments cover transgressively Permian volcanics forming several confined aquifers within a subsided, triangle shaped block. The aquifers are saturated with groundwater derived from the Khar Argalantyn Nuruu Mts. To the northwest and to the east this block is bordered by sealed faults. The significant recent seismic activity occurring in the area is related to Cenozoic faults as a response to the collision of the Indian and Eurasian continental plates. The mud volcanoes originated probably as a result of the Gobi-Altay Earthquake in 1957. The earthquake of magnitude 8.3 generated new fractures or reactivated existing fractures. The impulse of the earthquake exceeding the thixotropy of fine-grained sediments initiated the rise of the mud volcanoes. The recent equilibrium of pressure conditions in the area is labile. Earthquakes or increase in piezometric level of groundwater caused by heavy rainfalls can trigger activity of the mud volcanoes. A high content of smectites in sediments and loss of binding of clay particles due to soluble salts support mud outflows during such starting events.

Keywords: mud volcano, liquefaction, thixotropy, earthquake, Gobi Altay, Mongolia
Received: 18 March 2008; accepted 4 June 2008; handling editor: S. Vrána

1. Introduction

1.1 Origin of mud volcanoes

A mud volcano is a positive topographic feature constructed mainly of mud and other sedimentary constituents, which periodically or continuously vents liquid mud, including water, oil and gas (Hovland et al. 1997). Mud volcanoes, regardless of comparable morphology and manifestation on the Earth's surface, may be of variable origins. According to their genesis three fundamental groups are described: (1) mud volcanoes *sensu stricto* linked with hydrocarbon gas release (e.g. Dimitrov 2002), (2) hydrothermal mud volcanoes (e.g. Pitt and Hutchinson 1982) and (3) mud volcanoes as a manifestation of an earthquake or a sudden exogenetic event (e.g. Rogozhin et al. 2007).

Mud volcanoes *sensu stricto* occur mostly in areas of rapid sedimentation, lateral tectonic compression or recent magmatic activity (Milkov 2005). These mud volcanoes are often associated with hydrocarbon deposits. Gases, which are generated during hydrocarbon formation processes, and water force the mud ascent to the Earth's surface. This type of mud volcanoes occurs mostly in association with both thick sedimentary sequences, reaching several kilometres, and the existence of similarly thick layers of clay-rich sediments in deeper parts. The size of the mud volcanoes *s.s.* varies from small gryphons of about one meter in diameter to structures several kilometres across and with relative heights of first hundreds of metres (Dimitrov 2002; Kholodov 2002).

Mud volcanoes *sensu stricto* are irregularly clustered in separated areas forming belts, which coincide with active areas of the continental plate boundaries and zones of young orogenic structures (Dimitrov 2002). Most of the worldwide known mud volcanoes are located in eastern Azerbaijan and the Caspian Sea region (Panahi 2005).

Hydrothermal mud volcanoes occur in regions characterised by recent volcanic activity. Volcanic gas and hot water rising to the surface detach and entrain fine-grained particles of adjacent rocks. Cones of mud, usually no more than one or two metres in height, mud cauldrons and fumaroles are all apparent results of these geologic processes. High water temperature, formation of large volumes of water vapour and absence of hydrocarbon gases are characteristic of these mud volcanoes (Kholodov 2002). 'Mud pot' is an alternative term used for hydrothermal mud volcanoes, which are in fact recognized to be thermal springs. The best-known hydrothermal mud pots occur in Yellowstone National Park in USA (Pitt and Hutchinson 1982).

Mud volcanoes as manifestation of earthquake or sudden exogenetic events include small mud or often sand volcanoes, which arise as a subsequent effect of

sudden events such as earthquakes or floods causing rapid increase in strain in rocks or abrupt change in piezometric pressure in aquifers. In contrast to the previous two groups of mud volcanoes, the material ejected to the surface is derived from shallow depths, usually only a few tens of metres. The height of this type of mud volcanoes reaches generally several decimetres, rarely above one meter; their diameter may attain several metres.

Most of these small mud volcanoes are directly related to earthquakes. During earthquakes, pressure of pore water increases and soils saturated with groundwater lose their shear resistance, which leads to exceeding the threshold of thixotropy. This results in liquefaction of soils and sediments. If the liquefied layer is covered by dry/more compact sediments, by impermeable layers or by frozen ground, fluidized sediments are ejected to the surface through open ruptures and form mud or sand cones. Such ejections of mud and sand on the ground surface as a result of earthquakes are called mudvolcanic manifestations (Panahi 2005) and occur mainly in the areas with no mud volcanoes *sensu stricto*.

Mud volcanic manifestations have accompanied several strong earthquakes with magnitudes above 7. For example small mud mounds forming as a result of surficial effect of the 2003 Altay Earthquake (M_L = 7.5) are common in flood plains of the Chuya and Chagan-Uzun rivers in the Gorny Altay (Rogozhin et al. 2007). A number of small mud volcanoes appeared during the Olyutorsk Earthquake (M_L = 7.6) in 2006 on the Korf spit near the Kamchatka Peninsula (Pinegina and Konstantinova 2006).

1.2 Mud volcanoes in Mongolia

The territory of Mongolia is built by numerous geological blocks consolidated mainly during the Palaeozoic and became tectonically reactivated along the intracontinental deformation zones during the Cenozoic (Tapponier and Molnar 1979; Cunningham et al. 2003). Owing to lacking hydrocarbon occurrences, no mud volcanoes *sensu stricto* occur in this region.

The nearest group of mud volcanoes *sensu stricto*, located outside active belts, is known from the Xinjiang Uygur Autonomous Region in Northwest China (Seach 2007). Further Asian mud volcano areas are in the Central Sakhalin and Hokkaido–Sakhalin shear zones (Chigira and Tanaka 1997; Shakirov et al. 2004; Ershov and Mel'nikov 2007). These form a part of the Pacific Ocean mud volcano belt (Dimitrov 2002). The nearest mud volcano localities in the Alpine Himalayas active belt are in the Punjab region of Pakistan and India as well as in the Assam region of India (Snead 1964; Dimitrov 2002; Kholodov 2002).

Mongolian hydrothermal springs in the Khangay thermal area (Gendenjamts 2003) are developed within Cenozoic large arched uplifts. They belong to the Mongolian–Baikal hydrothermal water region (Lomonosov 1976). No hydrothermal mud volcanoes have yet been described here.

References to mudvolcanic manifestations in Mongolia are linked to strong Mongolian earthquakes on July 9th 1905 (Khangay Earthquake M_L = 8.4–8.7) and on December 4th 1957 (Gobi-Altay Earthquake, M_L = 8.3). Mud spouts are incorporated on the map of the Khangay Earthquake on the southern bank of Lake Bust Nuur in the northwest Mongolia (Voznesenskii and Dorogostaiskii 1914). Florensov and Solonenko (1963) registered clay outflows from fractures on the southern bank of Lake Orok Nuur (northern piedmont of NW Gobi Altay) related to the Gobi-Altay Earthquake. These fractures were caused by hydraulic pressure exerted on the layers of frozen ground during the earthquake in 1957. Liquefaction craters interpreted as sand blows formed during an earthquake were described from the Myanga Bulag oasis in the Biger Nuur Basin (Fig. 1) by Cunningham et al. (1996). Local people reported that the 1957 earthquake caused fountain-like ejections at Myanga Bulag oasis.

A new group of mud volcanoes was discovered during the geological survey (Hanžl and Aichler 2007) of the Zamtyn Nuruu area at junction of the Mongolian and Gobi Altay. The mud volcanoes occur in a nameless, local valley on the northern slopes of the Khar Argalantyn Nuruu Mts., 30 km W of Boon Tsagaan Nuur Lake. They belong to the earthquake-related type of mud volcanoes.

The spring of Dovyn Bulag is the closest feature incorporated on local topographic maps. Therefore, we name this occurrence of mud volcanoes "the Dovyn Bulag field". There are in fact four springs, two groups of mud volcanoes and one well with groundwater level near the surface. The Mongolian name "Dovyn Bulag" means in English "small hill spring". It is highly probable that the spring received its name when a cone of a mud volcano appeared.

2. Regional geography and geology of the area

2.1 Geography

The area of mud volcanoes is located in the western part of the Gobi Altay Range represented here by the Khar Argalantyn Nuruu Mts. (with the Khuren Ondor Uul summit reaching 2,724 m a.s.l.) as well as by the Shiliin Nuruu Highlands (Figs 1–2). The mud volcanoes are exposed on the northern foot of strongly eroded NW slopes

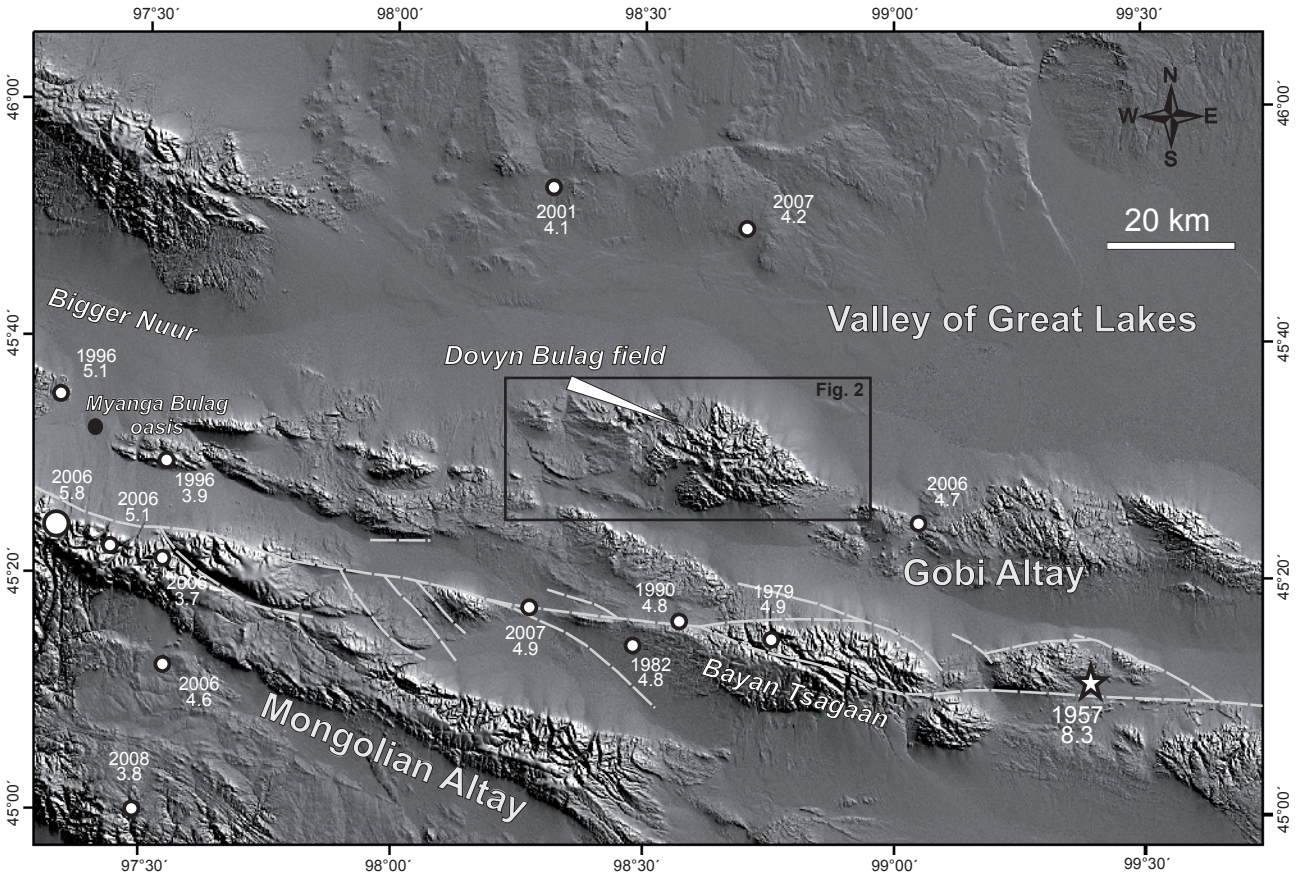

Fig. 1 Digital elevation model with positions of epicentres, years and magnitudes of earthquakes registered by NEIC (National Earthquake Information Centre, U.S. Geological Survey – NEIC 2007) since 1975 in the area of the junction of the Mongolian Altay and of the Gobi Altay. Epicentre of the Gobi Altay 1957 Earthquake is marked by star, epicentre of the Biger 2006 Earthquake by big circle, Dovyn Bulag mud volcanoes by the arrow (see also Fig. 2). Course of the western part of the Bogd fault system is marked by light grey line.

of the Khar Argalantyn Nuruu near the Dovyn Bulag spring at an altitude of *c.* 1,900 m a.s.l. The slopes are open towards the north to a wide intermountain endorheic depression of Ulaan Shalyn Khooloi, which is a part of the "Valley of Great Lakes". This inland drainage basin includes also Lake Boon Tsagaan Nuur, one of the largest Mongolian salt lakes. The region belongs to arid and semi-arid zones with the mean annual precipitation rates varying between 150 and 200 mm. There are only valleys with periodical water streams as typical in dessert areas. The groundwater is discharged from rare springs and is infiltrated back into the valley sediment filling, usually only a few metres from the discharge sites.

2.2 Geology

Gobi Altay has a basin-and-range type appearance. The geomorphology throughout the region suggests Cenozoic stages of an active orogeny (Cunningham et al. 1996). The Gobi Altay range represents one of the youngest mountain ranges in Central Asia. This is consistent with the idea of a northward propagation of the transpressional deformation from the Himalayan front to the Siberian Craton (Vassallo et al. 2007). The isolated mountain massif evolved as a restraining bend along the left-lateral intracontinental E–W trending and recently active fault (Cunningham et al. 2003). This structure (Fig. 1) is known as Bogd fault (Florensov and Solonenko 1963; Tapponier and Molnar 1979) or as North Gobi Altay fault system (Cunningham et al. 2003).

Geologically, the NW part of the Gobi Altay belongs to the Lake Zone Terrane after Badarch et al. (2002) which is composed of the Neoproterozoic to Lower Palaeozoic metamorphic and volcanosedimentary complexes. It is covered by the Lower Permian volcanic sequences and by the Upper Mesozoic continental sediments and volcanic rocks (Fig. 2) related to the western part of the Upper Mesozoic Gobi Altay rift (Yanshin 1976; Yarmolyuk 1986).

The Dovyn Bulag field with mud volcano manifestations is situated in the Quaternary infill of a small valley

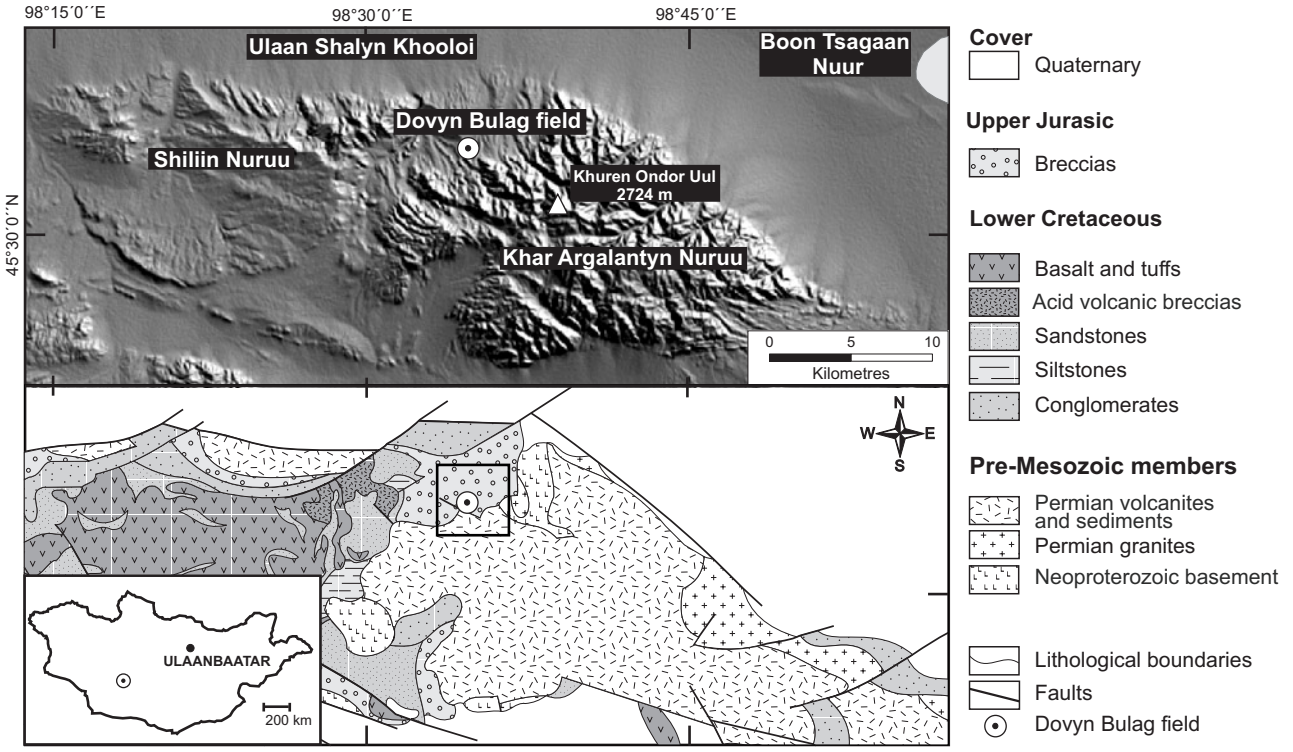

Fig. 2 Location, geomorphology and geology of the discovered Dovyn Bulag mud volcano field in the Khar Argalantyn Nuruu region, NW Gobi Altay, Mongolia.

incising into Jurassic sediments on the NW foothill of the Khar Argalantyn Mts. The basement of the Mesozoic sediments is formed here by the Neoproterozoic metabasalts and metadiorites (Khan Taishir Formation) and by Lower Permian bimodal volcanic rocks (Khar Argalantyn Formation) intruded by Permian granites (Hanžl et al. 2007).

The Mesozoic sequence is well exposed in the Shillin Nuruu syncline west of the studied locality. Sedimentation started with poorly sorted breccias and conglomerates of the Upper Jurassic age covering transgressively the pre-Mesozoic basement. The Upper Jurassic sedimentation was terminated by the Aptian–Albian volcanic activity (Buriánek et al. this volume). The gryphons of the Dovyn Bulag field are related to the lowermost sequence of the Mesozoic sediments of the Toromkhon Formation. Rauzer et al. (1987) estimated the thickness of the Jurassic Toromkhon Fm. to be of up to 650–700 m, but in the studied area there are no outcropping sections, which would confirm a thicknesses exceeding 250–300 m. The sediments of the Toromkhon Fm. consist of poorly sorted to extremely poorly sorted conglomerates, breccias and sandy conglomerates. The occurrence of siltstone horizons within the formation is rare. Poorly sorted and subangular clasts in not graded massive conglomerates indicate rapid sedimentation under arid to semiarid conditions. The lithification of the sediments is relatively low and they are interpreted as sediments of a proximal part of alluvial fans (Gilíková et al. 2007). Four lithological members of the Lower Jurassic sediments (from bottom to the top) were distinguished in the vicinity of the Dovyn Bulag (Fig. 3):

1. poorly sorted, weakly lithified breccias to conglomerates with matrix-supported fabric, matrix being silty to sandy,
2. alternation of weakly consolidated conglomerates, with layers of sandstones, siltstones and mudstones,
3. red siltstones with nets of tiny carbonate veins,
4. red siltstones alternating with sandstone layers and red to grey silty mudstones.

The breccias are usually the lowermost member of the sequence, nevertheless the boundaries between lithologies are transitional and facies substitute each other in a finger-like manner.

Bedding is monoclinal, dipping gently to the northwest, with the dip reoriented of up to 40° along the faults in vicinity of the tectonic contact with the southern Permian volcanic rocks.

Quaternary sediments are represented by Pleistocene–Holocene gravel plains covering the Mesozoic sediments. The thickness of poorly sorted, semi-angular gravels reaches up to 5 metres in the area of the Dovyn Bulag. These gravel plains are cut by valleys filled with the Holocene fluvial sediments of intermittent streams.

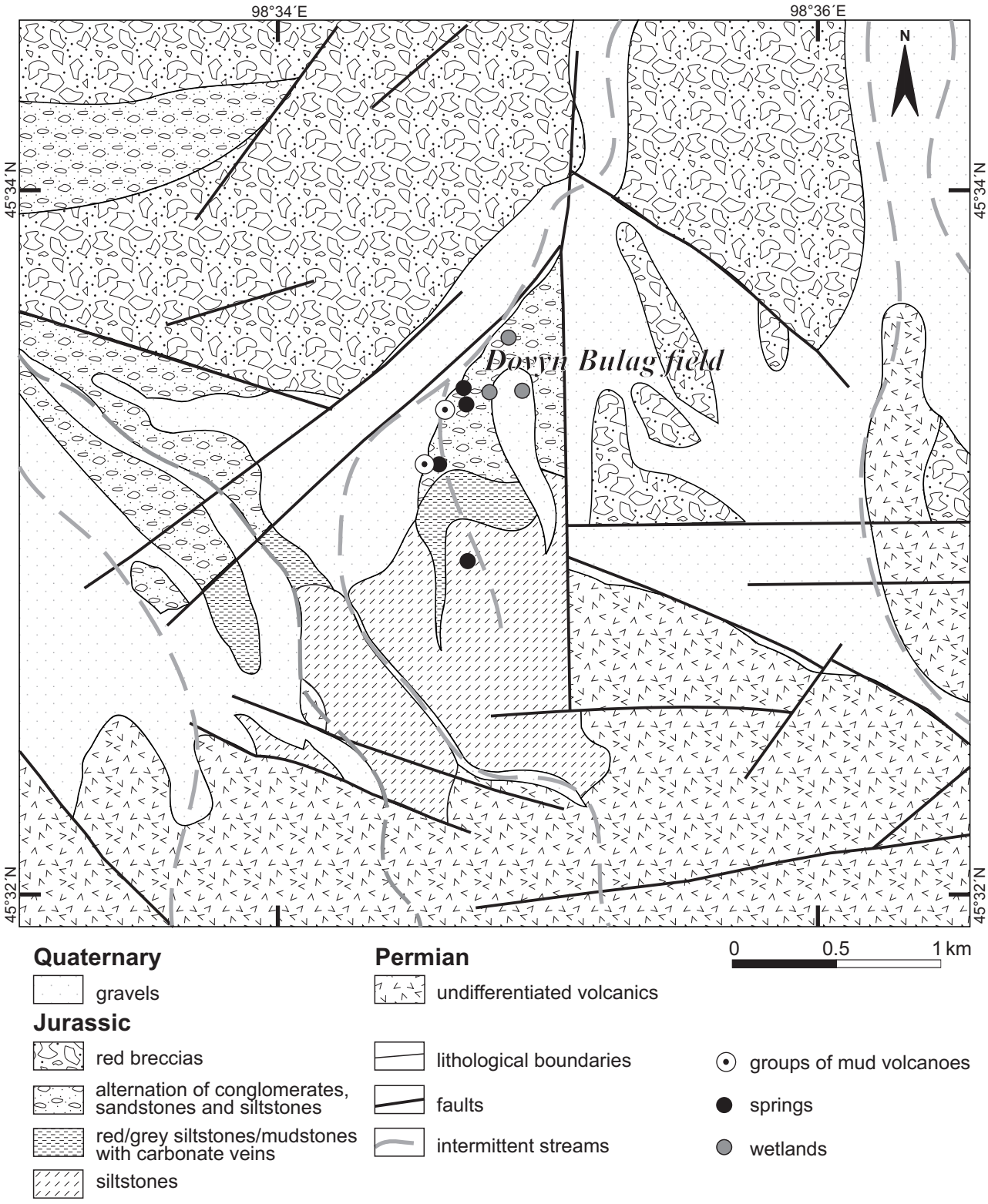

Fig. 3 Detailed geological map of the Dovyn Bulag field.

They are characterized by a large variation in grain size, from coarse-grained gravels to sands. In short, narrow valleys sands and silts dominate as the youngest fill.

In the area of the Dovyn Bulag field the pre-Mesozoic basement is represented by the Permian volcanic sequences. The transgressive basis is exposed approximately

1.5 km towards SW. The dominant part of the basement has suffered upheaval along the NNW–SSE oriented faults south of the locality (Figs 3–4). The Mesozoic sediments in the subsided area form separate blocks bound by numerous local dislocations. The Dovyn Bulag springs are situated along the northern edge of triangular block bordered by a N–S oriented fault in the east, a NW–SE oriented fault in the southwest and NE–SW oriented fault in the northwest. This block is sunken in adjacent poorly sorted Jurassic breccia sediments and represents higher members of the Jurassic sequence. Its lowest part is formed by the alternation of conglomerate benches with layers of red-brown sandstones and siltstones; the red siltstones and mudstones, which are pervaded by extensive nets of calcite veins, are exposed in the hanging wall. The uppermost member is represented by red siltstones with layers of grey mudstones. All strata are gently dipping to the NW and boundaries among them are transitional.

3. The mud volcanoes of the Dovyn Bulag field

3.1 Morphology

The mud volcanoes occur on the lower flat floor of a small valley near its opening to the larger one. The small valley is oriented N–S, being situated approximately at 1,900 m a. s. l. A flat slope composed of weathered Jurassic sediments with their tops about 5–7 m above the valley floor forms the right bank. The left bank is steep with the top formed by the Quaternary gravels 10–15 m over the floor. Benches of conglomerates are exposed in the slope and form also the footwall of the Quaternary fill of the valley. The valley is about 25 m wide near the mouth, then it broadens in the centre between two groups of mud spots and passes into a narrow gully towards the south. The floor of the valley is covered by a muddy crust with salt efflorescence (Fig. 5), the surface of the floor seems to be slightly domed. Mud is slightly eroded by an intermittent local stream. Sandy debris with pebbles accumulates along the banks.

Mud volcanoes form two groups, at a distance of 250 metres from each other (Fig. 3).

A northern group, downstream group occupied the right bank of the valley near its mouth. It is scattered irregularly over an area of 40×15 m. The group consists of several gryphons with a radius from first decimetres to 3 metres and an elevation up to 0.8 m. Small pools filled with muddy water with negligible discharge and direct mud outflows from the bottom of the valley occur there, as well. The thickness of the liquid mud measured in a gryphon is 1 m below the surface.

A southern group of mud volcanoes forms a partly continuous mound 20 m long and up to 6 m wide. It lies on the left bank of the valley.

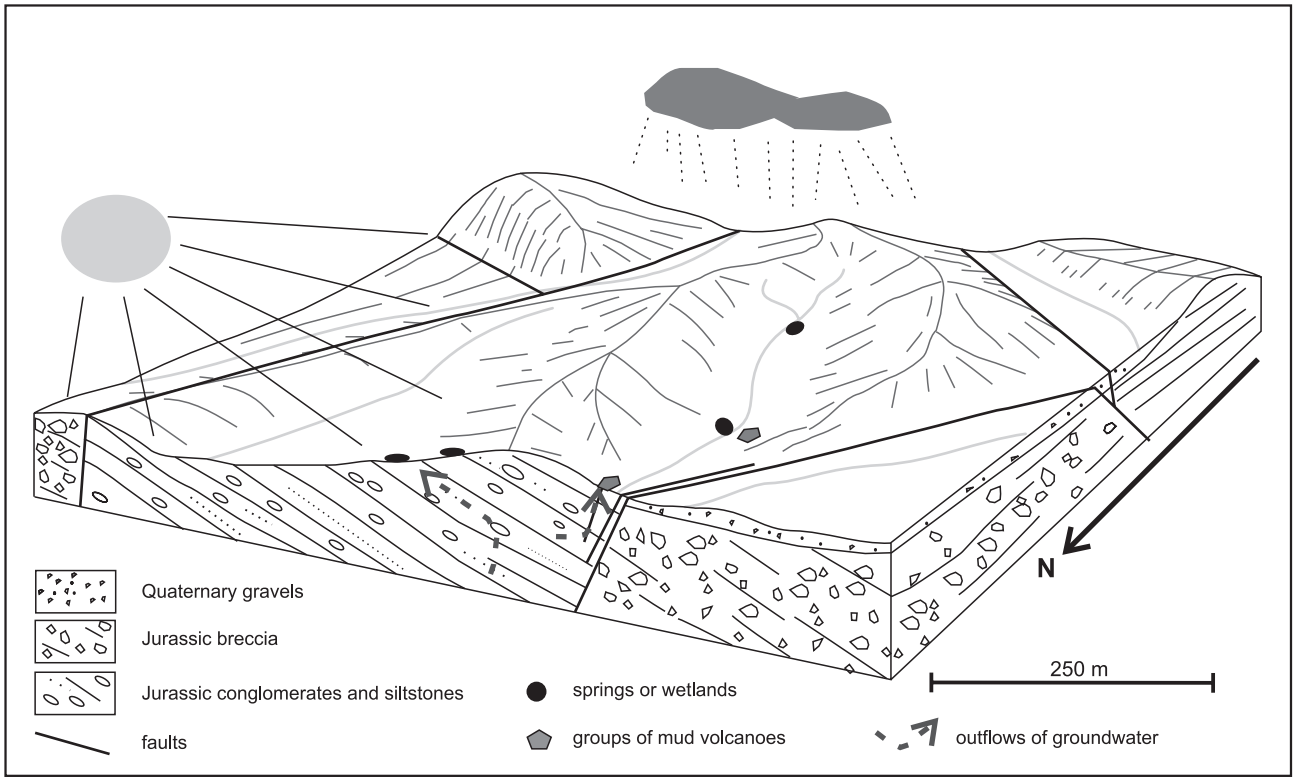

Fig. 4 Block diagram with simplified geology and geomorphology of the Dovyn Bulag field.

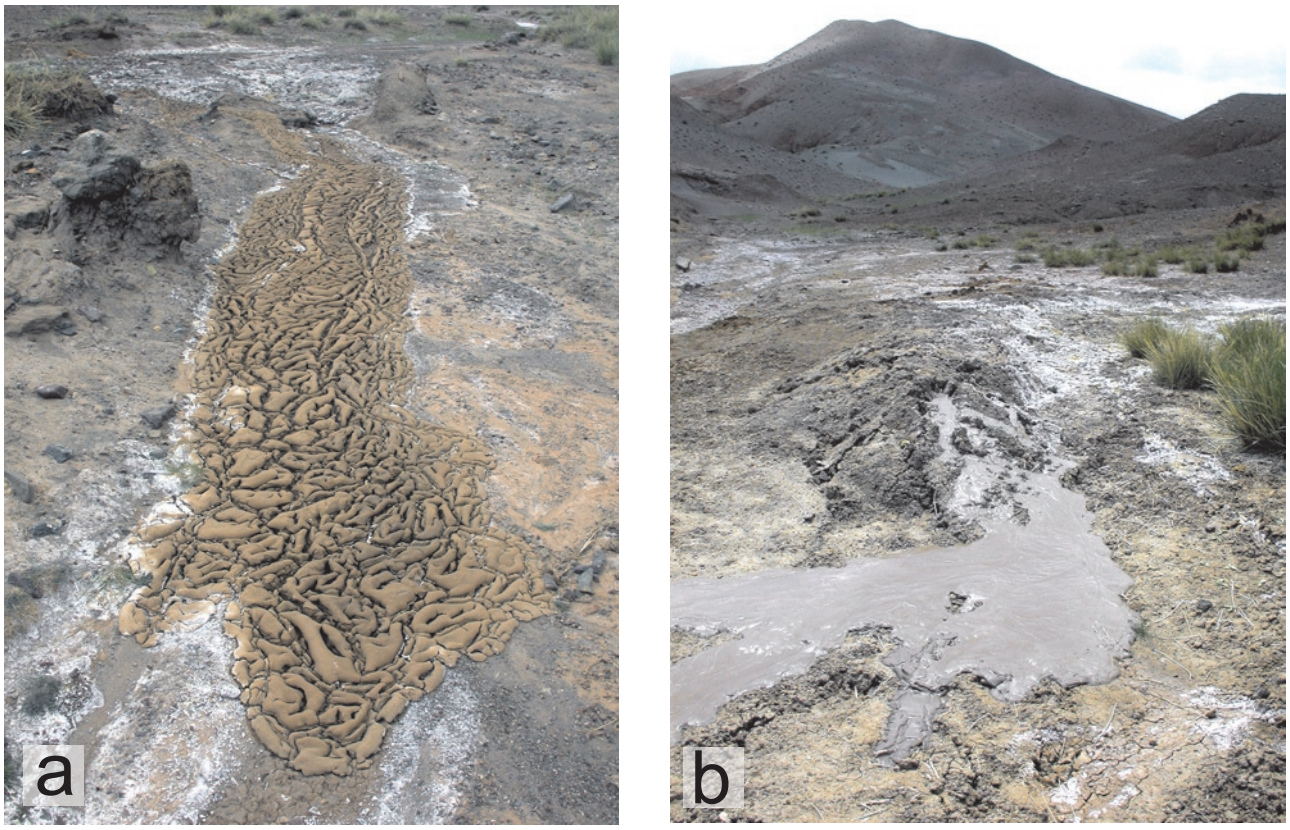

Fig. 5 Examples of mud volcanoes from the Dovyn Bulag field: **a** – Fresh mudflows from the northern group of the mud volcanoes, white spots on the floor are precipitated salts; **b** – A mud outflow from a top of a mound (southern group of the mud volcanoes) triggered by a small artificial mechanical perturbation on the top of the mound.

At the time of our discovery of the locality in June 2006, mud volcanoes were in the passive stage without visible mud outflows. But some of gryphons were active not long before our visit, since fresh mudflows occurred in their vicinity (Fig. 5a). The equilibrium of pressure conditions in the area was labile, as even a small artificial mechanical perturbation of a top part of a mound provoked a mud outflow (Fig. 5b). Other cones were much older according to the degree of their erosion.

Brown and dark-reddish colour of mud predominated, grey mud was less frequent and it flowed out only from mud volcanoes of the southern group.

3.2. Groundwater chemistry

Groundwater, which seeps in the mud volcanoes and in their vicinity, has strong basic character. Field measurements of pH in springs, the nearest well and in pools of muddy water have shown variation from 8.3 to 9.9. The highest measured values were directly in the mud volcanoes areas. Electrical conductivity of groundwater coincides with the values measured in the surrounding parts of the Gobi Altay and of the Mongolian Altay (Rukavičková 2007). It reached values of 900–2,200 μS.cm^{-1} corresponding to TDS (total dissolved solids) ranging from 700 to 1,700 mg.l^{-1} according to a correlation established for this area. Groundwater sampled in a small mud water pool in northern group of mud volcanoes is of Na-HCO_3 type (Tab. 1). A high proportion of hydrogen carbonate among the anions, which is unusual in the surrounding area (Rukavičková 2007), is caused by locally higher content of calciferous component in clays and siltstones. The high content of Na is typical of groundwater in Mesozoic sediments in the Shiliin Nuruu Highlands.

According to calculation performed by PHREEQC model (Parkhurst 1995), the water is Fe oversaturated and its ferruginous precipitation causes a red colour of mud. The mud particles in the water samples contain mainly quartz and clay minerals of the smectite group (montmorillonite) with subordinate amounts of feldspars, mica (muscovite) and hematite.

Tab. 1 Chemical analyses of groundwater from a muddy pool

Li	Na	K	NH4	Mg	Ca	Mn	Fe	Zn	Al
$\mu g.l^{-1}$	$mg.l^{-1}$	$mg.l^{-1}$	$mg.l^{-1}$	$mg.l^{-1}$	$mg.l^{-1}$	$\mu g.l^{-1}$	$mg.l^{-1}$	$\mu g.l^{-1}$	$mg.l^{-1}$
24	346	5.5	< 0.02	12.9	34.1	516	5.5	30	5.7
Cl	**F**	**NO_3**	**SO_4**	**HCO_3**	**SiO_2**	**TDS**	**El. Cond.**	**pH**	**T**
$mg.l^{-1}$	$mg.l^{-1}$	$mg.l^{-1}$	$mg.l^{-1}$	$mg.l^{-1}$	$mg.l^{-1}$	$mg.l^{-1}$	$\mu S.cm^{-1}$		°C
47.9	3.2	< 0.30	212	641	34.1	1,349	1,460.0	8.27	15

4. Origin of the Dovyn Bulag mudvolcanic manifestation

4.1 General conditions

Mud volcanoes at the Dovyn Bulag field belong to the group of mud volcanoes related to seismic events. Liquefaction during, and after, an earthquake shock resulting in exceeding the threshold of thixotropy is usually the major factor triggering formation of a mud volcano of this type.

Liquefaction manifestations occur mainly in young, unconsolidated, water-saturated sediments accumulated in lowland areas near the level of regional erosion base, where large aquifers are drained. River valleys, coastal areas and lakesides in basins of inland drainage (in case of arid climate) are the places meeting the requirements for liquefaction processes.

The mud volcanoes at the Dovyn Bulag field lie on the foot of the Khar Argalantyn Nuruu Mts. in a small barren valley, which, based solely on morphologic criteria, can be a local drainage path for shallow Quaternary aquifer during rare strong rains. An episodic stream appears in this case on the bottom of the valley.

The Gobi Altay is an area with a well-documented recent seismicity (for overview see Kurushin et al. 1997; Vassallo et al. 2007). Many earthquake events with magnitudes up to 8.3 were recorded in databases of ISC (International Seismological Centre) and of NEIC (National Earthquake Information Center, U.S.A.) from this area (ISC 2007; NEIC 2007).

4.2 Hydrogeology

The whole area of the Khar Argalantyn Nuruu Mountains has no natural groundwater seepages. This points to the fact that shallow, near surface groundwater flow is missing here. Water from rare rains infiltrates through regolith to the zone of a subsurface fracture open system. The depth of this zone usually reaches up to 80–100 m. Groundwater from deeper aquifers circulates into the covering sedimentary filling of adjacent basins.

There is a common drainage along a fault system, which borders the foothill of the Khar Argalantyn Nuruu Mountains. Springs associated with near-surface groundwater level frequently accompany these faults. In the springs, the groundwater has a low TDS level atypical of the conditions in the surrounding arid area (Rukavičková 2007). The low TDS levels of groundwater indicate a deeper circulation. In arid climate, a strong TDS increase occurs in groundwater in aquifers near the surface, since these layers contain soluble weathering products and evaporates. Deeper groundwater, in firm rocks with a low content of soluble salts and ascending quickly along fault to the surface, has relatively low TDS.

The mud volcanoes lie at the foot of the Khar Argalantyn Nuruu Mountains close to several faults with supposed groundwater drainage to Jurassic sediments in the subsided block, so that the sediments in the mud volcanoes vicinity are significantly saturated with groundwater.

The faults bordering this block with mud volcano manifestations inhibit the runoff of groundwater further to the centre of sedimentary basin on the eastern and northwestern sides. The faults were sealed by clay or silt components during, or gradually after, the movements and act now as hydraulic barriers. Breccias and conglomerates at the base of the sedimentary sequence form the main aquifer in the area. Alternating beds of conglomerates and sandstones (local aquifers) with layers of siltstones and mudstones (local aquitards) in the roof of the main aquifer altogether act as partial aquitard. The southern part of the subsided block is covered with an impermeable layer of red siltstones.

A single main closed and confined aquifer and a number of local confined or partly confined aquifers are the result of alternation of the impermeable and permeable beds and sealing of groundwater flow-off paths. Due to a high hydraulic gradient caused by steep morphology, piezometric levels of the aquifers are close to, or even above, the surface. High frequency of small springs, wetlands and areas with green vegetation in the mud volcanoes vicinity proves the high degree of the Jurassic sediments saturation and a small depth to the water table. This drainage occurs on the northern side of the block,

where siltstone aquitard is lacking and groundwater slowly soaks from coarse-grained layers.

No permanent stream occurs in the mud volcanoes valley, due to arid climate. Episodic rains flush away silts and clays from the upper, steep part of the valley to the lower, flat part. This fine-grained material dries out and forms an impermeable crust covered by evaporates.

4.3 Recent seismic activity

Earthquake events in the Gobi Altay area are related to Cenozoic faults, which evolved in response to the collision of the Indian and Eurasian tectonic plates. The master fault system, the western prolongation of the recent active, E–W oriented Bogd fault, is situated 35 km SW of the Dovyn Bulag field (Fig. 1). Foreberg structures described by Bayasgalan et al. (1999) at the northern foothill of the Bayan Tsagaan Mts., which were probably reactivated during the 1957 Gobi-Altay Earthquake (M_L = 8.3), are located even closer.

In the last ten years (1997–2007), 11 earthquakes were recorded with epicentres in a distance up to 100 kilometres from the Dovyn Bulag field according to the databases of ISC and NEIC (Fig. 1). Magnitudes of these earthquakes varied between 3.7 and 5.8 and the nearest epicentre was located 30 km from the studied locality. All the earthquakes were shallow, with hypocentres in depths of 10–30 km. According to Panahi (2005), solely such shallow earthquakes influence the mud volcanoes activity. Most of the epicentres concentrated in the close vicinity of the Bogd fault escarpment. However, two of them were localized north of the mud volcanoes in the Ulaan Shalyn Khooloi depression.

The mud volcanoes at the Dovyn Bulag field were discovered five days after a series of four earthquakes, recorded by the worldwide seismic network on 15th June 2006. The earthquakes were of magnitudes 3.9–5.8 and their epicentres were near the town Biger 90 km SW of the Dovyn Bulag (ISC 2007). Since raw mudflows (Fig. 5a) were present at the locality, it is obvious that the last period of mud volcanoes activity was related to these earthquakes. The strongest earthquake in June 2006 was the second largest occurring in the area after the major seismic event in December 1957 (M_L = 8.3) and its aftershocks in 1958. The epicentre of this Gobi-Altay 1957 Earthquake was localised 75 km E of the Dovyn Bulag field (Fig. 1).

5. Discussion

Mudvolcanic manifestations and liquefaction are produced mainly by strong earthquakes. Panahi (2005) reported that mudvolcanic manifestations accompany earthquakes of magnitude $M_L > 5.4$. According to Ambraseys (1988), liquefaction can occur for earthquakes with magnitudes as low as *c.* 5, however, magnitudes of *c.* 5.5 to 6 are the lower limit at which the liquefaction effect becomes relatively common. All available references about mudvolcanic manifestations from the Mongolian or from Russian parts of the Altay Mts. are related to earthquakes with magnitudes greater than 7. The Biger Earthquake (June 15th 2006) with magnitude 5.8 took place near the lower limit for mudvolcanic manifestation. Wang at al. (2006) evaluated worldwide data for earthquakes related to liquefaction occurrence and established a simple equation for liquefaction limit R_{max} (m) that represents the distance from the epicentre of a given magnitude M, beyond which the liquefaction is not observed:

$$Log\ R_{max} = 2.05\ (\pm\ 0.10) + 0.45\ M$$

According to this equation, the Biger Earthquake with magnitude 5.8 could have provoked liquefaction only in a distance up to 45 km. The Dovyn Bulag field is located 90 km from the epicentre of the Biger Earthquake; nevertheless active mud volcanoes with a provable relation to this earthquake occur here.

The mud volcano area of the Dovyn Bulag field with its principal vents was formed probably during the Gobi-Altay Earthquake in 1957. The earthquake intensity and the distance from the epicentre were sufficient for mudvolcanic (liquefaction) manifestation. During worldwide earthquakes with magnitude above 7.5, ejection of fluidized sediments occurred at distances of hundreds of kilometres from the epicentres (Rajendran et al. 2001).

The subsided block with Dovyn Bulag mud volcanoes forms a closed "basin" with confined groundwater surface. Additionally, high aquifer pore pressure increased during 1957 earthquake led to hydraulic fracturing and to opening of current fractures in the weakest part of the upper aquitard. Water, which flowed up during aquifer pressure compensation, entrained liquefied mud and first cones of mud arose on the earth surface. Fault permeability changes and increases in water discharges in springs are commonly observed after strong earthquakes (Rojstaczer and Wolf 1992; Montgomery and Manga 2003).

The groundwater level in the main and local aquifers is confined due to the permanent high hydraulic gradient and the equilibrium of pressure condition in the area is metastable. A small pressure impulse (increase of aquifer pressure) would be sufficient to exceed the threshold of thixotropy and could induce a mud and water ejection through conduits predisposed by the Gobi-Altay Earthquake. Even a weak or distant earthquake or an increase in piezometric level due to a high precipitation amount could be the decisive impulse.

Clay and silt particles are often bound by precipitated salts due to the arid climate. The salts are leached during water level increases and the sediments become susceptible to liquefaction. A relatively high content of smectites in mud may result in a significant role for swelling. We suppose that the stress caused by the increase in volume of sediments during their saturation is released by a mud outflow.

Preservation of mud cones in various stages of weathering and also the local name of the locality bear an evidence for repetitious activity of mud volcanoes at the Dovyn Bulag field.

6. Conclusions

A group of small mud volcanoes was discovered during a geological survey of the NW Gobi Altay in June 2006. The origin of mud volcanoes is closely associated with the recent seismic activity in the area. They arose probably during Gobi-Altay Earthquake in 1957.

If an earthquake shock encounters the sedimentologic, climatic and hydrogeologic prerequisites such as water saturated, unconsolidated sediments tending to a thixotropic behaviour in a closed, confined aquifer, then even weak or far earthquake could initialize the mudvolcanic manifestation. Such conditions concur at the Dovyn Bulag field and enable the mud cone rise.

The equilibrium between the force acting upwards (piezometric pressure, rock strain) and the resistance of sediments is labile. During an earthquake, this equilibrium is disturbed and a short active life period of mud volcanoes may start. We suppose that extreme hydrological events as long-lasting rains can distinctly increase piezometric level in aquifers and break the equilibrium in a manner similar to the earthquake.

Episodic activity of the mud volcanoes is manifested by formation of new mud cones and outflows. Old cones gradually vanish by erosion. The Dovyn Bulag field is a model example of repeated geological manifestation of earthquakes. Hence, the occurrences of mud volcanoes can be used to detect recent seismicity or palaeoseismicity in a particular area.

Acknowledgements. The fieldwork was carried out during the project Geological survey of the Mongolian Altay at the scale of 1 : 50 000 undertaken in the frame of the Program of the Development Assistance Project of the Czech Republic. We are grateful to the staff of the expedition, above all to excellent Mongolian drivers. We thank to F.H. Weinlich, S. Vrána, L. Kraftová, T. Pačes and K. Young for critical reading and help in improving the manuscript.

References

Ambraseys NN (1988) Engineering seismology. Earthq Eng Struct Dyn 17: 1–105

Badarch G, Cunningham WD, Windley BF (2002) A new subdivision for Mongolia: implications for Phanerozoic crustal growth in Central Asia. J Asian Earth Sci 21: 87–110

Bayasgalan A, Jackson J, Ritz JF, Carretier S (1999) Forebergs, flower structures, and the development of large intra-continental strike-slip faults: the Gurvan Bogd fault system in Mongolia. J Struct Geol 21: 1285–1302

Buriánek D, Hanžl P, Bolormaa K, Erban V (2008) The early Cretaceous volcanic activity in the western part of the Gobi-Altay rift (Shiliin Nuruu, Mongolia). J Geosci 53: 167–180

Chigira M, Tanaka K (1997) Structural features and the history of mud volcanoes in southern Hokkaido, northern Japan. J Geol Soc Japan 103: 781–791

Cunningham WD, Widley BF, Dorjnamjaa D, Badamgarov J, Saadar M (1996) Late Cenozoic transpression in southwestern Mongolia and the Gobi Altai–Tien Shan connection. Earth Planet Sci Lett 140: 67–81

Cunningham WD, Dijkstra A, Howard J, Quarles A, Badarch G (2003) Active intraplate strike-slip faulting and transpressional uplift in the Mongolian Altai. In: Storti F, Holdsworth RE, Salvini F (eds) Intraplate Strike-Slip Deformation Belts. Geol Soc London Spec Pub 210: pp 65–87

Dimitrov LI (2002) Mud volcanoes – the most important pathway for degassing deeply buried sediments. Earth Sci Rev 59: 49–76

Ershov VV, Meĕnikov OA (2007) Unusual eruption of the main Pugachevo gas-water-lithoclastic (mud) volcano in Sakhalin during the winter of 2005. Russ J Pac Geol 1: 366–370

Florensov NA, Solonenko VP (eds) (1963) The Gobi-Altay Earthquake. Akad Nauk USSR, Moscow, pp 1–394 (in Russian)

Gendenjamts O (2003) Interpretation of geochemical composition of geothermal fluids from Árskógsströnd, Dalvík, and Hrísey, N-Iceland and in the Khangai area, Mongolia. Geothermal Training Programme, Reykjavík, Reports 10: 219–252

Gilíková H, Budil P, Otava J, Hanžl P, Buriánek D (2007) Mesozoic. In: Hanžl P, Aichler J (eds) Geological survey of the Mongolian Altay at a scale of 1: 50,000 (Zamtyn Nuuu – 50), MS. Czech Geological Survey, Prague, MRPAM, Ulaanbaatar, pp 141–159

Hanžl P, Aichler J (eds) (2007) Geological survey of the Mongolian Altay at a scale of 1: 50,000 (Zamtyn Nuruu – 50), Final report. Czech Geological Survey, Prague, pp 1–377

Hanžl P, Buriánek D, Hrdličková K, Aichler J, Gerdes A, Byambasuren D (2007) Granite massifs in the Zamtyn Nuruu area, SW Mongolia. In: Breiter K (ed) Proceedings of the 3rd Meeting of the Czech Geological Society, Volary, 19–22 September 2007, pp 27 (in Czech)

Hovland M, Hill A, Stokes D (1997) The structure and geomorphology of the Dashgil mud volcano, Azerbaijan. Geomorphology 12: 24–37

ISC on-line data base, Bulletin 2007. *http://www.isc.ac.uk*, International Seismological Centre, Thatcham, United Kingdom.

Kholodov VN (2002) Mud volcanoes, their distribution regularities and genesis: communication 1. Mud volcanic provinces and morphology of mud volcanoes. Lithol Miner Res 37: 197–209

Kurushin RA, Bayasgalan A, Lziybat M, Enhtuvshin B, Molnar P, Bayarsayhan C, Hudnut KW, Lin J (1997) The surface rupture of the 1957 Gobi-Altay, Mongolia, earthquake. Geol Soc Am Spec Pap 320: pp 1–143

Lomonosov IS, Pissaesky BI, Khilko SD (1976) The role of neotectonics in the formation of the thermal springs of the Mongolian-Baikal orogenic belt. In: Rónai A (ed) Hydrogeology of Great Sedimentary Basins: Proceedings of an International Hydrogeological Conference IAH-IAHS, Budapest 1976, pp 663–670

Milkov AV (2005) Global distribution of mud volcanoes and their significance in petroleum exploration as source of methane in the atmosphere and hydrosphere as geohazard. In: Martinelli G, Panahi B (eds) Mud Volcanoes, Geodynamics and Seismicity. NATO Sci Ser 51, Springer, Amsterdam, pp 29–34

Montgomery DR, Manga M (2003) Streamflow and water well responses to earthquakes. Science 300: 2047–2049

NEIC 2007. Earthquake database. *http://neic.usgs.gov/*, National Earthquake Information Center, Denver, USA

Panahi B (2005) Mud volcanism, geodynamics and seismicity of Azerbaijan and the Caspian Sea region. In: Martinelli G, Panahi B (eds) Mud Volcanoes, Geodynamics and Seismicity. NATO Sci Ser 51, Springer, Amsterdam, pp 89–104

Parkhhurst DL (1995) User's guide to PHREEQC – a computer program for speciation, reaction-path, advective transport and inverse geochemical calculations. U.S. Geological Survey, Water-Resources Investigations Report 95–4227, Lakewood, Colorado

Pinegina TK, Konstantinova TG (2006) Macroseismic observation of consequences from April 21, 2006 "Olytorskoe" Earthquake. Vestn KRAUNC, Ser Nauki Zemle 1: 169–173 (in Russian)

Pitt AM, Hutchinson RA (1982) Hydrothermal changes related to earthquake activity at Mud Volcano, Yellowstone National Park, Wyoming. J Geophys Res 87(B4): 2762–2766

Rajendran K, Rajendran CP, Thakkar M, Tuttle MP (2001) The 2001 Kutch (Bhuj) Earthquake: coseismic surface features and their significance, Curr Sci 80: 1397–1405

Rauzer AA, Zhanchiv DI, Golyakov VI, Ykhina IF, Ivanov IG, Tsukernik AB, Afonin VV, Smirnov IG, Bykhover VI, Kravtsev AV, Baatarkhuyag A, Skoryukin MI, Khodikov IV, Mantsev NV, Okaemov SV, Mischin VA, Enkhsajkhan T (1987) Report on results of geological survey at a scale of 1: 200,000, performed in southeast part of the Mongolian Altay, Mongolian National Republic in 1983–1986. Tekhnoexport, Moscow, pp 1–352 (in Russian)

Rogozhin EA, Ovsyuchenko AN, Marakhov AV, Ushanova EA (2007) Tectonic setting and geological manifestations of the 2003 Altai Earthquake. Geotectonics 41: 87–104

Rojstaczer S, Wolf S (1992) Permeability changes associated with large earthquakes: an example from Loma Prieta, California. Geology 20: 211–214

Rukavičková L (2007) Hydrogeology. In: Hanžl P, Aichler J (eds) Geological survey of the Mongolian Altay at a scale of 1: 50,000 (Zamtyn Nuruu – 50), Final report. Czech Geological Survey, Prague, pp 240–266

Seach J (2007) Baiyanggou Mud Volcanoes. Volcano Live website, *http://www.volcanolive.com/baiyanggou.html*

Shakirov R, Obzhirov A, Sueze E, Salyuk A, Biebow N (2004) Mud volcanoes and gas vents in the Okhotsk Sea area. Geo-Mar Lett 24: 140–149

Snead RE (1964) Active mud volcanoes of Baluchistan, West Pakistan. Geogr Rev 54: 546–560

Tapponier P, Molnar P (1979) Active faulting and Cenozoic tectonics of the Tien Shan, Mongolia and Baykal region. J Geophys Res 84(B7): 3425–3459

Vassallo R, Ritz JF, Braucher R, Jolivet M, Carretier S, Larroque C, Chauvet A, Sue C, Todbileg M, Bourles DL, Arzhannikova A, Arzhannikova S (2007) Transpressional tectonics and stream terraces of the Gobi-Altay, Mongolia. Tectonics 26, DOI 10.1029/2006TC002081

Voznesenskii A, Dorogostaiskii V (1914) The map of the 9th and 23rd July 1905 earthquake area. In: Florensov NA, Solonenko VP (eds) (1963) The Gobi-Altay Earthquake. Akad Nauk USSR, Moscow (in Russian)

Wang CI, Wong A., Dreger DS, Manga M (2006) Liquefaction limit during earthquakes and underground explosions: implications on ground-motion attenuation. Bull Seismol Soc Am 96: 355–363

Yanshin AL (1976) Map of Mesozoic and Cenozoic Tectonics of the Mongolian People's Republic: 4 sheets, scale 1:1,500,000. Akad Nauk USSR, Moscow

Yarmolyuk VV (1986) The structural position of continental rift zones of Mongolia. Izv Akad Nauk SSSR, Ser Geol 9: 3–12 (in Russian)

Original paper

Geophysical cross-section through the Bogd fault system in the area of the Chandman rupture, SW Mongolia

Viktor VALTR[1*], Pavel HANŽL[2]

[1] *Sihaya, Ltd., Veleslavínova 6, 612 00 Brno, Czech Republic; sihaya@sihaya.cz*
[2] *Czech Geological Survey, Leitnerova 22, 658 69 Brno, Czech Republic*
[*] *Corresponding author*

The internal structure of the Bogd fault, which is one of the largest intra-continental faults in Asia, was studied using the geophysical methods of very low frequencies, vertical electrical sounding and induced polarization vertical sounding. The geophysical profile was situated on the eastern foothill of the Chandman Khayrkhan Uul (SW Mongolia) near the branching of the Chandman rupture, recently seismically active western part of the Bogd fault zone. Geophysical measurements confirmed several sub-parallel faults that are steeply dipping to the south. An imbricated structure inside the fault zone and anastomosing trends of mylonitic zones were revealed by the orientation of the low resistivity zones. The most distinct anomalies indicating the fault zone were localised in mylonitized graphitic limestones, which were preferentially involved in the structure of the fault. The orientations of geophysical anomalies together with geological and structural data from the surface indicate steep thrusting of the southern block over the northern one, accompanying the dominating strike-slip component of the movement along the Chandman rupture. Geometry of faults delimiting the Chandman Khayrkhan Uul, strong asymmetrical morphology of mountain and relics of the Quaternary gravels in its upper part indicate rapid uplift of the range during the Cenozoic in the restraining bend.

Keywords: Bogd fault, Gobi Altay, geophysics, vertical electrical sounding
Received: 31 March 2008; accepted 29 May 2008; handling editor: J. Kotková

1. Introduction

The Gobi Altay range shows a basin-and-range type appearance and geomorphology throughout the region, which suggests Quaternary tectonic activity (Cunningham et al. 1996a). It appears as one of the youngest mountain ranges in the Central Asia, which is consistent with the idea of a northward propagation of the transpressional deformation from the Himalayan front to the Siberian Craton (Vassallo et al. 2007).

The isolated mountain massifs of the Gobi Altay range evolved as bends along the recently active left-lateral intracontinental E–W trending structure known as the Bogd fault (Florensov and Solononko 1963; Tapponier and Molnar 1979) or the North Gobi Altay fault system (Cunningham et al. 2003).

The Bogd fault is a seismically active, right-stepping left-lateral strike-slip fault system that can be traced on the surface for nearly 400 km. It runs approximately between Artz Bogd Mt. in the east and Biger Nuur Lake in the west (Cunningham et al. 1996a, b). The eastern two thirds of the fault system ruptured during a major earthquake (M = 8.3) in 1957 (see Kurushin et al. 1977 for review). On the other hand, degraded fault scarps cutting alluvial deposits along the western third of the system indicate that this segment did not rupture during the 1957 event but has been active already during the Quaternary (Cunningham et al. 1996a). The western part of the Bogd fault is offset by the Bayan Tsagaan restraining bend and is known as a Chandman rupture (Fig. 1), It continues further west of the Chandman Khayrkhan Uul as a scarp visible on the Landsat imagery, termed the Myangan rupture (Baljinnyam et al. 1993).

The recent seismic activity in the area was confirmed also by macroseismic observations during the field works on June 15th, 2006. According to NEIC (National Earthquake Information Center, U.S. Geological Survey), a series of four earthquakes with magnitudes ranging from 4.0 to 5.6 was localized approximately 60 km west of the Chandman sum in an array sub-parallel with the Myangan rupture (Fig. 1a). The focal mechanism for the highest-magnitude event computed by NEIC corresponded to a strike-slip movement on the E–W-oriented fault. The last event of the year 2006 (magnitude 4.7) was localized north of the Bayan Tsagaan Mt. Recently, there was registered an earthquake (M = 4.9) on August 20th, 2007, which was localized by NEIC directly on the Chandman rupture, approximately 3 km E of the geophysical profile (Fig. 1b).

The geophysical profiles in the eastern foothill of the Chandman Khayrkhan Uul Mt. were situated over small geochemical anomaly of As, Au and Bi, which coincided with a mylonitic zone on the Chandman rupture of the Bogd fault and was ascertained during the geological

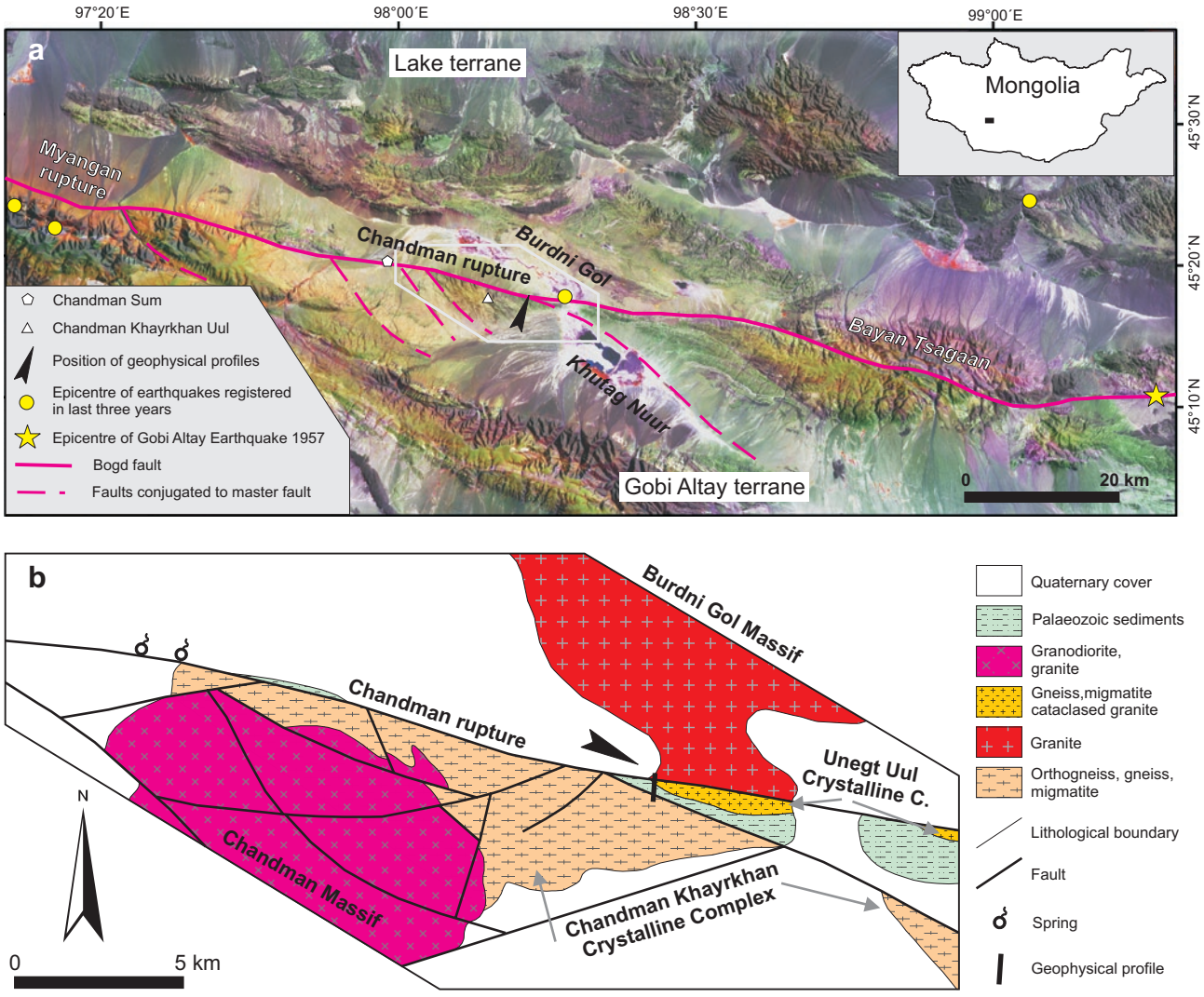

Fig. 1 Geomorphology and basic geology along the Chandman rupture of the Bogd fault: **a** – position of the studied area and Bogd fault on the digital elevation model combined with the Landsat ETM+ (4-5-3 as RGB); **b** – geological sketch along the Chandman rupture.

survey of the Zamtyn Nuruu area (Hanžl and Aichler 2007). The geophysical manifestations and the geological interpretation of the profile through the Chandman part of the important intracontinental fault are presented in this paper.

1.1 Geographical position

The Chandman Khayrkhan Uul is located in the eastern part of the Gobi Altay Province of the Western Mongolia, specifically, east of the Chandman sum. It is an isolated mountain massif on the junction between the Gobi Altay and Mongolian Altay Mts. and represents the easternmost promontory of the Bayan Tsagaan mountain range. The morphology of the Chandman Khayrkhan Uul (2,802 m a.s.l.) shows a pronounced N–S-oriented asymmetry. It rises steeply from the intermontane endorheic valley of the Burdni Gol River (~2,200 m a.s.l.) in the north. Relics of alluvial fan gravels are cut by short dry valleys on the northern slopes. Summit is flat as are slopes dipping towards the SW, which are cut by two NW–SE oriented fault steps and could be interpreted as an ancient erosion surface. Slopes oriented towards SE dip to endorheic depression of Khutag Nuur Lake; they are rocky with narrow dry valleys without gravel infill.

1.2 Geological setting

The Bogd fault is assumed to be a part of the so-called Main Mongolian lineament, a regional topographic and

structural boundary separating mostly Precambrian and Lower Palaeozoic rocks of the Lake Terrane in the north from dominantly Middle–Upper Palaeozoic units of the Gobi Altay Terrane in the south (Fig. 1a) (Marinov et al. 1973; Badarch et al. 2002).

In the area of the Chandman rupture, the fault separates metamorphic rocks, Carboniferous granites and the Lower Palaeozoic sediments of the Gobi Altay Terrane in the south from the Lake Zone in the north. The latter includes Neoproterozoic to Cambrian metamorphic and volcanosedimentary rocks accompanied by Cambrian granites with the Permian volcanics in the hanging wall (Hanžl and Aichler 2007).

The scarp of the Bogd fault is nearly E–W-oriented, tracing the northern foothills of the Chandman Khayrkhan Uul. This part of the fault was designated as the Chandman rupture (Baljinnyam et al. 1993). Springs accompanied by an accumulation of aeolian material are associated with the fault on the western edge of the mountain. The water-rich endorheic depression and flat land with Cambrian granites are exposed north of the fault. Variscan granites and diorites of the Chandman Massif (Economos et al. this volume) with metamorphic rocks of the Chandman Khayrkhan Crystalline Complex (Hrdličková et al. this volume) are exposed in the area of the Chandman Khayrkhan Uul south of the master fault (Fig. 1b). The fault splits into two branches at the eastern extremity of the Chandman Khayrkhan Uul. The northern one continues towards east, the southern one deflects to SE and disappears east of Khutag Nuur Lake. Tectonic melange composed of mylonitized granites, metamorphic rocks, serpentinites related to the Unegt Uul Crystalline Complex (Hrdličková et al. this volume) and Lower Palaeozoic sediments (Rauzer et al. 1987) including limestones is exposed in a wedge between these two fault branches. The NWN–ESE-trending foliation is a dominant feature in the metamorphic rocks south of the Chandman Uul. The foliation planes are medium to steeply dipping to the south and bear metamorphic lineations plunging variably to NW or SE. The asymmetric structures that developed locally along the feldspar porphyroblasts in the gneiss on the northern slope of the Chandman Khayrkhan Uul indicate strike slip movements sub-parallel to the strike of the Chandman rupture (Hanžl and Aichler 2007).

2. Geophysical measurements

2.1. Geophysical methods

The two parallel geophysical profiles were localized on the eastern tip of the Chandman Khayrkhan Uul, near the splitting of the master fault into two branches (Fig. 1a). The direction of the geophysical profiles was NNE–SSW; therefore the main profile No. 100 was approximately perpendicular to the surveyed fault axis. Second auxiliary profile no. 150 was placed at the distance of 50 m W of the profile No. 100. The length of each of the two profiles was 920 m.

The profile No. 150 was examined only by the method of very low frequencies (VLF), whereas on the main survey profile No. 100 the following complex of geophysical methods was applied:

The method of *vertical electrical sounding (VES)* was used to determine boundaries of quasi-homogeneous blocks of rocks according to their resistivity (rough determination of the volume of conductive fine fraction in sediments, estimation of the slope of tectonic zones, estimation of rock types and state of weathering etc.).

The method of *induced polarization vertical sounding* (time domain combined Schlumberger IPS and VES soundings) in its VES modification *(VES-IP)* was used to determine boundaries of quasi-homogeneous rock blocks according to their ability to be polarized by long-time (from 1 to 3 s) direct current charges. The apparent polarizability (apparent chargeability) of rocks was determined for various time windows: starting from 100 to 250 ms after current I_{AB} (A–B electrode current) switching-off and ending with the window: 1350 to 1500 ms after current I_{AB} switching-off. The parameter η_{app} is obtained using the following equation:

$$\eta_{app} = \frac{U^{MN}_{mx}}{U^{MN}_{inTW}} [\%]$$

U^{MN}_{mx} – *steady voltage (observed whilst the current is on) – the potential difference measured between voltage non-polarising electrodes M and N short time before I_{AB} switching-off,*

U^{MN}_{inTW} – *magnitude of the polarisation voltage – the potential difference average of discharging curve measured between M and N electrodes in given time window after I_{AB} switching-off.*

The positive anomaly of the η_{app} parameter was used to indicate ore mineralization, or increased graphite contents in underlying quasi-homogeneous rock blocks. The decrease of this parameter can, for instance, differentiate salt water from clay materials in pores of clastic sediments (Komarov 1980).

GEA-IV – the direct current geophysical instrument (24b A/D*2) with continuous sampling of potential electrodes voltage with rechargeable direct current source from 12 V to 400 V – was used for VES and VES-IP measurements.

Obtained VES curves and VES-IP discharge curves were interpreted by the VIS software (SIHAYA, Ltd.) directly to the form of depth section.

The method of *dipole electromagnetic profiling (DEMP)* was performed to subdivide efficiently the exposed rocks according to their apparent conductivity. This measurement was carried out using ground conductivity meter CM-031, manufactured by Geofyzika Brno, with the maximum investigation depth of approximately 6 m (depending on the ground conductivity).

The method of *very low frequencies (VLF)* was applied along both profiles (no. 100 and 150) to determine effectively the dip, shape, surface position and direction of long, deep conductors such as fault zones, graphitic zones and ore bodies, which are longer than 50 m. This continuous-wave electromagnetic technique records perturbations in a plane-wave radio signal (15–30 kHz) emanating from one of distant military transmitters. We used VLF instrument ENVI SCINTREX, which can measure both the primary and secondary fields in three frequencies simultaneously. The data acquired by this VLF instrument involve three separate parameters of the secondary magnetic field: the amplitude of the field, its quadrature (imaginary) and in-phase (real) components relatively to the horizontal primary field (or equivalently the elasticity and "tilt angle" of the field).

Acquired VLF data were interpreted using software VDV-PH (SIHAYA, Ltd.) based on Karous and Hjelt (1983) theories of apparent current density dependence upon the measured tilt angle of the VLF signal. It enables obtaining apparent current density distribution at certain pseudodepth levels and hence construction of pseudodepth–apparent current density sections according to the VLF. The interpretation process is generally qualitative and subjective in each case. VLF-located anomalous areas had to be further studied in detail by independent techniques.

The method of *single sensor magnetometry (MM)* was used to determine effectively the surface boundaries of magnetically different rocks (by measuring the total magnetic field – TF).

For MM we used instrument PMG 1.0 ver. 1.2 – proton magnetometer and gradiometer (Satis Geo). Modern magnetometers usually measure the gradient of the magnetic field (by two sensors separated vertically by two or three feet). We measured only the total field (single sensor mode) as it was more suitable for the aim of this mapping measurement. The resulting TF was corrected for TF variations measured by the same device in a near variation point or using variation station instrument ENVI SCINTREX – Mag.

On the auxiliary profile 150 only the VLF method was applied to verify the orientation of the observed anomalies.

2.2 Field geophysical measurements

Geophysical measurements along the profiles on the Chandman rupture were accomplished in July 2006 within the frame of the project "Geological survey of the Mongolian Altay at a scale of 1 : 50,000 (Zamtyn Nuruu-50)".

Position of all measured points and ends of geophysical profiles were acquired by GPS. In total 37 points of VES, 38 points of VES-IP, 397 points of DEMP, 498 points of MM and 494 points by method of VLF were acquired along the geophysical cross-section.

2.3 Results of geophysical measurements

The pseudodepth section of apparent current density according to the VLF method is shown in Fig. 2. One strong manifestation of a deep long intensive conductor appears on this section. Its outstanding anomaly (marked in red colour) reaches apparent current densities down to -26. This anomalous structure crops out at chainage 560 m. It is dipping steeply to the south and is probably caused by a graphitized zone along the major rupture zone. It is possible to find also several smaller anomalies of less intense manifestation. The second largest anomalous structure is the one surfacing around chainage 250 m (current density extends only to -11, shown in blue) with sense of dip towards N.

The isoohmic section of the measured apparent resistivities by VES (Fig. 3) correlates well with the VLF results. The zone of very low resistivities is rather well seen – representing a manifestation of the main fault zone (red, violet colours – for particular values see the hatch legend on figure) – even using raw measured apparent resistivity data (chainage from 550 m to 630 m).

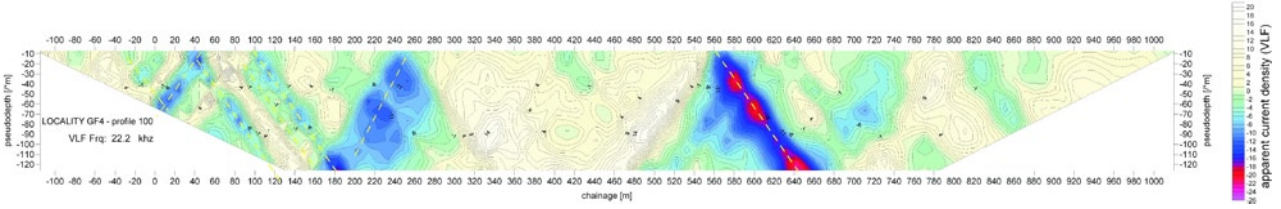

Fig. 2 The pseudodepth section of apparent current density according to VLF; indication of faults in blue to red colours.

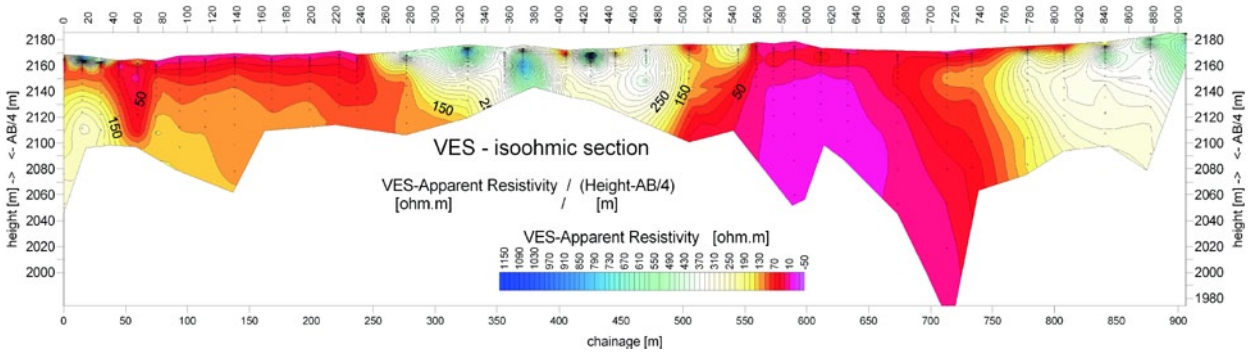

Fig. 3 The pseudodepth section of apparent resistivity according to VES; indication of faults in red to violet colors.

The VES-IP-resulting polarizability (0.8 sec after I_{AB} off) correlates with the modal ore and graphite contents in the rock marking the active fault zone by an yellow, red to violet area (η_{app} from 3.0 to 7.4 %; Fig. 4). The strongest anomaly (polarizability almost 7.5 %) was detected around the chainage 590 m (from 555 to 610 m). The highly prolonged discharging curves in this area imply graphitization.

A smaller anomaly is evident also around chainage 250 m, correlating well with the second strongest VLF anomaly.

The resulting interpreted resistivity section according to VES with diagrams of TF (total field magnetometry – violet line graph) and apparent resistivities according to DEMP (green and blue line graphs) are shown in Fig. 5. In this picture, summarizing results of all used methods, the fault boundary is far more precisely demarcated. There is also a notable decrease in apparent resistivities according to DEMP, accompanied by magnetometry total field increase at chainage 510–610 m. The shape of TF diagram in this anomalous sector is also significant for the fault dip to the south. The TF diagram is much more variable in the area between chainage 180 m to 510 m than in the area from chainage 600 m upwards.

Similarly, the highest apparent resistivities by DEMP have been reached in between chainage 280 m to 500 m and from 850 m upwards.

3. Geological interpretation of the geophysical data

Generally, the Chandman rupture of the Bogd fault zone separates the Cambrian granites of the Burdni Gol Massif (Hanžl and Aichler 2007) in the N from the metamorphic rocks in the roof of the Variscan Chandman Massif in the area of the eastern foothill of the Chandman Khayrkhan Uul. Palaeozoic sediments are enclosed by the branching faults in this zone (Fig. 1b).

Dominating trends of geophysically detected boundaries and anomalies along the profile on the eastern foothill of the Chandman Khayrkhan Uul are characterized by a homogeneous orientation. Geophysical anomalies are steeply dipping towards the south (Fig. 5), which is in accordance with the orientation of foliation, bedding and mylonitized zones observable on the surface. The southward oriented dip of these small-scale planar structures varies from 40° to 80°.

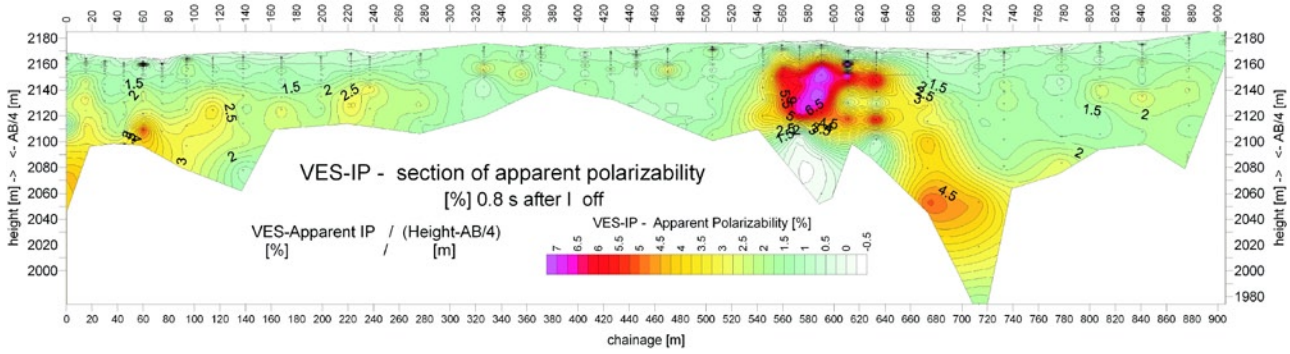

Fig. 4 The pseudodepth section of apparent polarizability by VES-IP; indication of faults in red to violet colours.

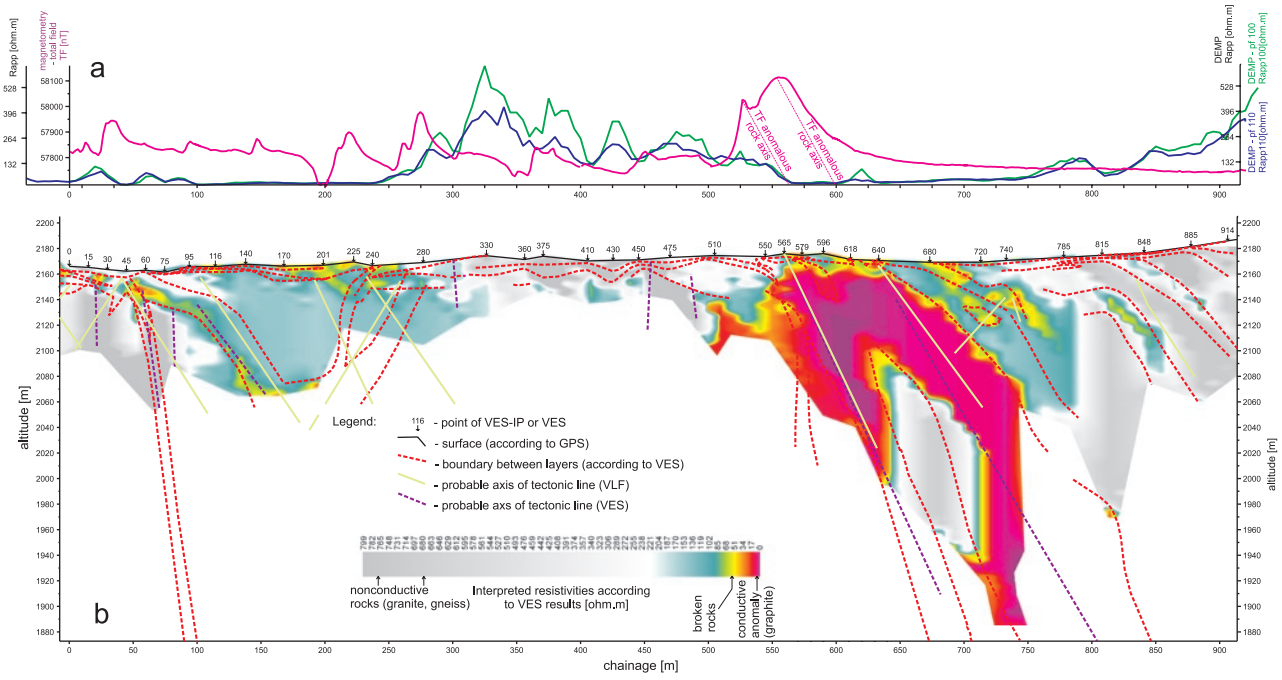

Fig. 5 Summary of geophysical data: a – TF^{mg}, R_{app}^{DEMP} diagrams with VLF conductor axes; b –interpreted vertical section according to resistivities VES and VLF.

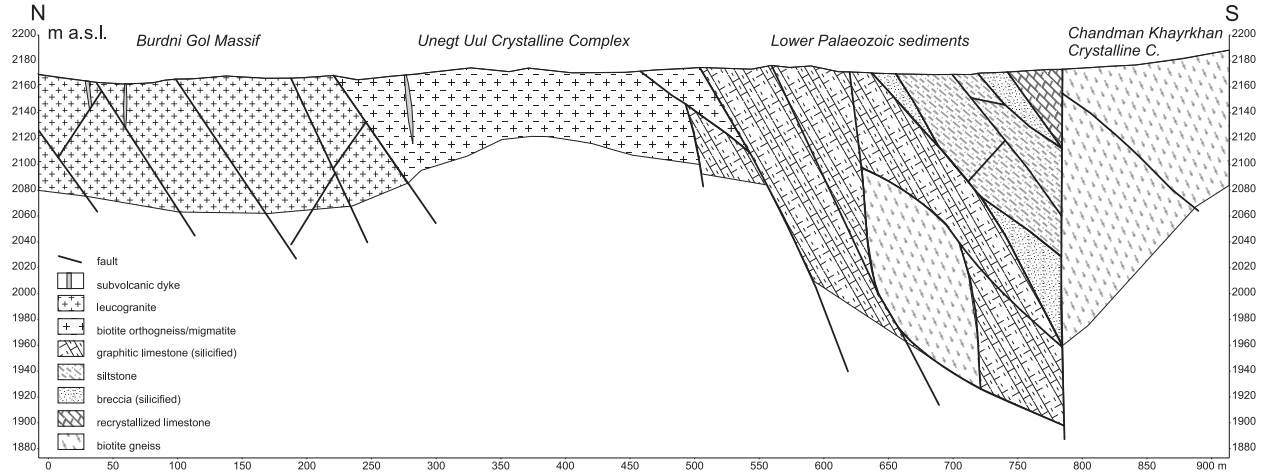

Fig. 6 Geological interpretation of the geophysical profile across the Chandman rupture of the Bogd fault zone.

The homogeneous fabric of the Burdni Gol Massif situated north of the fault is disturbed by a system of faults dipping to the south, as documented at profile chainage 50–250 m (Fig. 6). The zone of opposite dip (at the chainage 200–280 m) could be interpreted as an older fault zone or as a relic of wall rocks (mica schists) mapped in granites more to the north (Hanžl and Aichler 2007). A relatively homogeneous, tectonically restricted block composed of orthogneisses and migmatites of the Unegt Uul Crystalline Complex continues to chainage 500 m. The zone of extremely low resistivities at chainage 520–650 m corresponds to exposures of silicified, mylonitized and graphitic limestones, which can be related to the Lower Palaeozoic sedimentary and volcanosedimentary formations exposed more towards east (Rauzer et al. 1987). Limestones are brecciated, and tectonically bound boudines of adjacent rocks are incorporated in the fault zone (Fig. 6). The zone is dipping steeply to the south and is approximately 150 m wide. In the hanging wall of limestones, grey cataclastic siltstones are exposed. The fault, separating metamorphosed rocks of the Chandman Khayrkhan Crystalline Complex in the southern block and sedimentary sequences incorporated in the Bogd fault structure, is steep to nearly subvertical and can be interpreted as a master fault. Fault breccias and lenses of recrystallized limestones on the surface mark the contact between blocks. Towards the south, a homogeneous structure of gneisses is cut by faults which are sub-parallel with metamorphic foliation in this part of the Chandman Khayrkhan Crystalline Complex.

The sense of shearing along the Bogd fault has been generally considered to be sinistral (Tapponier and Molnar 1979), and the reverse faults were commonly described in the area of Baga Bogd and Ikh Bogd at the eastern termination of the Bogd fault zone (Vassallo et al. 2007). Position of tectonically restricted blocks of metamorphosed rocks in the hanging wall of the Palaeozoic sediments indicate thrusting of the southern block over the northern one. Cunningham et al. (1996a) described similar situation from the erosional cut on the western slopes of the Chandman Khayrkhan Uul. The strong asymmetry in geomorphology of the Chandman Khayrkhan Uul with inclined peneplain surface in the SW, relics of the Quaternary alluvial gravels on the northern slopes and rocky ramp oriented to SE indicate rapid and asymmetric uplift of the mountain due to movements on the Chandman rupture and conjugated faults. Orientation of the conjugated faults visible as scarps on the satellite imagery (Fig. 1a) and thrusting documented on the master fault of the Chandman rupture fit well the geometry of terminal restraining bend described by Cunningham (2005) from Jargalant Nuruu in the Mongolian Altay.

4. Conclusions

The geophysical cross-section on the eastern tip of the Chandman Khayrkhan Uul was situated near the branching of the Chandman rupture, which is a part of a large intracontinental tectonic zone – the Bogd fault. Geophysical measurements confirmed a steep dip to the south and its splitting into two branches east of the Chandman Khayrkhan Uul. The zone inside the northern block showing opposite dip could be interpreted as an older fault. Geophysical data indicate imbricated structure inside the fault zone and anastomosing trends of mylonitic zones. The more distinct fault zone is related to the layer of graphitic limestones. The orientation of geophysical anomalies together with geological and structural data from the surface implies thrusting of the southern over the northern block along the Chandman rupture.

Based on the field structural data and orientation of conjugated faults as seen from the satellite imagery, the origin of the Chandman Khayrkhan Uul can be interpreted as a restraining bend evolved on the left-lateral Bogd fault. The strong asymmetry in geomorphology of the Chandman Khayrkhan Uul is in accordance with a rapid uplift during the Quaternary. The seismic activity in the area is confirmed by the position of the recent earthquake epicentres along the segments of the Bogd fault as registered by the National Earthquake Information Center of the U.S. Geological Survey.

Acknowledgements. The geophysical measurements were carried out within the framework of the project "Geological Survey of the Mongolian Altay at a scale 1 : 50,000" which was a part of the Official Cooperation Assistance of the Czech Republic. We are indebted to H. Gilíková for help with drawing the figures. Last but not least, comments by reviewers J. Kněz, Ch. Krawczyk and handling editor J. Kotková have significantly helped us to improve this manuscript.

References

Badarch G, Cunningham WD, Windley BF (2002) A new terrane subdivision for Mongolia: implications for the Phanerozoic crustal growth of central Asia. J Asian Earth Sci 21: 87–110

Baljinnyam I, Bayasgalan A, Borisov BA, Cisternas A, Dem'yanovich MG, Ganbaatar L, Kochetkov VM, Kurushin RA, Molnar P, Philip H, Vashchilov YY (1993) Ruptures of major earthquakes and active deformation in Mongolia and its surroundings. Mem Geol Soc Amer 181: pp 1–62

Cunningham WD (2005) Active intracontinental transpressional mountain building in the Mongolian Altai: defining a new class of orogen Earth Planet Sci Lett 240: 436–444

Cunningham WD, Windley BF, Dorjnamjaa D, Badamgarov J, Saandar M (1996a) Late Cenozoic transpression in southwestern Mongolia and the Gobi Altai–Tien Shan connection. Earth Planet Sci Lett 140: 67–81

Cunningham WD, Windley BF, Dorjnamjaa D, Badamgarov J, Saandar M (1996b) A structural transect across the Mongolian Altai: active transpressional mountain building in central Asia. Tectonics 15: 142–156

Cunningham WD, Dijkstra A, Howard J, Quarles A, Badarch G (2003) Active intraplate strike-slip faulting and transpressional uplift in the Mongolian Altai. In: Storti F, Holdsworth RE, Salvini F (eds) Intraplate Strike-Slip Deformation Belts. Geol Soc London Spec Pub 210: 65-87

Economos R, Hanžl P, Hrdličková K, Buriánek D, Said LO, Gerdes A (in print) Geochemical and structural constraints on the magmatic history of the Chandman Massif of the eastern Mongolian Altay Range, SW Mongolia. J Geosci

Florensov NA, Solononko VP (1963) The Gobi-Altay Earthquake. Akademiya Nauk USSR, Moscow, pp 1–394 (in Russian)

Hanžl P, Aichler J (eds) (2007) Geological survey of the Mongolian Altay at a scale of 1: 50,000 (Zamtyn Nuruu – 50). MS, Geological Information Centre, MRPAM, Ulaanbaatar, pp 1–376

Hrdličková K, Bolormaa K, Buriánek D, Hanžl P, Gerdes A, Janoušek V (2008) Petrology and age of metamorphosed rock in tectonic slices inside the Palaeozoic sediments of the eastern Mongolian Altay, SW Mongolia. J Geosci 53: 139–165

Karous M, Hjelt SE (1983) Linear filtering of VLF dip-angle measurements. Geoph Prospecting 31: 782–794

Komarov VA (1980) Elektrorazvedka metodom vizvannoy polyarizatsii. Nedra USSR, St. Petersburg, pp 1–391 (in Russian)

Kurushin RA, Bayasgalan A, Olzybat M, Enhtuvshin B, Molnar P, Bayarsayhan C, Hudnut KW, Lin J (1977) The surface rupture of the 1957 Gobi-Altay, Mongolia, earthquake. Geol Soc Am Spec Pap 320, pp 1–143

Marinov NA, Zonenshain LP, Blagonravov VA (eds) (1973) Geologija Mongolskoi narodnoi respubliky. Nedra, Moscow, pp 1–782 (in Russian)

Rauzer AA, Zhanchiv DI, Golyakov VI, Ykhina IF, Ivanov IG, Tsukernik AB, Afonin VV, Smirnov IG, Bykhover VI, Kravtsev AV, Baatarkhuyag A, Skoryukin MI, Khodikov IV, Mantsev NV, Okaemov SV, Mischin VA, Enkhsajkhan T (1987) Otchot o rezultatach gruppovoj geologičeskoj syomki masštaba 1 : 200 000 provedennoj v yugo-vostočnoy časti Mongolskogo Altaya Mongolskoi Narodnoji Respubliki v 1983–1986 g. g. Tekhnoexport, Moscow, pp 1–352 (in Russian)

Tapponier P, Molnar P (1979) Active faulting and Cenozoic tectonics of the Tien Shan, Mongolia and Baykal region. J Geophys Res 84(B7): 3425–3459

Vassallo R, Ritz J, F., Braucher R, Jolivet M, Carretier S, Larroque C, Chauvet A, C. Sue C, Todbileg M, Bourle`s D, Arzhannikova A, Arzhannikov S (2007) Transpressional tectonics and stream terraces of the Gobi-Altay, Mongolia. Tectonics 26, TC5013, doi:10.1029/2006TC002081.

Journal of Geosciences, 53 (2008), 201–234 DOI: 10.3190/jgeosci.028

Original paper

Geology and geochemistry of the Palaeozoic plutonic bodies of the Trans-Altay Gobi, SW Mongolia: implications for magmatic processes in an accreted volcanic-arc system

Pavel HANŽL[1*], Dash BAT-ULZII[2], Miroslav REJCHRT[3], Jan KOŠLER[4], Khasbazaar BOLORMAA[5], Kristýna HRDLIČKOVÁ[1]

[1] *Czech Geological Survey, Leitnerova 22, 602 00 Brno, Czech Republic; pavel.hanzl@geology.cz*
[2] *Department of Geology and Mineralogy, Mongolian University of Science and Technology, Ulaanbaatar-46/520, Mongolia*
[3] *Czech Geological Survey, Klárov 3, 118 21 Prague, Czech Republic*
[4] *Department of Earth Science, University of Bergen, Bergen, N-5007 Norway*
[5] *Geological Investigation Centre, Songino Khayrkhan District, PO Box 37/307; Ulaanbaatar, Mongolia*
[*] *Corresponding author*

Three geological domains (Gobi Tien Shan, Shargyn Gobi and Trans-Altay) have been distinguished in the Trans-Altay Gobi (SW Mongolia) consolidated during the Carboniferous and intruded by numerous plutons of the Devonian, Carboniferous and Permian ages. According to relationship to the Variscan orogenic cycle, pre-orogenic, syn-orogenic and post-orogenic intrusive bodies have been recognized. A pre-orogenic phase is represented by the Gurvan Khar Massif composed of geochemically primitive granodiorites that are geologically related to the relics of the Silurian–Devonian oceanic crust in the Zoolen Terrane (Shargyn Gobi Domain). Calc-alkaline intrusive rocks of I-type in the Gobi Tien Shan and Naran Sevest intrusive complexes exposed in the Gobi Tien Shan Domain are syn-orogenic to post-orogenic. Laser ablation U-Pb ICP-MS dating on zircon yielded an Early Carboniferous age for the Zamyn Belgekh Pluton, representing the largest plutonic body in this domain. Other plutons (Bayan Ayrag, Trans-Altay and Ikh Bayan) are of high-K chemistry, have Late Carboniferous to Permian age and are clearly post-orogenic. Minor gabbro massifs and small oval bodies of granites of the Ikh Bayan Massif in the Baytag Terrane (Shargyn Gobi Domain) are spatially related to the Trans-Altay shear zone of Late Carboniferous to Permian age. This zone accommodated dextral lateral movements between the Shargyn Gobi and Trans-Altay domains.

Keywords: Trans-Altay Gobi, Variscan orogeny, granite, geochemistry, laser ablation, Trans-Altay shear zone, geotectonic position
Received: 31 March 2008; accepted 3 July 2008; handling editor: M. Štemprok

The online version of this article (doi: 10.3190/jgeosci.028) contains supplementary electronic material.

1. Introduction

The Palaeozoic and Mesozoic geological evolution of Central Asia was predominantly influenced by accretion of blocks of various geological character to the southern margin of Eurasia (e.g. Şengör et al. 1993; Windley et al. 2002; Jahn 2004). The orogenic belt has developed between the Siberian Block in the north, the Tarim Block in the south-west and the Sino-Korean Block in the south. It is known as the Central Asian Orogenic Belt (Mossakovsky et al. 1993) or the Altaids (Şengör et al. 1993) and it had evolved in a time span of 1000–250 Ma (Windley et al. 2007). It is composed of micro-continents, collapsed ocean basins, and associated accretionary volcano-sedimentary complexes, subduction-related volcanoplutonic arcs and anorogenic intrusive rocks (Hendrix et al. 1992). Şengör et al. (1993) interpreted this belt as a giant Palaeozoic subduction-accretion complex.

The Central Asian Orogenic Belt is characterised by an abundance of Palaeozoic and Mesozoic granitic intrusions as well as basaltic to rhyolitic volcanic rocks (e.g. Jahn et al. 2000) and is known as an important site of juvenile crustal growth during the Phanerozoic (Hu et al. 2000). The granitoids have a wide range of compositions and roughly show a temporal evolution from calc-alkaline, through alkaline to peralkaline series. The emplacement most of the granitic plutons fell between 500 to 120 Ma (Jahn et al. 2000).

Even though the Altaids can serve as an ideal site for a case study of magmatic processes in accreted volcanic-arc systems, the geological, geochemical and isotopic data on granite bodies are irregularly distributed. Whereas numerous data exist from NW China (e.g., Allen et al. 1992; Wei et al. 1997; Windley et al. 2002; Yuan, et al. 2007) some from Kazakhstan and Russian Altay (Kovalenko et al. 2004), Mongolian Altay (Mitrofanov et

al. 1981; Bibikova et al. 1992; Kozakov et al. 2007), eastern Gobi (Webb et al. 1999; Wang et al. 2003; Zhang et al. 2007) and southern Mongolia (Kozlovsky et al. 2005; Kovalenko et al. 2006), any data from the Trans-Altay Gobi are so far lacking. We present here new geological and geochemical data on granitic bodies in this remote, geologically little known area of SW Mongolia near its border with China.

1.1 Geographic position of the Trans-Altay Gobi

The Trans-Altay Gobi is situated SW of Edrengiin Nuruu Mts. in the SW corner of Mongolia. The studied area has been limited by the latitude 44° N in the N and the longitude 99° E, in the E as well as by the Mongolian–Chinese state border in the W and S (Fig. 1). Morphologically, it is formed by the E–W oriented Gobi Tien-Shan mountain range in the south, reaching maximum 2695 m a.s.l. (the summit of Atas Uul). The northern Edrengiin Nuruu range is a NW–SE trending structure with the highest point Ochir Khayrkhan Uul (1846 m a.s.l.) outside the studied area. The landscape between these mountain chains has a character of extensive uplands, in which no significant geomorphologic units can be distinguished. The northern slopes of the Gobi Tien Shan are lined by a system of endorheic intermountain depressions of the Shargyn Gobi. The lowermost point (~550 m a. s. l.) is located in the west in the Zagt Ikh Sayr valley at the Chinese border.

1.2 Geological setting of the Trans-Altay Gobi

The geologically very little known area of the Trans-Altay Gobi is formed by Palaeozoic volcanosedimentary and magmatic complexes locally covered by Mesozoic and Cenozoic sediments in the zone of junction between the Tien Shan and Altay orogenic belts. While the terrane division of Mongolia by Badarch et al. (2002) is generally used in a geological literature, our data from the Trans-Altay Gobi fit better with the geological subdivision of the South Mongolia by Ruzhentsev and Pospelov (1992) and Ruzhentsev (2001).

Based on a new geological survey (Šourek et al. 2003), three main Palaeozoic geological domains (Fig. 1) have been described in the Trans-Altay Gobi from north to south: **Trans-Altay (TA)** composed of Edren and Baaran

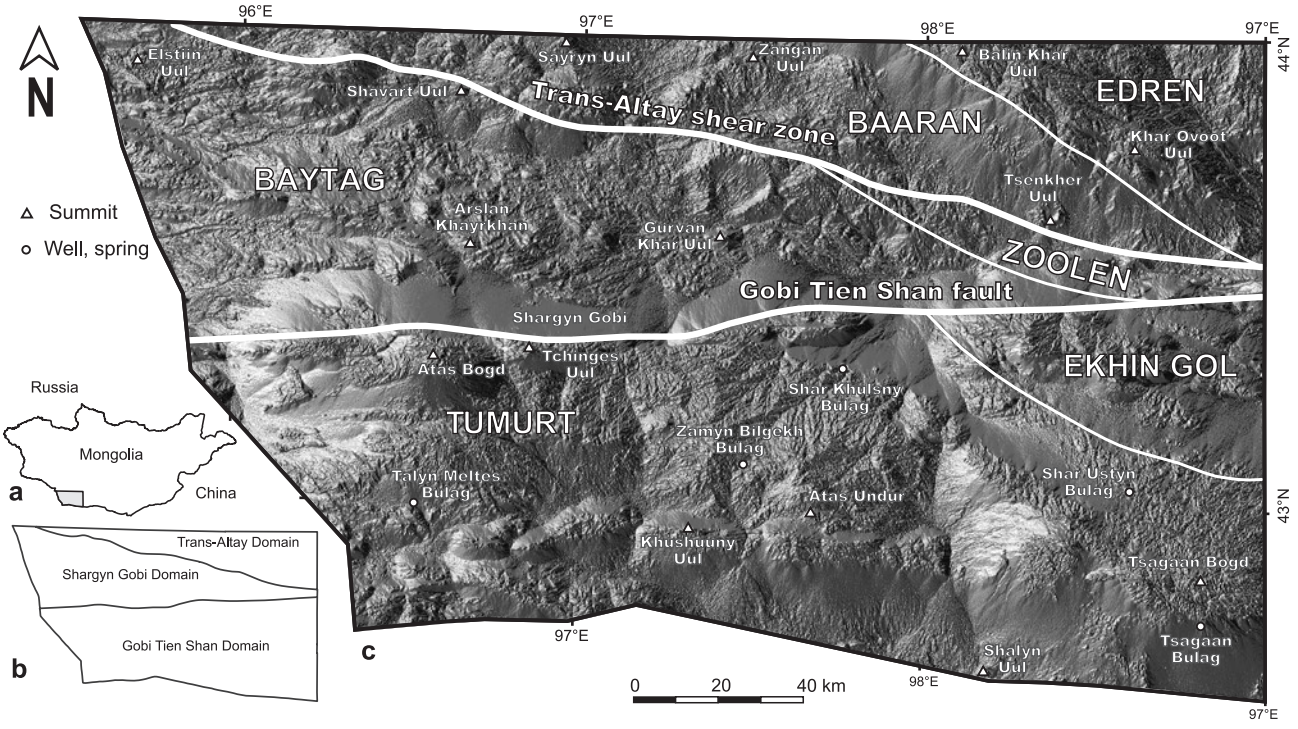

Fig. 1 Basic topography and geological nomenclature of the Trans-Altay Gobi: **a** – position of the Trans-Altay Gobi within the Mongolia; **b** – geological domains distinguished in Trans-Altay Gobi see also Tab. 1; **c** – digital elevation model of the Trans-Altay Gobi with important topographic points and subdivision to geological terranes (Edren, Baytag, Baaran, Zoolen, Ekhin Gol and Tumurt – set in capitals) and names of important geological boundaries (modified according to Ruzhentsev 2001; Badarch et al. 2002 and Hanžl et al. 2003).

terranes, **Shargyn Gobi (SG)** formed by Zoolen and Baytag terranes and **Gobi Tien Shan (GTS)** containing Tumurt and Ekhin Gol terranes. Generally speaking, the Trans-Altay Domain is built by Devonian island-arc basalts in Edren Terrane (Lamb and Badarch 2001) and by the Devonian to Carboniferous volcanic rocks and siliciclastic to volcaniclastic sediments (Hanžl et al. 2003). The Shargyn Gobi Domain is composed of Early Palaeozoic deep-water sediments, ophiolite remnants and Early Carboniferous siliciclastic turbidites covered by Late Carboniferous to Permian volcanic and volcaniclastic rocks (Ruzhentsev 1985). While Baytag Terrane was interpreted as an island arc and Zoolen Terrane as an accretionary wedge terranes by Badarch et al. (2002), rock association (Ruzhentsev 2001) and geochemical data (Helo 2006) point to an ophiolitic character of the Zoolen Terrane, at least. The Gobi Tien Shan Domain is of backarc/forearc basin character with accreted Ordovician to Carboniferous volcanic rocks, as well as siliciclastic and volcaniclastic sediments. These were accreted together with metamorphosed rocks of unknown age newly mapped in the Atas Bogd range (Šourek et al. 2003; Hanžl and Krejčí 2008).

A correlation between various interpretations and terrane-related terminology is summarised in Tab. 1. The suture developed between the GTS and SG is masked by the Cenozoic sediments in the Shargyn Gobi depression and was reactivated by the E–W trending Gobi Tien Shan fault system. The boundary between the SG and TA follows a NW–SE trending suture delineated by the exposures of serpentinite boudins and coloured mélange. Closing of this suture was post-dated by the intrusion of the Trans-Altay Intrusive Complex of (?) Early–Late Carboniferous age. The suture was reactivated in the latest stages of the Variscan tectonic activity and it could be interpreted as a dextral shear zone. This Trans-Altay shear zone resembles that described by Allen et al. (1992) from the northern Tien Shan in NW China.

2. Methodology

The presented geological interpretations and analytical data stem from available field documentation, maps and samples collected during the geological survey in the Trans-Altay Gobi (Šourek et al. 2003).

Petrography. The thin sections were prepared and described in Petrographical and Mineralogical Laboratory of the Geological Investigation Centre in Ulaanbaatar. Plagioclase basicity was determined by optical methods. Modal composition of rocks was computed by semi-automatic Eltinor 3 point counter.

Electron microprobe analyses were performed in the Joint Laboratory of Electron Microscopy and Microanalysis of the Masaryk University and the Czech Geological Survey (Brno). Operating conditions were 15 kV accelerating voltage, and beam current of 80 nA.

Geochemistry. Samples (each about 1–2 kg in weight) were pulverized in the Central Geological Laboratory in Ulaanbaatar and analysed at ACME Labs in Vancouver. Major oxides, LOI, C and S were analysed by ICP-ES (0.2 g sample, $LiBO_2$ fusion). Trace elements including REE were determined by ICP-MS (following a $LiBO_2$ fusion or aqua regia digestion in the case of precious and base metals). The only wet major-element whole-rock geochemical analyses performed at the Central Geological Laboratory in Ulaanbaatar are available for samples from the Bayan Ayrag Massif (Šourek et al. 2003). Whole-rock data were interpreted by the GCDkit software (Janoušek et al. 2006).

ICP-MS dating of zircons – samples and instrumentation. Samples of granite (*c.* 10 kg in weight) were crushed in iron mortar, heavy fractions were obtained by panning in the field. Zircons were extracted using heavy liquids and magnetic separation in laboratories of the Geomin Co., Jihlava. Hand-picked zircons were mounted in epoxy resin and polished. In order to better characterize their internal structure, all zircon grains

Tab. 1 Review of geological domains and terrane nomenclature of the Trans-Altay Gobi.

this paper		Ruzhencev (1985)		Ruzhencev and Pospelov (1992)		Tumurtogoo (1997, 2002)		Badarch et al. (2002)
domain	*terrane*	*domain*	*terrane*	*domain*	*terrane*	*domain*	*terrane*	*terrane*
Trans-Altay	Edren	Transaltay		Edrengiin	Edrengiin Nuriin	Transaltay	Edren	Edren
	Baaran			Transaltay			Aj Bogd	Baaran
Shargyn Gobi	Zoolen					Nemegt		Zoolen
	Baytag			South Baruun Khuurai		Baruun Khuurai	Khayrkhan	Baytag
Gobi Tien Shan	Ekhin Gol	Gobi Tien Shan	Ekhin Gol	South Gobi	Ekhingol	Gobi Tien Shan		Atasbogd
	Tumurt		Tumurtyn		Tumurtyn			

were imaged in BSE prior to the analysis by laser ablation ICP-MS.

In this study we utilized a VG PlasmaQuad 2 S+ instrument coupled to an in-house built 266 nm NdYAG laser at Memorial University, Newfoundland to measure Pb/U and Pb isotopic ratios in zircons. The sample introduction system was modified to enable simultaneous nebulisation of a Tl/^{233}U tracer solution and laser ablation of the solid sample. The tracer solution was aspirated to the plasma in an argon carrier gas through a Micromist concentric nebuliser, Scott-type double-pass spray chamber and a T-piece tube attached to the back end of the plasma torch. A helium gas line carrying the sample from the laser cell to the plasma was attached to the T-piece tube.

The laser was focused *c.* 100 μm above the surface of the sample and it was set up to produce energy of 0.8 mJ/pulse at a repetition rate of 10 Hz, and masked to produce laser pits with *c.* 10 μm diameter. The sample was mounted on a computer-driven motorised stage of a microscope and the stage was moved beneath the stationary laser beam to produce a square laser pit (40×40 μm) or line pit in the sample. The depth of pits varied from *c.* 10 to 15 μm. Typical acquisitions consisted of a 50s measurement of the gas blank and Tl/^{233}U solution signal just before the start of ablation. The U and Pb zircon ablation signal, along with the continuous Tl/^{233}U solution signal, were acquired for another 190 s. Data for the 1065 Ma old zircon 91500 standard periodically acquired during the course of this study gave a ^{238}U-^{206}Pb age of 1069 ± 8 Ma (2σ, n = 41).

Data were acquired in time resolved – peak jumping – pulse counting mode with one point measured per peak for masses 201 (flyback), 202 (Hg), 203 (Tl), 204 (Hg + Pb), 205 (Tl), 206 (Pb), 207 (Pb), 233 (U) and 238 (U). Quadrupole settling time was 3 ms and the dwell time was 8.3 ms on each mass except for 207, where it was 24.9 ms. The raw data were corrected for dead time of the electron multiplier (20 ns), laser-induced elemental fractionation, instrument mass bias (using the Tl/^{233}U signal of the tracer solution) and gas and tracer solution blank. The amount of common Pb present in zircons analysed in this study was insignificant and accordingly, no common Pb correction was applied to the data. Errors on ages are quoted at 2 sigma level.

3. Plutonic rocks of the Trans-Altay Gobi

Bodies of the plutonic rocks that are irregularly distributed in the Trans-Altay Gobi are the most widespread in the GTS, common in SG and subordinate in the studied part of the TA (Fig. 2 and map enclosed in this Volume). There are neither relevant radiometric data nor trace element analyses except for a few ICP-MS laser ablation U-Pb zircon ages of J. Košler (in Šourek et al. 2003). Thus the ages of plutons are estimated from their relationships with palaeontologically documented strata and interpretation of zircon laser ablation data. While the majority of plutons are spatially restricted to a given terrane, rocks of the Trans-Altay Intrusive Complex are distributed across the terrane boundaries. The names of plutonic complexes in Trans-Altay Gobi are used in accordance with Filippova et al. (1990b) and outlined in Tab. 2 (the term "intrusive complex" is used for extensive bodies composed of plutons of variable compositions). Modal and normative classifications of plutonic rocks are summarized in Fig. 3. Individual intrusive complexes are characterized in the order from the Trans-Altay Domain, through the Shargyn Gobi to the Gobi Tien Shan Domain.

Tab. 2 Outline of plutonic complexes exposed in the Trans-Altay Gobi.

Name	Terrane	Petrography	Age	Enclaves	Subvolcanic dykes
Bayan Ayrag	TA	Gabbro–diorite, monzonite, granite	C1	rare	common
Trans-Altay	TA, SG, GTS	Granodiorite, granite	C1–2 (P?)	rare	rare
Gabbro massifs	TA, SG	Gabbro	C2–P1	no	no
Ikh Bayan	SG	Granite	C2–P1	common	common
Gurvan Khar	SG	Metagranodiorite, metagranite, cataclased	D?	no	rare
Tsagaan Bogd	GTS	Alkali feldspar granite to granite	C2	no	no
Gobi Tien Shan	GTS	Gabbro, diorite, tonalite, granodiorite, granite	C1 (P?)	common	common
Naran Sevest	GTS	Granodiorite	D?	common	common

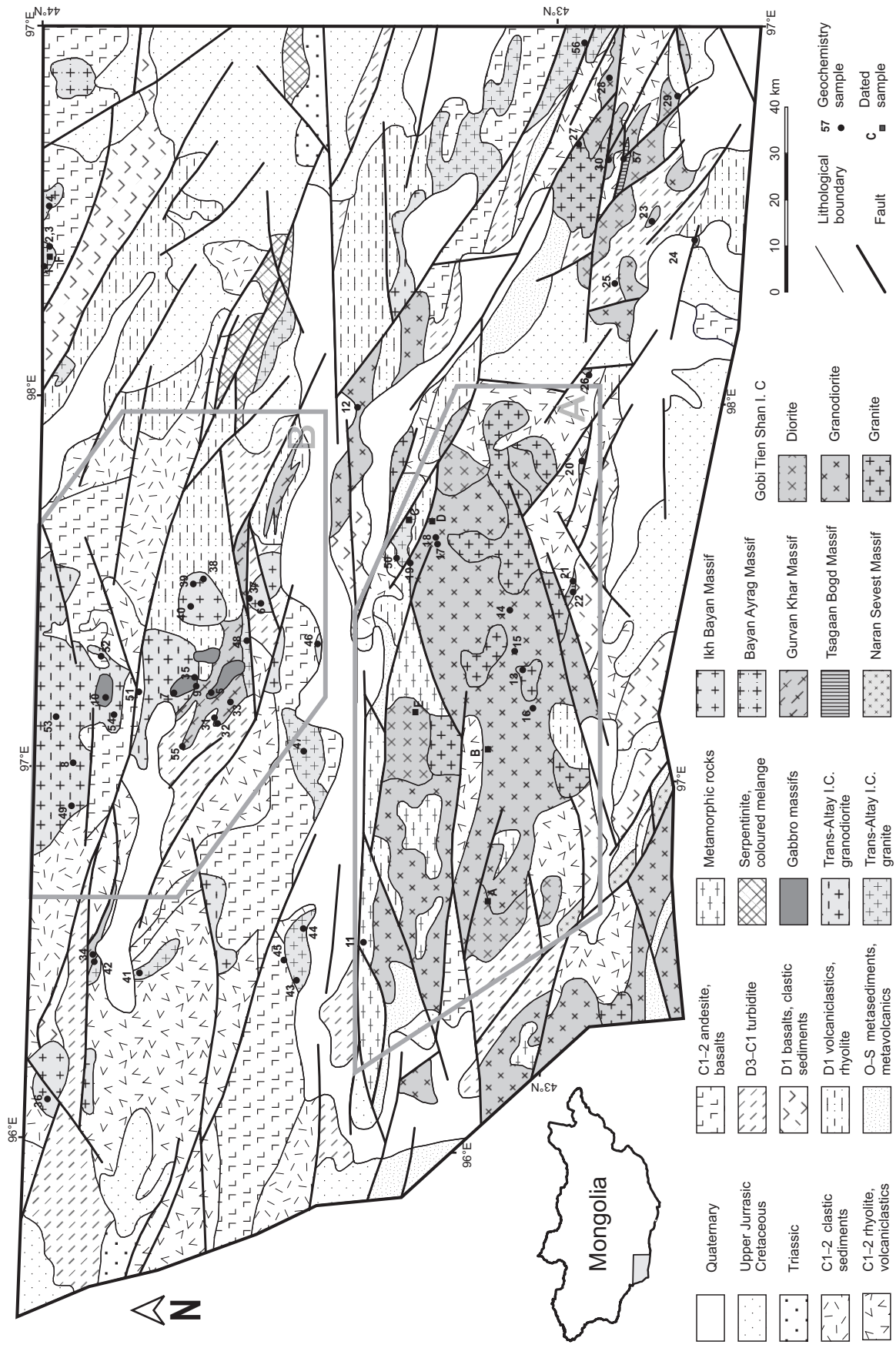

Fig. 2 Position of massifs and intrusive complexes of the Trans-Altay Gobi and localization of the analysed samples in the schematic geological map. Grey polygons A and B mark areas of sketches shown on Figs 12 and 15.

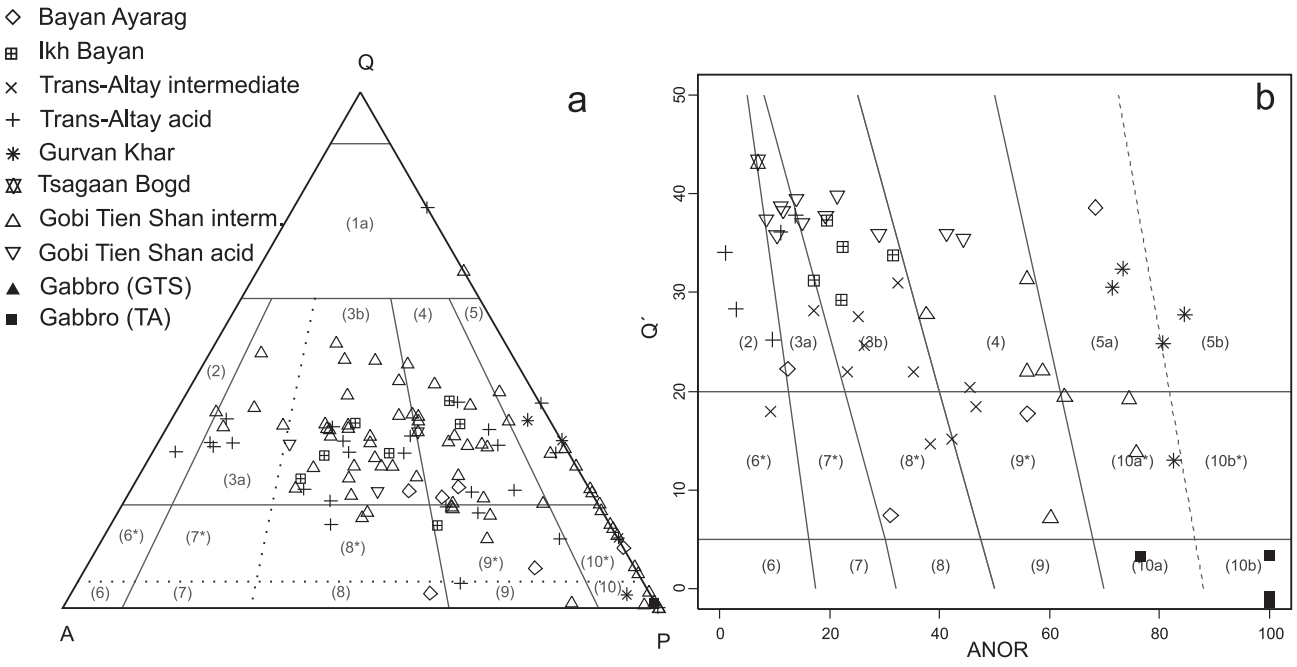

Fig. 3 Classification of plutonic rocks of the Trans-Altay Gobi in classification diagrams: **a** – QAP ternary plot based on modal compositions (Streckeisen 1976); **b** – Q´–ANOR mesonormative plot (Mielke and Winkler 1979; Streckeisen and Le Maitre 1979). Samples on both diagrams are not identical. Explanation: 2 – alkali feldspar granite, 3 – granite, 4 – granodiorite, 5 – tonalite, 6* – quartz alkali feldspar syenite, 7* – quartz syenite, 8* – quartz monzonite, 9* – quartz monzodiorite/quartz monzogabbro, 10* – quartz diorite/quartz gabbro, 6 – alkali feldspar syenite, 7 – syenite, 8 – monzonite, 9 – monzodiorite/monzogabbro 10 – diorite/gabbro.

3.1 The Bayan Ayrag Massif

Bayan Ayrag Massif crops out on the SE edge of the Edrengiin Nuruu range north of the Khar Ovoot Uul in the NW corner of the studied region (Fig. 2). The massif is related to the Edren Terrane of the TA. It intruded andesites and rhyolites of the Early Carboniferous age (Filippova et al. 1990a). Geological mapping confirmed comagmatic nature of the plutonic and volcanic rocks. Massif has a zoned structure with biotite-hornblende (monzo-) gabbro and diorite core surrounded by hornblende-biotite granodiorite to monzodiorite and coarse-grained biotite granite rim. Subvolcanic dykes of basaltic composition accompanying the pluton are relatively common.

Granodiorites to monzodiorites, which prevail in the Bayan Ayarg Massif, are grey, medium-grained rocks of hypautomorphic textures composed of plagioclase (40–65 %), K-feldspar (15–30 %), quartz (10–20 %), amphibole (5 %) and biotite (1–10 %). Elongated, oscillatory zoned laths of plagioclase have an oligoclase–andesine composition. Preferred orientation of feldspar crystals is common in more basic types. K-feldspar is in places perthitic, quartz fills interstices between the feldspars. Green amphibole forms euhedral columns. Biotite flakes enclose feldspar and quartz. Mafic minerals are commonly altered to chlorite and minerals of epidote group. Zircon, apatite, magnetite and titanite are the common accessories. More acid varieties are represented by **granodiorites** ranging **to granites**. The rocks are medium-grained, indistinctively porphyritic. K-feldspar forms isometric, twinned phenocrysts set in medium-grained equigranular mosaic usually with microgranophyric texture composed of plagioclase, K-feldspar and quartz. Biotite makes up to 5 % of the rock volume, amphiboles are rare.

Gabbros to diorites are exposed in the centres of small oval bodies in the Bayan Ayarg Massif (see map enclosed in this Volume). The rocks are medium- to coarse-grained, dark grey, composed of elongated tabular grains of plagioclase (55–70 %), quartz (0–10 %), hornblende (10 %), pyroxene (0–5 %) and biotite (2 %). Preferred orientation of tabular plagioclases of andesine–labradorite composition is common, ophitic texture has been observed in several samples. Apatite, titanite and opaque minerals are common accessories. Chlorite, prehnite and sericite are secondary.

3.2 Trans-Altay Intrusive Complex

The Trans-Altay Intrusive Complex is represented by numerous plutonic bodies of variable, oval to irregular shapes. The largest body of this complex, known as the

Sayryn Pluton, intruded the Late Carboniferous rocks. It has penetrated the terrane boundary of the TA and SG being exposed in the area between Sayryn Uul and Zangan Uul. In the SG, there are common ellipsoidal granitic bodies, which have intruded the Upper Carboniferous volcanosedimentary rocks and are related to the adjacent volcanic rocks. Smaller bodies of granites are widespread in the eastern part of GTS, where they intruded the Devonian and Carboniferous volcanosedimentary complexes. Borzakovskii and Suprunov (1990) supposed an Early to Middle Carboniferous age for the Trans-Altay Intrusive Complex; nevertheless, a Late Carboniferous to Permian age cannot be excluded. None or just a weak magmatic or submagmatic fabric has been observed in the bodies. Individual intrusions are usually composed of a single petrographic type of granite to quartz diorite composition. The enclaves are nearly missing. The number of subvolcanic dykes accompanying the granitic rocks is negligible. Granodiorites are cut by small elliptical gabbro bodies between the Sayryn Uul and Gurvan Khar Uul.

Hornblende-biotite granodiorites to quartz diorites dominate in the Sayryn Pluton, the largest body of this intrusive complex. It is of an irregular outcrop shape and composed of medium- to coarse-grained rocks. The rocks are composed of quartz (20–25 %), plagioclase (40–45 %), K-feldspar (10–25 %), biotite (0–5 %) and amphibole (5–10 %). Long-prismatic to tabular grains of plagioclase (oligoclase) are polysynthetically twinned and oscillatorilly zoned. Typical is intense sericitization, particularly in the more basic rocks. Irregular grains of K-feldspar are poikilitic, enclosing both the plagioclase and hornblende. Hornblende is thickly columnar, reaching up to 1 cm in length. This mineral is often euhedral, usually chloritized and epidotized. Using the amphibole–plagioclase thermometer (Holland and Blundy 1994), the temperature of crystallization was estimated at 714–612 °C. Biotite is chloritized with exsolutions of epidote and leucoxene. Accessoric are zircon, apatite and opaque minerals.

Biotite (leuco-) granites and granodiorites form a substantial part of the oval-shaped intrusions. These medium-grained rocks with subhedral to anhedral even-grained, locally porphyritic textures are composed of quartz (25–35 %), K-feldspar (40–50 %), plagioclase (15–30 %), biotite (0–5 %) and locally contain hornblende. Thick columnar to tabular plagioclases correspond to zoned oligoclase (An_{10} at the margin and An_{19} in the centre). Irregular grains of K-feldspar are usually strongly perthitic. Sporadically occurring biotite is light brown. An opaque mineral, titanite, allanite and apatite appear as accessories, secondary minerals are epidote and sericite. Indistinct phenocrysts of embayed K-feldspar, granophyric intergrowths and rare spicular amphibole (Fig. 4a–b) are characteristic of alkali-feldspar granites.

3.3 Ikh Bayan Massif

Leucocratic and biotite granites to granodiorites of the Ikh Bayan Massif form circular bodies spatially limited to the northern part of the SG. They intruded undifferentiated volcanosedimentary sequences of the Devonian age and the Early Carboniferous siliciclastic turbidite sediments. The largest intrusion has almost 15 km in diameter and is rimmed by a distinct contact aureole. Granites to granodiorites (Fig. 3) represent main lithological types; rocks of diorite composition are subordinate, forming microdiorite enclaves. Xenoliths of volcanosedimentary rocks (now hornfelses) are frequent in granites along the contact aureole, which reaches several hundreds of meters in thickness. In xenoliths, hornfelses sporadically pass to migmatized gneisses. The granites are accompanied by frequent subvolcanic dykes of bimodal composition with a prominent NE–SW oriented trend.

Biotite (leuco-) granites and granodiorites are medium-grained, their texture is hypidiomorphic even grained to slightly porphyritic. Plagioclases (25–45 %) and K-feldspars (15–45 %) are frequently equally represented. The proportion of quartz in these rocks is 25–35 % and of chloritized biotite 2–6 %; muscovite is exceptional. Amphibole appears only in a few samples, reaching up to 5 %. K-feldspar is tabular, often occurring in distinctly elongated usually twinned phenocrysts with uneven grain margins (Fig. 4c). The plagioclase (oligoclase) is slightly zoned and polysynthetically twinned. Accessory minerals are zircon, magnetite, garnet, titanite, apatite and fluorite. Secondary minerals are represented by epidote, chlorite, sericite and kaolinite.

3.4 Gurvan Khar Massif

The largest body of the Gurvan Khar Massif of an irregular outcrop shape is exposed NW of the Gurvan Khar Uul in the centre of the Shargyn Gobi Terrane. It is composed of hornblende-biotite metagranodiorite and biotite orthogneiss. Smaller bodies of similar rocks are exposed in tectonic slices along the faults subparallel with the Trans-Altay shear zone, where they are mylonitized and altered. The massif intruded volcaniclastic rocks of Silurian to Early Devonian age. The metagranodiorites are cut by oval bodies of gabbro and apophyses of red granites probably related to the Trans-Altay Intrusive Complex. The contact aureole developed around the massif in the Carboniferous flysh is indistinct and is influenced by later gabbro intrusions.

Hornblende-biotite metagranodiorite to biotite orthogneiss are grey to reddish grey, fine- to medium-grained, composed of plagioclase (55–70 %), quartz (5–30 %), K-feldspar (5 %), biotite (5–8 %), and amphi-

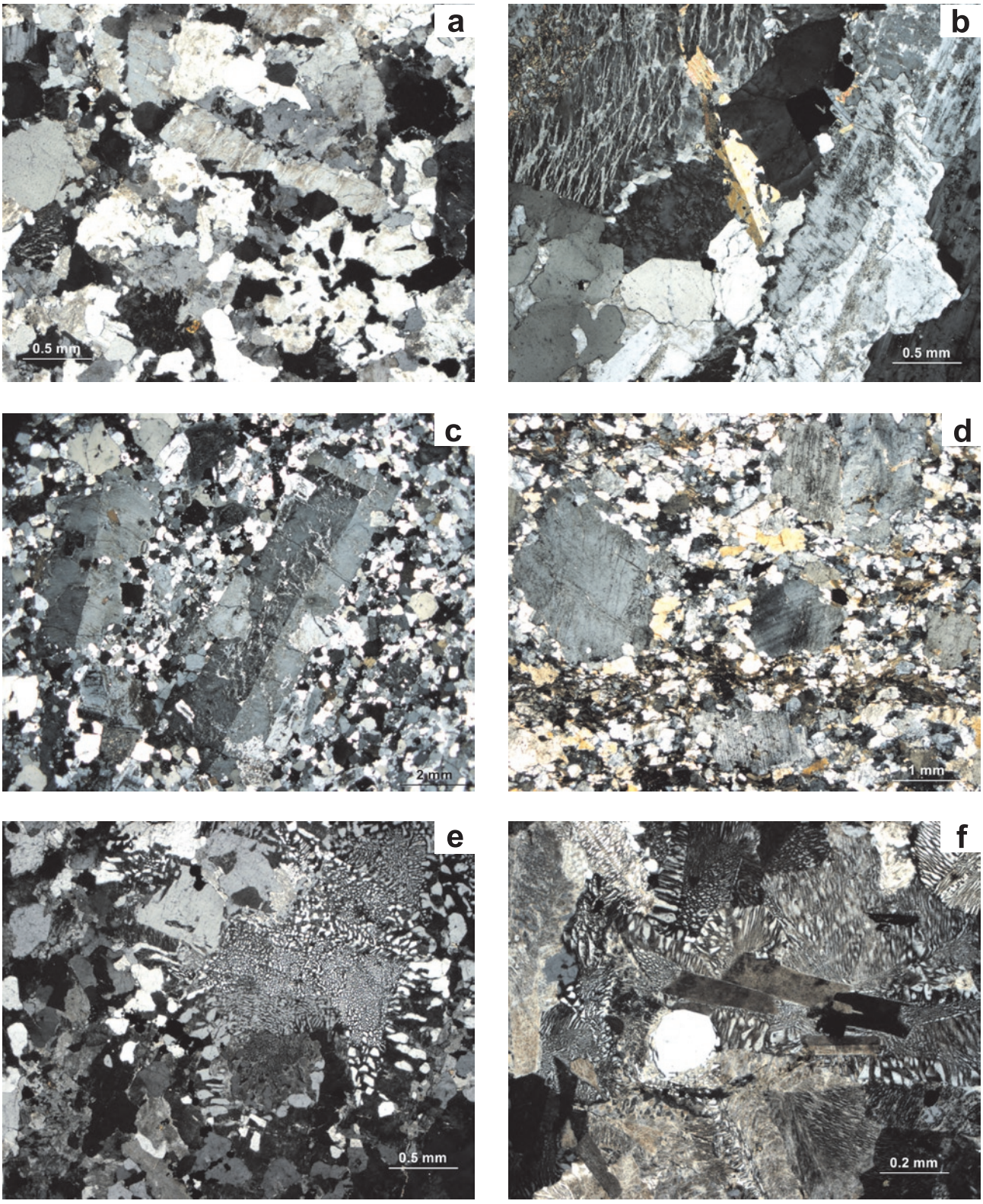

Fig. 4 Photomicrographs of selected granites from the Trans-Altay Gobi: **a, b** – examples of granites with alkaline affinity from the Trans-Altay Intrusive Complex; **c** – phenocrysts of strongly perthitic K-feldspars in granite from the Ikh Bayan Massif; **d** – orthogneiss from the Gurvan Khar Massif; **e, f** – examples of granophyric textures from granites of the Gobi Tien Shan Intrusive Complex.

bole (2–10 %). The plagioclase forms tabular subhedral crystals with irregular margins, K-feldspar is oval-shaped, biotite is brown, chloritized, anhedral quartz is recrystallized with uneven margins. Porphyroclastic texture is developed in some orthogneisses (Fig. 4d). Opaque minerals, decomposed titanite and exceptionally grains of oval garnet appear as accessories. The rocks are recrystallized with attendant development of metamorphic foliation. The strike of foliation follows the shape of the younger gabbro intrusions.

3.5 Gabbro massifs

Granites of the Gurvan Khar and Sayryn massifs (polygon B in Fig. 2) between the Gurvan Khar Uul and the Sayryn Uul are intruded by oval-shaped bodies of gabbro, which caused a great deal of alteration and deformation along their contacts. The **gabbros** are fine- to medium-grained, dark grey rocks. They are formed by plagioclase (42–80 %), clinopyroxene (0–35 %), olivine (5–21 %), and biotite (0–6 %). In some of the samples, also orthopyroxene is present. Brown biotite and light brown clinopyroxene enclose oval-shaped grains of olivine. Amphibole rims often appear around the pyroxene grains. Prismatic plagioclase corresponds to labradorite. Slight alteration is documented by the presence of talc, tremolite and carbonate. An opaque mineral occurs as an accessory.

3.6 Gobi Tien Shan Intrusive Complex

The Gobi Tien Shan Intrusive Complex crops out in several relatively isolated massifs that are arranged in the form of an E–W trending belt in the Gobi Tien Shan range. The Gobi Tien Shan Intrusive Complex is of Late Devonian to Early Carboniferous age (Filippova et al. 1990a, b). The largest body of this complex forms an E–W elongated pluton (polygon A in Fig. 2) in the western part of a mountain range known as the Zamyn Belgekh Pluton (Batulzii et al. 2003). Plutonic bodies in the eastern part of the range are disrupted by numerous NW–SE oriented faults. The Zamyn Belgekh Pluton exceeds 100 km in length and reaches up to 40 km in width. In the eastern part, granites intrude the Early Carboniferous rocks as a partly independent circular body (Fig. 2). The primary intrusive contacts with the Early Devonian and Ordovician/Silurian volcaniclastic rocks along the northern and southern margins of the Zamyn Belgekh Pluton are usually modified by faults. Only a narrow zone of thermally-metamorphosed rocks containing microscopic andalusite is developed around the granites in the E part of the pluton. A wide zone of very fine-grained biotite gneisses with polygonal textures and common cordierite is exposed at the exocontact of the pluton in the NW parts of the Gobi Tien Shan range.

Biotite gneiss with garnet has been locally found in wall-rock xenoliths along the northern endocontact of the Zamyn Belgekh Pluton. The garnet is dominated by the almandine component with subordinate proportion of the pyrope molecule. The garnet zoning with rimward decrease in Mn and Ca contents can be interpreted as crystallization at rising temperature and decreasing pressure, which can correspond well with the conditions during the granite emplacement. Two phases of garnet growth was revealed in the larger grains, while smaller garnets crystallized during the later phase only. The crystallization temperature estimated on the basis of the biotite thermometer (Ferry and Spear 1978) at ~ 680 °C corresponds to the range typical of the water-saturated melting (Clarke 1992). The metamorphic conditions of T ~ 700 °C and P ~ 8 kbar computed by THERMOCALC (version 3.21; Powell and Holland 1985; Holland and Powell 1985, 1998; update February 2002) fail the recommended statistical tests. This can point to the disequilibrium between mineral phases in this exceptional garnet-bearing xenolith.

Granitic rocks of the Gobi Tien Shan Intrusive Complex intruded in the form of small apophyses and dykes metamorphic rocks (migmatized biotite gneiss and amphibolite) of unknown age occurring in the mountain ranges of the Atas Uul and Tchinges Uul in the NW.

The Gobi Tien Shan Intrusive Complex is formed by varied igneous rocks of gabbro, diorite, quartz diorite to monzodiorite, granodiorite and granite composition. The gabbros to gabbrodiorites are exposed as small, discrete bodies inside the granitic rocks but they also occur in the Lower Palaeozoic wall rocks and their genetic relation to the massif is ambiguous. Three main magmatic suites have been revealed by geological mapping (Šourek et al. 2003) inside this intrusive complex: **biotite (leuco-) granite and granodiorite, locally granophyric; hornblende-biotite granodiorite to monzodiorite with mafic enclaves** and **biotite-hornblende diorite to gabbro**. Contacts between the lithological types are usually transitional, and sometimes also untraceable. A typical feature of the Gobi Tien Shan Intrusive Complex is the intimate association of coexisting basic and acid igneous rocks and the evidence for their mutual interaction (magma mingling and mixing) in the form of lobate embayments, syn-plutonic dykes, swarms of mafic microgranular enclaves and disintegrated batches of mafic magma in the acid one (Fig. 5). Magmatic flow active during the lifespan of pluton is documented by magmatic foliation defined by schlieren, preferred orientation of mafic minerals and flattening of mafic enclaves. Submagmatic foliation is developed in the plutonic rocks especially along the northern contact of the Zamyn Belgekh Pluton,

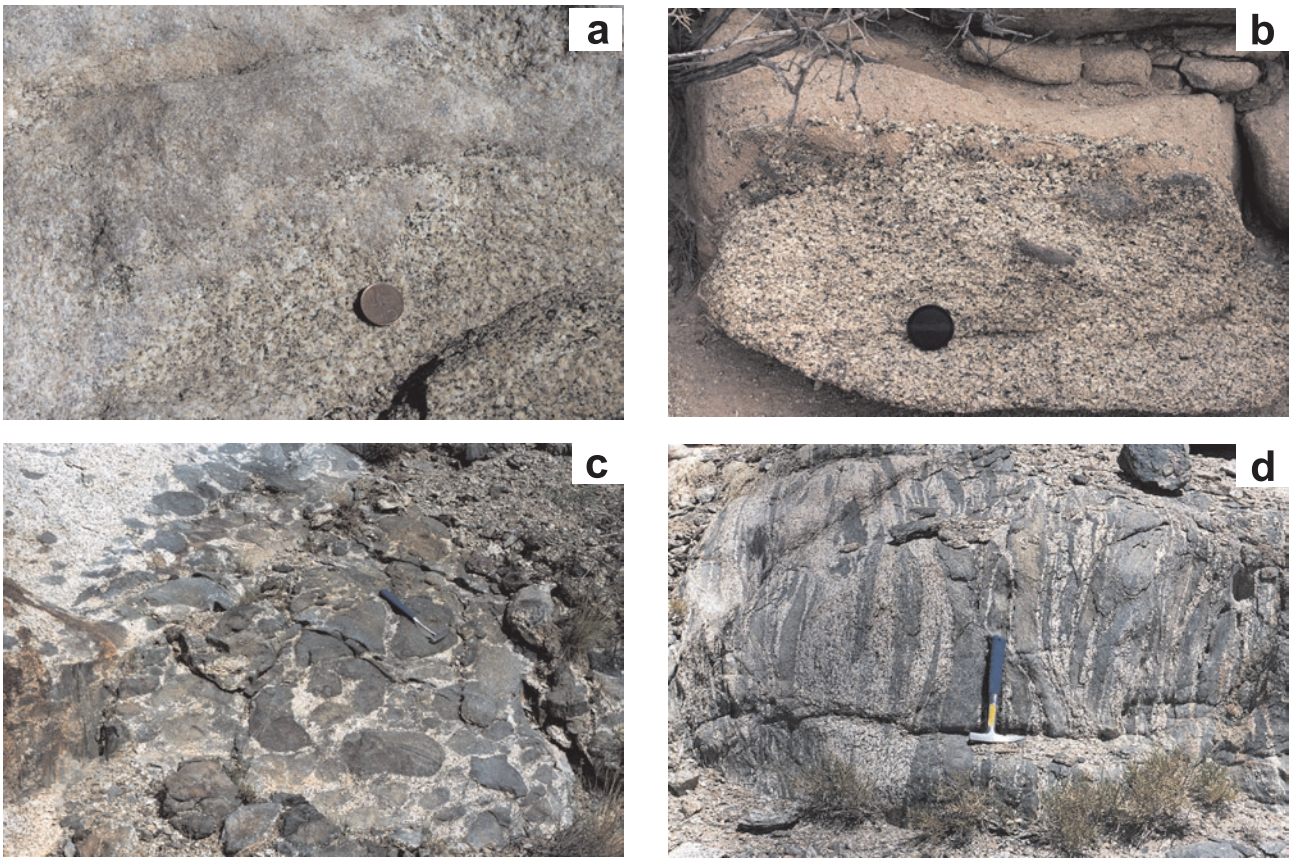

Fig. 5 Field photographs documenting magma interaction processes in the Zamyn Belgekh Pluton: **a, b** – lobate contacts between granites and granodiorites; **c** – swarm of mafic microgranular enclaves of dioritic composition in granodiorite; **d** – strongly deformed mafic enclaves near the northern margin of the pluton.

and granites and granodiorites attain even an orthogneiss appearance.

Subvolcanic dykes commonly accompany rocks of the Gobi Tien Shan Intrusive Complex and occur also in other Paleozoic units. Subvertical dykes of subvolcanic character, reaching a thickness of first meters and a length of up to 15 km, strike in two dominant W–E and WNW–ESE directions. They can be subdivided into basic (predominantly basaltic), and intermediate to acid porphyries. Contacts between the dykes and host rocks are usually sharp.

3.6.1 Petrography of the main rock types in the Gobi Tien Shan Intrusive Complex

Biotite (leuco-) granite to granodiorite is a medium- to coarse-grained, light grey to light red or pink rock with hypautomorphic granular texture. It is composed of quartz (15–45 %), K-feldspar (15–54 %), plagioclase (20–50 %) and biotite (0–7 %); hornblende is exceptional. The feldspars are usually tabular, in some of the samples of hypersolvus character. Tabular subhedral K-feldspars are perthitic, often showing Carlsbad twinning. Up to 2 cm large subhedral phenocrysts of poikilitic and perthitic K-feldspars were observed in porphyritic varieties. The slightly sericitized plagioclases of oligoclase composition are polysynthetically twinned or oscillatory-zoned. Quartz is anhedral with undulatory extinction. Myrmekites are frequent. Biotite is brown, slightly pleochroic. Zircon, monazite, apatite, opaque mineral, exceptionally allanite and titanite appear as accessories. Secondary minerals are chlorite, epidote, leucoxene and sericite. Biotite granite to granodiorite occurs particularly in the south-eastern part of the Zamyn Belgekh Pluton and forms smaller bodies inside the massif.

Granophyric leucocratic granites are light grey, reddish, fine- to medium-grained rocks. Granophyric granites occur together with common biotite granites. They are composed of quartz (20–40 %), K-feldspar (22–55 %), plagioclase (12–45 %) and biotite (1–10 %); muscovite is rare and hornblende exceptional. They are characterized by mutual graphic intergrowths of quartz and K-feldspar forming granophyric, micrographic or

aplitic structures. K-feldspars are often strongly perthitic. The polysynthetically twinned plagioclase corresponds to oligoclase, locally indistinctly zoned and slightly altered in the core. In some of the samples, plagioclase crystals up to 3 mm in size form interconnected framework, their interstices being filled by the granophyric quartz–K-feldspar intergrowths (Fig. 4e). In the types transitional to the subvolcanic rocks, feldspars or, more rarely, quartz, form cores of granophyric intergrowths (Fig. 4f). Zircon, monazite, apatite, opaque mineral, and exceptionally allanite and titanite appear as accessories. Secondary minerals are chlorite, epidote, leucoxene, sericite, and rarely carbonate.

Hornblende-biotite to biotite-hornblende granodiorite to tonalite is a medium-grained, exceptionally even a coarse-grained rock. It is the prevailing type in the Gobi Tien Shan Intrusive Complex and always contains enclaves of melanocratic biotite-hornblende diorites. Phenomena indicative of magma mixing and fluidal textures are characteristic. This rock type is composed of quartz (11–45 %), plagioclase (24–65 %), K-feldspar (0–26 %), biotite (0–20 %), and amphibole (0–14 %). Structure is subautomorphic, granular. The plagioclases of oligoclase to andesine composition are tabular, rarely even euhedral, polysynthetically lamellar and also normally zoned. Basic cores are intensively saussuritized and sericitized. K-feldspars are of irregular shape, poikilitic and perthitic. Quartz is anhedral with undulatory extinction. Biotite is brown, strongly pleochroic. Amphibole forms thick columnar, subhedral to euhedral grains of green-brown colour. Acicular and oval apatite, zircon, abundant titanite and an opaque mineral appear as accessories. Dark minerals are often altered to a mixture of chlorite, opaque and epidote-groups minerals; titanite is altered to leucoxene.

Biotite-hornblende diorite to quartz diorite forms enclaves in granodiorites and also individual bodies. The largest of them are situated in the eastern and western parts of the Zamyn Belgekh Pluton. The diorites are medium- to coarse-grained, grey to dark grey rocks with hypautomorphic granular structure. The tabular minerals in the rock are usually oriented in magmatic foliation. Diorites consist of quartz (0–15 %), plagioclase (44–62 %), K-feldspar (0–20 %), biotite (0–18 %), and amphibole (3–43 %). The main mineral is a polysynthetically lamellar or, more often, oscillatory zoned plagioclase of andesine composition. The plagioclases are intensively saussuritized and sericitized. K-feldspar, if present, is anhedral. Euhedral, poikilitic amphibole is thickly columnar, enclosing elongated plagioclase grains. It usually predominates over brown biotite. In one of the microdiorite samples, pyroxene was identified. A very common accessory is titanite, other include apatite, zircon and opaque minerals. The rocks are commonly epidotized and chloritized.

Gabbro to gabbrodiorite forms part of the mafic enclaves in granodiorites and is exposed in small massifs bound to the W and NW margins of the Zamyn Belgekh Pluton and also a body south of the Tsagaan Bogd. It is a dark grey to green-grey, medium- to coarse-grained rock. Texture is ophitic with preferred orientation of plagioclase laths. It is composed of plagioclase (38–56 %), olivine (0–25 %), pyroxene (9–31 %), biotite (0–14 %) and amphibole (5–8 %). Plagioclases of andesine–labradorite composition are saussuritized. The pyroxenes are often rimmed by hornblende and biotite and/or almost completely replaced by these minerals. Olivine grains are serpentinized. Hornblende is light green-brown and altered to actinolite. Magnetite and ilmenite occur subordinately in many gabbros and melanocratic diorites. Subhedral apatite grains are accessoric.

3.7 Naran Sevest Massif

The Naran Sevest Massif is exposed on highly weathered outcrops and eluvia in the SW part of Gobi Tien Shan Domain SE of Talyn Meltes bulag near the Chinese border. Its age was considered to be the Early Devonian by Ruzhentsev (1985), who described Lower Devonian conglomerates transgressively overlying the plutonic rock and having tectonic contacts with the Ordovician/Silurian volcanosedimentary rocks. The massif is built by grey medium-grained **hornblende-biotite granodiorites to diorites** with composition corresponding to rocks of the Gobi Tien Shan Intrusive Complex. They are often altered and mylonitized. They are composed generally of intensely sericitized, oscillatorilly zoned plagioclase of andesine composition in its core, kaolinized K-feldspar, chloritized biotite flakes, pseudomorphs of chlorite and carbonate probably after hornblende and anhedral quartz. Numerous enclaves of dioritic and gabbroic rocks have been recorded.

3.8 Tsagaan Bogd Massif

The Tsagaan Bogd Massif is restricted to a narrow, E–W elongated body in the vicinity of the Tsagaan Bogd Mt. It consists of brownish red to brownish yellow alkali-feldspar granite and biotite granite, with a distinctly developed porphyritic texture. According to Filippova (1990a) it is comagmatic with the Middle–Upper Carboniferous rhyolites. Among the felsic minerals in the granites, K-feldspar (25–35 %) dominates over quartz and oligoclase. K-feldspar phenocrysts are up to 1 cm across and are intensively haematitized. The content of biotite reaches 15 %, the mineral being intensively chloritized. In terms of their petrology, the rocks of the massif can be related to the acid members of the Gobi Tien Shan Intrusive Complex.

4. Geochemistry

The presented analytical data represent available lithogeochemical samples collected during the geological survey of Trans-Altay Gobi (Šourek et al. 2003). The list of samples is provided in Tab. 3. Analytical results are shown in Tables 4 and 5.

4.1 Bayan Ayrag Massif

Only major-element data are available from this massif. Classification in the Q′–ANOR diagram (Streckeisen and Le Maitre 1979) shows in accordance with petrographical data large compositional variation spanning from granite to quartz monzonite, quartz monzogabbro and tonalite (Fig. 3). The rocks belong to the high-K calc-alkaline series of Peccerillo and Taylor (1976) (Fig. 6b) with SiO_2 abundances ranging between 56 and 69 wt. %. The potassium contents are high (2.3–5.6 wt. % K_2O) and the K_2O/Na_2O ratios low (0.6–0.9). The rocks are distinctly metaluminous with the values for the Shand's alumina saturation index (A/CNK, Shand 1947) ranging between 0.75 and 1.00 (Fig. 6c).

4.2 Trans-Altay Intrusive Complex

Rocks of the Trans-Altay Intrusive Complex can be classified as alkali feldspar granite, granite, quartz monzonite and quartz monzodiorite on the basis of the Q′–ANOR diagram (Fig. 3). Silica abundances range between 60 and 76 wt. %. They are calc-alkaline and belong to the high-K series (Peccerillo and Taylor 1976) with alkaline affinity of some samples. Two suites with different trends can be distinguished in the SiO_2–K_2O diagram (Fig. 6b), but other petrochemical parameters do not corroborate those trends. The K_2O/Na_2O ratio is very variable with the median close to 1. Metaluminous rocks dominate (A/CNK = 0.8–1.0). The K/Rb ratios vary between *c.* 300 and 800, samples from the Gobi Tien Shan Domain showing values below 250. The Rb/Sr ratios (Fig. 7b) are usually below 0.6 except for two samples of cataclased rocks reaching Rb/Sr of 5. The NMORB-normalized spider plots (Fig. 8) display a marked depletion in Nb, P, Ti, while LILE are enriched. The Ba and Sr are generally slightly enriched but are distinctly depleted in two samples. Chondrite-normalized (Boynton 1984) REE patterns (Fig. 9) show a good fractionation of LREE, while HREE trends are flat (La_N/Yb_N = 4.5–14.2; La_N/Sm_N = 2.6–6.2, Gd_N/Yb_N = 0.8–2.0). Negative Eu anomaly is

Tab. 3 List of analysed samples. Explanations: BA – Bayan Ayrag Massif; GBR – gabbro massifs; GTS – Gobi Tien Shan Intrusive Complex; GV – Gurvan Khar Massif; IB – Ikh Bayan Massif; TA – Trans-Altay Intrusive Complex; TSB – Tsagaan Bogd Massif.

No.	Ref. Point	Rock	Unit	E (°)	N (°)
1	5-1019	Bt Hbl monzonite	BA	98.3561	43.9694
2	5-1070	Hbl Bt quartz monzonite	BA	98.489	43.9961
3	5-1074	Bt Hbl granodiorite	BA	98.4089	43.9829
4	5-1075	Monzodiorite	BA	98.3649	43.9991
5	15-1250	Gabbro	GBR	97.2146	43.6572
6	15-1287	Gabbro	GBR	97.4590	43.5636
7	3-1035	Gabbro	GBR	97.2115	43.7299
8	3-1083	Gabbro	GBR	97.0202	43.9225
9	3-1096	Gabbro	GBR	97.2342	43.6873
10	3-1113	Gabbro	GBR	97.1976	43.8619
11	14-1235A	Metagranite	GTS	96.5592	43.3475
12	17-1142	Porphyritic granite	GTS	97.7668	43.7203
13	27-1225	Bt granodiorite	GTS	97.2935	43.0514
14	27-1226	Granite	GTS	97.4532	43.0788
15	27-1230B	Granite	GTS	97.3441	43.0698
16	27-1240	Granite	GTS	97.1927	43.0303
17	28-5298	Bt Hbl quartz monzonite	GTS	97.6260	43.2237
18	28-5301	Bt Hbl granodiorite	GTS	97.6402	43.2262
19	28-5333a	Bt Hbl monzonite	GTS	97.5767	43.2821
20	40-1010b	Granite	GTS	97.8495	42.9439
21	40-1061	Granite	GTS	97.5310	42.9587
22	40-1062b	Granite	GTS	97.5063	42.9574
23	41-1002	Hbl Bt granodiorite	GTS	98.4867	42.8127
24	41-1007A	Monzonite	GTS	98.4385	42.7289
25	41-1025	Bt Hbl granodiorite	GTS	98.3187	42.8832
26	41-1062	Gabbro	GTS	98.0794	42.9323
27	42-1004	Granite	GTS	98.6896	42.9557
28	42-1098	Hbl diorite	GTS	98.8649	42.8966
29	42-1121	Granite	GTS	98.8159	42.7642
30	42-P59B	Granite	GTS	98.6485	42.8985
31	15-1247	Bt metagranodiorite	GV	97.1337	43.6428
32	15-1248	Bt porphyric granite	GV	97.1484	43.6497
33	15-1254	Bt metagranite	GV	97.1902	43.6196
34	2-1054	Hbl diorite	GV	96.5039	43.8736
35	3-1060	Bt Hbl diorite	GV	97.2556	43.6899
36	1-1071a	Bt porphyric granite	IB	96.1118	43.9546
37	15-1202A	Bt granite	IB	97.4699	43.5861
38	3-1052	Bt granite	IB	97.4487	43.6998
39	4-1036A	Bt granite (± Hbl)	IB	97.5206	43.6759
40	4-1038	Porphyric granite	IB	97.5045	43.6951
41	1_2200	Bt porpyric granite	TA	96.4608	43.7828
42	1_2237	Bt granite	TA	96.4858	43.8713
43	13-1027	Hbl Bt quartz monzonite	TA	96.4544	43.4772
44	14-1203	Bt porpyritic granite	TA	96.5933	43.4673
45	14-1205	Hbl Bt granite	TA	96.5048	43.4996
46	15-1208	Bt quartz monzonite	TA	97.3509	43.4529
47	15-1224	Bt granophyric granite	TA	97.0650	43.4745
48	15-1293	Bt Hbl quartz monzonite	TA	97.3584	43.5902
49	2-1017	Bt granite	TA	96.9018	43.9218
50	28-5335	Porphyritic granite	TA	97.5839	43.3033
51	3-1064	Hbl monzonite	TA	97.2139	43.7962
52	3-1068	Hbl quartz monzonite	TA	97.3088	43.8739
53	3-1079a	Hbl quartz monzonite	TA	97.1426	43.9559
54	3-1112	Hbl quartz monzonite	TA	97.1503	43.8451
55	3-1150	Granite	TA	97.0702	43.7097
56	42-1104	Bt granite	TA	98.9563	42.9396
57	42-1019	Leucogranite	TSB	98.6501	42.8693

Tab. 4 Major-element analyses (wt. %).

	Bayan Ayrag				Gabbro						Gobi Tien Shan								
Sample	1	2	3	4	5	6	7	8	9	10	11	12	13	14	15	16	17	18	19
SiO_2	59.09	68.22	68.50	56.28	46.95	50.49	49.45	48.94	47.78	44.72	75.92	75.68	68.57	72.32	75.29	76.95	64.72	63.27	59.09
TiO_2	0.90	0.40	0.77	0.91	1.05	0.76	0.29	1.14	0.13	2.70	0.16	0.19	0.49	0.22	0.15	0.14	0.60	0.63	0.94
Al_2O_3	16.95	14.48	14.16	15.89	14.41	19.41	14.52	19.62	23.71	16.74	12.59	12.91	14.82	14.28	12.09	12.11	16.12	16.99	18.32
Fe_2O_3	3.83	2.25	1.40	4.91	11.47	8.35	9.35	9.67	4.23	14.83	1.56	1.95	3.48	2.60	1.85	1.24	4.66	4.88	6.14
FeO	2.90	1.26	3.67	3.74	n.d.	n.d.	n.d.	n.d.	n.d.	n.d.	n.d.	n.d.	n.d.	n.d.	n.d.	n.d.	n.d.	n.d.	n.d.
MnO	0.16	0.15	0.13	0.21	0.15	0.11	0.14	0.16	0.06	0.19	0.03	0.05	0.08	0.06	0.04	0.03	0.09	0.08	0.10
MgO	2.60	0.83	1.22	4.18	13.91	4.81	14.79	3.27	7.26	6.48	0.19	0.40	1.06	0.47	0.19	0.14	1.22	1.42	1.84
CaO	4.83	2.50	2.86	6.80	6.84	9.93	7.27	10.26	11.40	8.12	0.68	1.08	2.93	2.14	0.71	0.63	3.17	4.21	5.01
Na_2O	3.83	4.43	3.76	3.58	2.74	2.96	1.98	3.47	2.65	3.76	3.64	3.89	4.36	4.08	3.34	3.34	5.33	5.14	5.26
K_2O	3.21	4.09	2.28	2.49	0.66	0.81	0.11	0.75	0.19	0.57	4.87	3.41	2.96	2.73	4.67	5.14	2.03	1.82	1.55
P_2O_5	0.34	0.17	0.14	0.31	0.25	0.13	0.03	0.43	0.03	0.94	0.02	0.03	0.10	0.03	n.d.	0.03	0.18	0.18	0.23
Cr_2O_3	n.d.	n.d.	n.d.	n.d.	0.08	0.01	0.10	0.01	0.04	0.01	0.00	n.d.	n.d.	n.d.	n.d.	n.d.	n.d.	n.d.	n.d.
LOI	1.53	0.80	1.25	1.38	0.60	1.50	1.30	1.60	1.90	0.30	0.50	0.40	0.40	0.60	0.40	0.20	0.90	1.00	1.20
H_2O^-	0.11	0.05	0.10	0.08	n.d.	n.d.	n.d.	n.d.	n.d.	n.d.	n.d.	n.d.	n.d.	n.d.	n.d.	n.d.	n.d.	n.d.	n.d.
TOT/C	n.d.	n.d.	n.d.	n.d.	0.04	0.07	0.07	0.03	0.02	0.02	0.02	0.03	0.04	0.04	0.05	0.06	0.04	0.08	0.04
TOT/S	n.d.	n.d.	n.d.	n.d.	0.17	0.01	0.20	0.02	0.06	0.16	n.d.	0.01	n.d.	0.02	0.01	n.d.	0.01	0.01	0.02
Total	98.75	98.83	98.99	99.38	99.17	99.31	99.39	99.38	99.42	99.42	100.20	100.07	99.31	99.60	98.77	99.97	99.11	99.72	99.74
A/NK	1.73	1.24	1.64	1.85	2.76	3.38	4.30	3.01	5.19	2.46	1.12	1.28	1.43	1.48	1.15	1.10	1.47	1.63	1.77
A/CNK	0.91	0.89	1.02	0.76	0.82	0.82	0.87	0.78	0.94	0.78	1.01	1.07	0.94	1.05	1.02	0.99	0.96	0.94	0.94
K_2O/Na_2O	0.84	0.92	0.61	0.70	0.24	0.27	0.06	0.22	0.07	0.15	1.34	0.88	0.68	0.67	1.40	1.54	0.38	0.35	0.29

	Gobi Tien Shan											Gurvan Khar					Ikch Bayan		
Sample	20	21	22	23	24	25	26	27	28	29	30	31	32	33	34	35	36	37	38
SiO_2	75.40	71.33	72.52	65.77	57.99	61.74	46.37	75.48	53.05	75.46	74.14	67.64	71.07	70.51	60.19	57.16	72.91	72.98	75.16
TiO_2	0.25	0.32	0.25	0.64	1.10	0.74	3.27	0.23	1.36	0.05	0.29	0.31	0.18	0.17	0.47	0.76	0.22	0.16	0.13
Al_2O_3	12.17	14.57	13.83	14.96	16.11	15.94	17.39	12.46	17.06	14.16	12.61	16.79	15.93	16.00	17.17	18.35	13.35	13.95	13.11
Fe_2O_3	1.60	2.46	2.14	5.88	7.66	5.24	12.03	1.90	8.18	1.08	2.10	2.94	1.89	1.80	6.02	6.26	2.15	2.18	1.57
FeO	n.d.	n.d.	n.d.	n.d.	n.d.	n.d.	n.d.	n.d.	n.d.	n.d.	n.d.	n.d.	n.d.	n.d.	n.d.	n.d.	n.d.	n.d.	n.d.
MnO	0.02	0.05	0.06	0.07	0.15	0.07	0.14	0.03	0.15	0.06	0.02	0.06	0.04	0.04	0.10	0.10	0.04	0.03	0.03
MgO	0.11	0.97	0.47	1.08	3.15	2.72	4.60	0.29	5.03	0.19	0.52	0.97	0.53	0.48	2.59	2.54	0.44	0.25	0.27
CaO	0.65	2.18	1.68	3.68	4.63	5.02	9.85	0.96	8.54	0.65	1.18	4.08	3.17	3.01	6.31	7.02	1.41	1.02	1.27
Na_2O	3.77	4.20	3.76	3.53	4.56	4.04	2.80	3.54	3.24	4.25	3.47	5.12	5.05	5.33	3.48	4.68	3.73	4.37	3.48
K_2O	4.03	2.63	3.58	2.71	1.74	2.06	0.67	4.53	1.24	3.17	4.20	1.02	1.18	1.19	1.35	0.60	4.12	4.11	4.32
P_2O_5	0.05	0.07	0.04	0.18	0.34	0.16	0.03	0.03	0.31	0.04	0.04	0.11	0.05	0.07	0.15	0.31	0.05	0.03	0.05
Cr_2O_3	n.d.	n.d.	n.d.	0.00	n.d.	0.00	n.d.	n.d.	0.02	n.d.	n.d.	0.00	n.d.	0.00	0.01	0.00	0.00	0.00	0.00
LOI	1.70	1.30	1.20	1.40	2.60	1.60	2.90	1.00	1.90	0.80	0.70	0.70	0.40	0.60	1.50	1.60	0.70	0.60	0.70
H_2O^-	n.d.	n.d.	n.d.	n.d.	n.d.	n.d.	n.d.	n.d.	n.d.	n.d.	n.d.	n.d.	n.d.	n.d.	n.d.	n.d.	n.d.	n.d.	n.d.
TOT/C	0.18	0.02	0.06	0.11	0.01	0.06	0.23	0.04	0.05	0.01	0.03	0.04	0.04	0.04	0.03	0.03	0.03	0.03	0.04
TOT/S	0.05	0.01	0.01	0.02	0.01	0.01	0.15	n.d.	0.01	0.01	0.01	n.d.	0.02	0.01	0.01	0.02	0.01	n.d.	0.01
Total	99.78	100.15	99.61	99.97	100.08	99.37	100.09	100.48	100.12	99.97	99.30	99.79	99.55	99.26	99.39	99.43	99.19	99.78	100.17
A/NK	1.15	1.49	1.37	1.71	1.72	1.80	3.26	1.16	2.56	1.36	1.23	1.76	1.66	1.59	2.39	2.20	1.26	1.20	1.26
A/CNK	1.04	1.06	1.05	0.97	0.90	0.89	0.75	1.00	0.77	1.22	1.02	0.99	1.04	1.03	0.92	0.87	1.01	1.03	1.03
K_2O/Na_2O	1.07	0.63	0.95	0.77	0.38	0.51	0.24	1.28	0.38	0.75	1.21	0.20	0.23	0.22	0.39	0.13	1.10	0.94	1.24

pronounced and its magnitude generally increasing with SiO_2 (Eu/Eu* = 0.8–0.1). The rare values exceeding 1 in acid to intermediate rock samples can be associated with later alteration of the rocks.

4.3 Ikh Bayan Massif

Granites of this massif are chemically homogenous. Samples fall into granite field in the Q′–ANOR clas-

Tab. 4 Major-element analyses (wt. %) continued.

	Ikch Bayan		Trans-Altay																TSB
Sample	39	40	41	42	43	44	45	46	47	48	49	50	51	52	53	54	55	56	57
SiO_2	70.93	71.41	73.83	75.83	66.75	74.74	69.61	68.68	68.94	64.98	70.29	68.71	60.24	61.99	63.17	63.51	75.93	68.61	78.63
TiO_2	0.35	0.25	0.19	0.10	0.56	0.23	0.46	0.56	0.52	0.95	0.42	0.57	1.04	0.61	0.55	0.66	0.13	0.38	0.09
Al_2O_3	14.45	14.38	13.37	12.34	14.89	12.42	14.44	15.12	14.79	16.99	14.10	14.30	16.09	16.98	15.13	16.29	12.23	13.53	11.10
Fe_2O_3	2.79	2.24	1.62	1.31	2.45	1.56	3.03	3.31	3.13	4.43	2.52	3.97	6.60	4.19	4.71	4.59	2.15	2.40	0.63
FeO	n.d.	n.d.	n.d.	n.d.	n.d.	n.d.	n.d.	n.d.	n.d.	n.d.	n.d.	n.d.	n.d.	n.d.	n.d.	n.d.	n.d.	n.d.	n.d.
MnO	0.07	0.05	0.04	0.02	0.03	0.01	0.05	0.07	0.07	0.08	0.03	0.04	0.11	0.09	0.06	0.06	0.05	0.03	0.01
MgO	0.59	0.63	0.11	0.21	1.61	0.46	1.01	0.68	0.74	0.95	0.48	1.04	2.01	1.38	2.07	1.91	0.04	0.62	0.09
CaO	1.36	1.92	0.51	0.95	4.06	1.20	2.07	1.58	1.90	2.84	1.30	2.19	4.44	3.50	3.71	3.06	0.36	2.36	0.42
Na_2O	4.40	3.88	4.37	3.16	4.48	2.77	4.15	5.51	5.02	5.36	3.62	3.69	4.59	4.90	4.01	4.59	4.12	3.79	2.94
K_2O	4.04	3.58	5.16	4.96	3.29	5.64	4.11	3.40	3.41	3.01	5.88	3.97	2.72	3.33	3.32	3.50	4.68	3.98	4.84
P_2O_5	0.07	0.09	0.04	0.02	0.19	0.07	0.11	0.11	0.13	0.15	0.07	0.15	0.32	0.23	0.26	0.24	n.d.	0.11	n.d.
Cr_2O_3	0.00	0.00	0.01	0.01	0.01	0.01	0.01	n.d.	n.d.	0.00	0.00	0.00	n.d.	0.00	0.01	0.01	n.d.	n.d.	n.d.
LOI	0.90	0.70	0.50	0.40	0.60	0.70	0.20	0.40	0.50	0.40	0.70	1.10	1.10	1.70	2.70	1.20	0.30	3.20	0.50
H_2O^-	n.d.	n.d.	n.d.	n.d.	n.d.	n.d.	n.d.	n.d.	n.d.	n.d.	n.d.	n.d.	n.d.	n.d.	n.d.	n.d.	n.d.	n.d.	n.d.
TOT/C	0.02	0.03	0.05	0.04	0.07	0.03	0.02	n.d.	0.02	0.01	0.07	0.07	0.03	0.11	0.34	0.04	0.03	0.49	0.04
TOT/S	0.02	0.01	n.d.	0.02	0.02	n.d.	n.d.	0.01	n.d.	0.01	0.01	0.02	0.03	0.02	0.01	0.02	0.01	n.d.	0.03
Total	100.05	99.22	99.76	99.37	99.00	99.87	99.29	99.53	99.24	100.31	99.46	99.81	99.36	99.08	99.80	99.72	100.00	99.09	99.27
A/NK	1.24	1.40	1.05	1.17	1.36	1.16	1.28	1.19	1.24	1.41	1.14	1.38	1.53	1.46	1.48	1.44	1.03	1.28	1.10
A/CNK	1.03	1.05	0.98	1.00	0.81	0.97	0.96	0.97	0.96	0.99	0.96	1.00	0.87	0.94	0.89	0.96	0.98	0.91	1.02
K_2O/Na_2O	0.92	0.92	1.18	1.57	0.73	2.04	0.99	0.62	0.68	0.56	1.62	1.08	0.59	0.68	0.83	0.76	1.14	1.05	1.65

sification (Streckeisen and Le Maitre 1979). They are acid with SiO_2 = 71–73 wt. %, high-K calc-alkaline and subaluminous (Fig. 6). The K_2O/Na_2O ratios fall within the range of 0.9–1.2, K/Rb ratios range from 270 to 500 and Rb/Sr ratios from 0.4 to 0.7. They are enriched in LILE in the NMORB-normalized spider plot (Fig. 8); Nb, P, and Ti are strongly depleted, while Pb and Nd are slightly enriched. The REE patterns (Fig. 9) show slight fractionation of LREE with the HREE trends being flat (La_N/Yb_N = 5.4–7.6; La_N/Sm_N = 2.9–4.9, Gd_N/Yb_N = 1.1–1.4). Negative Eu anomaly is well developed (Eu/Eu* = 0.3–0.6).

4.4 Gurvan Khar Massif

Samples plotted into the Q´–ANOR diagram fit the tonalite field, only one corresponds to diorite. They are intermediate to acid (SiO_2 = 57–71 wt. %) and very low in K_2O (0.6–1.4 wt. %), corresponding to tholeiite series of Peccerillo and Taylor (1976). The A/CNK values equal 0.9 to 1.0 (Fig. 6). The K_2O/Na_2O ratios are low (0.1–0.4). The K/Rb ratios are very high (ranging between 430 and 680) and Rb/Sr = 0.01–0.4. NMORB normalized spider plot shows distinctive trends. The rocks are strongly enriched in Ba, and Sr, slightly enriched in U, Pb and Nd. Niobium only shows marked depletion, while Rb, Th, P and Ti are depleted slightly. The Cs, Pb and Zr have varied trends (Fig. 8). The REE abundances are very low (ΣREE = 29–56 ppm), chondrite-normalized trends showing slight fractionation (Fig. 9), with a weak negative or negligibly positive Eu anomaly (La_N/Yb_N = 3.3–7.1, La_N/Sm_N = 2.1–5.3, Gd_N/Yb_N = 1.1–1.9, Eu/Eu* = 0.7–1.1).

4.5 Gabbroic rocks

Basic rocks accompanying the Gurvan Khar Massif and the largest body of the Trans-Altay Intrusive Complex could be geochemically classified as gabbro in accordance with the petrography. Silica abundances range between 44 and 50 wt. %. These are calc-alkaline to tholeiitic rocks except for one sample with alkaline affinity. The K/Rb ratios are very high and variable, ranging from 300 to 2000, with the lowest value in a sample from the GTS. This corresponds well with very low Rb/Sr ratios (0.001–0.01), again with the maximum (0.03) in the GTS (Fig. 7b). The NMORB-normalized spider diagrams show high variation in trends (Fig. 10a). Generally, there is only a distinct depletion in Rb, Th, Nb and Zr accompanied by an enrichment in Ba and Sr. Chondrite-normalized REE patterns reflect differences in the total abundance (ΣREE = 10–160 ppm) and variable fractionation (La_N/Yb_N = 32.4–4.8, La_N/Sm_N = 1.6–2.7, Gd_N/Yb_N = 1.5–1.9). Three samples show positive Eu

Tab. 5 Trace-element analyses (ppm).

	Gabbro massifs						Gobi Tien Shan						
Sample	5	6	7	8	9	10	11	12	13	14	15	16	17
Rb	8.0	16.5	0.6	12.4	2.1	2.3	162.8	84.1	120.3	92.1	156.2	176.8	44.1
Cs	0.4	0.7	n.d.	0.2	n.d.	n.d.	0.9	1.9	6.5	3.1	1.9	3.1	0.8
Sr	509.2	1145.9	520.4	802.1	889.5	968.0	48.5	163.7	271.6	229.3	90.9	41.8	409.2
Ba	170	312	74	355	72	331	365	696	465	594	360	205	821
Nb	3.7	1.9	n.d.	2.3	n.d.	9.2	13.2	5.0	8.0	5.6	6.2	10.3	6.3
Ta	0.2	0.1	n.d.	0.2	n.d.	0.5	1.2	0.4	0.7	0.5	0.7	1.1	0.4
Zr	103.8	36.9	5.5	47.9	6.6	135.1	155.3	124.3	167.2	130.7	84.0	94.1	284.6
Hf	2.6	1.0	n.d.	1.5	n.d.	3.5	5.5	3.8	5.3	4.2	3.0	3.7	7.4
Ga	15.2	19.9	11.3	20.8	13.1	20.7	16.9	14.6	18.0	17.4	14.2	15.6	20.0
Th	0.4	0.8	n.d.	1.0	0.1	0.4	22.9	8.5	13.8	8.5	16.1	19.4	4.1
U	0.2	0.6	n.d.	0.4	n.d.	n.d.	3.0	1.6	1.3	1.2	1.7	1.4	1.6
Ni	303.9	39.5	239.7	6.3	210.2	74.4	3.2	1.6	4.9	6.5	5.8	5.0	4.9
Co	73.0	31.5	66.0	22.9	30.1	49.2	1.5	1.6	5.8	3.3	2.0	1.1	6.0
V	153	290	82	306	25	334	6	12	58	18	8	5	64
Sc	18	26	21	33	9	27	4	5	5	4	3	5	11
Pb	0.8	0.7	0.4	1.7	0.5	0.2	5.8	5.9	3.3	4.4	6.7	7.1	2.1
Cu	98.5	60.8	153.8	118.5	95.6	89.5	5.6	1.7	6.9	9.1	10.8	7.6	8.5
Zn	51	32	22	35	18	53	23	29	27	38	10	12	59
Sn	1	1	1	n.d.	n.d.	2	4	1	2	2	1	2	3
W	0.1	0.7	n.d.	0.2	0.1	0.2	0.2	0.2	1.7	0.4	0.5	0.7	0.6
Mo	0.5	0.1	0.2	0.4	0.6	0.7	0.3	0.4	0.6	0.9	1.0	0.8	0.5
Cd	n.d.	0.1	0.1	0.1	n.d.	0.1	n.d.	n.d.	n.d.	0.1	n.d.	0.1	n.d.
As	0.9	0.5	n.d.	n.d.	n.d.	n.d.	n.d.	1.1	3.3	2.1	0.6	1.7	1.0
Sb	n.d.	n.d.	n.d.	0.1	n.d.	n.d.	n.d.	0.1	0.2	0.1	n.d.	0.1	n.d.
Bi	n.d.	n.d.	n.d.	n.d.	n.d.	n.d.	n.d.	n.d.	0.1	n.d.	n.d.	0.1	0.1
Au (ppb)	0.5	n.d.	8.2	n.d.	n.d.	0.9	0.8	n.d.	0.7	0.9	1.5	0.7	1.2
Ag	n.d.	0.1	0.1	n.d.	n.d.	n.d.	n.d.	n.d.	n.d.	n.d.	n.d.	0.1	n.d.
Hg	n.d.	n.d.	n.d.	n.d.	n.d.	n.d.	n.d.	n.d.	n.d.	0.01	n.d.	0.01	n.d.
Tl	n.d.	n.d.	n.d.	n.d.	n.d.	n.d.	n.d.	n.d.	0.1	0.2	n.d.	n.d.	n.d.
La	8.5	6.7	2.0	11.8	1.7	22.3	40.6	18.5	24.8	21.6	26.1	29.4	24.9
Ce	21.7	15.1	3.7	26.3	3.3	54.4	79.2	33.6	58.3	46.6	53.8	64.7	53.4
Pr	2.95	2.04	0.49	3.68	0.45	7.88	9.11	3.78	6.40	5.03	5.65	7.13	6.56
Nd	15.2	10.1	2.6	18.9	2.3	40.8	35.7	16.4	27.8	20.9	20.8	27.0	30.8
Sm	3.4	2.1	0.5	4.5	0.4	8.5	7.4	3.2	5.4	3.8	3.7	4.9	6.0
Eu	1.06	0.70	0.36	1.48	0.38	2.47	0.46	0.65	0.95	0.69	0.46	0.41	1.35
Gd	3.63	1.94	0.78	4.32	0.45	7.65	7.12	3.00	5.01	3.22	2.63	3.89	5.08
Tb	0.56	0.30	0.11	0.69	0.07	1.18	1.21	0.58	0.77	0.61	0.45	0.71	0.78
Dy	3.26	1.57	0.63	3.94	0.40	6.61	7.30	3.20	4.71	3.34	2.64	4.13	4.44
Ho	0.62	0.31	0.15	0.75	0.07	1.23	1.46	0.64	0.89	0.59	0.50	0.87	0.78
Er	1.83	0.93	0.48	2.13	0.21	3.67	4.81	1.97	2.69	1.81	1.58	2.73	2.32
Tm	0.26	0.13	0.06	0.31	n.d.	0.52	0.73	0.33	0.44	0.29	0.29	0.49	0.38
Yb	1.82	0.93	0.55	1.99	0.24	3.16	4.97	2.26	3.54	2.14	2.14	3.51	2.37
Lu	0.25	0.12	0.07	0.31	0.03	0.49	0.72	0.33	0.47	0.29	0.31	0.50	0.33
Y	18.8	9.9	4.1	22.3	2.1	38.6	48.2	20.9	30.3	20.5	18.3	29.9	26.0
Eu/Eu*	0.92	1.06	1.76	1.03	2.74	0.94	0.19	0.64	0.56	0.60	0.45	0.29	0.75
La_N/Yb_N	3.15	4.86	2.45	4.00	4.78	4.76	5.51	5.52	4.72	6.80	8.22	5.65	7.08
La_N/Sm_N	1.57	2.01	2.52	1.65	2.67	1.65	3.45	3.64	2.89	3.58	4.44	3.77	2.61
Gd_N/Yb_N	1.61	1.68	1.14	1.75	1.51	1.95	1.16	1.07	1.14	1.21	0.99	0.89	1.73
∑ REE	65.04	42.97	12.48	81.10	10.00	160.86	200.79	88.44	142.17	110.91	121.05	150.37	139.49
K/Rb	684.86	407.52	1521.91	502.09	751.07	2057.28	248.33	336.59	204.25	246.06	248.19	241.34	382.12
Rb/Sr	0.02	0.01	0.00	0.02	0.00	0.00	3.36	0.51	0.44	0.40	1.72	4.23	0.11
Rb/Cs	20.00	23.57	n.d.	62.00	n.d.	n.d.	180.89	44.26	18.51	29.71	82.21	57.03	55.13

Tab. 5 continued. Trace-element analyses (ppm).

	Gobi Tien Shan												
Sample	18	19	20	21	22	23	24	25	26	27	28	29	30
Rb	39.3	53.9	122.3	86.0	126.2	94.4	45.7	49.3	18.4	158.3	34.8	116.4	126.2
Cs	1.3	1.8	3.9	2.1	2.0	5.5	2.3	1.6	3.5	3.0	1.2	4.5	2.2
Sr	463.8	547.9	80.7	370.2	188.7	222.0	447.9	534.4	562.9	75.2	436.3	144.5	93.0
Ba	798	511	292	577	730	575	490	402	265	313	301	605	306
Nb	5.2	7.6	11.6	4.5	4.9	7.7	5.4	5.0	3.1	10.2	5.7	7.2	8.9
Ta	0.3	0.5	0.9	0.5	0.6	0.6	0.4	0.4	0.2	1.3	0.4	0.9	0.8
Zr	228.6	437.2	247.7	112.1	126.0	209.5	200.5	195.3	66.6	214.4	177.7	38.1	198.2
Hf	6.1	10.6	7.8	3.6	3.7	5.9	5.4	5.6	1.7	7.2	4.2	2.0	7.3
Ga	20.9	24.9	16.4	18.0	15.4	21.2	19.3	20.7	20.7	20.0	20.4	17.2	18.7
Th	3.1	4.4	13.9	11.6	12.3	10.5	3.8	6.4	1.4	25.6	2.8	5.0	22.3
U	1.2	1.4	6.5	1.7	1.8	2.2	1.4	1.9	0.5	4.3	0.8	1.1	3.9
Ni	5.9	7.3	5.4	4.9	1.5	2.4	7.9	16.9	3.2	1.7	13.3	1.0	5.8
Co	8.0	10.8	1.1	5.1	2.8	6.6	16.5	13.6	39.9	1.8	24.2	n.d.	3.8
V	74	103	13	37	21	81	158	117	587	15	192	n.d.	21
Sc	10	12	8	4	4	25	16	9	34	2	30	n.d.	2
Pb	1.1	2.4	7.1	5.4	5.1	26.7	5.6	1.7	1.6	13.5	3.8	18.1	8.6
Cu	10.5	15.3	5.4	1.6	1.7	3.9	12.9	9.9	18.4	2.4	24.1	1.3	11.6
Zn	49	65	44	39	30	40	81	29	56	30	26	33	21
Sn	2	3	4	1	4	2	1	1	1	2	1	3	3
W	0.3	0.4	1.4	0.3	0.8	1.3	0.4	0.3	0.1	0.8	0.6	0.9	0.7
Mo	0.6	0.8	2.0	0.1	0.3	0.3	0.3	0.2	0.3	0.5	0.5	0.1	0.4
Cd	n.d.	n.d.	0.1	n.d.	0.1	0.1	n.d.	n.d.	n.d.	n.d.	n.d.	n.d.	n.d.
As	0.7	1.5	6.4	2.5	1.2	3.2	5.7	1.3	4.9	0.5	12.1	1.1	2.2
Sb	n.d.	0.1	0.2	n.d.	n.d.	0.3	0.1	0.1	0.1	0.1	0.2	0.1	0.1
Bi	n.d.	n.d.	n.d.	n.d.	n.d.	n.d.	n.d.	n.d.	n.d.	0.1	n.d.	0.1	n.d.
Au (ppb)	1.5	2.4	n.d.	1.3	n.d.	2.1	n.d.	n.d.	1.5	0.9	n.d.	1.7	n.d.
Ag	n.d.	n.d.	n.d.	n.d.	n.d.	n.d.	n.d.	n.d.	n.d.	n.d.	n.d.	n.d.	n.d.
Hg	n.d.	n.d.	0.02	0.02	0.01	0.05	0.08	0.04	0.04	0.03	0.03	0.02	0.02
Tl	0.1	0.1	n.d.	n.d.	n.d.	n.d.	n.d.	n.d.	n.d.	0.1	n.d.	n.d.	0.1
La	21.2	25.1	36.9	20.6	21.6	27.8	19.6	23.5	5.6	40.7	19.6	11.3	31.3
Ce	43.5	56.3	81.7	41.5	45.9	56.4	40.7	49.1	11.6	83.9	41.7	23.4	75.4
Pr	5.43	7.88	10.03	4.57	4.81	6.92	5.37	6.11	1.57	10.13	5.37	2.48	7.91
Nd	24.5	40.9	41.7	18.6	18.9	32.0	26.7	29.0	8.3	42.4	26.2	10.7	34.7
Sm	4.4	8.7	8.4	3.1	3.6	7.2	6.1	5.6	2.0	9.3	5.7	2.4	6.5
Eu	1.35	2.04	0.99	0.73	0.72	1.34	1.75	1.33	0.90	0.71	1.54	0.36	0.67
Gd	4.08	8.56	7.60	2.29	3.75	7.07	6.38	5.01	2.13	8.54	6.01	2.04	6.03
Tb	0.61	1.35	1.22	0.37	0.67	1.24	1.06	0.76	0.38	1.60	0.89	0.39	1.03
Dy	3.38	7.34	6.89	2.05	3.86	7.23	6.15	3.88	2.14	10.06	5.08	2.10	6.52
Ho	0.66	1.34	1.35	0.39	0.80	1.34	1.20	0.73	0.38	1.81	0.94	0.40	1.17
Er	1.75	3.78	3.98	1.07	2.43	3.93	3.47	2.00	1.07	5.79	2.72	1.11	3.65
Tm	0.27	0.58	0.65	0.18	0.41	0.61	0.54	0.31	0.17	0.92	0.41	0.19	0.60
Yb	1.87	3.81	4.63	1.27	2.93	4.50	3.56	2.34	1.18	7.00	2.90	1.33	4.61
Lu	0.26	0.51	0.65	0.17	0.42	0.63	0.56	0.32	0.17	0.95	0.38	0.17	0.59
Y	19.6	40.9	43.8	12.5	25.1	42.8	37.1	22.8	11.8	62.4	29.2	14.1	39.0
Eu/Eu*	0.97	0.72	0.38	0.84	0.60	0.57	0.86	0.77	1.33	0.24	0.80	0.50	0.33
La_N/Yb_N	7.64	4.44	5.37	10.94	4.97	4.17	3.71	6.77	3.20	3.92	4.56	5.73	4.58
La_N/Sm_N	3.03	1.81	2.76	4.18	3.77	2.43	2.02	2.64	1.76	2.75	2.16	2.96	3.03
Gd_N/Yb_N	1.76	1.81	1.32	1.46	1.03	1.27	1.45	1.73	1.46	0.98	1.67	1.24	1.06
∑ REE	113.26	168.19	206.69	96.89	110.80	158.21	123.14	129.99	37.59	223.81	119.44	58.37	180.68
K/Rb	384.44	238.72	273.54	253.87	235.49	238.31	316.07	346.87	302.28	237.55	295.79	226.07	276.27
Rb/Sr	0.08	0.10	1.52	0.23	0.67	0.43	0.10	0.09	0.03	2.11	0.08	0.81	1.36
Rb/Cs	30.23	29.94	31.36	40.95	63.10	17.16	19.87	30.81	5.26	52.77	29.00	25.87	57.36

Tab. 5 continued. Trace-element analyses (ppm).

	Gurvan Khar					Ikch Bayan					Trans-Altay		
Sample	31	32	33	34	35	36	37	38	39	40	41	42	43
Rb	14.1	16.9	14.5	25.9	7.2	126.3	93.6	122.4	66.8	83.4	136.1	49.2	44.2
Cs	0.3	0.3	0.4	0.6	n.d.	3.0	1.8	2.0	0.9	1.0	1.6	0.4	0.9
Sr	829.6	783.7	766.0	578.3	1107.5	170.8	143.3	171.3	166.6	227.1	26.6	129.5	562.6
Ba	447	557	506	418	399	526	841	742	870	809	86	448	709
Nb	3.1	2.2	2.1	3.3	2.7	7.0	7.6	6.6	13.1	9.3	8.8	2.1	7.7
Ta	0.2	0.1	0.1	0.2	0.1	0.5	0.4	0.7	0.6	0.9	0.6	0.3	0.6
Zr	77.2	57.0	51.9	105.6	67.7	121.6	154.7	88.2	339.2	150.2	185.3	68.6	203.2
Hf	2.3	2.1	1.8	3.0	2.0	4.0	5.0	3.6	9.1	5.1	7.0	3.0	6.1
Ga	18.8	17.8	16.8	17.7	23.6	16.1	19.6	13.9	17.9	16.1	19.6	11.2	18.3
Th	1.4	0.7	0.4	2.1	0.3	6.2	7.2	14.0	6.0	15.5	9.3	9.7	6.1
U	0.7	0.3	0.4	0.6	0.3	1.3	1.6	3.5	1.9	2.6	2.5	1.4	1.5
Ni	4.5	3.1	3.3	14.9	12.1	6.1	4.8	6.6	5.7	9.2	6.5	6.3	4.3
Co	4.5	2.6	2.2	13.3	15.3	3.3	1.8	1.6	2.6	3.1	1.0	1.8	4.4
V	56	24	26	138	186	20	8	7	22	31	8	17	56
Sc	10	5	6	21	15	4	9	8	14	10	8	4	10
Pb	0.3	0.4	0.7	1.2	2.0	2.8	6.5	4.3	6.3	2.8	8.7	4.5	4.4
Cu	5.5	4.8	4.3	61.6	75.7	11.2	14.6	9.4	5.2	12.5	12.3	7.7	7.9
Zn	38	37	42	43	75	29	34	21	48	37	33	12	7
Sn	n.d.	n.d.	n.d.	n.d.	n.d.	2	2	n.d.	3	2	2	n.d.	2
W	0.1	0.2	1.6	0.2	0.2	0.3	0.3	0.2	0.5	0.3	0.8	0.2	0.4
Mo	0.2	0.4	0.2	1.0	0.9	0.6	0.7	0.5	0.4	0.7	2.3	0.5	0.4
Cd	n.d.	n.d.	n.d.	n.d.	0.1	n.d.	n.d.	n.d.	0.1	n.d.	0.1	n.d.	n.d.
As	0.5	n.d.	0.5	0.8	n.d.	0.9	0.5	n.d.	n.d.	n.d.	0.8	1.0	3.9
Sb	n.d.	n.d.	n.d.	n.d.	n.d.	n.d.	n.d.	n.d.	n.d.	n.d.	0.1	n.d.	0.1
Bi	n.d.	n.d.	n.d.	n.d.	0.1	n.d.	n.d.	n.d.	n.d.	0.1	0.1	n.d.	0.1
Au (ppb)	n.d.	0.5	0.7	0.6	2.1	n.d.	n.d.	2.7	n.d.	n.d.	2.7	6.2	1.4
Ag	n.d.	n.d.	n.d.	n.d.	n.d.	n.d.	n.d.	n.d.	n.d.	n.d.	n.d.	n.d.	n.d.
Hg	0.01	n.d.	n.d.	n.d.	n.d.	n.d.	n.d.	n.d.	n.d.	0.01	n.d.	n.d.	n.d.
Tl	n.d.	n.d.	n.d.	n.d.	n.d.	0.1	0.1	n.d.	n.d.	n.d.	n.d.	n.d.	n.d.
La	8.0	6.5	4.9	9.3	9.1	18.3	20.1	25.3	43.5	28.7	32.8	19.9	19.7
Ce	17.3	14.0	11.0	19.5	20.6	34.6	44.8	46.0	89.3	55.7	64.5	40.1	37.5
Pr	2.18	1.76	1.32	2.44	2.80	3.98	5.16	4.86	11.14	6.18	7.19	3.51	4.31
Nd	10.1	8.1	6.0	11.7	13.5	16.8	23.0	18.5	47.8	25.6	28.9	12.4	18.6
Sm	1.9	1.6	1.2	2.4	2.8	3.0	4.4	3.2	8.6	4.6	4.7	2.0	3.5
Eu	0.55	0.35	0.30	0.71	0.85	0.54	0.37	0.40	1.24	0.66	0.37	0.43	0.68
Gd	1.59	1.69	1.27	2.37	2.02	2.67	3.72	2.23	6.61	3.40	3.53	1.31	3.38
Tb	0.25	0.29	0.18	0.38	0.31	0.46	0.63	0.42	1.15	0.56	0.57	0.21	0.54
Dy	1.56	1.83	1.09	2.18	1.75	2.65	3.90	2.17	6.56	3.47	3.18	1.23	3.02
Ho	0.28	0.37	0.21	0.44	0.29	0.53	0.77	0.46	1.20	0.68	0.63	0.24	0.57
Er	0.93	1.22	0.67	1.42	0.89	1.67	2.40	1.30	3.75	2.12	2.06	0.98	1.83
Tm	0.15	0.19	0.10	0.20	0.12	0.26	0.37	0.25	0.58	0.32	0.35	0.15	0.29
Yb	1.02	1.31	0.73	1.39	0.86	1.83	2.50	1.70	3.69	2.54	2.38	1.26	2.07
Lu	0.16	0.20	0.09	0.20	0.12	0.28	0.35	0.26	0.56	0.38	0.36	0.21	0.28
Y	10.0	12.9	7.2	14.3	9.5	17.1	24.9	15.2	39.8	22.5	21.1	8.6	19.4
Eu/Eu*	0.97	0.65	0.74	0.91	1.09	0.58	0.28	0.46	0.50	0.51	0.28	0.81	0.60
La_N/Yb_N	5.29	3.35	4.53	4.51	7.13	6.74	5.42	10.03	7.95	7.62	9.29	10.65	6.42
La_N/Sm_N	2.65	2.56	2.57	2.44	2.04	3.84	2.87	4.97	3.18	3.92	4.39	6.26	3.54
Gd_N/Yb_N	1.26	1.04	1.40	1.38	1.90	1.18	1.20	1.06	1.45	1.08	1.20	0.84	1.32
∑ REE	45.97	39.41	29.06	54.63	56.01	87.57	112.47	107.05	225.68	134.91	151.52	83.93	96.27
K/Rb	600.52	579.62	681.28	432.69	691.78	270.79	364.51	292.99	502.05	356.34	314.73	836.88	617.90
Rb/Sr	0.02	0.02	0.02	0.04	0.01	0.74	0.65	0.71	0.40	0.37	5.12	0.38	0.08
Rb/Cs	47.00	56.33	36.25	43.17	n.d.	42.10	52.00	61.20	74.22	83.40	85.06	123.00	49.11

Tab. 5 continued. Trace-element analyses (ppm).

	Trans-Altay													TSB
Sample	44	45	46	47	48	49	50	51	52	53	54	55	56	57
Rb	100.6	98.7	70.7	66.9	45.6	120.9	152.9	58.4	54.4	77.8	68.3	55.4	142.8	139.6
Cs	2.0	2.0	1.7	1.8	0.6	1.4	4.0	0.9	0.6	0.6	0.6	0.4	2.3	3.1
Sr	177.8	252.8	225.0	235.3	469.2	258.8	285.4	547.1	898.6	443.4	684.7	11.3	194.7	71.8
Ba	600	466	886	767	1496	379	651	798	1561	858	909	36	681	206
Nb	3.4	11.0	12.7	9.3	13.4	16.6	12.3	8.5	7.4	6.3	7.2	7.9	9.7	8.0
Ta	0.3	0.8	0.8	0.6	0.6	1.1	1.0	0.4	0.4	0.6	0.5	0.4	0.8	1.0
Zr	65.1	212.3	368.1	286.2	905.4	341.0	313.1	64.0	227.9	89.9	176.4	174.0	231.6	52.5
Hf	2.2	6.1	9.6	8.1	19.3	10.6	8.1	2.7	5.7	2.7	5.2	5.2	5.9	2.7
Ga	13.2	19.9	22.2	19.8	21.1	20.8	20.4	22.9	20.1	15.8	18.4	21.8	17.1	12.4
Th	3.6	7.1	5.8	5.9	4.7	15.8	16.8	5.7	4.8	5.6	5.0	3.9	18.9	24.6
U	0.8	1.9	1.9	1.4	1.4	3.1	1.8	1.1	1.2	2.2	1.6	1.1	4.3	3.4
Ni	7.3	7.3	3.7	4.7	2.7	9.7	9.3	6.8	14.3	27.7	22.2	9.8	2.0	0.4
Co	3.3	5.7	3.0	3.9	4.3	4.6	5.8	12.2	6.9	12.0	11.1	0.5	4.0	n.d.
V	17	40	34	35	28	32	55	141	81	96	112	7	32	5
Sc	2	6	10	12	12	3	9	17	9	12	11	2	6	5
Pb	4.4	8.3	7.9	5.2	4.2	4.0	7.7	6.4	2.1	3.6	3.3	2.1	10.1	4.4
Cu	8.7	6.8	9.5	9.8	7.2	8.7	13.7	125.8	16.2	58.3	44.2	9.4	29.8	1.2
Zn	10	32	32	34	43	21	16	56	40	44	35	21	34	7
Sn	n.d.	2	3	2	2	1	3	2	n.d.	n.d.	n.d.	2	1	n.d.
W	0.2	0.8	0.5	1.1	0.7	0.4	1.1	0.7	0.5	0.5	0.6	0.4	1.0	0.4
Mo	0.4	0.7	0.9	0.7	0.6	1.3	22.7	1.2	1.2	1.4	1.0	1.2	0.9	0.3
Cd	n.d.	0.1	0.1	0.1	n.d.	n.d.	n.d.	n.d.	n.d.	n.d.	n.d.	n.d.	n.d.	n.d.
As	2.2	2.6	n.d.	1.3	n.d.	1.3	0.9	1.8	1.2	1.2	0.6	0.7	2.8	6.5
Sb	0.1	0.1	n.d.	0.1	n.d.	0.1	0.1	0.1	0.1	n.d.	n.d.	n.d.	0.1	0.3
Bi	n.d.	n.d.	n.d.	0.1	n.d.	n.d.	0.1	n.d.	n.d.	n.d.	n.d.	n.d.	n.d.	n.d.
Au (ppb)	0.5	1.1	2.0	1.1	n.d.	1.2	0.9	n.d.	n.d.	n.d.	n.d.	n.d.	2.3	1.1
Ag	n.d.	n.d.	n.d.	n.d.	n.d.	n.d.	n.d.	n.d.	n.d.	n.d.	n.d.	0.1	n.d.	n.d.
Hg	n.d.	0.01	n.d.	n.d.	n.d.	n.d.	n.d.	0.01	n.d.	n.d.	n.d.	n.d.	0.02	0.03
Tl	n.d.	0.1	n.d.	n.d.	n.d.	n.d.	0.1	0.1	n.d.	n.d.	n.d.	n.d.	n.d.	n.d.
La	11.7	27.8	30.2	25.9	32.1	30.1	44.6	26.8	24.5	21.3	22.8	52.3	39.5	18.8
Ce	20.2	57.0	73.2	54.7	70.4	63.7	95.7	56.9	44.4	37.9	42.8	105.0	74.0	26.2
Pr	2.16	6.66	8.39	6.35	8.58	7.41	11.51	7.18	4.99	4.21	5.07	12.58	8.14	2.12
Nd	8.4	27.2	37.7	28.0	39.0	30.0	50.6	32.7	22.5	17.8	21.9	54.6	30.4	7.0
Sm	1.3	5.0	7.2	5.3	7.0	4.8	9.0	6.2	3.6	3.1	3.9	8.2	5.3	0.9
Eu	0.54	0.81	1.38	1.05	2.48	0.62	1.82	1.14	1.01	0.79	0.91	0.19	0.86	0.16
Gd	1.20	4.29	6.39	4.62	5.89	3.59	8.32	4.86	2.69	2.17	2.59	5.52	3.93	0.64
Tb	0.18	0.65	1.07	0.79	0.96	0.50	1.32	0.77	0.37	0.31	0.38	0.79	0.63	0.15
Dy	0.92	3.91	6.69	5.09	5.58	2.68	7.27	4.37	1.91	1.67	2.08	4.24	3.20	0.91
Ho	0.19	0.72	1.31	1.05	1.08	0.51	1.37	0.80	0.37	0.29	0.38	0.76	0.55	0.23
Er	0.61	2.33	4.04	3.38	3.47	1.57	4.03	2.43	1.13	0.81	1.05	2.48	1.69	0.88
Tm	0.10	0.38	0.65	0.51	0.53	0.25	0.65	0.37	0.18	0.12	0.18	0.43	0.24	0.19
Yb	0.75	2.66	4.01	3.85	3.69	1.76	4.51	2.20	1.20	0.85	1.16	3.03	1.87	1.74
Lu	0.11	0.36	0.64	0.56	0.59	0.27	0.58	0.41	0.18	0.12	0.16	0.49	0.26	0.30
Y	6.8	24.6	41.4	33.8	33.8	16.0	45.0	25.4	11.7	8.9	12.2	22.4	17.8	9.8
Eu/Eu*	1.32	0.53	0.62	0.65	1.18	0.46	0.64	0.63	0.99	0.93	0.88	0.09	0.58	0.64
La_N/Yb_N	10.52	7.05	5.08	4.54	5.86	11.53	6.67	8.21	13.76	16.89	13.25	11.64	14.24	7.28
La_N/Sm_N	5.66	3.50	2.64	3.07	2.88	3.94	3.12	2.72	4.28	4.32	3.68	4.01	4.69	13.14
Gd_N/Yb_N	1.29	1.30	1.29	0.97	1.29	1.65	1.49	1.78	1.81	2.06	1.80	1.47	1.70	0.30
∑ REE	48.36	139.77	182.87	141.15	181.35	147.76	241.28	147.13	109.03	91.44	105.36	250.61	170.57	60.22
K/Rb	465.40	345.68	399.21	423.13	547.96	403.74	215.54	386.64	508.15	354.25	425.40	701.27	231.37	287.81
Rb/Sr	0.57	0.39	0.31	0.28	0.10	0.47	0.54	0.11	0.06	0.18	0.10	4.90	0.73	1.94
Rb/Cs	50.30	49.35	41.59	37.17	76.00	86.36	38.23	64.89	90.67	129.67	113.83	138.50	62.09	45.03

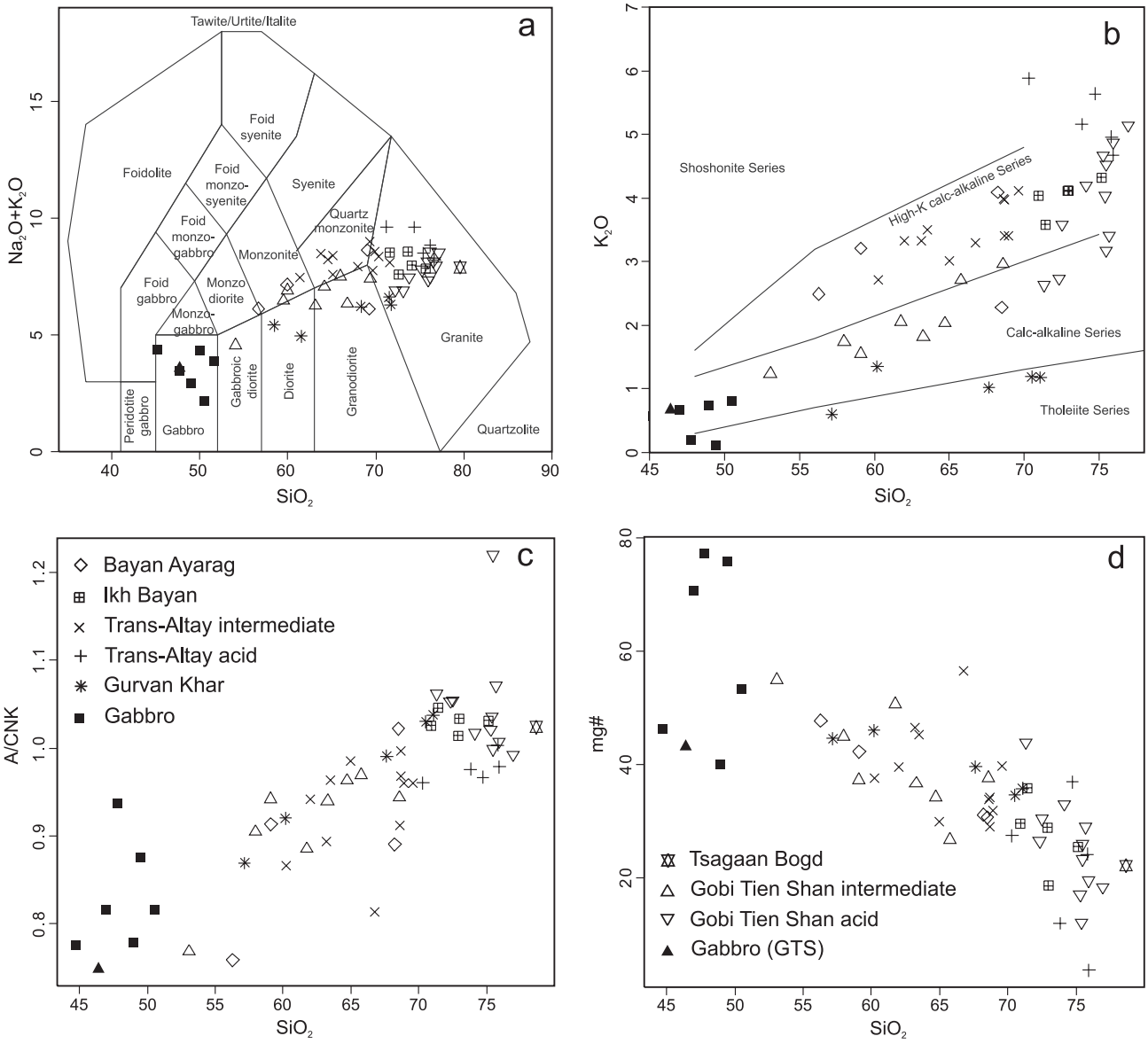

Fig. 6 Major-element chemistry of the plutonic rocks in the Trans-Altay Gobi: **a** – TAS classification (Middlemost 1994); **b** – SiO_2 vs. K_2O plot of Peccerillo and Taylor (1976); **c** – plot of alumina saturation index (Shand 1947) vs. SiO_2; **d** – binary plot of mg# vs. SiO_2, mg# = 100(MgO/(FeO^t + MgO)) in mol %.

anomaly (Eu/Eu* = 1.7–2.7), which is otherwise negligible (Eu/Eu* = 0.92–1.06) (Fig. 10b).

4.6 Gobi Tien Shan Intrusive Complex

Geochemical data from the Gobi Tien Shan Intrusive Complex correlate well with petrographic classification established for the individual rock types. Analysed samples can be classified as granite, granodiorite and quartz monzodiorite on the basis of the Q′–ANOR diagram (Fig. 3). They are calc-alkaline and belong to the medium K-series (Peccerillo and Taylor 1976). As for the Trans-Altay Intrusive Complex granites, two trends can be distinguished in SiO_2–K_2O diagram, whereby the rocks with SiO_2 > 70 wt. % are of high-K character (Fig. 6b). The K_2O/Na_2O ratios are very variable (0.3–0.8) for the intermediate rocks as well as for samples with SiO_2 > 70 wt. % (0.6–1.5). The rocks are metaluminous (A/CNK = 0.7–1.2); elevated values of Shand's index probably reflect secondary loss of alkalies accompanying intense sericitization. The K/Rb ratios fall between *c.* 200 and 390. The Rb/Sr ratios are low (0.1–0.4) in intermediate rocks, but generally higher although variable (0.2–4.2) in acid rocks (Fig. 7). The NMORB-normalized spider plots (Fig. 8) display marked depletion in Nb, P, Ti while Cs and Pb are generally enriched; P, Zr and Ti are slightly depleted, Nd

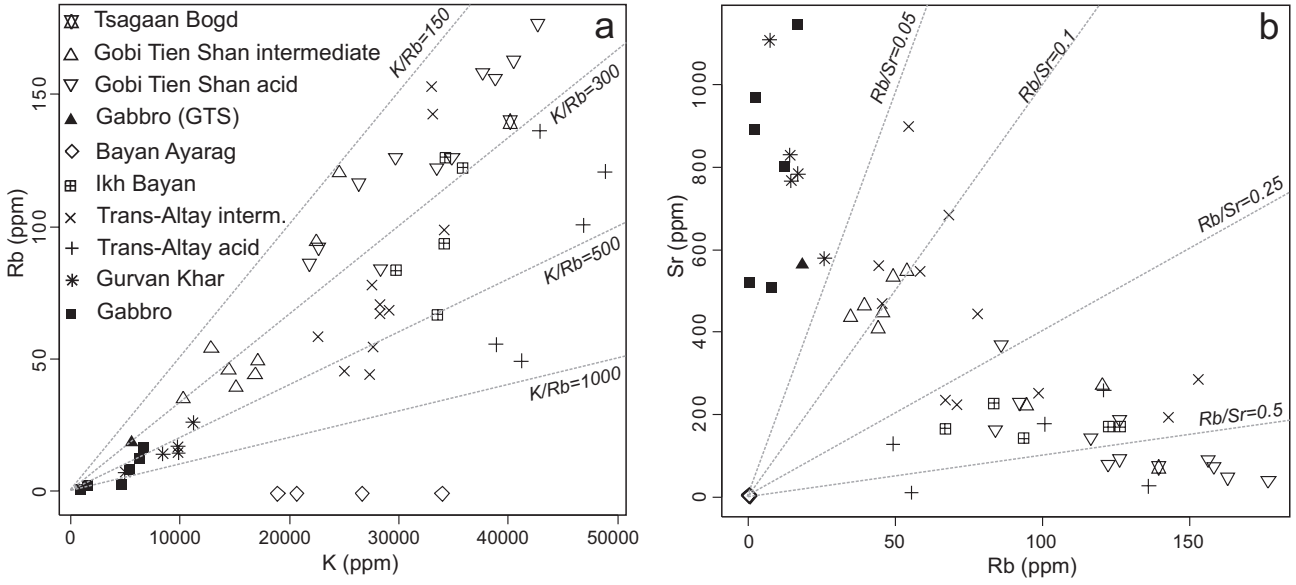

Fig. 7 Binary plots K–Rb (a) and Rb–Sr (b) for plutonic rocks of the Trans-Altay Gobi.

slightly enriched. The Ba, Sr and Th contents are consistently, slightly to moderately, enriched in acid rocks but are variable in intermediate rocks. Chondrite-normalized REE patterns (Fig. 9) show moderate to strong fractionation of LREE, while HREE display flat trends (La_N/Yb_N = 3.7–10.9, La_N/Sm_N = 1.8–4.4, Gd_N/Yb_N = 0.9–1.8). Negative Eu anomaly is well developed in acid (Eu/Eu* = 0.2–0.6) and less so in intermediate rocks (Eu/Eu* = 0.6–0.9).

There are no trace-element data available from the Naran Sevest Massif, but the major-element analyses suggest similarity with the Zamyn Belgekh Pluton (Šourek et al. 2003).

4.7 Tsagaan Bogd Massif

The only available sample from the Tsagaan Bogd granite has an affinity to alkali feldspar granite, and it is very acid (SiO_2 = 79 wt. %). The K_2O/Na_2O ratio is high (1.6) and A/CNK close to unity. Its K/Rb ratio is 287 and Rb/Sr ratio 1.9 (Fig. 7). The NMORB-normalized spider plot shows marked depletion in Ba, Nb, P and Ti, while Cs, Th, K, and Pb are enriched (Fig. 8) This trend is very similar to the rocks of GTS in LILE but the REE abundances are rather different. Chondrite-normalized pattern is V-shaped (Fig. 9), reflecting strong fractionation of LREE (La_N/Sm_N = 13.14) and enrichment in HREE (Gd_N/Yb_N = 0.3).

5. Laser ablation ICP-MS dating of zircons

The radiometric ages are not available yet in the Trans-Altay Gobi. Filippova et al. (1990a) described the Gobi Tien Shan Intrusive Complex as being Late Devonian–Early Carboniferous based on K-Ar dating. No original results were, nevertheless, presented in their report. Sample of granodiorite from NW part of the Trans-Altay Gobi corresponding to the Gurvan Khar Massif has been dated by the zircon evaporation method at 399 ± 1 Ma by A. Kröner (K. Schulmann pers. comm).

Most of the zircons extracted from the nine granitic samples showed substantial heterogeneity in ages, often on scale smaller than the analysed volume of zircon. Therefore only 50, out of the total of 123 analyses carried out on the unknown zircon samples, produced ages that could be interpreted as single-component ages corresponding to the zircon crystallization from the granitic melt. Yet, small number of concordant data points allows more precise age determination within the period of the Variscan magmatic activity in the studied area. Available data (Fig. 11) characterize the evolution of the Zamyn Belgekh Pluton, one sample is from an equivalent of the Trans-Altay granite in GTS and one from the Bayan Ayrag Massif.

Regression of data points from sample **D-28/1145** (biotite-hornblende granodiorite) gives the Early Carboniferous upper concordia intercept age of 354 ± 37 Ma. However, zircon analyses from this sample form two separate clusters in the concordia diagram, first represented by four slightly discordant data points with a weighted mean ^{238}U-^{206}Pb age of 309 ± 9 Ma, second being somewhat older with one concordant point yielding a concordia age of 346 ± 14 Ma. All zircons from sample **D-28/1145** are euhedral with igneous oscillatory zoning, and hence their ages can be interpreted as recording two separate phases (309 and 346 Ma) or one

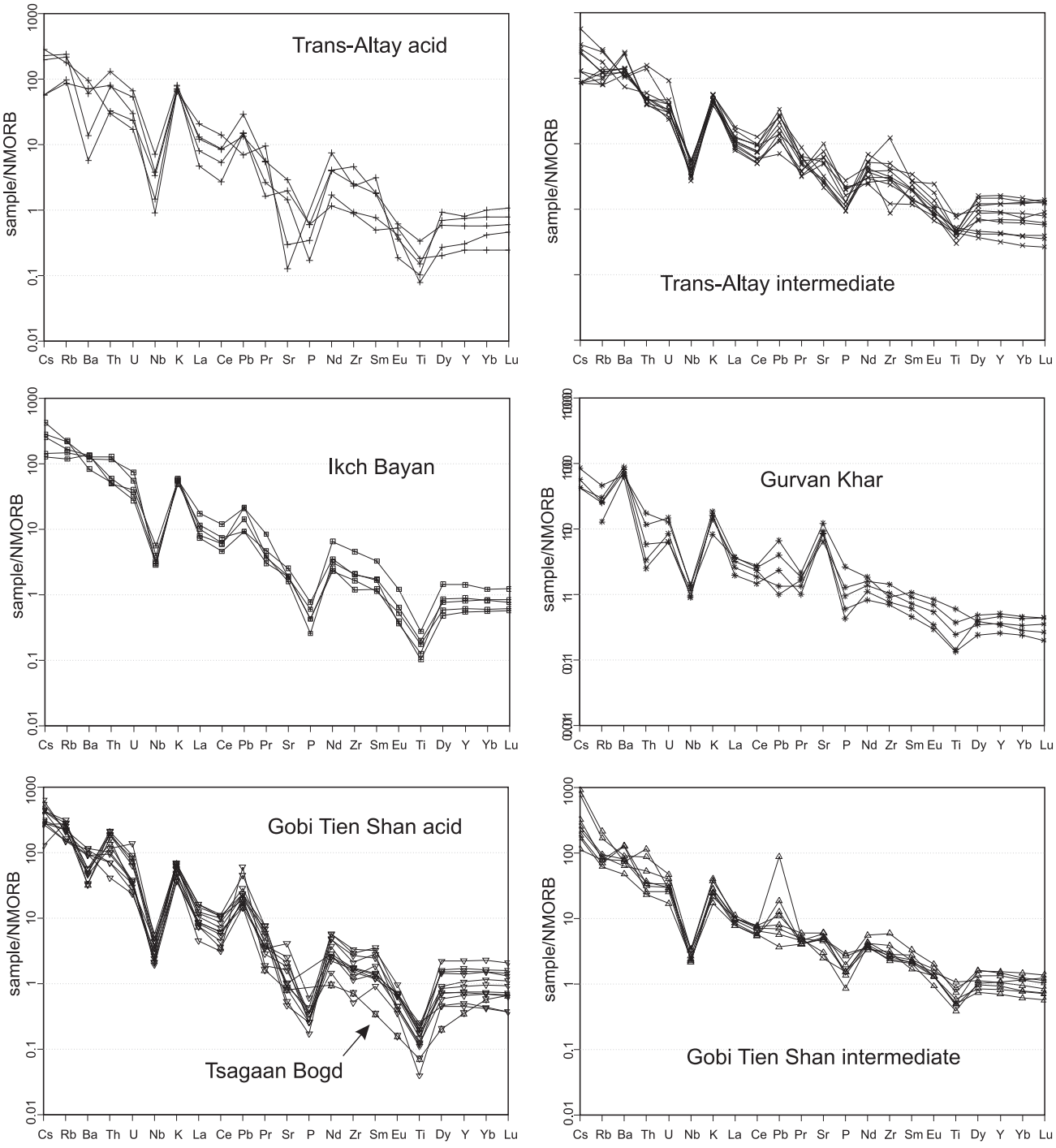

Fig. 8 NMORB (Sun and McDonough 1989) normalized spider diagrams for granitic rocks of the Trans-Altay Gobi.

prolonged phase of zircon magmatic crystallization during the Carboniferous period. All analysed zircons from sample **E-27/1138** (biotite-hornblende granodiorite) are slightly discordant, giving a weighted mean ^{238}U-^{206}Pb age of 335 ± 15 Ma and a corresponding lower concordia intercept age of 326 ± 33 Ma. Given the morphology and character of oscillatory zoning in the zircons, this age can again be interpreted as corresponding to the zircon magmatic crystallization. On the other hand, samples **A-26/1018** (biotite-hornblende granodiorite) and **B-27/1149** (leucogranite) yielded somewhat younger (Late Carboniferous–Early Permian) weighted mean ^{238}U-^{206}Pb ages of 299 ± 8 Ma and 288 ± 15 Ma (7 more concordant data points), respectively. Younger still lower concordia

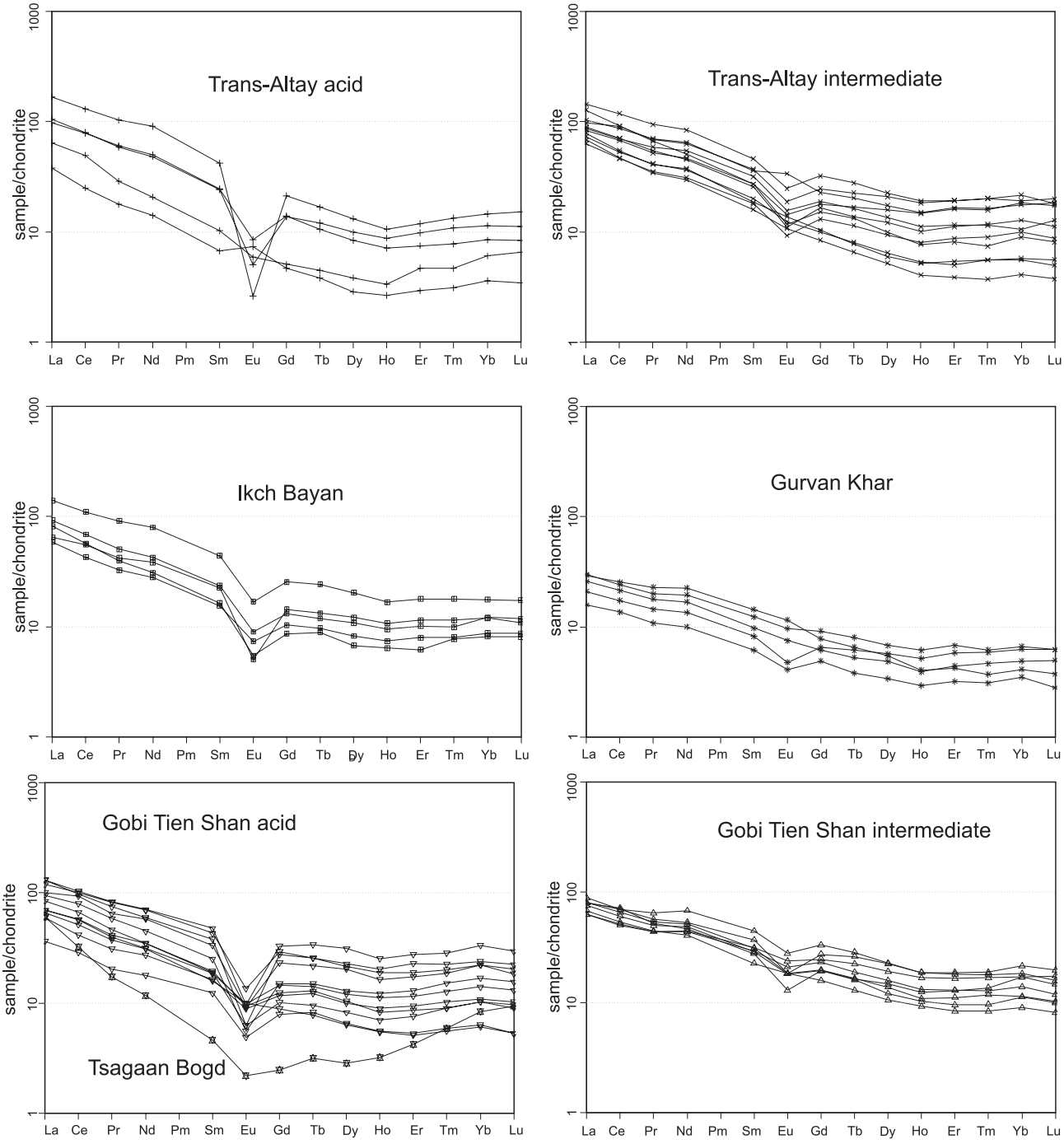

Fig. 9 Chondrite (Boynton 1984) normalized REE patterns for granitic rocks of the Trans-Altay Gobi.

intercept age of 263 +14/-13 Ma can be derived from zircon analyses from sample **A-26/1018**; however, this date is likely to be biased towards younger ages by one discordant data point and it is therefore not considered as being very accurate. In summary, the age of magmatic activity in the Gobi Tien Shan area, as recorded by magmatic (euhedral and oscillatory-zoned) zircons extracted from nine granitic samples spans the time interval from Early to Late Carboniferous, and perhaps even to Early Permian times.

A weighted mean ^{238}U-^{206}Pb age of 330 ± 12 Ma and a corresponding lower concordia intercept age of 331 ± 23 Ma can be derived from zircon analyses of the sample **F-5/1020** representing granodiorite with granophyric texture of the Bayan Ayrag Massif in the Edrengiin Nuruu Mts.

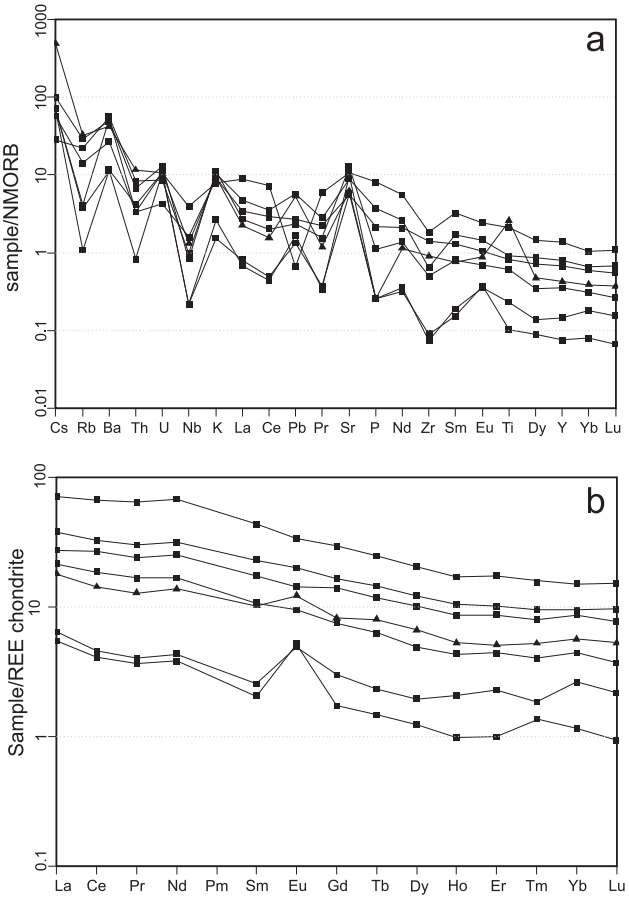

Fig. 10 Multielement trace-element patterns for gabbros of the Trans-Altay Gobi normalized by: **a** –NMORB (Sun and McDonough 1989); **b** – chondrite (Boynton 1984).

Two concordant data points in biotite granite sample **C-28/1028** forming an independent body of Trans-Altay Intrusive Complex situated west of the Shar Khulsny Bulag in GTS gave Carboniferous concordia ages of 333 ± 8 and 308 ± 14 Ma. Both ages derived from euhedral magmatic zircons may be interpreted as either recording two separate phases of zircon crystallization from the magma, or as reflecting a prolonged phase of zircon magmatic crystallization during the Carboniferous period.

6. Structures in granitic bodies

Internal structures of plutonic rocks of the Trans-Altay Gobi have developed in a regime of the Variscan magmatic activity as well as during the postmagmatic deformation. Magmatic and late magmatic structures are characteristic of the largest body in the GTS, the Zamyn Belgekh Pluton, and are represented by magma mingling structures and magmatic foliation. Planes interpreted as magmatic foliation are sporadic only in the northernmost part of the Trans-Altay Intrusive Complex. The rocks of the Bayan Ayrag and Ikh Bayan massifs are usually without macroscopically observable magmatic structures. Post-magmatic structures are connected with the development of ductile to brittle–ductile foliation and brittle–ductile to brittle mylonitic zones, joint systems and the origin of tension joints that are filled with subvolcanic dykes. Late to post-magmatic foliation is characteristic of the NW part of the Zamyn Belgekh and Gurvan Khar massifs.

6.1 Bayan Ayrag Massif

Only the presence of fine-grained dark grey microdiorite enclaves could be described as magmatic fabric in the Bayan Ayrag Massif. Neither the magmatic foliations in intrusive rocks nor bedding in the wall-rock volcanic rocks have been found. Contacts of plutonites with their volcanic country rocks are fuzzy, granites intruded basalt and andesite in the form of dykes and loaf-shaped apophyses. Textures of a character transitional between plutonic and volcanic are developed in granites near the contacts with volcanic rocks.

6.2 Trans-Altay Intrusive Complex

Bodies of this complex are of oval or irregular shape. Country-rock xenoliths are exceptional. Magmatic to submagmatic foliation is very rarely developed in granodiorites of the Sayryn Pluton of the Trans-Altay Intrusive Complex. It is steep, NE–SW trending south of, and flat north of, the Trans-Altay shear zone. There is a very narrow or almost indistinct zone of thermal metamorphism around Trans-Altay granites. They intruded volcanic or volcaniclastic rocks usually without pronounced bedding. Transitional subvolcanic textures have locally developed along the contacts of granite apophyses with adjacent rhyolites. The contact has a clearly discordant character in places with preserved bedding. Rocks are mylonitized in exposures along the faults parallel with the Trans-Altay shear zone.

6.3 The Ikh Bayan Massif

Definitely post-orogenic are the circular intrusions of the Ikh Bayan Massif. A distinct contact aureole with thermally metamorphosed volcanosedimentary rocks has developed around intrusions, the bedding and cleavage in wall rocks are cut by granites. The plutonic bodies contain, particularly at their margins, wall-rock xenoliths of various sizes. The pronounced bending of the structural trends in adjacent geological units around the massifs, which is clear from the geological maps (see

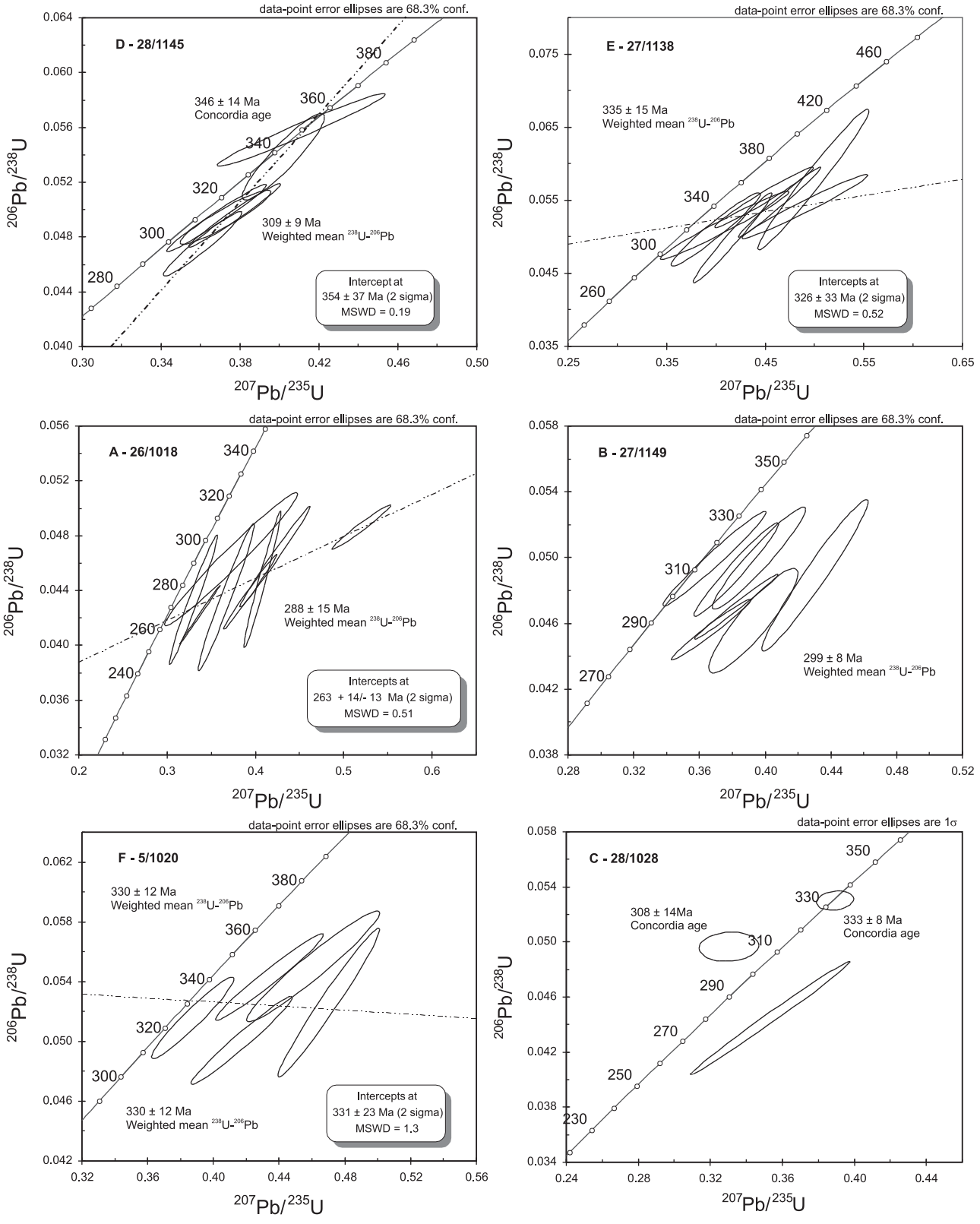

Fig. 11 U-Pb concordia diagrams for zircon LA ICP-MS analyses from the Zamyn Belgekh Pluton (samples A, B, D and E), granite from GTS corresponding to the Trans-Altay Intrusive Complex (sample C) and from Bayan Ayrag Massif (sample F).

map enclosed in this Volume) as well as satellite images was caused by the post-magmatic deformation during the movements on the Trans-Altay shear zone.

6.4 Gurvan Khar Massif

Metamorphic foliation is developed solely in the rocks of the Gurvan Khar Massif. The foliations in recrystallized metagranodiorites and orthogneisses are of predominant NNW–SSE trend, with variable but usually subvertical dips. Such an orientation is subparallel with cleavage in the adjacent Early Carboniferous flysch sediments. The foliation trend is reoriented along the intrusions of the gabbro massifs to produce ring structures identifiable from the satellite images.

6.5 Gobi Tien Shan Intrusive Complex

Structures bound to the Gobi Tien Shan Intrusive Complex are best exposed in the granitoids of the Zamyn Belgekh Pluton. Structures indicative of hybridization between granodiorites and diorite/gabbrodiorites are typical part of much of the massif. These structures (Fig. 5) are well exposed along the path between the Shar Khulsny and Zamyn Belgekh springs. Magma of granite–granodiorite composition was invaded by dioritic melt, forming syn-plutonic dykes which were often disintegrated into swarms of enclaves varying in size and degree of roundness. Basic enclaves are usually aligned in direction of the magmatic flow, flattened with varying intensity, thus defining magmatic foliation and lineation. Magmatic lineations are particularly highlighted by the preferred orientation of feldspars and hornblende grains. In the diorite body in the eastern part of the pluton, magmatic foliation is commonly defined by schlieren.

Strikes of magmatic foliation in the Zamyn Belgekh Pluton show predominant N–S to NE–SW orientations – closely resembling the foliation trends in the crystalline complex as well as bedding in country-rock sediments

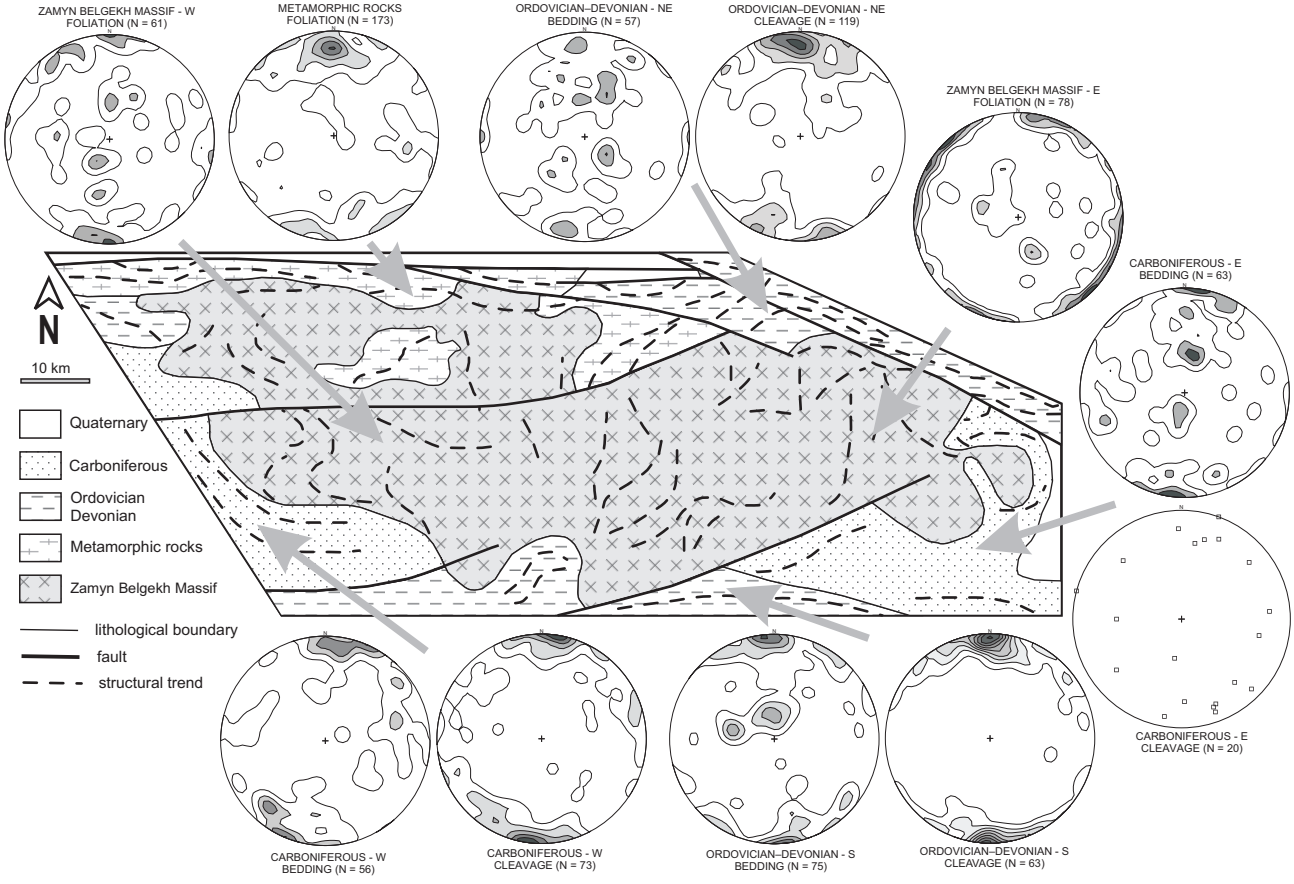

Fig. 12 Schematic map of the Zamyn Belgekh Pluton and contour diagrams summarizing orientation of planar structures in granites and adjacent rocks. Schmidt projection on the lower hemisphere. Step of contours 2 sigma. For position see Fig. 2.

of the pluton (Fig. 12). Flat lying and NW–SE trending steep foliations are subordinate.

7. Discussion

The Trans-Altay Gobi is a part of the southern domain of Mongolia with accreted arc-related volcanic and volcaniclastic rocks (Lamb and Badarch 1997) of dominantly Silurian to Lower Devonian and Carboniferous to Permian ages. Wide compositional range, different structural features and irregular distribution of the Palaeozoic granitic intrusions reflect magmatic processes during accretion of separate domains of the Trans-Altay Gobi. Even though there exist differences in chemical composition among the individual Late Palaeozoic massifs in the Trans-Altay Gobi, they are all metaluminous and characterised by pronounced depletion in Nb, Ti and P, whereby the depletion in Nb and Ti is indicative of arc magmatism (Wilson 1989; Draut and Clift 2002). Luchitskaya and Tikhomirov (2007) described Nb and P minima in the Cretaceous subduction-related granitoids in the northeast Asia. Interpretation of the Trans-Altay Gobi granites as arc-related rocks is consistent with positions of the samples in the VAG field (Fig. 13) of geotectonic discrimination diagrams by Pearce et al. (1984). Relatively primitive geochemistry of granites is in accordance with the results of Jahn et al. (2000) and Jahn (2004) who emphasized juvenile character of granites in the Central Asian Orogenic Belt and short crustal residence since the separation of magmas from the source.

Although nearly all the plutons studied in the course of the present work are of igneous-arc character, there are several samples of granites from the Trans-Altay and Gobi Tien Shan Intrusive complexes indicating apparently an alkaline affinity (Fig. 14). These rocks are usually acid members of the individual intrusive complexes. Their geochemical signature resembling the intermediate members (Fig. 8) points rather to highly fractionated rocks of magmatic suites, especially in the Gobi Tien Shan Intrusive Complex.

Subvolcanic dyke rocks of bimodal composition are particularly associated with the Ikh Bayan Massif, Gobi Tien Shan Intrusive Complex and the Bayan Ayrag Massif. Their age is unknown. By analogy with the dated occurrences of similar rocks in NW China they can be connected to Permian post-collisional extension in the area (Zhang et al. 1998).

Pre-orogenic, syn-collisional and post-collisional plutonic bodies can be distinguished in relation to the accretionary processes culminating during the Late Carboniferous in the area of the Trans-Altay Gobi. The evolution of Early Carboniferous calc-alkaline granites

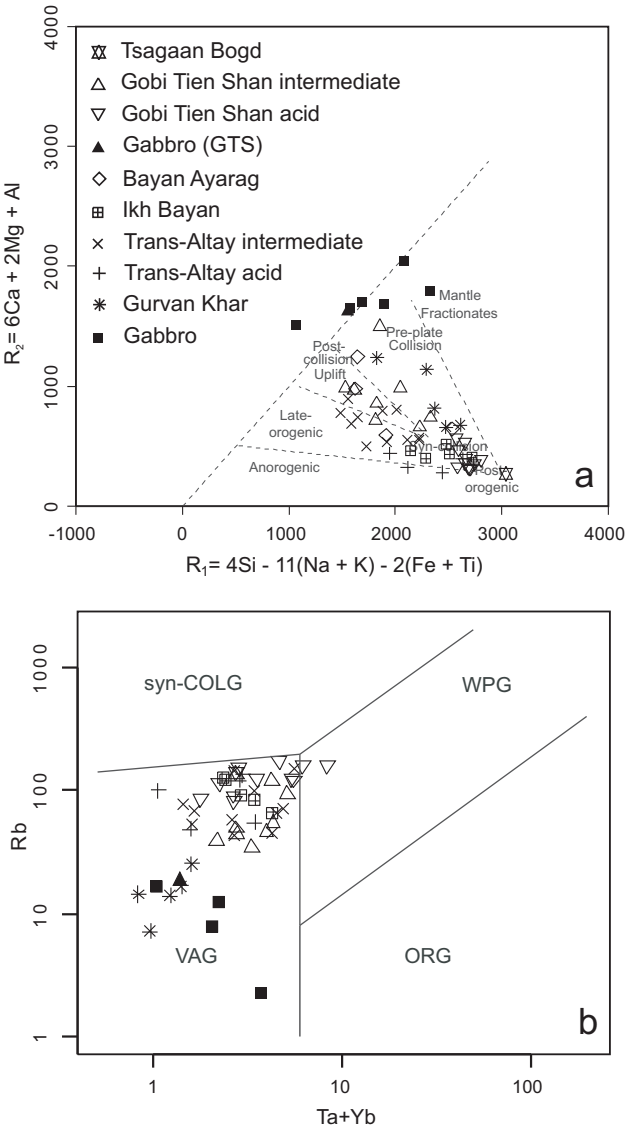

Fig. 13 Geotectonic discrimination diagrams for rocks of the Trans-Altay Gobi: **a** – R_1-R_2 plot of Batchelor and Bowden (1985); **b** – Ta + Nb vs. Rb diagram of Pearce et al. (1984). VAG – Volcanic Arc Granite, syn-COLG – syn-Collisional Granite, WPG – Within Plate Granite, ORG – Ocean Ridge Granite.

to Late Carboniferous/Permian high-K rocks in time and similar trend in space from the south to the north indicate the presence of a Carboniferous subduction zone dipping north and situated south (in relation to present-day coordinates) of the Gobi Tien Shan Domain. The final closure took place most likely during the Upper Carboniferous and Permian. Such a scenario is in accord with palaeotectonic interpretations in the southern Mongolia (Ruzhentsev and Pospelov 1992; Windley et al. 2007) as well as the Chinese Tien Shan (Windley et al. 1990; Allen et al. 1992; Xiao et al. 2004).

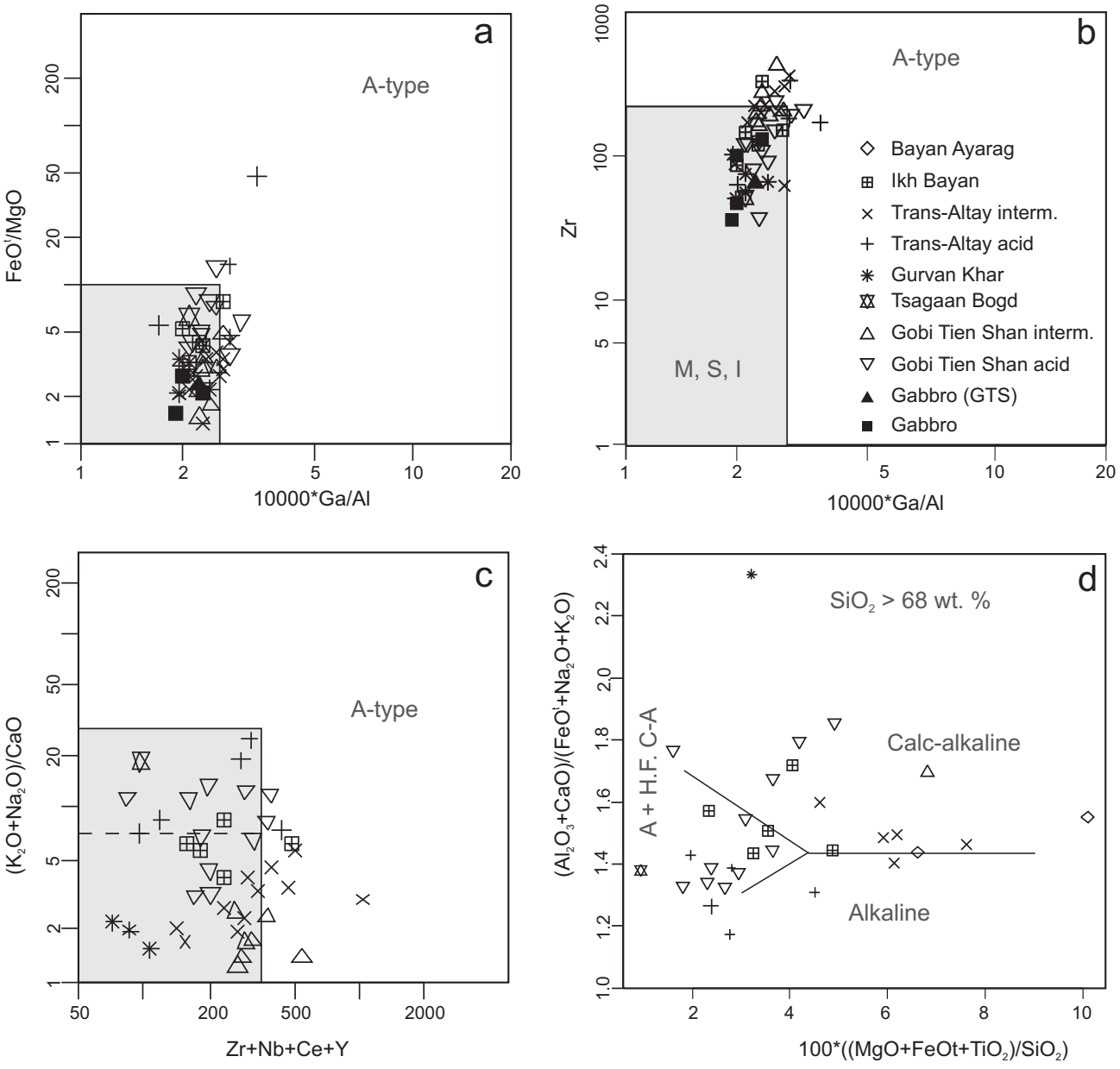

Fig. 14 Position of granitic samples in A-type granite discrimination diagrams: **a, b** – 1000*Ga/Al vs. FeO^t/MgO resp. Zr diagrams (Whalen et al. 1987); **c** – Zr + Nb + Ce + Y vs. $(K_2O/Na_2O)/CaO$ (Eby 1990); **d** – classification diagram $100*((MgO + FeO^t + TiO_2)/SiO_2)$ vs. $(Al_2O_3 + CaO)/(FeO^t + Na_2O + K_2O)$ (Sylvester 1989). Explanations: M, S, I – field of M, S and I type granites; A + H.F. CA – alkaline and highly fractionated calc-alkaline granites.

7.1 Pre-tectonic igneous activity

Only the **Gurvan Khar Massif** can be assumed as being a pre-tectonic granite body in relation to Variscan orogeny in the area. It was incorporated into the geological structures of the adjacent rocks by post-magmatic tectonometamorphic processes. Metagranodiorites and orthogneisses representing this massif are exposed in tectonic slices within the Palaeozoic volcaniclastic sediments of the Baytag Terrane along the boundary between the SG and TA domains. Long axes of tectonic slices are subparallel with structural trends in adjacent volcaniclastic sequences and rocks are usually mylonitized in the fault zones along the contacts of geological formations. In the less affected parts of the massif, metamorphic foliation developed due to the recrystallization of quartz, feldspars and biotite. The massif was intruded by oval bodies of gabbro and cut by dykes of massive red granites corresponding to rocks of the Trans-Altay Intrusive Complex. Trends of foliation are subparal-

lel with cleavage in the adjacent Late Devonian–Early Carboniferous flysch sediments (Fig. 15). Interpretation of the post-magmatic relationships between metagranodiorites and flysch is complicated by the development of a thermal metamorphic aureole. Indeed this aureole could be related to intrusions of the oval-shaped gabbro massifs, around which circular structures with bending of foliation have formed especially north of the Gurvan Khar Mt.

Deformed granitoids of the massif differ chemically from the other granitic rocks in the area. They are characterised by very low contents of K_2O, corresponding to tholeiitic rocks. The low K_2O/Na_2O and Rb/Sr ratios point, together with the very low degree of fractionation of REE, to a primitive source of parental magmas. High and variable K/Rb ratios with weak enrichment in U, Ba and Pb can indicate mobility of elements during the metamorphism and deformation.

The primitive chemical features of the rocks, position of samples in Pre-plate Collision Field of the R_1-R_2 diagram (Batchelor and Bowden 1985, Fig. 13a) imply a largely different character in comparison with other granitic bodies of the Trans-Altay Gobi. Even though there are no geochronological data available except for the unpublished Early Devonian zircon age obtained by Kröner (Šourek et al. 2003), geological and structural data can indicate older than Carboniferous age. The rock chemistry points to an evolution in a primitive magmatic arc. This is in agreement with geological position of the Gurvan Khar Massif which is bounded to the zone situated along the suture between Bayatag and Baaran terranes. It is marked by relics of Ordovician–Devonian (Ruzhentsev 1985; Ruzhentsev et al. 1985), tectonic mélange with deep water sediments, pillow lavas and fragments of serpentinites exposed in a narrow structure known as the Zoolen accretionary prism Terrane (Badarch et al. 2002). On the other hand, Helo et al. (2006) interpreted eastern exposures of this terrane as single intra-oceanic island arc–forearc according to geochemical characteristics. The U-Pb SHRIMP single zircon dating of metavolcaniclastic rocks from eastern part of the Zoolen Terrane gave ages of 421± 3 Ma and 417± 2.2 Ma (Helo et al. 2006). These data may support the presumed Devonian age of the Gurvan Khar Massif.

7.2 Syn-collisional plutonism

The **Gobi Tien Shan Intrusive Complex** is represented by numerous bodies forming an E–W trending belt between the Gobi Tien Shan fault zone in the north and the Mongolia–China border in the south. The Zamyn Belgekh Pluton in the western part of Gobi Tien Shan range is the largest body among them. It is a composite pluton with newly-established intrusion age of 355–310 Ma corresponding to the Carboniferous. Permian ages of about 260–290 Ma can be related to a younger magmatic phase. Monzodiorites to diorites which form relatively independent bodies in the N and NE parts of the Zamyn Belgekh Pluton are its relatively oldest facies. In the main body of the pluton, predominant granodiorites to granites had been intruded by biotite-hornblende diorites, while still (largely) molten, giving rise to magma mingling textures. Magmatic foliation developed in the intermediate members shows a weak preferred orientation but the maxima in structural contour diagrams correlate well with the bedding orientation in Silurian–Devonian as well as Carboniferous sediments preserved as a roof pendants of the pluton (Fig. 12). The magmatic foliation was reoriented to a prevailing E–W trend along the N margin of the pluton and corresponds with metamorphic foliation within the rocks of the Atas Uul–Tchinges Uul mountain range. The ellipsoidal structural trends in thermally metamorphosed wall rocks, structures indicative of magmatic flow in the western part of pluton, submagmatic deformation along the northern endocontact and the oval-shaped, relatively separate intrusion in the east part of the pluton, which are well visible from the geological maps and satellite imagery indicate as the dominating mechanism of intrusion. It was combined with magma stoping processes as proved by the occurrence of the common septa in NW part of pluton.

Erosional processes have exposed deeper facies of the massif, connected with more intense thermal metamorphism in the N and NW. Granites without preserved magmatic fabrics and granophyric granites are typical of the central and SE parts of the pluton. The presence of granophyric textures in the granites and very narrow contact aureole point to a intrusion level with the pressure of up to 5 kbar. Cordierite and andalusite in the contact zone indicate temperatures of 500–600 °C (Bucher and Frey 1994) in the SE part of pluton, while garnet–biotite thermometer in migmatized gneiss xenolith in diorites in NE part points to temperatures 680 °C, possibly reflecting the higher temperature of the dioritic magma. Granophyric granites passing to granites with corroded quartz and feldspars phenocrysts in granophyric matrix are exposed commonly close to the Carboniferous volcanic rocks in the roof pendant of the pluton, which points to comagmatic evolution during the youngest phases of the pluton evolution. The granophyric granites probably correspond to the apical part of the intrusion, which, rich in fluids, intruded in subvolcanic conditions.

Plutonic rocks of the GTS have an I-type character corresponding to the volcanic arc-granites according to Pearce et al. (1984). Nevertheless, the chemical composition of rocks indicates – in accordance with structural features – two different rock groups. The intermediate rocks are calc-alkaline with low Rb/Sr ratios, correspond-

ing to Syn-Collisional to Post-Collisional Uplift field of the R_1-R_2 diagram (Fig. 13a), seem to be related to earlier stages of the igneous-arc evolution. Acid rocks usually without internal fabric are high-K calc-alkaline. Higher and variable K_2O/Na_2O and Rb/Sr ratios point to more evolved source and/or contamination during the ascent. These rocks are of distinctly post-collision character as seen from the R_1-R_2 diagram.

Linear arrangement of plutonic bodies of the Gobi Tien Shan indicates development of intrusive rocks at an Andean-type continental margin. Geological relationships, petrography and geochemical data in the Zamyn Belgekh Pluton suggest following stages in evolution during the Early Carboniferous:

- generation of basic magma above the subduction zone and its ascent,
- melting of overlying rocks in the igneous arc triggered by basic magma emplacement,
- generation and segregation of the granitic magma, processes of mixing with underlying basic magma and construction of the batholith,
- emplacement of granophyric granites accompanied by subaerial volcanic activity.

7.3 Post-collisional bodies

Post-tectonic intrusive bodies should cut both the bedding and metamorphic fabric in their country rocks (Clarke 1992). The oval bodies of the Trans-Altay Intrusive Complex, circular intrusions of Ikh Bayan and the Bayan Ayrag massifs indeed penetrate Variscan geological structures in the Trans-Altay Gobi. They usually have no visible internal fabric and could be interpreted as post-tectonic massifs. This also concerns some small bodies of granites in the Gobi Tien Shan Domain. Even though all these massifs are of post-collisional character, they differ in some features.

The only one sample from the **Tsagaan Bogd Massif** is not possible to interpret. Moreover, unusual REE trend points to late- or post-magmatic alteration.

Bayan Ayrag Massif crops out in the NE part of studied region in the Edren Terrane. Its high-K calc-alkaline granites are of Early Carboniferous age according to zircon dating (330 Ma). They are comagmatic with bimodal Carboniferous volcanics.

The circular bodies of the **Ikh Bayan Massif** are clearly post-collisional. Their exposures rim the suture zone between the Baaran and Baytag terranes. The geochemical composition is typical of high-K, I-type granites. The higher K/Rb and lower Rb/Sr ratios are similar to values in the Trans-Altay granites. They correspond to volcanic arc granites *sensu* Pearce et al. (1984) and fit the field of Syn-Collision Granites in the R_1-R_2 diagram (Fig. 13). Circular shape and regular zoning of the thermal metamorphism suggest ballooning as a possible mechanism of intrusion. No radiometric data are available but a distinct contact aureole has developed in the Devonian and Lower Carboniferous rocks around the massif indicating its Early Carboniferous–Permian age. As there are no radiometric data confirming the Permian intrusive age in the Trans-Altay Gobi, this age is documented by Lamb et al. (2008) from granites in the Shinjinst area of the Gobi Altay range NE of the studied area. Also Kovalenko et al. (2006) described the Permian Khan Bogd alkali granite pluton in the Gobi Tien Shan Rift Zone E of the Trans-Altay Gobi area.

In the map sheet area, isolated bodies which are related to the **Trans-Altay Gobi Intrusive Complex** occur both in the Trans-Altay and Shargyn Gobi terranes. Similar granites forming the Gobi Tien Shan Terrane have a slightly different chemistry and the question of their mutual relationships remains still open. In the studied region, the majority of individual plutons are situated in the Shargyn Gobi Domain. The plutons cut palaeontologically dated Lower Carboniferous volcaniclastic sequences north of the Shargyn Gobi intermountain depression. Microdiorite enclaves are rare and wall-rock xenoliths are usually absent in these rocks. The Late Carboniferous age of the massif is also confirmed by radiometric dating (sample C in Fig. 11), but the number of dated zircons is too low for relevant interpretation. Rocks are of I-type; relatively primitive source is confirmed by high K/Rb and low Rb/Sr ratios. On the other hand, high-K calc-alkaline character, fractionated REE trends and enrichment in Rb, Th and Pb in the NMORB-normalized spiderplots could indicate contamination by crustal material. The rocks are of Volcanic-Arc Granite type according to Pearce et al. (1984) and show a trend from Late- to Post-orogenic Granites in the R_1-R_2 diagram. The low Ba, Sr and Eu abundances corresponding to a post-orogenic granite (Bonin et al. 1998) can be related with extensive fractionation of feldspars.

Geochemistry of a few samples (Fig. 14) and textures with K-feldspar laths and amphibole can indicate alkaline affinity of some isolated bodies of the Trans-Altay Intrusive Complex and also of the Bayan Ayrag Massif. These massifs are related with the Carboniferous to Permian volcanic rocks of alkaline character (Yarmolyuk 1983). The best example is the NW–SE elongated red granite pluton NW of the Arslan Khayrkhan Mt. in the Baytag Terrane. Alternation of ring-like parts of the granitic massif with acid volcanics and transition between granitic and volcanic textures in adjacent rocks could indicate cauldron subsidence as a key emplacement process.

Small gabbro massifs seem to be the youngest intrusive rocks in the Trans-Altay Gobi. They are preferentially distributed close to the oval-shaped intrusions of

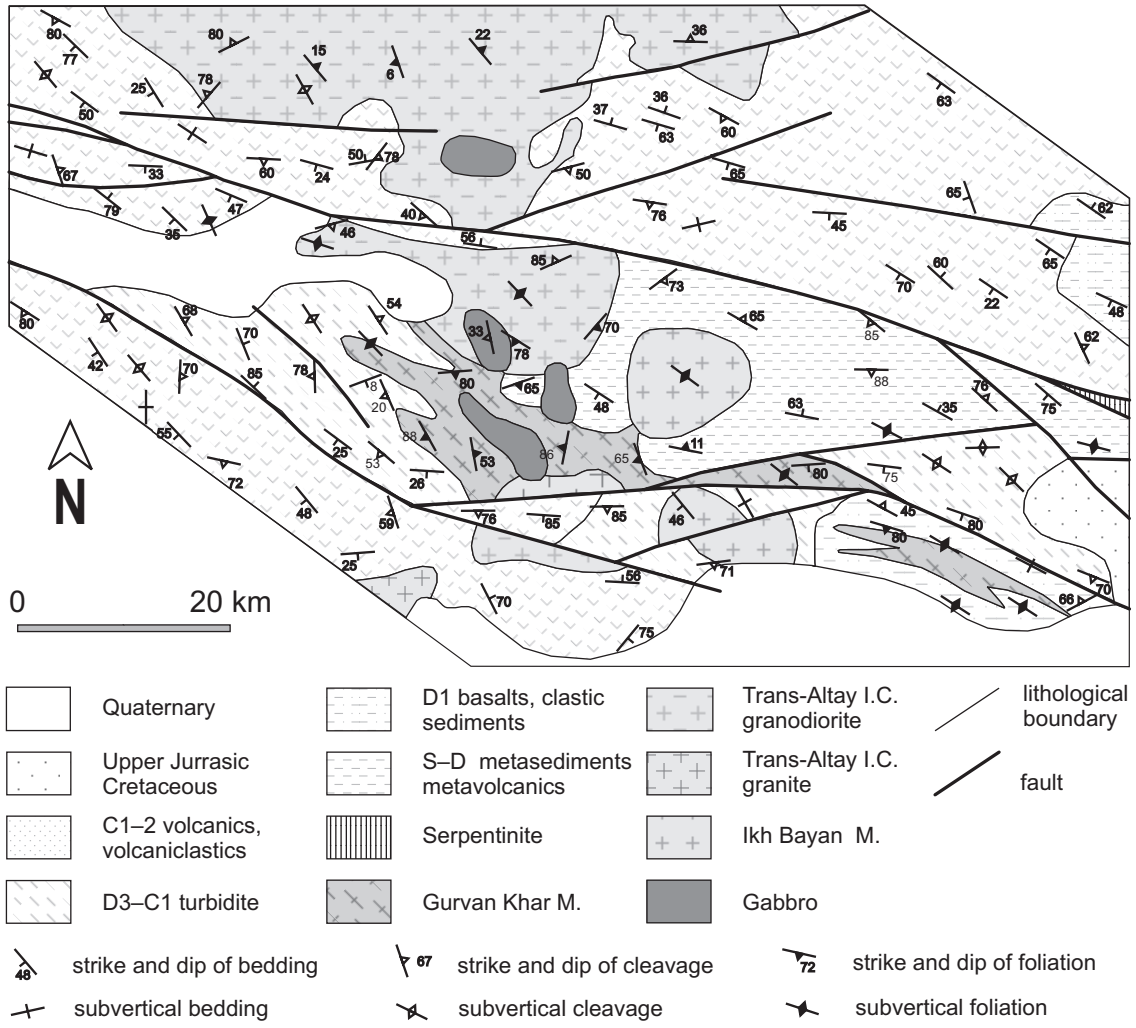

Fig. 15 Schematic structural map along the Trans-Altay shear zone north of the Gurvan Khar Mt. For position see Fig. 2.

the Ikh Bayan Massif north of Gurvan Khar Mt. Invasion of gabbros into the granitoids caused probably partial remobilisation of the granitic melt and netveining of the gabbros by the granitic melt (Fig. 15).

7.4 Trans-Altay shear zone

The NW–SE oriented zone separating the Baytag and Baaran terranes is marked by a mylonitic zone, ultrabasic bodies, alternation of tectonic slices with rocks from both of the terranes, relics of Triassic sediments and granite bodies of the Ikh Bayan Massif. It corresponds with a suture separating Baytag and Baaran terranes, in which relics of ophiolites are preserved (Zoolen Terrane) more to the SE. Regional structural trends are markedly bent around circular granite bodies. This is apparent from the satellite images, geological maps, and also confirmed by orientation of small-scale structures (Fig. 15). The geometry of regional structures corresponds to sigma porphyroclasts (Passchier and Simpson 1986; Hanmer 1990) used as a shear-sense indicator. Granite massif in the centre seems to have behaved as a rotated rigid block during the movements between the terranes. Bedding and cleavage in adjacent volcaniclastic formations was bent during rotation of the Ikh Bayan Massif caused by strike-slip movements on the zone. Asymmetric geometry of the described structures indicates dextral sense of movement along the Trans-Altay shear zone. The location of gabbros in the areas of pressure shadows behind the rotated massifs suggests syn-tectonic formation contemporaneous with the movements on this shear zone.

As bodies of the Trans-Altay Intrusive Complex are exposed on both sides of the Trans-Altay shear zone (Fig. 1), they might have post-dated the movements on this zone. The zone was reactivated during the Cenozoic movements on the Gobi Tien Shan fault (Tapponier and Molnar 1979; Cunningham et al. 1996) but its formation is probably older because of similar shear zones have

been described and dated from the Chinese and Kazakhstan parts of Central Asian Orogenic Belt. Allen et al. (1992) depicted post-collisional but Palaeozoic (Late Carboniferous–Early Permian), dextral shear zone accompanied by the intrusion of basic and acid magmas in the northern suture of the Chinese Tien Shan. Early Permian age for the dextral motion on the Tien Shan Shear zone (Shu et al. 1999) is confirmed by dating of newly formed muscovite in dextrally sheared mylonite.

A tectonic feature, which can be geographically linked with the Trans-Altay shear zone, is a 5–10 km wide sinistral NW–SE trending Erqishi shear zone (Laurent-Charvet et al. 2002), known also as Ertix fault (Briggs et al. 2007). It stretches from Qinhe in the Chinese Altay to Kazakhstan, where it is named the Irtysh shear zone (Melnikov et al. 1997). In Kazakhstan, the initiation of this shear zone occurred about 290 Ma ago as determined from $^{40}Ar/^{39}Ar$ mica dating in syn-tectonic granite (Melnikov et al. 1998). The main movement was sinistral and occurred along the Erqishi zone between 280–290 Ma. It was followed by a complex succession of dextral and sinistral shearing episodes dated at 245 Ma (Laurent-Charvet et al. 2003).

8. Conclusions

The Trans-Altay Gobi, as a part of the Central Asian Orogenic Belt consolidated during the Carboniferous, is composed of the Trans-Altay, Shargyn Gobi and Gobi Tien Shan domains which are constituted by individual (sub)terranes. All these were intruded by numerous pre-orogenic to post-orogenic granitic bodies of Devonian to Permian ages. Plutons are I-type, calc-alkaline, exceptionally with alkaline affinity of some acid rocks. They thus were most likely derived in a Late Palaeozoic volcanic arc related to the north-dipping Carboniferous subduction zone situated further south (in the present-day coordinates). According to geological position, six granitic intrusive complexes and independent gabbro massifs have been distinguished. These are, going generally from north to south:

- The Early Carboniferous **Bayan Ayrag Massif** in the Edren Terrane which is of post-orogenic character and comagmatic with the adjacent bimodal volcanics.
- The **Trans-Altay Intrusive Complex** is of Carboniferous to probably Permian age. Individual plutons are scattered throughout all terranes but the largest ones are bound mostly to the Shargyn Gobi and Trans-Altay domains. Intermediate to acid magmatic suites can be recognized. They are usually high-K calc-alkaline, highly fractionated rocks, with a signature resembling some individual plutons of alkaline affinity in Shargyn Gobi.
- The Carboniferous to Permian(?) **Ikh Bayan Massif** intruded along the Trans-Altay shear zone in the form of conspicuously circular plutons of a purely granitic composition.
- The **Gurvan Khar Massif** is probably of Devonian age, being composed of granodioritic orthogneiss. Geological relationships and primitive chemistry with very low-K character suggest evolution in an oceanic-island or primitive island-arc environment and could be related to ophiolite remnants in the Zoolen Terrane exposed in the suture between Trans-Altay and Shargyn Gobi domains.
- The **Gobi Tien Shan Intrusive Complex** is represented by numerous plutonic bodies in the Gobi Tien Shan range intruding accreted Ordovician to Carboniferous volcaniclastic complexes. In the NW part of the mountain range it also cuts metamorphic rocks of unknown age. Three magmatic suites have been recognized forming a gabbro – diorite – quartz diorite to monzodiorite – granodiorite – granite sequence. According to laser ablation ICP-MS data, the largest body of the complex – the Zamyn Belgekh Pluton – is Carboniferous. Nevertheless, Permian magmatic activity was documented in two samples. Magma mingling structures between basic and intermediate/acid magmas are characteristic of the magmatic complex and, together with I-type chemistry, point to an evolution above a subduction zone. Close spatial relations with the Carboniferous volcanics, granophyric textures in granites and mineral association in thermally metamorphosed rocks around the pluton point to an intrusion into the upper crustal level. Small bodies of the **Naran Sevest** and **Tsagaan Bogd** massifs represent relatively independent facies of the Gobi Tien Shan Intrusive Complex.
- **Gabbro massifs** of clearly post-orogenic character in respect to the Variscan accretion are closely related to the Late Carboniferous–Permian dextral shearing on the Trans-Altay shear zone separating Shargyn Gobi and Trans-Altay domains.

Acknowledgements. This study was based on data collected during the project "Geological and Geochemical mapping of Trans-Altay Gobi". It was prepared by Geomin Co., Jihlava in cooperation with Mineral Resources Authority of Mongolia within the framework of the International Co-operation Program of the Czech Republic in 1999–2003. The primary results including geological maps on a scale of 1 : 200,000 are available in Geological Information Centre in Ulaanbaatar. We are grateful to colleagues from the Mongolian Geological Survey and Mongolian University of Science and Technology who helped us with the field work as well as with the processing of maps. We are grateful to the staff of the expedition, above all to the excellent Mongolian drivers and especially we thank to J. G. Holák

for his logistic support in the field. Comments by I. Petrík, an anonymous reviewer and handling editor M. Štemprok have significantly helped us to improve this manuscript. We are also indebted to V. Janoušek for help with the preparation of the final version of manuscript.

Electronic supplementary material. The tables 4 and 5, as well as GPS coordinates of the studied samples, are available online at the Journal web site (http://dx.doi.org/10.3190/jgeosci.028).

References

Allen MB, Windley BF, Zhang C (1992) Paleozoic collisional tectonics and magmatism of the Chinese Tienshan, central Asia. Tectonophysics 220: 89–115

Badarch G, Cunningham WD, Windley BF (2002) A new terrane subdivision for Mongolia: implications for the Phanerozoic crustal growth of central Asia. J Asian Earth Sci 21: 87–110

Batchelor RA, Bowden P (1985) Petrogenetic interpretation of granitoid rock series using multicationic parameters. Chem Geol 48: 43–56

Batulzii D, Hanžl P, Orolzodmaa O, Naranbaatar TS (2003) Chemistry of the Carboniferous batholite Zambilgekh in Trans Altai Region. Mongol Geosci 21: 57–60

Bibikova EV, Kirnozova TI, Kozakov IK, Kotov AB, Neymark LA, Gorokhovskiy BM, Shuleshko IK (1992) U-Pb ages for polymetamorphic complexes on the southern flank of the Mongolian and Gobi Altai. Geotectonics 26: 166–172

Bonin B, Azzouni-Sekkal A, Bussy F, Ferrag S (1998) Alkali-calcic and alkaline post-orogenic (PO) granite magmatism: petrologic constraints and geodynamic settings. Lithos 45: 45–70

Borzakovskii YA, Suprunov EA (1990) Geological and mineral resources maps of western Mongolia on scale 1 : 500,000 with explanatory notes. Geological Information Centre, Mongolia, File Report no. 4496, Ulaanbaatar (in Russian)

Boynton WV (1984) Cosmochemistry of the rare earth elements: meteorite studies. In: Henderson PE (ed) Rare Earth Element Geochemistry. Elsevier, Amsterdam, pp 63–114

Briggs SM, Yin A, Manning CE, Chen ZL, Wang XF, Grove M (2007) Late Paleozoic tectonic history of the Ertix fault in the Chinese Altai and its implications for the development of the Central Asian Orogenic System. Geol Soc Am Bull 119: 944–960

Bucher K, Frey M (1994) Petrogenesis of Metamorphic Rocks. Springer-Verlag, Berlin, pp 1–318

Clarke DB (1992) Granitoid Rocks. Chapman & Hall, London, pp 1–283

Cunningham WD, Windley BF, Dorjnamjaa D, Badamgarov J, Saandar M (1996) Late Cenozoic transpression in southwestern Mongolia and the Gobi Altai–Tien Shan connection. Earth Planet Sci Lett 140: 67–81

Draut AE, Clift PD (2002) The origin and significance of the Delaney Dome Formation, Connemara, Ireland. J Geol Soc, London 159: 95–103

Eby GN (1990) The A-type granitoids: a review of their occurrence and chemical characteristics and speculations on their petrogenesis. Lithos 26: 115–134

Ferry JM, Spear FS (1978) Experimental calibration of the partitioning of Fe and Mg between biotite and garnet. Contrib Mineral Petrol 66: 113–117

Filippova IV, Suetenko OD, Levintov ME (1990a) Explanation text to Geological map of Western Mongolia on the scale 1 : 500,000. Volume 1 Stratigraphy, AN SSSR, Moscow (in Russian)

Filippova IV, Suetenko OD, Levintov ME (1990b) Geological map of Western Mongolia on the scale 1 : 500,000. AN SSSR, Moscow (in Russian)

Hanžl P, Krejčí Z eds (2008): Geological map of the Trans-Altay Gobi 1 : 500,000. Czech Geological Survey, Prague

Hanžl P, Otava J, Rejchrt M, Naranbaatar D, Coggerel J, Bajanjargal B, Lexa O, Černý M (2003) Geology of the Trans-Altai Gobi, SW Mongolia. J Czech Geol Soc 48: 55–56

Hanmer S (1990) Natural rotated inclusions in non-ideal shear. Tectonophysics 176: 245–255

Helo C, Hegner E, Kröner A, Badarch G, Tomurtogoo O, Windley BF, Dulski P (2006) Chemical signature of Paleozoic accretionary complexes of Central Asian Orogenic Belt in South Mongolia: constraints on arc environments and crustal growth. Chem Geol 227: 236–257

Hendrix MS, Graham SS, Carroll AR, Sobel ER, Mc Knight CL, Schulein BJ, Wang Z (1992) Sedimentary record and climatic implications of recurrent deformation in the Tianshan: evidence from Mesozoic strata of the north Tarim, south Junggar and Turpan basins, northwest China. Geol Soc Am Bull 104: 53–79

Holland T, Blundy J (1994) Non-ideal interactions in calcite amphiboles and their bearing on amphibole–plagioclase thermometry. Contrib Mineral Petrol 116: 433–447

Holland TJB, Powell R (1985) An internally consistent thermodynamic dataset with uncertainties and correlations: 2. Data and results. J Metamorph Geol 3: 343–370

Holland TJB, Powell R (1998) An internally consistent thermodynamic data set for phases of petrological interest. J Metamorph Geol 16: 309–343

Hu A, Jahn BM, Zhang G, Chen Y, Zhang Q (2000) Crustal evolution and Phanerozoic crustal growth in northern Xinjiang: Nd isotopic evidence. Part 1. Isotopic characterization of basement rocks. Tectonophysics 328: 15–51

Jahn BE (2004) The Central Asian Orogenic Belt and growth of the continental crust in the Phanerozoic. In: Malpas J, Fletcher CJN, Ali JR, Aitchinson JC (eds) Aspects of the Tectonic Evolution of China. Geol Soc London Spec Pub 226: pp 73–100

Jahn BM, Wu F, Chen B (2000) Massive granitoid generation in Central Asia: Nd isotope evidence and implication for continental growth in the Phanerozoic. Episodes 23: 82–92

Janoušek V, Farrow CM, Erban V (2006) Interpretation of whole-rock geochemical data in igneous geochemistry: introducing Geochemical Data Toolkit (GCDkit). J Petrol 47: 1255–1259

Kovalenko VI, Yarmolyuk VV, Salnikova EB, Kartashov PM, Kovach VP, Kozakov IK, Kozlovskiy AM, Kotov AB, Ponomarchuk VA, Listratova EN, Yakovleva SZ (2004) The Khaldzan-Buregtei Massif of peralkaline rare-metal igneous rocks: structure, geochronology, and geodynamic setting in the Caledonides of Western Mongolia. Petrologiya 12: 467–494 (in Russian)

Kovalenko VI, Yarmoluyk VV, Salnikova E, Kozlovskiy AM, Kotov A, Kovach VP, Savatenkov V, Vladykin N, Ponomarchuk VA (2006) Geology, geochronology, and geodynamics of the Khan Bogd alkali granite pluton in southern Mongolia. Geotektonika 40: 450–466 (in Russian)

Kozakov IK, Kovach VP, Bibikova EV, Kirnozova TI, Zagornaya NY, Plotkina YV, Podkovyrov VN (2007) Age and sources of granitoids in the junction zone of the Caledonides and Hercynides in southwestern Mongolia: geodynamic implications (in Russia). Petrologiya 15: 126–150

Kozlovskiy AM, Yarmolyuk VV, Salnikova EB, Savatenkov VM, Kovalenko VI (2005) Age of bimodal and alkali granite magmatism of the Gobi-Tien Shan rift zone, Tost Range, southern Mongolia. Petrology 13: 197–203

Lamb M, Badarch G (1997) Paleozoic sedimentary basins and volcanic-arc systems of southern Mongolia: new stratigraphic and sedimentologic constraints. Int Geol Rev 39: 542–576

Lamb M, Badarch G (2001) Paleozoic sedimentary basins and volcanic-arc systems of southern Mongolia: new stratigraphic and petrographic constraints. In: Hedrix MS, Davis GA (eds) Paleozoic and Mesozoic Tectonic Evolution of Central Asia – From Continental Assembly to Intracontinental Deformation. Geol Soc Am Memoir 194: 117–150

Lamb M, Badarch G, Navratil T, Poier R (2008) Structural and geochronologic data from the Shin Jinst area, eastern Gobi Altai, Mongolia: implications for Phanerozoic intracontinental deformation in Asia. Tectonophysics 451: 312–330

Laurent-Charvet S, Charvet J, Monie P, Shu LS (2003) Late Paleozoic strike-slip shear zones in eastern central Asia (NW China): new structural and geochronological data. Tectonics 22: 1099–1101

Laurent-Charvet S, Charvet J, Shu LS, Ma RS, Lu HF (2002) Palaeozoic late collisional strike-slip deformations in Tianshan and Altay, Eastern Xinjiang, NW China. Terra Nova 14: 249–256

Luchitskaya M, Tikhomirov P (2007) Cretaceous granitoid magmatism of north-east Asia: tectonic setting, rock chemistry, isotopy and P-T conditions of formation. Geoph Res Abstr 9

Melnikov A, Delvaux D, Travin A, Buslov MM, Vladimirov A, Smirnova L, Theunissen K (1997) Late Paleozoic–Early Mesozoic sinistral movement along the Irtysh shear zone, NE Kazakhstan. In: Tectonic Studies Group Annual General Meeting, 17–19 Dec, 1997, Durham (UK)

Melnikov A, Travin A, Plotnikov A, Smirnova L, Theunissen K (1998) Kinematics and Ar/Ar geochronology of the Irtysh Shear Zone in NE Kazakhstan. In: Continental Growth in the in Phanerozoic: evidence from East-Central Asia, IGCP-420 Meeting, Urumqi, China, pp 30

Middlemost EAK (1994) Naming materials in the magma/igneous rock system. Earth Sci Rev 37: 215–224

Mielke P, Winkler HGF (1979) Eine bessere Berechnung der Mesonorm für granitische Gesteine. Neu Jb Mineral, Mh 471–480.

Mitrofanov FP, Kozakov IK, Palei IP (1981) Precambrian of west Mongolia and South Tuva. In: Mitrofanov FP, Kozakov IK, Palei IP (eds) Transactions of the Joint Soviet–Mongolian Scientific-Research Geological Expedition vol 32. Nauka, Leningrad, pp 90–102 (in Russian)

Mossakovsky AA, Ruzhentsev SV, Samygin SG, Kheraskova TN (1993) Central Asian fold belt: geodynamic evolution and history of formation. Geotectonics 6: 3–33

Passchier CW, Simpson C (1986) Porphyroclast systems as kinematic indicators. J Struct Geol 8: 831–843

Pearce JA, Harris NBW, Tindle AG (1984) Trace element discrimination diagrams for the tectonic interpretation of granitic rocks. J Petrol 25: 956–983

Peccerillo A, Taylor SR (1976) Geochemistry of Eocene calc-alkaline volcanic rocks from the Kastamonu area, northern Turkey. Contrib Mineral Petrol 68: 61–81

Powell R, Holland TJB (1985) An internally consistent thermodynamic dataset with uncertainties and correlations: 1. Method and a worked example. J Metamorph Geol 3: 327–342

Ruzhentsev SV (1985) Geology of the Gobi Tien Shan and problems of South-Mongolian ocean. Izvestiya Vysshei Shkoly. Geologiya i Razvedka 6: 12–19 (in Russian)

Ruzhentsev SV (2001) The Variscan belt of South Mongolia and Dzungaria. In: Dergunov AB (ed) Tectonics, Magmatism, and Metallogeny of Mongolia, London, pp 61–94

Ruzhentsev SV, Pospelov II (1992) The South-Mongolian Variscan fold system. Geotektonika 5: 45–62 (in Russian)

Ruzhentsev SV, Badarch G, Voznesenskaya TA (1985) Tectonics of Trans-Altay zone of Mongolia. Geotektonika 4: 28–40

Şengör AMC, Natalin BA, Burtman VS (1993) Evolution of the Altaid tectonic collage and Paleozoic crustal growth in Eurasia. Nature 364: 299–307

Shand SJ (1947) Eruptive Rocks, Their Genesis, Composition, Classification and Their Relation to the Ore-Deposits. 3rd edition, J. Wiley & Sons, New York, 1–488 pp.

Shu LS, Charvet J, Guo LZ, Lu HF, Laurent-Charvet S (1999) A Large scale Paleozoic dextral strike-slip shear zone: the Aqikkudug-Weiya zone along the Northern margin of Central Tianshan belt, Xinjiang, NW China. Acta Geol Sinica 73: 148–162

Šourek J, Černý M, Rejchrt M eds (2003) Geological and geochemical mapping of Trans-Altay Gobi on the scale 1 : 200,000. MS, MRPAM, Ulaanbaatar, 1–64 pp

Streckeisen A, 1976. To each plutonic rock its proper name. Earth Sci Rev 12: 1–33.

Streckeisen A, Le Maitre RW (1979) A chemical approximation to the modal QAPF classification of igneous rocks. Neu Jb Mineral, Abh 136: 169–206

Sun SS, McDonough WF (1989) Chemical and isotopic systematics of oceanic basalts: implications for mantle composition and processes. In: Saunders AD, Norry MJ (eds) Magmatism in Ocean Basins. Geol Soc London Spec Pub 42: pp 313–345

Sylvester PJ (1989) Post-collisional alkaline granites. J Geol 97: 261–281

Tapponier P, Molnar P (1979) Active faulting and Cenozoic tectonics of the Tien Shan, Mongolia and Baykal region. J Geophys Res 84(B7): 3425–3459

Tumurtogoo O (1997): A new tectonic scheme of the Palaeozoides in Mongolia. In: Zhaqin X, Yufeng R, Xiaoping Q (Eds.). Proceedings of the 30th Int. Geol. Congr. VSP 7, 75-82

Tumurtogoo O (2002): Tectonic map of Mongolia, scale 1 : 1 000 000 (with Brief Explanatory Notes, 23 pp.), Geological Information Centre MRPAM, 15 sheets, Ulaanbaatar

Wang YX, Qiu YZ, Gao JY, Zhang QA (2003) Proterozoic anorogenic magmatic rocks and their constraints on mineralizations in the Bayan Obo deposit region, Inner Mongolia. Sci China, series D – Earth Sci 46: 26–40

Webb LE, Graham SA, Johnson CL, Badarch G, Hendrix MS (1999) Occurrence, age, and implications of the Yagan–Onch Hayrhan metamorphic core complex, southern Mongolia. Geology 27: 143–146

Wei CJ, Congqiang L, Masuda A (1997) Complex trace-element effects of mixing-fractional crystallization composite processes: applications to the Alaer granite pluton, Altay Mountains, Xinjiang, northwestern China. Chem Geol 135: 103–124

Whalen JB, Currie KL, Chappel BW (1987) A-type granites: geochemical characteristics, discriminations and petrogenesis. Contrib Mineral Petrol 95: 407–419

Wilson M (1989) Igneous Petrogenesis. Harper Collins Academic, London, pp 1–466

Windley BF, Allen MB, Zhang C, Zhao Z, Wang G (1990) Paleozoic accretion and Cenozoic redeformation of the Chinese Tien Shan range, central Asia. Geology 18: 128–131

Windley BF, Kröner A, Guo JH, Qu GS, Li YY, Zhang C (2002) Neoproterozoic to Paleozoic geology of the Altai orogen, NW China: new zircon age data and tectonic evolution. J Geol 110: 719–737

Windley BF, Alexeiev D, Xiao W, Kröner A, Badarch G (2007) Tectonic models for the accretion of the Central Asian orogenic belt. J Geol Soc, London 164: 31–47

Xiao WJ, Windley BF, Badarch G, Sun S, Li J, Qin K, Wang Z (2004) Palaeozoic accretionary and convergent tectonics of the southern Altaids: implications for the growth of central Asia. J Geol Soc, London 161: 339–342

Yarmolyuk VV (1983) Late Paleozoic volcanism of continental rifting structures of Central Asia. Nauka, Moscow, pp 1–198 (in Russian).

Yuan C, Sun M, Xiao W, Li X, Chen H, Lin S, Xia X, Long X (2007) Accretionary orogenesis of the Chinese Altai: insights from Paleozoic granitoids. Chem Geol 242: 22–39

Zhang Z, Guo Z, Liu S (1998) Age and tectonic significance of the mafic dyke swarm in the Kuruktag region, Xinjiang. Acta Geol Sinica 72: 29–36

Zhang SH, Zhao Y, Song B, Yang ZY, Hu JM, Wu H (2007) Carboniferous granitic plutons from the northern margin of the North China Block: implications for a late Paleozoic active continental margin. J Geol Soc, London 164: 451–463